ISAS - INTERNATIONAL SCHOOL
FOR ADVANCED STUDIES

A Global Hα-Emission Survey

of the Cluster

Abell 1367

Magister Philosophiæ

CANDIDATE

Joseph E. Pesce

SUPERVISOR

Dr. Chris Moss

Anno 1990-1991

TRIESTE

SISSA - SCUOLA
INTERNAZIONALE
SUPERIORE
STUDI AVANZATI
TRIESTE
Strada Costiera 11

ERRATUM

For the two photographs, Figures 3.1 and 3.5, North is up, as labelled but East is to the LEFT.

Summary

Using a high dispersion, objective prism, 201 CGCG galaxies in the irregular cluster Abell 1367 have been surveyed for global Hα emission. The emission, indicative of star formation, is observed in 23 per cent of cluster galaxies, all of which are of Hubble type S0-a and later. Emission frequency increases for later type galaxies.

In addition, an objective prism survey for [OII] λ3727 Å emission, the first of its kind, is made and we find four per cent of the galaxies in Abell 1367 in emission. Galaxies with [OII] emission are the strongest Hα emitters as well. Further work needs to be done in order to say anything definitive about the [OII] emission. For example, the lack of detection may be an effect of the survey technique.

We attempt to determine the effects of the cluster environment on individual galaxies and find that Hα emission is not correlated with apparent and absolute magnitude nor with position within the cluster. However, emission frequency may increase with increasing local galaxy density. When compared with field galaxies, the cluster spiral galaxies of early-type Sa – Sab exhibit more strong emission than field spirals of similar type. Conversely, late-type cluster spirals, Sc – Irr. exhibit less strong emission than field galaxies of the same type. Interactions between the intracluster medium and galaxies and galaxy – galaxy interactions may account for the observations. These subjects are discussed in view of the results herein presented.

Haec sic pernosces parva perductus opella;
namque alid ex alio clarescet, nec tibi caeca
nox iter eripiet quin ultima naturai
pervideas: ita res accendent lumina rebus.

"If you take a little trouble you will attain
a thorough understanding of these truths. For one thing
will be illumined by another, and eyeless night will
not rob you of your road till you have looked into
the heart of nature's darkest mysteries. So surely will
facts throw light upon facts."

Lucretius, *De rerum natura*, I.1114 – 1117

CONTENTS

TABLES

FIGURES

CHAPTER I

Introduction

1.1 Galaxy segregation by morphological type

Clusters of galaxies are the largest structures in the universe containing tens (poor clusters) to thousands (rich clusters) of galaxies, extending over a region of approximately three megaparsecs and with masses greater than 5 $\times 10^{14}$ $M_{\odot}$ (Sarazin 1988). Although only about five per cent of galaxies are collected in groups and clusters whose space density is larger than one galaxy per cubic megaparsec (Dressler 1984), they provide an interesting laboratory in which to study topics such as galaxy evolution, segregation by morphological type and environmental effects on galaxies. Galaxies not associated with a cluster or group are said to be "field" galaxies and reside in low-density regions with space density less than or equal to one galaxy per cubic megaparsec (Dressler 1984).

Numerous systems have been devised to classify clusters, based upon varying properties. We briefly mention two classification schemes here in order to facilitate the discussion given below. An excellent review of the many systems of cluster classification can be found in Sarazin (1988).

Abell (1975) classifies clusters of galaxies on a system varying from *regular* to *irregular*. *Regular* clusters are highly symmetric in shape and have a

core with a high concentration of galaxies toward the centre. *Irregular* clusters have little or no symmetry, no central concentration and exhibit substantial subclustering.

Oemler (1974) has constructed a classification scheme based upon the galaxy content of clusters, *i.e.*. the fraction of galaxies which are spirals, S0s and ellipticals. He has refined the system of Morgan (1962), defining three classes of clusters: *spiral-rich* clusters in which spirals are the most common galaxies and with the ratios of E:S0:S galaxies of 1:2:3; *spiral-poor* in which spirals are less common and S0s are the more common galaxies with ratios E:S0:S of 1:2:1; and *cD* clusters which are dominated by a central cD galaxy and in which the majority of galaxies are elliptical or S0 and with ratios E:S0:S of 3:4:2. Dressler (1980) finds that representative populations of *spiral-rich*, *spiral-poor* and *cD* clusters have projected galaxy surface densities of approximately 3.2, 32 and 63 galaxies per square megaparsec, respectively, for $m_v < 16.5$ and $z \lesssim 0.06$.

Regular clusters tend to be Oemler *spiral-poor* or *cD* and have a high mean density of galaxies. The Coma cluster is a nearby example of a typical regular cluster. A typical irregular cluster is the Virgo cluster. Clusters of this sort are usually Oemler *spiral-rich*. In comparison, the field contains approximately 81 per cent spiral, 17 per cent S0 and 2 per cent elliptical galaxies (Christensen 1975).

These classification schemes show that there is a link between galaxy content and environmental density. The percentage of spiral galaxies increases as the galaxy density decreases with a lower fraction of spiral galaxies in regular clusters than in the field. Conversely, the percentage of elliptical and S0 galaxies decreases as the galaxy density decreases.

Dressler (1980) finds that a well-defined relation exists over five orders

of magnitude in density between the local density of galaxies and the proportion of different morphological types. The morphology-density relation is monotonic but changes slowly so that the low density field is dominated by 80 – 90 per cent spirals and the high density regions are composed of 80 – 90 per cent ellipticals and S0s (although all types are represented in all regions) (Dressler 1984).

The fundamental question that may be asked is why there are the differences in the ratio of morphological types in different density regions. Two possibilities have been suggested. The first states that the initial conditions in which galaxies form determine differences in the ratio of morphological types. Perhaps spiral galaxies require relatively isolated, low-density regions to form; they are destroyed or their formation suppressed in regions where the galaxy density is high. The second possibility is that environmental influences are more important than initial conditions and these cause galaxies to evolve and change morphological type. High-density regions may cause spirals to change into S0 and/or elliptical galaxies. Because clusters are regions of high galaxy density they provide excellent laboratories in which to observe the effects, or lack of them, of environment on individual galaxies.

1.2 Initial conditions of galaxy formation

Initial conditions at the time of galaxy formation may be more important than later, environmentally induced changes in determining the variations in ratio of morphological types from region to region. This view holds that regular clusters *never* had many spiral galaxies (Abell 1975) but were formed as they appear now.

Gott & Thuan (1976) argue that the efficiency of star formation during galaxy formation is set by the density of the protogalaxy. In a protogalaxy with sufficiently high density, gas will be largely converted into stars during collapse, forming elliptical galaxies. If the initial density is low, star formation is not effective and the left-over gas continues to collapse gravitationally. The gas can efficiently transfer angular momentum as it collapses, through viscous forces, because it is a collisional fluid. A disk will be the result of such a collapse. Stars formed subsequently will have circular orbits in the plane of the disk.

If, on the other hand, the gas is totally converted into stars before it can collapse to a disk the system can no longer be operated on by viscous forces since the stars are collisionless particles. The stars will not collapse into a disk but will have random, radial orbits with no preferred plane, forming an elliptical galaxy. Regular clusters are denser than irregular clusters and if density is the factor that determines galaxy morphology, then the relationship of galaxy morphology to cluster morphology can be understood easily. Denser environments favour the formation of elliptical galaxies.

However, regular clusters do contain some spiral galaxies. One possible explanation, in light of the above argument, is that spiral galaxies formed in the lower density regions outside of regular clusters and were accreted later.

Butcher & Oemler (1978) observed that a number of clusters at high redshift ($z \sim 0.4$) contain a high proportion of blue galaxies which lie at larger projected distances from the cluster centre than the redder galaxies. These galaxies have colours which are indistinguishable from spirals, but no nearby cluster contains such active spirals. This observation was taken as evidence that the galaxies were falling into the cluster and experiencing star formation. Later workers (Dressler & Gunn 1982; Dressler 1984; Dressler, Gunn & Schneider 1985) have shown that while some of the galaxies are indeed cluster members,

many are foreground and background objects. The blue cluster galaxies have spectra unlike present day spirals and may be active galaxies. These may be galaxies that are just entering the high-density intracluster medium and their star formation rates may have been enhanced.

Several authors (Moss & Dickens 1977; Tammann & Binggeli 1987) suggest that the high velocity dispersions and peripheral positions of spiral galaxies in clusters signify that these galaxies are presently falling into the cluster core region. This observation seems to be confirmed by Sodre *et al.* (1989) who, based upon an analysis of 15 clusters, find that spiral and irregular galaxies have higher velocity dispersions than elliptical and S0 galaxies. They speculate that this fact indicates that the late-type galaxies may have been accreted by the cluster more recently.

Thus, regions of high density may have precluded the formation of late-type galaxies because they preferentially, and more efficiently, formed early-type galaxies. Spiral galaxies are, in fact, seen in regular clusters, albeit in small fractions. These galaxies may have formed in the lower density regions and were then added to the high density regions through accretion.

A difficulty with the view of Gott & Thuan (1976) is raised in the objection of Gott (1977) who argues that at the time of galaxy formation ($z \sim 20 - 30$) [1] a density enhancement that is to become a cluster of galaxies has a very small amplitude. Therefore, if galaxies form early and rapidly, they can not "know" the environment in which they will reside and all regions should contain all types of galaxies.

[1] It may be noted that there is no consensus on the formation epoch of galaxies. Many workers believe that galaxies form at $z \sim 3 - 5$ (see, for example, Peebles 1989 and Majewski 1989). However, a thorough discussion of the topic of galaxy formation is beyond the scope of the present work.

1.3 Environmental influences on galaxy evolution

If the view of Gott (1977) is correct, it is difficult to see how initial conditions have led to differences in the ratio of morphological types. Another possibility is that environmental effects cause the differences. Gott (1977) hypothesizes that density enhancements destined to become regular and irregular clusters start out with very small differences. All galaxy types may begin to form in all regions. Eventually, small density variations grow to become large differences and as the potential well of a high-density region deepens, its gas is heated more than the gas in a low-density region. Incipient spirals in the high-density regions are then destroyed by the hot, intracluster gas. For example, clusters like Coma may never have included fully developed spirals and their subsequent development may have been precluded when the intracluster medium was heated to $T \sim 10^8$ K.

Therefore, environmental effects may be more important in determining the differences in the ratio of morphological types. Such environmental effects may also lead to interactions of galaxies with each other or with the cluster in such a way that their morphologies are changed. Two possibilities have been suggested, the transformation of spiral galaxies into S0 galaxies because of gas stripping (*cf.* Gunn & Gott 1972) and the merging of two galaxies to form a galaxy of another type (*e.g.* Schweizer 1983).

1.3.1 THE TRANSFORMATION OF SPIRALS INTO S0 GALAXIES

The increase in S0 galaxies and the decrease in spiral galaxies in higher density regions may be due to the fact that spirals evolve to become S0s. Spirals

are stripped of interstellar gas as they fall through the intracluster medium. Continuing star formation then exhausts any remaining gas and the spiral "becomes" an S0 galaxy (Spitzer & Baade 1951).

However, there are arguments against the view that environmental influences cause spirals to become S0 galaxies. Dressler (1980) points out a few:

1.) The bulges of S0s are systematically larger (brighter) than those of spiral galaxies. Similarly, the disk-to-bulge ratios of spirals are much larger than those of S0 galaxies. This observation would seem to indicate that spirals and S0 galaxies are not from the same parent population and is certainly inconsistent with the view that S0 galaxies are swept spirals.

2.) Significant numbers (80 per cent) of S0 galaxies are found in low density environments, such as the field and the outskirts of clusters, which are $10^2 - 10^3$ times less dense than regions where stripping is thought to take place. Also, spiral galaxies and S0 galaxies coexist. The gas deficiencies in spirals in intermediate density environments are modest (2 – 3 times) whereas S0s have deficiencies of hundreds of times (Dressler 1984).

An alternative process to produce S0 galaxies has been proposed by several authors (Norman & Silk 1979; Sarazin 1979) who suggest that all spiral galaxies have large, extended haloes. These envelopes resupply gas that has been exhausted in the disks. A spiral that has lost the envelope through stripping will exhaust its internal gas supply by normal star formation and become an S0 galaxy. While spirals probably do have extended haloes, Keel (1983) traces the distribution and extent of the optical emission lines in the nuclei of a number of spirals and concludes that the distribution seems to follow the starlight in outline, supporting an internal origin for the gas, rather than recent infall from outside. However, not much is known about the haloes nor

about the effects of gas, returning to the interstellar medium from outside, on star formation.

1.3.2 GALAXY MERGERS

While the view that spirals evolve to become S0 galaxies appears to have serious problems, the environment can change a spiral in other ways. For example, the merging of two spirals may form an S0 or elliptical galaxy. Toomre & Toomre (1972) first showed that the unusual structures observed in many peculiar systems are the results of two galaxies merging. These mergers manifest themselves by, for example, exhibiting tails, arcs and bridges of matter that has been liberated from the galaxies as they pass through or near one another. The obvious signatures of mergers are short lived but most likely the galaxies stay together after interacting (Toomre 1977). Other observational evidence for merging includes multiple cores in cluster ellipticals, the presence of counter-rotating cores, disks of dusty material and asymmetric envelopes around ellipticals (Schweizer 1983).

Approximately one-half of the bright field elliptical galaxies show signs of having accreted disks or parts of disks recently (Schweizer 1983). Schweizer also concludes that the accretion process must have tended to reduce the number of disk galaxies and increase the luminosity of bright elliptical galaxies. If such a large number of mergers have occurred in the field, it might be expected that mergers are much more common in the high density cluster environment. Galaxy mergers between various combinations of small and large ellipticals, disk galaxies and gas clouds can be invoked to produce observed galaxies. For example, Schweizer believes that S0 galaxies with polar rings or disks can be

produced when large and small disk galaxies merge. This would explain the coexistence of S0 and spiral galaxies in the field.

Barnes (1988) finds that the merging of disks with haloes leave slowly rotating remnants that are consistent with slowly rotating, bright elliptical galaxies. Thus, the merger process seems to provide a mechanism for decreasing the number of spirals and increasing the number of ellipticals and S0s and may be relatively common in the cluster environment.

There are, however, critics of the hypothesis. Tremaine (1990) suggests that the presence of multiple nuclei in some cluster ellipticals is due to projection effects of foreground galaxies. In addition, van den Bergh (1990) suggests that ellipticals could not have been formed by the merging of two spirals because the frequency of globular clusters in elliptical galaxies is many orders of magnitude greater than in spirals. The merging process is not thought to produce the extra globular clusters.

The subject of mergers in galaxies is a vast one and is being debated widely. We can only touch upon the surface here but it is one viable alternative to explain the transformation of spiral galaxies into galaxies of earlier type.

1.4 Observed environmental effects on spiral galaxies

What sort of environmental effects on spiral galaxies might be caused by the cluster? The intracluster gas may interact with the interstellar gas of a galaxy. If this is the case, what effect will such interactions have on the gas content and star formation of spiral galaxies? These topics are discussed in the following sections. Interactions between individual galaxies may be more frequent in the cluster and they will be discussed in Chapter VIII.

1.4.1 GAS CONTENT

As a spiral galaxy moves through the intracluster medium, one might expect its gas to be stripped. In fact, observations suggest that removal of gas has occurred in cluster spirals. Cluster spirals are deficient in neutral hydrogen when compared to similar galaxies in the field.

Spitzer & Baade (1951) were the first to suggest that direct collisions between galaxies would ionize and liberate interstellar gas but leave stars unaffected, a relatively efficient process. Assuming that all galaxies in the Coma cluster were equivalent and that the galaxies had radial orbits, Spitzer and Baade found that a galaxy would be stripped in about 10^8 years.

However, direct Spitzer–Baade collisions are rare. With an increase in the cosmic distance scale it is now realized that stripping of this sort will take about a Hubble time, far too long to be effective (Bothun 1982).

Gunn & Gott (1972) proposed a model of ram pressure stripping to sweep the H I from disk galaxies in clusters. In this scenario, the external pressure exerted on the interstellar gas as the galaxy moves rapidly through the intracluster medium would strip the galaxy. According to Bothun (1982), the effects of ram pressure stripping may be a strong function of the orientation of a galaxy as it moves through the intracluster medium. Galaxies moving through the intracluster medium face-on will have their gas easily swept. However, if a galaxy moves through the intracluster medium edge-on the interstellar medium may not be swept, but compressed.

Cowie & Songaila (1977) hypothesized that the high temperature (T $\sim 10^8$ K), intracluster gas interacts with cooler gas embedded within galaxies causing thermal evaporation of the galaxy gas. According to these authors, this effect, rather than ram pressure stripping, may be responsible for the absence

of the [OII] λ3727 Å line in elliptical galaxies within rich clusters, since ram pressure stripping will not remove nuclear gas but thermal evaporation will.

Davies & Lewis (1973) were the first to observe that spiral galaxies in the Virgo cluster exhibited deficiencies of H I when compared to field spirals. This finding was later confirmed (Chamaraux, Balkowski & Gerard 1980; Giovanardi *et al.* 1983; Giovanelli & Haynes 1983).

Giovanelli & Haynes (1985), from H I data for galaxies in nine clusters, argue that spirals in regions of high galaxy density are substantially deficient in their H I content. The H I disks of deficient Virgo cluster spirals are clearly smaller than those of field galaxies of the same or earlier morphological type. The H I deficiency strongly correlates with radial distance from the cluster centre; galaxies near the core exhibit the greatest deficiencies. In clusters in which the deficiency is pronounced, the proportion of swept spirals is larger. If a deficiency is observed, then most, if not all, spirals passing through the core are affected. These results are confirmed by Haynes & Giovanelli (1986) who find that Virgo galaxies are undergoing gas removal by interactions with the surrounding medium. Giovanelli & Haynes (1985) find that H I deficiency correlates with the presence of a hot X-ray intracluster medium. The largest deficiencies are found in clusters with the highest X-ray luminosity.

Similarly, Gavazzi (1987) finds that in a sample of 53 galaxies in Coma/Abell 1367, spiral galaxies within one Abell radius from the core of Coma contain three times less H I, on average, than isolated galaxies. However, spiral galaxies in the groups and multiple systems of Coma have H I content not dissimilar to isolated galaxies. The average deficiency increases to five times in the core of Coma, a high density region of this regular cluster, and drops to about two times in Abell 1367, an irregular, spiral-rich cluster. There is a tendency for galaxies that are more severely depleted to be redder

and of earlier Hubble type. Late-type spirals in Abell 1367 have "normal" H I content, suggesting that they have not yet entered the dense intergalactic environment or that they have resided in it for a time shorter than the stripping timescale (consistent with the hypothesis that these galaxies have been accreted recently).

According to Stauffer (1983), the majority of spirals in Virgo that are H I deficient have had time to adjust their colours to the H I content, thus the H I deficiency can not have occurred recently ($T \leq 10^9$ years). In contrast to the *global* H I deficiency, Stauffer finds that the nuclei of Virgo spirals have apparently normal supplies of ionized gas as inferred from the nuclear Hα emission-line strength. This finding is contrary to Gisler's (1978) result that there is less ionized gas in the nuclei of spirals in clusters. Obviously the mechanism for causing H I deficiency is more efficient at removing gas from the disk of a spiral than from its nucleus.

1.4.2 EMISSION-LINES FROM IONIZED GAS

Osterbrock (1960) was the first to point out that the frequency of emission of the [OII] λ3727 Å line is lower for cluster ellipticals than for ellipticals in the field and that there are differences between the cluster and field populations. Gisler (1978) found, for a sample of 1316 galaxies collected from the literature, that the total fraction of galaxies observed in emission increases toward later galaxy types and there is a strong tendency for galaxies in less compact associations to be reported more frequently in emission. He also found that ionized gas in the nuclei of spiral galaxies occurs less frequently in dense clusters and that H II regions in the nuclei of galaxies (spiral and elliptical) are less commonly found in galaxies inside dense clusters than among galaxies

in general. He concluded that the substantial intracluster medium *does* hinder the formation of H II regions in the *nuclei* of galaxies.

Dressler, Thompson & Shectman's (1985) *nuclear* observations of 1095 galaxies in rich clusters and 173 field galaxies confirm the earlier results that the frequency of emission line galaxies in the field is higher than in clusters. Emission-line galaxies comprise 31 per cent of the field galaxies but only 7 per cent of the cluster galaxies.

However, based on photometric observations of 200 spirals in 9 clusters, Bothun, Schommer & Sullivan (1982) conclude that cluster galaxies are not unlike field galaxies in many of their integrated properties. These authors state that the data argue against environmental effects as having been important in the evolution of most cluster members and that only in Coma is there evidence for environmental modification.

Stauffer (1983) agrees with this conclusion. Using previously published 21 cm data and optical emission-line fluxes from a *nuclear* survey of Virgo cluster spirals, he concludes there is *no significant difference* in Hα emission equivalent width between field and Virgo cluster spirals. He also finds that the [NII]/Hα ratio correlates well with the nuclear magnitude; in the sense that large ratios correspond to bright nuclei, and concludes large [NII]/Hα ratios are internally generated and not due to an external process.

Kennicutt & Kent (1983), in their study of 200 field and Virgo cluster galaxies, found that Hα emission is only weakly correlated with H I content. This suggests that the H I gas density is probably not the only causative parameter which determines the global rate of star formation.

These authors can identify distinct nuclear and disk components in the Hα emission. The strong nuclear components consist of large H II regions in the inner disk and bulge regions. Sa – Sab galaxies with strong Hα invariably

turn out to have such nuclei. They find *no* correlation between disk and nuclear emission properties among the galaxies surveyed (*cf.* their Figure 6).

Kennicutt (1983a) combines *global* Hα measurements with published H I and B – V colour data to compare the properties of Virgo cluster spirals with a large sample of field spirals. The Virgo core members exhibit significantly weaker emission compared to the field. A substantial fraction of the spirals are also gas poor. Taken together with Stauffer's (1983) data, Kennicutt agrees that the Virgo environment has significantly altered the *gaseous* and *stellar* content of the disks *without* significantly altering the nuclear regions.

Kennicutt, Bothun & Schommer (1984), in a global, photometric study of 65 field and cluster spirals, report that Hα fluxes and colours indicate H I deficiency has not altered the star formation or stellar content of the galaxies. Cluster members in general, possess a distribution of gas exhaustion timescales not unlike those for field galaxies. They find **no** evidence for a strong deficiency of Hα emission from spirals in rich clusters. In fact, there is a sizable population of high emission galaxies in the very centre of Coma and Abell 1367, indicating recent, high rates of star formation. Imaging shows that the emission arises from the disk H II regions, not the nuclei. Similarly, Moss (1988) shows that early-type spirals (S0-a – Sb) in clusters are more likely to be detected in emission than field spirals of the same type.

1.4.3 RADIO EMISSION FROM SPIRAL GALAXIES

Based upon a study of Coma and Abell 1367 cluster members, Gavazzi & Jaffe (1985, 1986) conclude that the stripping of gas, which is supposed to be a major cause for hydrogen deficiency in spirals, *does not* prevent but *enhances* radio-continuum emissivity and star formation (in agreement with Kennicutt,

Bothun & Schommer 1984). These authors suggest that interactions with the intracluster medium lead to a collapse of molecular clouds, enhanced star formation, generation of cosmic rays via supernovae and the observed optical peculiar morphologies. Cluster systems have stronger H I deficiency with respect to field galaxies and, yet, have higher ratios of radio to optical luminosity, which indicates enhanced star formation.

1.4.4 DISCUSSION

Does the observed gas deficiency in cluster spirals lead to less star formation? Removal of gas *is* thought to slow down star formation activity in spiral galaxies (Kennicutt & Kent 1983). Evidence from various authors (Osterbrock 1960; Gisler 1978; Dressler, Thompson & Shectman 1985) suggests that emission from spiral galaxies is, indeed, reduced when compared to field galaxies. However, there is also surprising evidence that emission from cluster spirals may be no different than emission from field spirals (Bothun, Schommer & Sullivan 1982; Stauffer 1983; Kennicutt 1983a; Kennicutt & Kent 1983) and may even be *enhanced* (Kennicutt, Bothun & Schommer 1984; Gavazzi & Jaffe 1985, 1986; Moss 1988).

Obviously, the observations are contradictory. If, however, there is emission in cluster spirals how does it come about? Shocks induced by ram pressure effects have been proposed by some authors (Kennicutt, Bothun & Schommer 1984; Gavazzi & Jaffe 1985, 1986; Gavazzi 1987) to cause star formation activity. Star formation occurs in molecular clouds that may be too dense to be stripped and are, perhaps, more centrally concentrated. Ram/thermal pressure of the cluster medium may trigger collapse of these clouds. Stripped from the periphery of galaxies, H I does not contribute to star formation in

any case. Young, Scoville & Brady (1985) and Kenney & Young (1989) find that CO and molecular gas is *not* deficient in stripped spirals, supporting this hypothesis.

The idea that shocks lead to star formation is an old one (Shu *et al.* 1972; Elmegreen & Lada 1977; Larson & Tinsley 1978). Schweizer (1987) states that as a shock propagates through the gas, most pre-existing H_2 molecules dissociate but dust survives. These grains then allow the H_2 to form again in the high density post-shock regions where the gas can actually become fully molecular. Such gas at high densities cools very fast forming ideal conditions for fragmentation and rapid star formation. Large-scale dynamical collisions appear to make big differences because they lead to the formation of shocks of galactic dimensions which in turn form 10 to 100 times more molecular gas than normal.

Giant molecular clouds resist removal because of their large surface densities and location deep in the gravitational potential well of the inner disk. Kenney & Young (1989) rule-out galaxy collisions, tidal stripping and thermal evaporation as mechanisms for gas removal and conclude that ram pressure stripping is the one simple model consistent with observations. These authors conclude that ram pressure stripping may facilitate the conversion of H I to H_2, but it is less plausible that it causes the enhancement of star formation. Magnetic and turbulent forces which support molecular clouds are generally much stronger than the ram pressure forces making it unlikely that the galaxy–cluster interaction will accelerate the collapse of molecular clouds and increase star formation.

Another, alternative mechanism to enhance star formation may be tidal effects caused by galaxy-galaxy interactions. (Interactions are discussed in detail in Chapter VIII). Such interactions drive a large amount of gas into

the nuclear regions of the galaxies, fueling activity, and, incidentally, removing gas from the disks (Byrd *et al.* 1986; Noguchi 1988; Byrd & Valtonen 1990). Star formation is expected to be enhanced in the outer disk regions while nuclear starbursts and the formation of bars are induced, according to models by Noguchi (1988).

1.5 The present survey

It is obvious from Section 1.4 that the observations have led to contradictory and confusing conclusions. One of the more surprising results is that even though cluster galaxies show gas deficiencies, star formation may be enhanced.

Clues to some of the above mentioned problems may be gained from a systematic study of the star formation in cluster galaxies. In addition, more data will help to clarify the confusion in the field. With these ideas in mind, we have surveyed the galaxies of the irregular cluster Abell 1367 for global Hα + [NII] emission.

Subsequent sections of this work are organized as follows. Star formation indicators in general, and the justification for the use of Hα + [NII] emission as an indicator of star formation in particular, are the subjects of Chapter II. The survey method, which follows the technique developed by Moss, Whittle & Irwin (MWI) (1988), is discussed in Chapter III. This technique allows for rapid surveys of nearby ($z < 12000$ km s^{-1}) clusters, determination of radial velocities and measurements of Hα flux and equivalent width. Chapter IV discusses the radial velocity measurements, and Hα fluxes and equivalent widths are presented in Chapter V. In addition to the Hα survey, a high dispersion, objective prism survey for the [OII] λ3727 Å emission line in

cluster galaxies was made. The survey is the first of its kind and the results are presented in Chapter VI.

Using the data, we then investigate how star formation rates in the galaxies depend upon various galaxy properties (*e.g.* magnitude and type). This material is discussed in Chapter VII. The effects of the cluster environment on star formation in cluster galaxies (*i.e.*, how emission varies with position within the cluster and the comparison of cluster and field galaxies) are discussed and possible explanations are presented in Chapter VIII. Finally, the conclusions are given in Chapter IX.

CHAPTER II

Star Formation Indicators

2.1 Summary of indicators

2.1.1 GALAXY COLOUR

Larson & Tinsley (1978) studied a sample of galaxies taken from the *Hubble Atlas of Galaxies* (Sandage 1961) and the *Atlas of Peculiar Galaxies* (Arp 1966) with measured *UBV* colours. The Hubble galaxies (which these authors assumed to be "normal") exhibit a well-defined relation between U – B and B – V with the scatter approximately the mean error. The Arp galaxies have a much greater scatter and extend to considerably bluer colours in both B – V and U – B. The authors state that the scatter is **not** due to larger errors for the Arp galaxies, since the quoted average errors are no larger than for the Hubble group.

Although reddening is the greatest source of error it does not greatly affect the overall distribution in the two-colour diagram. Similarly, gaseous emission lines and non-thermal emission are not considered important for the galaxies studied. Chemical composition affects a galaxy's colour but not enough information is known to correct for this effect. In addition, the variation of the initial mass function of stars in the galaxies can affect the colours and may account for some, but not all, of the observed scatter in the two-colour

diagram. Therefore, the scatter in the observed UBV colours of galaxies must be due mainly to differences in the star formation history.

Models of star formation show that the position of a galaxy on the common two-colour line is almost uniquely determined by the star formation rate per unit mass averaged over the past 10^8 years. The spread of galaxies perpendicular to the normal distribution of the two-colour diagram can be explained as being due to *recent* bursts of star formation. Bluer U – B colours indicate more recent star formation bursts.

2.1.2 OPTICAL EMISSION LINES

Gaseous nebulae in star forming regions are photoionized by ultraviolet radiation from hot stars with surface temperatures $T_* \gtrsim 3 \times 10^4$ K (Osterbrock 1989). The emission-line spectra of such nebulae include forbidden lines such as [OIII] $\lambda\lambda$4959,5007 Å, [NII] $\lambda\lambda$6548,6583 Å and [OII] $\lambda\lambda$3726,3729 Å and the permitted lines of Hα λ6563 Å, Hβ λ4861 Å, Hγ λ4340 Å, He I λ5876 Å and He II λ4686 Å. Weak forbidden lines and faint permitted lines of other elements are also seen, such as C II, C III, C IV, O II, *et cetera*.

One indicator of star formation is the Hα λ6563 Å emission, which will be discussed in more detail below, in Section 2.2. Cohen (1976) observed emission from Hα and [NII] lines in the disks of 53 spiral and irregular galaxies and concluded that the amount of emission at Hα correlates with the B – V colour of a galaxy in the sense that the bluer the galaxy, the larger the Hα emission. She shows that the emission itself does not directly affect the B – V colour to produce the correlation and that two-thirds of the observed light comes from the disk. The Hα emission in the normal spirals can be accounted for by emission from ordinary H II regions of reasonable size and number. The

conclusion of the study is that the range of Hα emission is a result of the varying properties of O and B stars capable of photoionizing the gas relative to cooler stars.

Gallagher, Bushouse & Hunter (1989) find [OII] λ3727 Å flux highly correlated to Hβ flux and that the equivalent width of an emission line produced via photoionization from OB stars is a measure of recent star formation histories. Therefore, the [OII] line flux can also be used to derive approximate star formation rates in galaxies.

2.1.3 INFRARED

Almost all energy produced by newly born stars emerges as infrared radiation from the parental gas and dust clouds. Thus, the infrared is an excellent waveband to study the distribution of energetics and rates of star formation in galaxies (de Jong *et al.* 1984). Infrared emission lines from the gaseous nebulae are also expected. These include [NeII] λ12.8 μm and [OIII] λ88.4 μm (Osterbrock 1989).

Lamb *et al.* (1988) studied 108 colliding pairs of spiral galaxies and 83 isolated spirals and find that Hα correlates with infrared flux at 60 and 100μm for the interacting pairs. They conclude that interactions can lead to enhanced star formation. Similarly, Trinchieri *et al.* (1989) find tight correlations between far-infrared, Hα, and blue luminosities for a sample of 178 normal galaxies observed by Kennicutt & Kent (1983) in Hα.

2.1.4 RADIO

Supernovae may be intimately connected to star forming regions. Massive stars form and "die" as supernovae, which in turn compress the surrounding gas to initiate the next generation of star formation (Mueller & Arnett 1976). Radio emission from supernovae and their remnants would, therefore, indirectly indicate star formation. Synchrotron emission is expected from supernovae remnants while supernovae, themselves, emit 6 cm continuum and 20 cm line radiation (Weiler & Sramek 1988 and references therein). In addition, emission nebulae in star forming regions have strong radio continua, mostly due to thermal bremsstrahlung (Osterbrock 1989).

Gavazzi & Jaffe (1985), in a study of Coma and Abell 1367 cluster galaxies, find that the ratio of radio luminosity to optical luminosity, R, correlates well with B–V and the Hα equivalent width suggesting that R is a good indicator of star formation.

Fitt *et al.* (1988) believe that non-thermal radio emission in the disks of spiral galaxies arises from the cosmic rays energized by supernovae in regions of active star formation. They find a tight correlation between far-infrared and radio emission. However, the far-infrared emission is powered not only by young star forming regions but also by the old disk population. An even better correlation is found between the radio and far-infrared emission when the contribution from the old disk population is removed from the far-infrared emission. Therefore, the authors suggest that the radio luminosity at low frequencies is a better tracer of young star forming activity than the far-infrared emission.

2.2 The use of global Hα + [NII] emission as a star formation indicator

Global Hα + [NII] (herein after referred to as simply Hα) emission has been shown to be associated with H II regions (Cohen 1976). The emission is related to the total number of OB stars in a galaxy and, therefore, is thought to be an indicator of current, massive star formation. The equivalent width of these lines (the line-to-continuum ratio) represents the ratio of young to old stars and, hence, the relative star formation rate (Kennicutt & Kent 1983). These authors obtained photometric and spectrophotometric observations of Hα emission for 200 field and Virgo cluster galaxies and find that Hα equivalent width increases for later type galaxies with a large dispersion among galaxies of the same Hubble type.

Kennicutt & Kent attempt to verify that the Hα emission measures the relative rate of star formation and that the dispersion is not due to extraneous factors such as instrumental error, nuclear emission, large H II regions, [NII]/Hα variations or variations of extinction by dust. Their discussion proceeds as follows.

Instrumental errors are small, on the order of 2 Å for equivalent width measurements. Therefore, these authors conclude that this source of error is not expected to affect the observed dispersion of Hα equivalent widths.

Strong nuclear emission arises from large H II regions in the inner disk and bulge of galaxies. While this fact may present a problem for small-slit spectrometer data, it rarely dominates the integrated photometry. In any case, Kennicutt & Kent find that the nuclear emission amounts to a few per cent or less of the total disk emission. The conclusion drawn is that nuclear emission is rarely significant and that the large dispersion in the emission-line properties

of the late-type galaxies is a 'property of the star forming disks and not the nuclei.

While emission may be dominated by several large H II regions, Kennicutt & Kent find that this is not the case. For high luminosity galaxies, the contribution of the largest H II regions is uniform and small, about 10 per cent of the total emission (although they warn that this *may* not hold for lower luminosity irregular galaxies).

Variations in Hα and [NII] emission lines from galaxy to galaxy could account for the large observed dispersion in emission properties, especially if [NII]/Hα is large. However, [NII]/Hα variations are shown to cause only ± 5 – 20 per cent of the observed dispersion in Hα emission.

Finally, dust extinction is found to be the largest source of uncertainty in interpreting Balmer line fluxes. Extinction by dust is considerable in most galaxies and extinction variations may produce considerable variations in the Hα emission, independent of the star formation rate. However, Kennicutt & Kent state that the effect can hardly explain the very large dispersion in emission properties observed in their analysis and that there is little or no anti-correlation observed between the stellar absorption and the Hα equivalent width.

The authors conclude that although dust may play a significant role in the dispersion of the Hα emission, the other contributions to the dispersion are small. Therefore, for spiral galaxies of types Sab and later, *the large dispersion in observed Hα properties must reflect a real dispersion in the relative star formation activity.* Galaxies with very large equivalent widths ($\geq$ 50 Å) invariably prove to be galaxies which appear to be undergoing intense star formation bursts. Galaxies with low equivalent widths almost always possess morphologies and integrated colours which are consistent with low star for-

mation rates. Equivalent widths of Hα emission are strongly correlated with colour in the sense that galaxies with blue colour have large equivalent widths. Kennicutt & Kent conclude that *the Hα + [NII] emission of a spiral galaxy is a good measure of the current rate of massive star formation.*

Kennicutt (1983b) confirms these findings and assumptions. He performed the first attempt at measuring the total star formation rate in a large sample of field spirals and irregulars using photometry of Hα emission. *Nuclear* emission is found to be negligible ($\leq$ 5 per cent of total) in most of the spirals studied. Absorption by Hα in the underlying red continuum is small, as well, since the light is dominated by G and K giants with typical equivalent width of $\sim$ 1 – 2 Å. Therefore, the uncertainties in the Hα flux are small.

Emission of Hα is produced by massive stars (10 – 100$M_\odot$) while the red continuum is provided mostly by low mass (0.7 – 3$M_\odot$) red giants. Thus, the Hα equivalent width is a sensitive indicator of the initial mass function slopes over that range of stellar masses. Using this fact, Kennicutt finds that star formation has proceeded at a relatively constant rate over the lifetimes of most late-type galaxies and that the Hα emission is an indicator of the current rate of star formation normalized to the average past star formation rate.

2.3 Low mass star formation

The above mentioned indicators all relate to massive star formation. Low mass stars may be less easy to detect but their presence may lead to an enhancement of red continuum light. Johnstone & Fabian (1989) explain *i*-band excesses in the surface brightness profile of a giant elliptical galaxy as being due to stars in the mass range 0.2 – 0.5 $M_\odot$.

CHAPTER III

An Objective Prism Hα Survey of Abell 1367

3.1 Abell 1367

Abell 1367 is an irregular, Bautz-Morgan *Type II-III* cluster with a moderately high spiral fraction (Bahcall 1977) and is part of the Coma – Abell 1367 supercluster (Gregory & Thompson 1978). Clusters designated as Bautz-Morgan *Type II-III* are intermediate between Bautz-Morgan *Type II* clusters whose dominant galaxies are between cD and normal giant ellipticals and Bautz-Morgan *Type III* with no dominant cluster galaxies (Bautz & Morgan 1970). Oemler (1974) categorizes Abell 1367 as *spiral-rich* (E:S0:Sp; 1:2:3) with a total luminosity of 3.3×10^{12} $L_{\odot}$. The redshift of the cluster is $z = 0.0215$ with a velocity dispersion of 832 km s^{-1} (Struble & Rood 1987). An optical photograph of Abell 1367, from the Palomar Sky Survey red plate, is shown Figure 3.1.

The cluster X-ray luminosity is relatively low, $L_x \sim 1.6 \times 10^{44}$ h^{-2} erg s^{-1} (where $h = H_o/100$ km s^{-1} Mpc^{-1}) with an inferred temperature of the intracluster gas, $T_g \sim 3 \times 10^7$ K (Mushotzky 1984). The X-ray emission of Abell 1367 has an irregular, clumpy appearance typical of an unrelaxed cluster (Jones *et al.* 1979). Bechtold *et al.* (1983) observed the cluster with the *Einstein* satellite and discovered 11 resolved peaks in the X-ray emission associated with cluster galaxies, constituting about six per cent of the total

cluster X-ray emission. These galaxies have X-ray luminosities in the range 10^{40-42} h^{-1} erg s^{-1}. Bechtold *et al.* find the X-ray core radius to be r_x = (1.6 × 0.8) h^{-1} Mpc for the semimajor and semiminor axes of the distribution.

Hanisch (1980) finds that the radio emission (at 430 and 1400 MHz) of Abell 1367 is dominated by the strong radio galaxy 3C 264 (= NGC 3862 = CGCG no. 097.127) and that a diffuse source of emission remains when the contribution from 3C 264 is subtracted. The diffuse emission is significantly different than that of a regular cluster such as Coma in that it is located well away from the cluster centre, is in a region not well populated with galaxies and the source size is small (~ 0.2 Mpc).

3.2 Observations

3.2.1 PLATE MATERIAL

Observations of Abell 1367 were made by C. Moss using the Burrell Schmidt telescope (61-/94-cm) on Kitt Peak equipped with a 2° + 4° objective prism combination for plates A and B (in Table 3.1) and a 10° objective prism for plates C and D. The dispersion of the 10° prism is 400 Å mm^{-1} (MWI) and 780 Å mm^{-1} for the 2° + 4° prism combination (see below, Section 4.2.3), at the rest wavelength of Hα. The dispersion direction of the prisms was oriented north–south. Four exposures were made on IIIaF emulsion, hypersensitized by baking at 65° C in forming gas (2 per cent hydrogen and 98 per cent nitrogen). Exposure times range from 75 minutes to 120 minutes. The physical plate size is 19.8 × 19.8 cm and the Burrell Schmidt plate scale is 96.6 arcsec mm^{-1} providing a usable field of 5°.1 × 5°.1. A square RG 645 filter was used for plates A and B in Table 3.1, while for plates C and D a circular RG 630 filter was

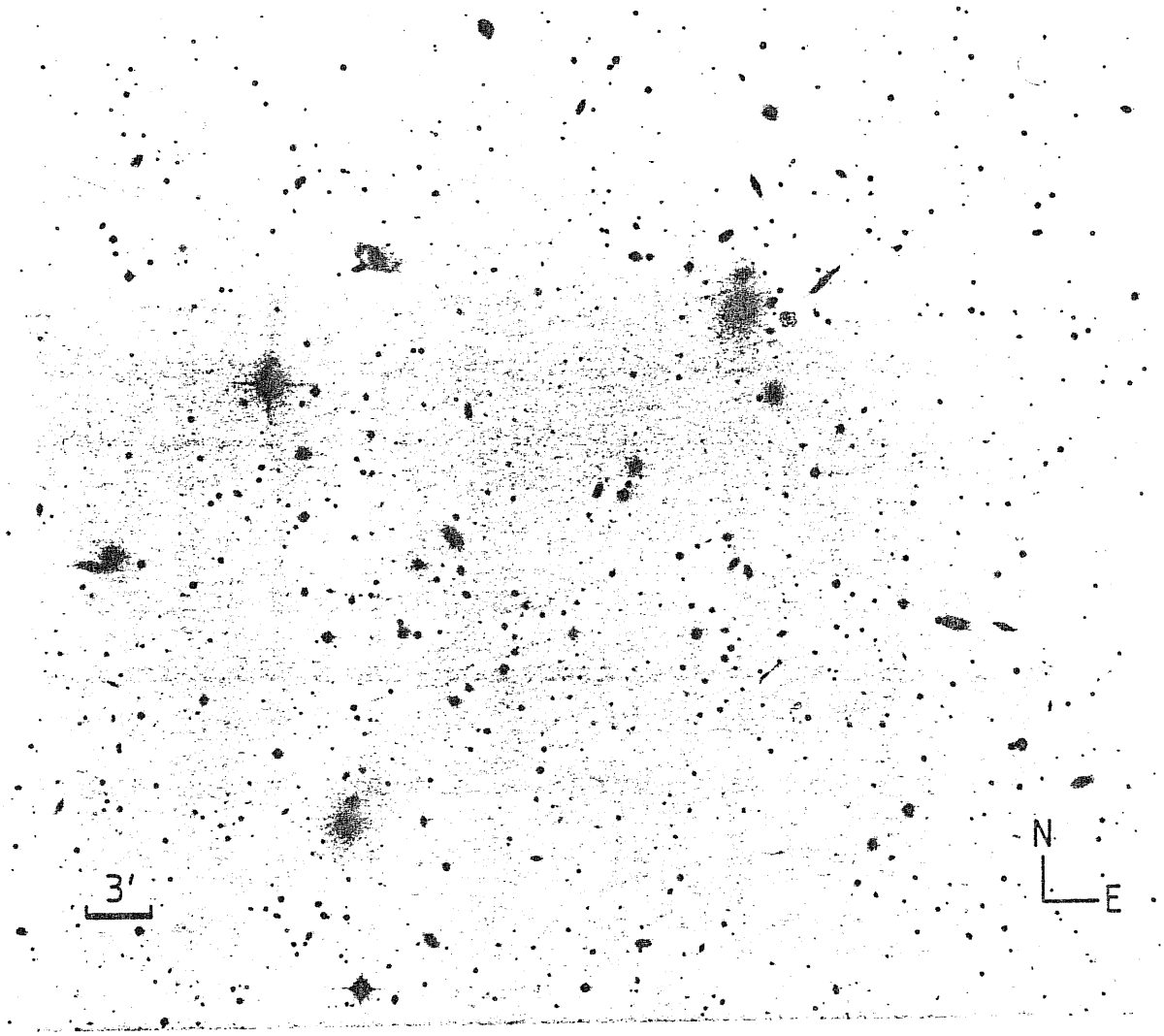

Figure 3.1: The cluster, Abell 1367, in a photograph reproduced from the Palomar Sky Survey red plate.

employed, giving a field of 5°.1 diameter. (See MWI for a thorough discussion of the survey of Abell 1367 using plates C and D).

The RG 645 filter is preferable to the RG 630 since it blocks the two [OI] night sky lines at 6300 and 6364 Å (McCarthy & Treanor 1970). In addition, since the filter is square it allows the entire 5°.1 × 5°.1 field to be used. The combination of RG 645 + IIIaF emulsion gives a bandpass which has a full width at half maximum of ∼ 350 Å centred on 6655 Å with a peak sensitivity at ∼ 6717 Å (the peak sensitivity of the IIIaF emulsion) (MWI). The sensitivity curve for this filter-emulsion combination is shown in Figure 3.2.

Two plate pairs of the cluster field were obtained using the 10° prism and 2° + 4° prism combination to allow one to reject spurious detections due to plate flaws and photographic grain clumping (sometimes resembling weak emission features). In addition, weak emission features can be confirmed more easily when two plates are used. Plates were taken with the telescope on the east and west side of the pier. This procedure has the effect of reversing the prism and, hence, the dispersion direction, and is useful in cases when a galaxy spectrum is overlapped by a nearby object (more common for clusters at low Galactic latitude but not a problem in the present study). Reversing the prism also allows one to measure redshifts, employing the method discussed below in Section 4.2.

In addition, plates E and F in Table 3.1 are two exposures of Abell 1367 using IIIaJ emulsion, a 4°.5 UV prism and a circular UG5 filter on the Burrell Schmidt telescope. The field of view is 5°.1 in diameter. The filter-emulsion combination gives a bandpass of ∼ 750 Å centred on ∼3600 Å with a peak sensitivity at ∼ 3700 Å. The relative sensitivity of the IIIaJ emulsion and UG5 filter is shown in Figure 3.3. These plates are used for the [OII] λ3727 Å emission survey of Abell 1367 discussed below in Chapter VI.

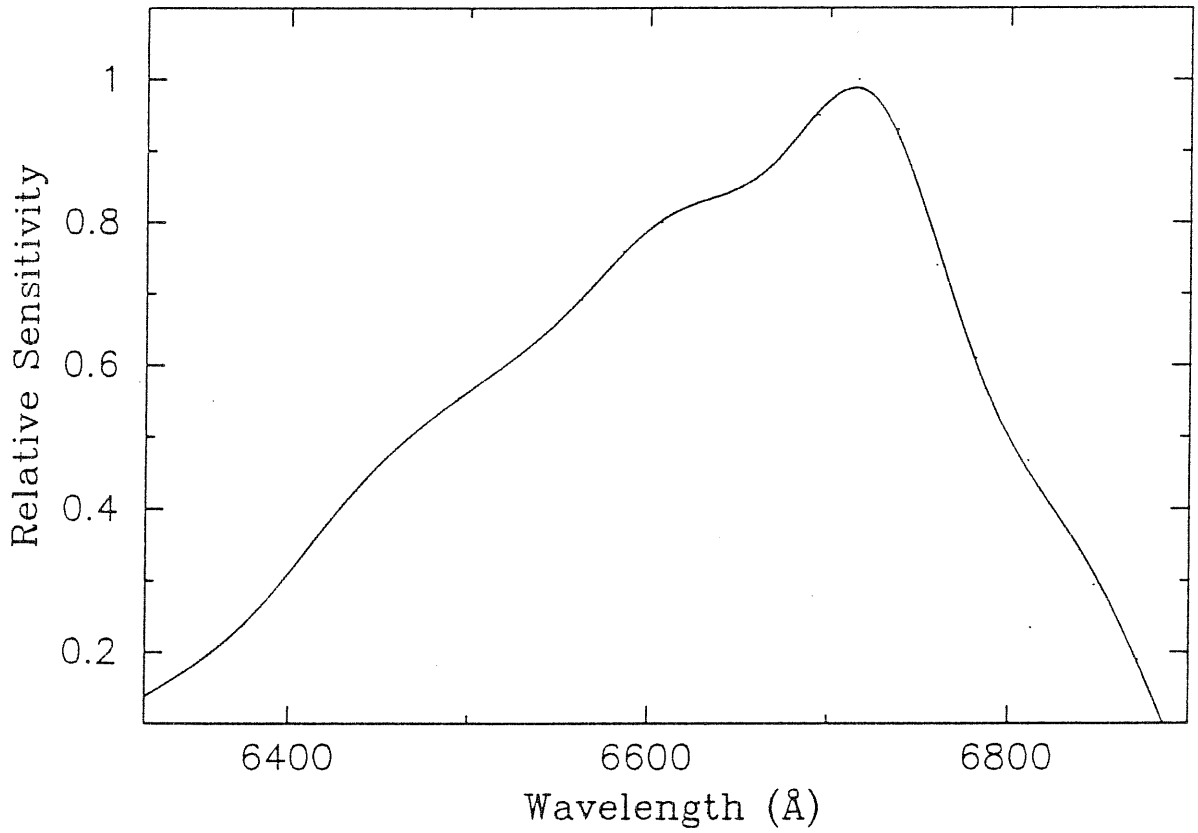

Figure 3.2: The relative sensitivity of the IIIaF emulsion + RG 645 filter combination plotted as a function of wavelength. The steep cutoff redward of the peak at 6717 Å is due to the loss of sensitivity of the IIIaF emulsion.

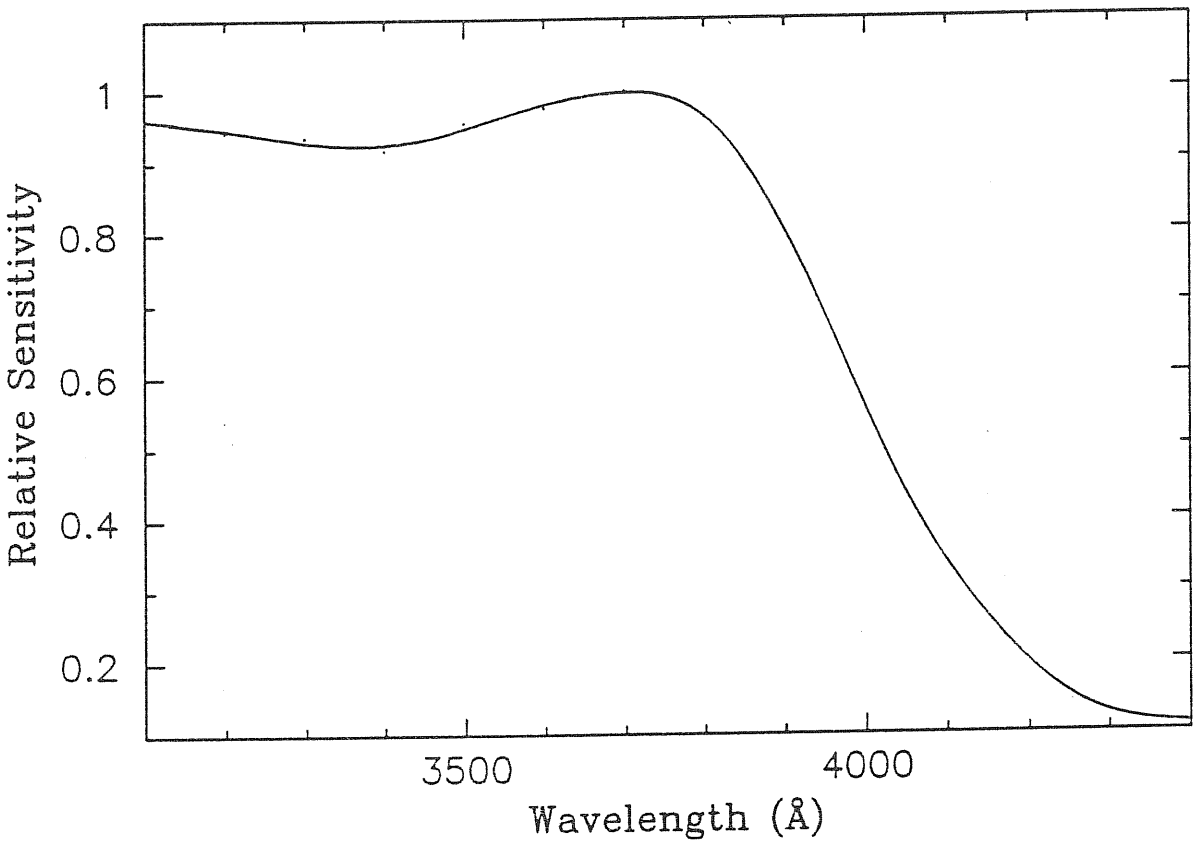

Figure 3.3: The relative sensitivity of the IIIaJ emulsion + UG5 filter combination plotted as a function of wavelength. The loss of sensitivity redward of the peak at 3700 Å is due to the cutoff of the filter. The atmosphere attenuates ultraviolet flux blueward of 3200 Å.

Finally, plate G in Table 3.1 is an excellent quality, direct plate centred on Abell 1367 and taken with the Palomar Schmidt by C. Mackay. A Wratten 2C filter, which has a sharp cutoff for $\lambda \leq 3850$ Å, and IIIaJ emulsion were used for the exposure. This plate was used to determine the morphological types of the galaxies in the survey.

The plate material used in this survey is summarized in Table 3.1. Shown in the table are the plate designations (column 1) and, in column 2, plate number. Column 3 gives the date of observation while columns 4 and 5 give the right ascension and declination of the plate centres. The prism, filter and emulsion used for the exposures are given in columns 6, 7 and 8, respectively. Column 9 gives the exposure time and column 10 gives the telescope on which the exposure was made (BS = Burrell Schmidt and PS = Palomar Schmidt) and the orientation of the telescope (East or West of the pier).

Plates A and B were taken on the Burrell Schmidt telescope equipped with a $2° + 4°$ objective prism combination, an RG 645 filter and IIIaF emulsion. The present study makes use of these two plates for the first time. Plates C and D were used in the study of MWI and were taken with the Burrell Schmidt telescope equipped with a 10° objective prism, an RG 630 filter and IIIaF emulsion. In addition to these four plates used for the main survey, plates E and F are used for the survey of [OII] λ3727 Å emission. They were taken on the Burrell Schmidt equipped with a 4°.5 UV prism, a UG5 filter and IIIaJ emulsion. Plate G is a Palomar Schmidt direct plate on IIIaJ emulsion with a WR 2C filter. All plates are of high quality.

The present study is important for the following reasons. A larger area is studied in this analysis than in any previous study using objective prism plates, and we have, therefore, a larger sample of galaxies. Because the area covered by the MWI study lies within the overlap region of plates A and B we

Table 3.1: Plate material used in the survey of Abell 1367.

	Plate no.	U.T. Date	Plate Centre R.A. (1950.0) h m s	Dec. ° ′ ″	Prism	Filter	Emulsion	Exposure (min)	Telescope & Orientation
(1)	(2)	(3)	(4)	(5)	(6)	(7)	(8)	(9)	(10)
A	15272	1985 April 12	11 42 57	+20 00 06	2° + 4°	RG 645	IIIaF	90	BS E
B	15273	1985 May 12	11 43 22	+20 20 19	2° + 4°	RG 645	IIIaF	90	BS W
C	14077	1983 April 3	11 37 54	+19 59 18	10°	RG 630	IIIaF	75	BS E
D	14200	1983 May 3	11 41 55	+20 00 03	10°	RG 630	IIIaF	120	BS W
E	15275	1985 April 13	11 44	+19 56	4°.5 UV	UG5	IIIaJ	120	BS E
F	15276	1985 April 13	11 44	+19 56	4°.5 UV	UG5	IIIaJ	180	BS W
G	8882	1973 May 2	11 41 54	+20 07 00	direct	WR2C	IIIaJ	60	PS —

Note: Telescope Type, BS = Burrell Schmidt
PS = Palomar Schmidt

can compare the performance and efficiency at detecting emission-line galaxies between the lower dispersion 2° + 4° prism combination and the 10° prism. For emission-line galaxies in common between the two studies we will compare independent measurements of flux and equivalent width. These measurements will be compared, in turn, to measurements obtained with photoelectric methods. In addition, the spectra could be used to study the two-dimensional nature of the Hα emission. However, this is not done in the present analysis. Finally, the objective prism plate method is employed for the first time to search for [OII] λ3727 Å emission in galaxies.

3.3 The galaxy sample

Figure 3.4 shows the area of the cluster covered by the four prism plates A, B, C and D. The largest overlap region of a plate pair is between plates A and B and constitutes an area of 23 square degrees, more than 1.6 Abell radii from the core, in which there are 172 CGCG galaxies. It may be noted that there are no galaxies in the non-overlap region of plates A and B. In what follows, we will refer to the "overlap region" as that region overlapped by plates A and B. The overlap region of plates C and D is elliptical and is practically contained within the overlap region. This is the region studied by MWI and we are, therefore, able to compare many aspects of the present study with their work.

Whereas MWI looked at all galaxy spectra in the overlap region of plates C and D, this study analyzes CGCG galaxies only. We have limited the present study to CGCG galaxies because it is easy to obtain morphological types for these galaxies, this being more difficult for fainter galaxies. MWI find that the magnitude limit of the CGCG, $m_p = 15.7$, is an approximate

detection limit for the survey method. While there are a considerable number of detected emission-line galaxies with magnitudes fainter than $m_p = 15.7$ (35 per cent of the MWI sample have magnitudes greater than this limit), the fraction of galaxies detected in emission drops steeply compared to the fraction of brighter galaxies detected in emission. For $m_p < 15.7$ the detected fraction of galaxies is relatively constant (*cf.* Section 7.2).

Plates A and B were systematically searched using a low power ($\sim \times$ 12) binocular microscope. In this way, the objective prism spectra of a total of 201 CGCG galaxies in the fields of view of all four plates were studied for Hα emission.

Table 3.5 (on page 46) lists the CGCG galaxies observed. In column 1 the CGCG number is given (an asterix indicates that the galaxy appears on only one plate). The NGC (IC with an asterix) and UGC (Nilson 1973) numbers are given in columns 2 and 3, respectively. The galaxy coordinates are given in columns 4 and 5. These were measured with an accuracy of $\sim$ 2 arcsec from the Palomar Sky Survey (PSS) prints using a coradograph (a manual XY measuring machine) and are the centres of the optical images. Photographic magnitudes from Zwicky & Herzog (1963) are given in column 6, and morphological types of the galaxies in column 7. Galaxy types were estimated from an examination of the high-quality, Palomar Schmidt plate, plate G in Table 3.1. Types marked with an asterix are off the edge of the field of plate G and were examined on the PSS blue print. These types are less well determined. Column 8 gives the plates on which the galaxy spectra are observed. Heliocentric velocities, taken from the literature, are given in column 9 along with source references in column 10. In most cases, velocities are derived from 21 cm observations. Finally, references to notes on individual objects are given in column 11. In total, 201 CGCG galaxies are observed in

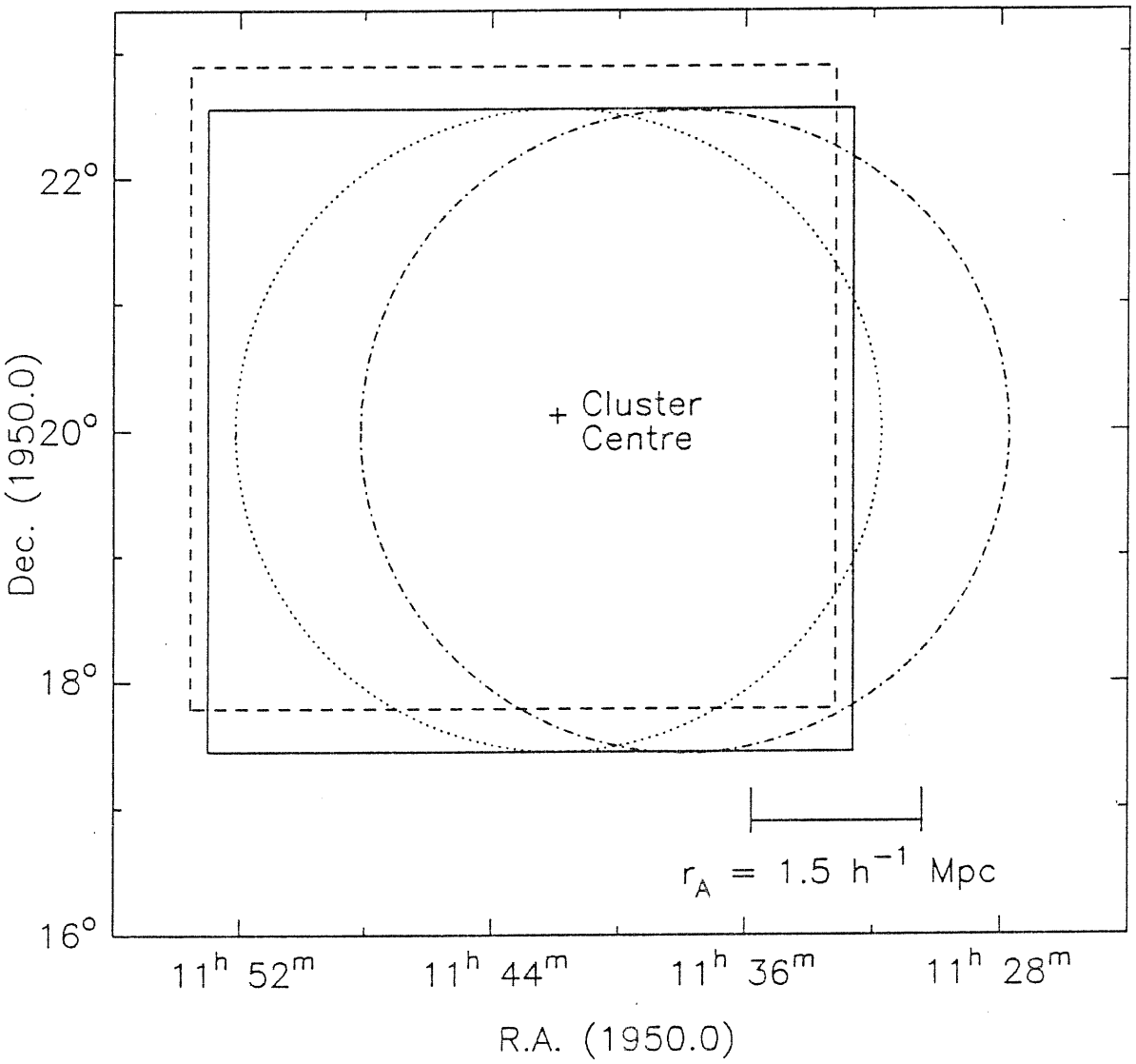

Figure 3.4: The area of the cluster Abell 1367 covered by the four objective prism plates. The cluster centre (at R.A. and Dec (1950): $11^h\ 41^m.9\ +20°\ 07'$) is marked and the cluster scale, in Abell radii (Abell 1958) is indicated. Plate A is represented by the solid line, plate B by the dashed line, plate C by the dot-dashed line and plate D by the dotted line. Plates A and B are 5°.1 square and plates C and D have a 5°.1 diameter.

the area covered by one or more plates. In the overlap region, 172 galaxies are observed while 130 galaxies are in the overlap region of plates C and D.

3.4 Identification of emission-line galaxies

All of the CGCG galaxies were examined for Hα emission and the results are given in Table 3.6 (on page 57). The CGCG numbers are given in column 1. An asterix indicates that a galaxy appears on only one plate. These are galaxies that appear on plate C only. Columns 2 and 3 give the galaxy numbers on plates C and D, respectively, and refer to the previous study of these plates by Moss, provided here for reference purposes. A qualitative description of the emission visibility on all plates A, B, C and D is given in columns 4, 5, 6 and 7, respectively. The presence or absence of emission is described as follows: an ellipsis indicates that the galaxy does not appear on the plate; "No" indicates no detection of emission; S, MS, M, MW and W indicate that emission was detected and refers to the visual appearance ('Strong', 'Medium-strong', 'Medium', 'Medium-weak' and 'Weak', respectively). MWI find that the parameter correlates loosely with the Hα flux but not with the Hα equivalent width (this is confirmed in the present study). The visibility parameters for galaxies on plates C and D (columns 6 and 7, respectively) are taken from MWI. Columns 8 – 11 contain a qualitative description of the concentration of the emission regions: very diffuse (VD), diffuse (D), concentrated (C) or very concentrated (VC). A blank space in these columns indicates that there is no emission, or that the concentration appearance is unremarkable. The concentration parameter for galaxies on plates C and D (columns 10 and 11, respectively) are taken from the analysis of MWI. Finally, references to notes on individual objects are given in column 12.

Figure 3.5 shows three representative galaxies (left) and their spectra (right). The top panel is CGCG no. 126.110, with emission characterized as visually strong and very concentrated. The emission of CGCG no. 097.093 is characterized as visually medium and with normal concentration and is shown in the middle panel. Weak and very diffuse emission from CGCG no. 097.033 is shown in the lower panel.

Independent analysis of the concentration parameters indicate that while these are subjective qualities, classification of an emission region is relatively constant from individual to individual. As a test, the concentration parameter for galaxies on plates C and D (columns 10 and 11, respectively, in Table 3.6) were re-examined by Pesce and the results were found to correlate well with the parameter as determined by Moss. The results of the analysis are shown in Table 3.2, with the measurements of Pesce in the rows and those of Moss in the columns. The numbers represent the number of galaxies with the concentration as given by Pesce and Moss. If there were no differences between the way individuals classify emission we would expect all measurements to lie on the diagonal line from top left to bottom right. In general, the agreement is good. If we were to limit the classification of emission concentration to categories, either VC, C and normal or VD and D as is done below, we are in total agreement.

Galaxies were included in a final list of emission-line galaxies if they appeared in emission on two or more of the four plates surveyed. Exceptions to this criterion were galaxies which lie on single plates only, and with visually strong emission. There are three such galaxies, CGCG nos. 126.074, 126.075 and 126.091 (all on plate C). In the total sample of 201 CGCG galaxies, 23 per cent (n = 46) show Hα emission. Of the 172 CGCG galaxies in the overlap region 25 per cent (n = 43) show emission.

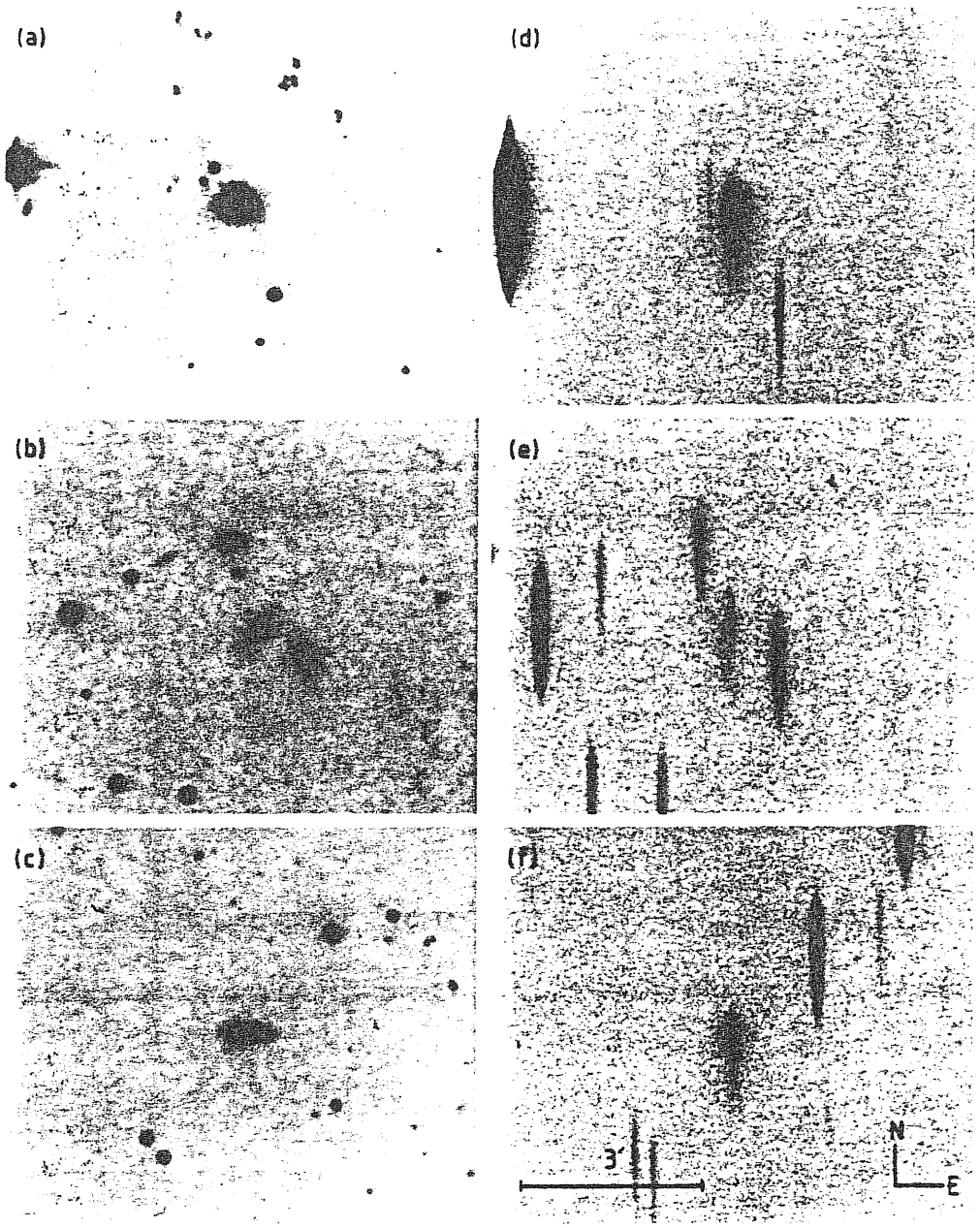

Figure 3.5: Representative spectra of emission-line galaxies. The panels on the left are the galaxy images from the Palomar Sky Survey red plate while the panels on the right show the spectra from plate B. The top panel shows CGCG no. 126.110 whose emission is characterized as visually strong and very concentrated. CGCG no. 097.093 is characterized as visually medium and with normal concentration and is in the middle panel. Weak, very diffuse emission from CGCG no. 097.033 is shown in the lower panel.

Table 3.2: Comparison of concentration parameter classifications.

P \ M	VC	C	—	D	VD
VC	1	1	1		
C			1		
—			15		
D				5	1
VD				1	3

The final list of emission-line galaxies is given in Table 3.7 (on page 62). The first line of column 1 is the CGCG number and the second line gives the alternate CGCG number. The first line of column 2 gives the NGC number (IC number if proceeded by an asterix) and the second line is the UGC number. Line 1 of column 3 is the MCG number and line 2 the *IRAS* number. Note that because of the proximity of CGCG nos. 097.122 and 097.120, these two galaxies are given the same *IRAS* identification. Ellipses in columns 2 and 3 indicate that the galaxies are not found in the catalogues. Positions measured with a coradograph and accurate to $\sim$ 2 arcsec are given in columns 4 and 5, while CGCG photographic magnitude is given in column 6. The morphological type, as determined for Table 3.5 (see above, Section 3.3) appears in column 7. Columns 8 and 9 give the emission visibility and concentration parameters, respectively. The plates on which the galaxy appears is given in column 10. Heliocentric velocities are given in column 11 with references on line 2, and references to notes on individual objects are given in column 12.

The final list of emission-line galaxies consists of 46 (43 in the overlap region) galaxies, none of which have morphological types earlier than S0.

The fraction of emission-line galaxies detected is 23 per cent, similar to that detected by MWI.

3.5 Comparison with the MWI survey

It is desirable to compare the performance of the 2° + 4° prism combination to that of the 10° prism in detecting emission-line galaxies. Table 3.3 shows the number of galaxies detected on the prism plate combinations, in the overlap region of all four plates. Based on detection of emission-line galaxies we can rank the plates according to their quality, from best to worst. Plates A and B are the best, plate D the second best while plate C is the worst. In the overlap region of all the plates, no galaxies were detected on plate C that were not detected on other plates, *i.e.,* the poor quality of plate C did not cause spurious galaxy detections.

The exposure time, as given in Table 3.1, for plate C is 20 to 40 per cent lower than the exposure times for the other plates. One might assume that the plate's poor quality is due to this factor alone. However if true, plate D, with the longest exposure, should be the best which is clearly not the case. It is well known that seeing affects the quality of a plate. Most probably, seeing is the other major factor, besides exposure time, affecting plate quality.

At present it is not possible to determine if the 2° + 4° prism combination is better than the 10° prism. However, the current analysis indicates that the 2° + 4° prism combination is, at least, no worse at detecting emission-line galaxies than the 10° prism. This signifies that the lower dispersion of the 2° + 4° prism combination (780 Å mm^{-1}) compared to the dispersion of the 10°

Table 3.3: Emission-line galaxies detected on plate combinations.

Plate Combination	Number Detected
A + B	32
A + D	25
B + D	25
A + C	22
B + C	22
C + D	20

prism (400 Å mm^{-1}) does not adversely affect the detection of emission-line galaxies.

3.6 Sizes of galaxies and emission regions

Table 3.4 lists measurements of the major axis diameter, D, of the emission-line galaxies taken from plate G. Diameters of emission regions were measured from plates A and B and the average is listed as d_e. The ratio d_e/D is given also and all measurements are in arcmin.

Diameters were measured with a binocular microscope at × 56 using a reticule placed directly onto the surface of the plates. The reticule has 28 divisions per millimeter. CGCG nos. 097.087 and 127.095 were not measured because they have several emission regions, nor was CGCG no. 097.067 because it is a foreground object.

For strong, concentrated emission the diameters of the emission re-

gions can be measured relatively accurately because the outer edge of such regions is clearly defined. On the other hand, it is difficult to ascertain the outer extent of weak emission regions, so these values are, perhaps, less accurately measured.

3.7 Individual objects

Several emission-line galaxies may be noted for their interesting appearance; CGCG no. 097.087 (*cf.* Gavazzi *et al.* 1984) has four or five distinct knots and CGCG no. 127.095 is a barred spiral with emission knots at the centre and at locations that correspond to regions at either end of the bar visible on the PSS prints. Véron-Cetty & Véron (1989) classify CGCG nos. 126.110 and 127.052 as Seyfert 1 galaxies. CGCG no. 097.067 is a foreground galaxy ($V_{\odot}$ = 918 km s^{-1}) and individual H II regions are seen. Note that Zwicky & Herzog (1963) misidentify CGCG no. 127.085 as IC 2958.

Table 3.4: Sizes of galaxies and emission regions.

CGCG no.	D (arcmin)	d_e (arcmin)	$r = d_e/D$
(1)	(2)	(3)	(4)
126.103	0.48	0.35	0.73
126.104	0.92	0.37	0.40
126.110	0.48	0.29	0.60
097.027	0.60	0.29	0.48
097.026	0.68	0.29	0.43
097.033	0.76	0.23	0.30
097.044	0.76	0.32	0.42
097.062	0.64	0.29	0.45
097.063	0.40	0.20	0.50
097.068	0.88	0.29	0.33
097.070	0.88	0.55	0.62
097.072	0.92	0.23	0.25
097.073	0.64	0.38	0.59
097.079	0.56	0.35	0.58
097.092	0.60	0.20	0.33
097.091	1.00	0.20	0.20
097.093	0.60	0.20	0.33
097.114	0.40	0.17	0.43
097.120	1.32	0.17	0.13
097.122	1.01	0.40	0.40
097.125	0.36	0.17	0.47
127.046	0.79	0.32	0.41
127.045	1.04	0.29	0.28
097.130	0.32	0.14	0.45
097.138	0.60	0.38	0.63
127.049	0.88	0.20	0.23
127.051	0.72	0.23	0.32
127.052	1.32	0.20	0.15
127.055	0.40	0.20	0.50
127.056	0.88	0.35	0.44
127.058	0.36	0.20	0.56
097.160	0.44	0.17	0.39
127.067	0.32	0.23	0.72
127.068	0.64	0.35	0.55
127.071	0.48	0.17	0.35
127.074	0.64	0.23	0.36
097.168	0.68	0.40	0.59
127.082	0.60	0.40	0.67
127.085	0.84	0.17	0.20
097.180	0.92	0.35	0.38

Table 3.4 – *continued*

Explanation of Columns

Column 1: CGCG number from Zwicky & Herzog (1963).
Column 2: Galaxy major axis in arcmin, measured from plate G.
Column 3: Diameter of the emission region in arcmin. This is an average of the values determined from the emission diameters on plates A and B.
Column 4: The ratio of the diameters of the emission regions to the galaxy diameters.

Table 3.5: CGCG galaxies in the field of the plates.

Galaxy identification			R.A. (1950.0)	Dec. (1950.0)	m_p	Type	Plates	$V_\odot$ (km s^{-1})	Refs.	Notes
CGCG	NGC/IC*	UGC	h m s	° ′ ″						
(1)	(2)	(3)	(4)	(5)	(6)	(7)	(8)	(9)	(10)	(11)
126.073*	...	...	11 28 21.0	+20 42 15	15.7	S–Irr?*	C			s
126.074*	701*	06503	11 28 23.5	+20 44 43	14.7	SBb*	C	6155	3	q
126.075*	...	...	11 28 26.6	+20 30 43	15.4	SBc*	C			
126.077*	...	...	11 28 29.7	+21 33 23	15.5	S?*	C			s
126.081*	...	...	11 29 11.9	+20 40 44	15.2	SBb*	C			
097.002*	...	...	11 29 53.8	+20 26 01	15.4	E–S0*	C			
097.001*	...	...	11 29 56.6	+18 25 27	15.5	Sab	C			
097.003*	...	...	11 29 59.8	+18 25 11	15.5	S0–a	C	12385	22	
126.083*	...	06525	11 30 04.5	+20 42 55	14.9	SBc*	C	6050	3	
097.005*	...	...	11 30 10.5	+20 18 56	15.5	S0 pec*	C	6122	5	q
097.007*	...	...	11 30 29.8	+20 00 57	15.5	S0–SB0*	C			
097.008*	...	...	11 30 34.7	+20 04 11	15.7	Sc–Irr*	C			s
097.009*	...	...	11 30 37.1	+20 05 35	15.6	Sc–Irr*	C			s
126.091*	707*	06543	11 31 07.8	+21 39 23	14.4	Sbc	C	6575	3	
097.011*	...	...	11 31 13.9	+20 18 13	15.6	Sb*	C			
126.097	...	...	11 31 58.8	+20 38 49	15.5	E–S0	C,D	10606	3	
097.013*	...	...	11 31 59.0	+18 57 35	15.6	E–S0	C			
126.100	...	...	11 32 16.9	+20 45 53	15.6	S(B)ab	C,D			s
126.102	...	...	11 32 31.3	+20 57 13	15.7	Sab pec	A,C,D			
097.017*	...	...	11 32 32.8	+18 03 25	15.7	S(B)0	C			
126.103	...	...	11 32 46.7	+20 35 20	15.7	S0–a	A,B,C,D	10300	14	
126.104	...	...	11 32 58.4	+20 46 57	15.6	S pec	A,B,C,D	6679	3	

Table 3.5 – *continued*

Galaxy identification			R.A.	Dec.	m_p	Type	Plates	$V_\odot$	Refs.	Notes
CGCG	NGC/IC*	UGC	(1950.0)					(km s^{-1})		
			h m s	° ′ ″						
(1)	(2)	(3)	(4)	(5)	(6)	(7)	(8)	(9)	(10)	(11)
097.018*	···	06569	11 33 16.1	+17 43 29	15.7	SBa	C			
126.106	3743	···	11 33 20.5	+21 59 59	15.6	E–S0	A,B			
126.108	···	···	11 33 43.5	+20 47 56	15.5	(S0)–a	A,B,D	6555	13	
126.110	3758	···	11 33 52.4	+21 52 25	14.8	Sab	A,B,C,D	8897	4	
097.021	···	···	11 33 53.1	+20 05 19	14.6	E–S0	A,B,C,D	6646	13	
097.022	···	···	11 34 04.0	+17 55 14	15.2	SB0	B,C			
097.023	···	···	11 34 16.3	+20 16 56	15.3	SB0	A,B,C,D	6630	5	
127.002	···	···	11 34 16.6	+21 16 49	15.5	Sa pec	A,B,C,D	9001	13	
097.027	···	···	11 34 17.8	+20 16 24	14.6	S(B)a pec	A,B,C,D	6630	5	q
097.026	···	06583	11 34 17.9	+20 14 51	13.9	S pec	A,B,C,D	6202	5	q
097.025	3764	···	11 34 19.2	+18 09 58	14.9	E + S0	B,C			o,r
097.030	3768	06589	11 34 39.1	+18 07 01	13.7	S0	B,C	3301	7	
097.033	···	···	11 34 59.6	+20 26 23	15.6	S(B)a	A,B,C,D	7736	3	s
127.006	3746	06597	11 35 06.9	+22 17 13	15.3	SB(r)ab	A,B,C	9022	5	
127.007	3748	···	11 35 12.3	+22 18 12	15.5	S0–a	A,B,C	9336	19	
127.009	3750	···	11 35 14.9	+22 15 05	15.2	E–S0	A,B,C,D	8934	19	
127.011	3751	06601	11 35 15.9	+22 04 33	15.3	E–S0	A,B,C,D	9592	22	
127.012	3753	06602	11 35 17.0	+22 15 31	14.6	Irr–S pec	A,B,C	8717	22	p
127.010	···	···	11 35 21.8	+21 03 19	15.7	S0	A,B,C,D	6950	13	
127.013	···	···	11 35 46.7	+20 48 06	15.5	S0–a	A,B,C,D	7721	13	
127.014	···	06607	11 35 48.7	+21 01 01	15.2	S(B)c	A,B,C	3357	8	
127.015	···	06609	11 35 53.3	+20 48 16	14.9	E	A,B,C,D	7641	13	

Table 3.5 – *continued*

Galaxy identification			R.A. (1950.0)	Dec. (1950.0)	m_p	Type	Plates	$V_\odot$ (km s^{-1})	Refs.	Notes
CGCG	NGC/IC*	UGC	h m s	° ′ ″						
(1)	(2)	(3)	(4)	(5)	(6)	(7)	(8)	(9)	(10)	(11)
097.035*	···	···	11 36 00.8	+18 06 01	15.2	S0	B			
097.036	···	···	11 36 15.8	+19 52 43	15.7	Sa	A,B,C,D			
097.037	···	···	11 36 32.5	+19 38 26	15.6	S0	A,B,C,D			
127.016	···	···	11 36 40.2	+20 42 17	15.6	Sa	A,B,C,D			s
097.041	···	···	11 36 49.4	+19 48 44	15.5	Sa	A,B,C,D	6708	13	
127.017	3787	···	11 37 01.8	+20 43 55	14.7	E–S0	A,B,C,D	7055	13	
097.044	···	06625	11 37 11.5	+20 12 36	14.2	S pec	A,B,C,D	10964	7	q
097.043	3790	06624	11 37 12.2	+17 59 23	14.5	SBa	A,B,C,D	3434	20	
097.046	···	···	11 37 19.1	+18 09 35	15.7	E–S0	A,B,C,D			
097.048	···	06631	11 37 36.6	+17 35 22	14.3	Sa	A,C	3543	22	
097.050	···	···	11 37 41.1	+17 44 05	14.6	SAB0	A,C,D	3297	22	
097.051	3801	06635	11 37 41.8	+18 00 21	13.3	SB0 pec	A,B,C,D	3254	7	
097.052	3802	06636	11 37 42.9	+18 02 39	14.7	Sb	A,B,C,D	3321	20	
097.053	···	···	11 37 51.1	+19 41 31	15.7	S pec	A,B,C,D			
127.024	3805	06642	11 38 05.8	+20 37 13	13.8	E–S0	A,B,C,D	6472	7	
097.054	3806=3807	06641	11 38 11.6	+18 04 22	14.6	SABc	A,B,C,D	3495	20	
097.055	···	···	11 38 47.3	+20 14 23	15.3	E–S0	A,B,C,D	6554	9	
097.060	3816	06656	11 39 13.1	+20 22 52	13.6	S0–a	A,B,C,D	5548	7	
127.032	3821	06663	11 39 33.2	+20 35 35	13.8	SBa	A,B,C,D	5600	8	
097.061	···	···	11 39 38.1	+18 40 54	15.5	E–S0	A,B,C,D	7001	13	
097.062	···	···	11 39 38.9	+20 15 12	15.5	Sa pec	A,B,C,D	7800	8	s
097.064	···	···	11 39 39.6	+20 22 31	15.6	S0–a	A,B,C,D	5968	5	

Table 3.5 – *continued*

Galaxy identification			R.A.	Dec.	m_p	Type	Plates	$V_\odot$	Refs.	Notes
CGCG	NGC/IC*	UGC	(1950.0)					(km s^{-1})		
			h m s	° ′ ″						
(1)	(2)	(3)	(4)	(5)	(6)	(7)	(8)	(9)	(10)	(11)
097.063	...	...	11 39 39.8	+20 19 32	15.7	S pec	A,B,C,D	6102	5	r
097.068	...	...	11 39 48.7	+20 23 44	14.7	SBc	A,B,C,D	5960	3	
097.066	...	...	11 39 51.7	+18 02 20	15.7	S	A,B,C,D			
097.067	...	06670	11 39 53.7	+18 36 40	14.3	Sbc	A,B,C,D	918	2	s
097.069	...	...	11 39 56.9	+18 03 45	15.6	E–S0	A,B,C,D			
097.070	3827	06673	11 40 00.6	+19 07 25	13.6	Sbc	A,B,C,D	3226	9,10	
097.072	...	...	11 40 09.4	+20 18 30	15.0	SBbc	A,B,C,D	6334	8	
097.073	...	...	11 40 20.7	+20 14 37	15.6	Scd pec	A,B,C,D	7275	5	s
097.074	...	...	11 40 24.1	+20 21 53	15.4	S0	A,B,C,D	6494	11	
097.076	...	06680	11 40 27.3	+19 55 37	15.5	SAB(rs)b	A,B,C,D	13125	13	
097.079	...	...	11 40 37.5	+20 16 54	15.7	S pec	A,B,C,D	7000	5	o,r,s
097.078	...	06683	11 40 41.4	+20 01 37	15.2	S0–a	A,B,C,D	7608	9,15	s
097.077	...	...	11 40 42.9	+19 39 42	15.5	S(B)0	A,B,C,D	6529	11	
127.036	...	06689	11 40 48.6	+21 55 43	15.5	Sab	A,B,C,D	3524	5	s
097.082	2951*	06688	11 40 49.8	+20 01 40	15.0	S(r)a	A,B,C,D	6100	8	
097.083	...	...	11 40 56.5	+19 54 20	15.2	S(r)b	A,B,C,D	14000	11	
097.085	...	...	11 41 02.2	+19 52 59	15.7	E–S0	A,B,C,D	6562	11	
097.084	3834	...	11 41 02.9	+19 22 05	15.1	E–S0	A,B,C,D	6533	21	
097.086	...	...	11 41 11.9	+20 19 02	15.7	S0–a	A,B,C,D	6397	11	
097.087	...	06697	11 41 12.7	+20 14 52	14.3	Irr–Sd	A,B,C,D	6723	5	s
127.040	...	...	11 41 08.8	+20 32 58	15.3	S0–a	A,B,C,D	6906	13	s
097.089	3837	06701	11 41 21.9	+20 10 20	14.2	E	A,B,C,D	6248	7	

Table 3.5 – *continued*

Galaxy identification			R.A. (1950.0)	Dec. (1950.0)	m_p	Type	Plates	$V_\odot$ (km s^{-1})	Refs.	Notes
CGCG	NGC/IC*	UGC	h m s	° ′ ″						
(1)	(2)	(3)	(4)	(5)	(6)	(7)	(8)	(9)	(10)	(11)
097.092	···	···	11 41 22.5	+20 27 44	15.5	S0–a pec	A,B,C,D	6373	5	o,r
097.090	···	···	11 41 22.8	+20 13 54	15.3	E–S0	A,B,C,D	6038	11	p
097.091	3840	06702	11 41 23.2	+20 21 14	14.7	Sbc	A,B,C,D	7367	3	
097.088	···	···	11 41 24.9	+20 03 24	15.2	S0–a	A,B,C,D	5622	11	a
097.097	3844	06705	11 41 26.1	+20 18 26	14.9	S0–a	A,B,C,D	6840	9,15	
097.093	···	···	11 41 26.3	+20 03 42	15.5	Sab	A,B,C,D	4924	11	b,s
097.095	3842	06704	11 41 27.5	+20 13 39	13.3	E	A,B,C,D	6237	7	
097.096	3841	···	11 41 27.5	+20 14 59	15.0	E	A,B,C,D	6214	11	
097.094	···	···	11 41 28.5	+20 04 44	15.7	S0	A,B,C,D	8002	11	
097.100	3845	···	11 41 30.9	+20 16 27	15.1	Sa?	A,B,C,D	5643	9	
097.099	···	···	11 41 33.0	+20 00 55	15.7	E–S0	A,B,C,D	7731	11	
097.102	···	···	11 41 42.6	+20 30 02	15.1	Sa + S0	A,B,C,D	6300	5	c
097.101	···	···	11 41 44.3	+20 07 20	15.3	SB0	A,B,C,D	6451	11	
097.106	3851	···	11 41 45.7	+20 15 31	15.2	E–S0	A,B,C,D	6467	11	
097.105	···	···	11 41 46.1	+20 06 14	15.4	SB0	A,B,C,D	5439	15	
097.108	···	···	11 41 48.9	+17 35 23	15.5	E–S0	A,B,C,D			s
097.111	···	···	11 41 50.5	+20 23 08	15.5	E–S0	A,B,C,D	7918	18	p
097.110	···	···	11 41 50.6	+20 06 21	15.5	S0	A,B,C,D	4525	11	
097.109	···	···	11 41 53.8	+20 00 48	15.5	E–S0	A,B,C,D	6821	11	
097.112	···	···	11 41 55.9	+20 21 16	14.9	S0	A,B,C,D	6755	9,11	s
097.113	···	···	11 42 12.1	+20 02 10	15.6	S0–a	A,B,C,D	6417	11	
097.114	···	···	11 42 12.1	+20 03 02	15.4	S0–a pec	A,B,C,D	8293	5	s

Table 3.5 – *continued*

Galaxy identification			R.A. (1950.0)	Dec. (1950.0)	m_p	Type	Plates	$V_\odot$ (km s^{-1})	Refs.	Notes
CGCG	NGC/IC*	UGC	h m s	° ′ ″						
(1)	(2)	(3)	(4)	(5)	(6)	(7)	(8)	(9)	(10)	(11)
097.121	···	06719	11 42 12.5	+20 24 12	14.6	S pec	A,B,C,D	6573	8	
097.115	···	···	11 42 12.9	+20 09 15	15.5	S0	A,B,C,D	7792	15	
097.116	···	···	11 42 13.2	+18 08 42	15.5	S–Irr	A,B,C,D			
097.119	···	···	11 42 13.4	+19 57 59	15.7	SB0–a	A,B,C,D	5256	8	
097.120	3860	06718	11 42 13.6	+20 04 21	14.5	SBab	A,B,C,D	5595	8	p
097.117	3857	···	11 42 15.5	+19 48 39	15.1	S0–a	A,B,C,D	6253	11	
097.122	3859	06721	11 42 16.8	+19 43 59	14.9	S pec	A,B,C,D	5466	8	
097.118	···	···	11 42 17.6	+19 53 17	15.7	S0–a	A,B,C,D	6554	11	
097.125	···	···	11 42 19.3	+20 03 15	15.6	Sa pec	A,B,C,D	8288	5	
097.123	···	···	11 42 21.3	+19 46 18	15.7	S0	A,B,C,D	6455	11	
097.124	···	···	11 42 22.4	+20 00 34	15.3	E–S0	A,B,C,D			p
097.128	2955*	···	11 42 29.3	+19 53 56	15.2	E–S0	A,B,C,D	6343	11	
097.129	3861	06724	11 42 29.5	+20 15 07	14.0	SB(r)bc	A,B,C,D	5082	5	p
127.046	···	···	11 42 29.9	+21 41 24	15.6	S pec–Irr	A,B,C,D	7814	3	
127.045	···	06725	11 42 30.5	+20 42 57	14.5	Sb	A,B,C,D	6878	7	
097.127	3862	06723	11 42 30.6	+19 53 03	14.0	E	A,B,C,D	6462	7	d
097.130	3864	···	11 42 40.2	+19 40 13	15.5	Sa	A,B,C,D	6697	8	r
097.131	···	···	11 42 40.4	+20 07 26	15.1	S0	A,B,C,D	7646	11	
097.133	···	···	11 42 43.1	+20 17 52	15.7	S pec + S0	A,B,C,D	5290	5	p,q,r
127.047	···	···	11 42 48.3	+20 36 09	14.6	S0–a	A,B,C,D	7243	9	
127.048	···	···	11 42 52.1	+21 05 03	15.0	E–S0	A,B,C,D	6935	13	
097.134	3867	06731	11 42 55.1	+19 40 44	14.6	S...	A,B,C,D	5000	6	

Table 3.5 – *continued*

Galaxy identification			R.A.	Dec.	m_p	Type	Plates	$V_\odot$	Refs.	Notes
CGCG	NGC/IC*	UGC	(1950.0)					(km s^{-1})		
			h m s	° ′ ″						
(1)	(2)	(3)	(4)	(5)	(6)	(7)	(8)	(9)	(10)	(11)
097.135	3868	···	11 42 55.4	+19 43 21	14.8	SB0	A,B,C,D	6653	9	
097.136	···	···	11 43 08.3	+18 01 34	15.4	E–S0	A,B,C,D			
097.138	···	···	11 43 09.3	+20 18 30	15.5	Scd	A,B,C,D	5313	8	
097.137	3873	06735	11 43 11.7	+20 03 09	14.2	E–S0	A,B,C,D	5438	7	
127.049	···	···	11 43 13.4	+20 54 24	15.5	SBb	A,B,C,D	7061	3	s
097.139	3875	06739	11 43 15.0	+20 02 42	14.8	S0–a	A,B,C,D	6934	11	s
127.050	···	06743	11 43 19.9	+21 18 11	14.8	SAB(r)c	A,B,C,D	6752	8	
097.140	···	···	11 43 24.4	+19 48 26	15.4	SB0	A,B,C,D	5484	11	
127.051	732*	···	11 43 24.4	+20 43 01	15.1	SB0–a	A,B,C,D	7288	5	e,r
097.141	···	···	11 43 28.6	+19 42 55	15.6	S0	A,B,C,D	5163	11	
097.143	···	···	11 43 31.7	+20 04 05	15.3	SBa	A,B,C,D			p
097.142	···	···	11 43 31.9	+19 54 44	15.7	SB0	A,B,C,D	6355	11	
127.052	3884	06746	11 43 36.8	+20 40 08	14.0	Sa	A,B,C,D	6842	8	
097.144	···	···	11 44 02.6	+19 23 17	15.3	E–S0	A,B,C,D	6158	13	
127.055	···	···	11 44 11.2	+21 33 00	15.1	Sa	A,B,C,D	6665	12	
127.054	3883	06754	11 44 11.8	+20 57 10	14.2	S(r)cd	A,B,C,D	7026	8	
097.147	3886	06760	11 44 31.2	+20 06 54	14.3	E–S0	A,B,C,D	5431	9	
097.148	···	···	11 44 38.7	+19 12 15	15.5	S0	A,B,C,D	11209	13	
097.149	···	···	11 44 40.7	+19 27 15	15.6	S0–a	A,B,C,D			
097.151	···	···	11 44 54.1	+18 19 56	15.6	Sb	A,B,C,D			s
097.152	···	···	11 45 05.1	+20 13 04	15.5	Sa	A,B,C,D	6188	3	s
097.153	···	06770	11 45 14.4	+18 49 55	15.6	Irr? + SBb	A,B,C,D			f

Table 3.5 – *continued*

Galaxy identification			R.A.	Dec.	m_p	Type	Plates	$V_\odot$	Refs.	Notes
CGCG	NGC/IC*	UGC	(1950.0)					(km s^{-1})		
			h m s	° ′ ″						
(1)	(2)	(3)	(4)	(5)	(6)	(7)	(8)	(9)	(10)	(11)
097.154	...	...	11 45 28.9	+18 55 42	15.7	S0–a	A,B,C,D			
097.155	...	...	11 45 29.1	+20 17 03	15.0	S0–a	A,B,C,D	7280	9	
127.056	...	...	11 45 52.3	+21 26 05	15.7	Sb	A,B,C,D	6834	3	s
127.058	...	...	11 46 13.4	+22 17 17	15.7	SBb	A,B,D			
127.059	...	...	11 46 14.5	+22 02 03	15.6	Sb pec	A,B,D			q
127.062	...	...	11 46 55.3	+21 19 17	15.5	SBa	A,B,D			s
127.063	3910	06800	11 47 24.2	+21 36 42	14.4	E–S0	A,B,D	7768	16	
127.066	...	...	11 47 45.7	+22 17 28	15.6	Sab	A,B,D			
097.160	...	...	11 47 58.6	+18 08 10	15.6	S0–a	A,B,D			
127.067	...	...	11 48 04.7	+21 11 07	15.5	S pec?	A,B,D			
097.161	3919	06810	11 48 07.6	+20 17 35	14.5	E	A,B,C,D	6244	7	
127.069	...	...	11 48 16.1	+21 40 02	15.7	S0–a	A,B,D			s
127.070	...	06820	11 48 16.5	+20 46 30	15.4	S(B)0–a	A,B,D			
097.162	...	...	11 48 16.9	+20 19 35	15.7	S0	A,B,C,D			
127.068	...	...	11 48 17.7	+21 26 51	15.3	S pec	A,B,D			q
127.071	...	...	11 48 20.5	+21 25 26	15.4	pec	A,B,D	6388	5	q
127.072	...	06821	11 48 26.2	+20 40 38	14.6	SBc	A,B,D	6438	6	
127.073	742*	06822	11 48 27.4	+21 04 39	15.1	SB(r)b	A,B,D	6439	8	
127.074	...	...	11 48 39.8	+21 16 47	15.0	S0	A,B,D	3358	1	
127.075	3925	...	11 48 46.3	+22 10 02	15.3	S0–a	A,B,D			
127.076	3926	06829	11 48 53.4	+22 18 16	14.7	E + S0	A,B,D	8514	17	g
127.079	...	...	11 49 02.8	+22 20 11	15.7	E–S0	A,B,D			

Table 3.5 – *continued*

Galaxy identification			R.A. (1950.0)	Dec. (1950.0)	m_p	Type	Plates	$V_\odot$ (km s^{-1})	Refs.	Notes
CGCG	NGC/IC*	UGC	h m s	° ′ ″						
(1)	(2)	(3)	(4)	(5)	(6)	(7)	(8)	(9)	(10)	(11)
127.078	···	···	11 49 03.3	+21 44 26	15.3	S0–a	A,B,D			
127.080	3929	06832	11 49 07.8	+21 16 50	14.5	E–S0	A,B,D	7113	22	
097.168	···	···	11 49 13.9	+19 38 09	15.7	S	A,B,D			s
097.169	···	06837	11 49 17.8	+18 49 30	15.7	Sc	A,B,D	5975	3	s
127.082	···	···	11 49 25.0	+21 23 13	14.7	Sbc	A,B,D	6654	6	
097.172	···	···	11 49 40.8	+18 55 46	15.7	SBa	A,B,D			
127.083	···	···	11 49 45.2	+21 22 48	15.1	S(B)a	A,B,D	6743	3	
127.085	···	···	11 49 55.9	+20 54 14	15.5	S(B)a	A,B,D			h
097.173	···	···	11 50 07.6	+20 25 32	15.7	E	A,B,D			o
127.088	3937	06851	11 50 07.9	+20 54 34	14.0	E–S0	A,B,D	6618	7	
097.174	···	···	11 50 10.6	+18 53 35	15.7	Sb	A,B,D			
127.089	3940	06852	11 50 11.8	+21 16 02	14.3	E–S0	A,B,D	6500	7	
127.090	3943	···	11 50 22.1	+20 45 25	14.7	SBa	A,B,D	6538	5	
127.092	···	···	11 50 36.5	+20 56 12	15.3	E–S0	A,B,D			
127.095	3947	06863	11 50 45.8	+21 01 49	14.2	SBb	A,B,D	6199	6	
127.096	3946	···	11 50 46.1	+21 17 57	15.5	S0–a	A,B,D			
127.098	3954	06866	11 51 07.2	+21 09 36	14.4	E	A,B,D	6800	16	
097.176	···	···	11 51 16.7	+20 01 46	15.5	S(r)a	A,B,D			
127.100	···	06876	11 51 25.2	+20 51 01	14.9	SBb	A,B,D	6854	6	q
097.178	···	···	11 51 26.3	+20 14 11	15.6	Sab	A,B,D			i,s
097.180	···	···	11 51 39.4	+20 18 19	15.6	Sab	A,B,D	6187	3	j,s
097.182	···	06891	11 52 43.4	+17 46 02	15.4	SBb	A,C	6633	6	k,s

Table 3.5 – *continued*

Galaxy identification			R.A. (1950.0)	Dec. (1950.0)	m_p	Type	Plates	$V_\odot$ (km s^{-1})	Refs.	Notes
CGCG	NGC/IC*	UGC	h m s	° ′ ″						
(1)	(2)	(3)	(4)	(5)	(6)	(7)	(8)	(9)	(10)	(11)
097.183	...	...	11 53 02.9	+18 18 30	15.5	E–S0	A,B,D			l
097.184*	...	...	11 53 10.6	+17 37 35	15.7	S(r)bc	C			m
097.185	...	...	11 53 11.4	+18 10 05	15.5	S	A,B,D	6346	3	n,s

References: (1) Markarian *et al.* 1984. (2) Fisher & Tully 1981. (3) Bothun *et al.* 1985. (4) Petrosyan, Saakyan & Khachikyan 1979. (5) Gavazzi 1987. (6) Chincarini *et al.* 1983. (7) Huchra *et al.* 1983. (8) Giovanelli & Haynes 1985. (9) Dickens & Moss 1976. (10) Kirshner 1977. (11) Tifft 1978. (12) Denisyuk *et al.* 1976. (13) Huchra 1988. (14) Moss & Whittle 1991. (15) Gudehus 1976. (16) Jaffe *et al.* 1986. (17) Jaffe & Gavazzi 1986. (18) Bicay & Giovanelli 1987. (19) Burns *et al.* 1987. (20) Schneider *et al.* 1986. (21) Barbon *et al.* 1989. (22) Paturel *et al.* 1989.

Explanation of columns.

Column 1. CGCG number from Zwicky & Herzog (1963). An asterix indicates that the object is on one plate only.
Column 2. NGC number or IC number (with asterix).
Column 3. UGC number (Nilson 1973).
Columns 4. and 5. 1950.0 coordinates in HHMMSS.S+DDMMSS format.
Column 6. Photographic magnitude taken from CGCG.
Column 7. Morphological type. Galaxies were typed using plate G. Types with an asterix were determined from the PSS blue prints.
Column 8. Plates on which the galaxy is detected.
Column 9. and 10. Heliocentric velocity and references.
Column 11. References to notes on individual objects, described below.

Notes on individual objects.

a. Interacting with CGCG 097.093 (Moss & Whittle 1991).
b. Interacting with CGCG 097.088 (Moss & Whittle 1991).
c. Also CGCG 127.042. Double system (Zwicky & Herzog, 1963).
d. This elliptical is the radio galaxy 3C 264, it dominates the cluster radio emission at 430 and 1400 Mhz (Hanisch 1980). It is also the brightest X-ray galaxy in Abell 1367 (Jones *et al.* 1979).
e. This galaxy is in a double system, the components of which are 33 arcsec apart. The coordinates refer to the SE component, which shows emission. The magnitude of each galaxy is 15.9 (Moss & Whittle 1991).
f. Double system (Nilson 1973).
g. Double system with common envelope (Nilson 1973).
h. Zwicky & Herzog (1963) incorrectly identify this object as IC 2958.
i. Also CGCG 098.001.
j. Also CGCG 098.002.
k. Also CGCG 098.004.
l. Also CGCG 098.005.
m. Also CGCG 098.006.
n. Also CGCG 098.007.
o. Double nebula (Zwicky & Herzog 1963).
p. Double system (Zwicky & Herzog 1963).
q. Appears disturbed on plate G and/or the PSS blue prints.
r. Appears to be interacting on plate G and/or the PSS blue prints.
s. Galaxy is edge-on.

Table 3.6: Hα emission in CGCG galaxies.

CGCG	Galaxy no.		Emission visibility				Emission Concentration				Notes
no.	C	D	A	B	C	D	A	B	C	D	
(1)	(2)	(3)	(4)	(5)	(6)	(7)	(8)	(9)	(10)	(11)	(12)
097.001*	...	...	...	...	No	...	...	...		...	
097.002*	8	...	...	...	M	...	...	...	D	...	
097.003*	...	...	...	...	No	...	...	...		...	
097.005*	9	...	...	...	M	...	...	...	VD	...	
097.007*	...	...	...	...	No	...	...	...		...	
097.008*	...	...	...	...	No	...	...	...		...	
097.009*	...	...	...	...	No	...	...	...		...	
097.011*	...	...	...	...	No	...	...	...		...	
097.013*	...	...	...	...	No	...	...	...		...	
097.017*	...	...	...	...	No	...	...	...		...	
097.018*	34	...	...	...	M	...	...	...	VD	...	
097.021	...	...	No	No	No	No					
097.022	33	...	...	MW	MW	...	...	D	D	...	16
097.023	...	...	No	No	No	No					
097.025	...	...	...	No	No	...	...			...	
097.026	25	8	S	S	S	S					
097.027	...	...	W	W	No	No	VD	VD			
097.030	...	...	...	No	No	...	...			...	
097.033	...	...	W	W	No	No	VD	VD			
097.035*	...	...	...	No	...	...	...		...	...	
097.036	...	...	No	No	No	No					
097.037	...	...	No	No	No	No					1
097.041	...	...	No	W	No	No		VD			
097.043	...	...	No	No	No	No					
097.044	38	17	MW	W	No	W	D	D		D	
097.046	...	...	No	W	No	No		VD			2
097.048	...	...	W	...	No	...	VD	...		...	
097.050	...	...	No	...	No	No		...			
097.051	...	...	No	No	No	No					
097.052	...	...	No	No	No	No					
097.053	...	...	W	No	No	No	VD				
097.054	...	...	No	W	No	No		VD			
097.055	...	...	No	No	No	No					1
097.060	...	...	No	No	No	No					
097.061	...	...	No	No	No	No					
097.062	66	44	M	M	M	S					
097.063	...	45	W	W	No	W					
097.064	...	...	W	No	No	No	VD				
097.066	...	...	No	W	No	No		VD			
097.067	78	55	M	M	S	S	VC	VC	C	VC	3
097.068	65	46	S	S	S	S					
097.069	...	...	No	W	No	No		VD			1
097.070	75	54	M	M	S	S	D	D	D	D	3
097.072	64	43	W	W	W	W	VD	VD	VD	VD	
097.073	...	42	MW	M	No	S	D	D		VD	
097.074	...	...	No	No	No	No					
097.076	...	...	No	No	No	No					
097.077	...	...	No	No	No	No					
097.078	...	...	No	No	No	No					
097.079	63	41	S	S	S	M					1

Table 3.6 – *continued*

CGCG	Galaxy no.		Emission visibility				Emission Concentration				Notes
no.	C	D	A	B	C	D	A	B	C	D	
(1)	(2)	(3)	(4)	(5)	(6)	(7)	(8)	(9)	(10)	(11)	(12)
097.082	···	···	No	No	No	No					
097.083	···	···	No	No	No	No					
097.084	···	···	No	No	No	No					
097.085	···	···	No	No	No	No					
097.086	···	···	No	No	No	No					
097.087	62	40	S	S	S	S					4
097.088	···	···	No	No	No	No					5
097.089	···	···	No	No	No	No					
097.090	···	···	No	No	No	No					
097.091	61	39	M	M	S	S					
097.092	59	37	M	MS	S	S					
097.093	67	47	MW	M	M	S					6
097.094	···	···	No	No	No	No					
097.095	···	···	No	No	No	No					
097.096	···	···	No	No	No	No					
097.097	···	···	No	No	No	No					
097.099	···	···	No	No	No	No					
097.100	···	···	No	No	No	No					
097.101	···	···	W	No	No	No					
097.102	···	···	No	No	No	No					7
097.105	···	···	No	No	No	No					
097.106	···	···	No	No	No	No					1
097.108	81	···	No	No	W	No			VD		
097.109	···	···	No	No	No	No					
097.110	···	···	No	No	No	No					
097.111	···	···	No	No	No	No					
097.112	···	···	No	No	No	No					
097.113	···	···	W	No	No	No					
097.114	70	49	M	M	S	S					1
097.115	···	···	No	No	No	No					
097.116	···	57	No	No	No	W				VD	
097.117	···	···	No	No	No	No					
097.118	···	···	No	No	No	No					
097.119	···	51	No	No	No	No					
097.120	···	48	M	W	No	M	D	VD		D	
097.121	···	···	No	No	No	No					
097.122	71	52	S	M	S	S					
097.123	···	···	No	No	No	No					
097.124	···	···	No	No	No	No					
097.125	69	50	M	M	M	S					
097.127	···	···	No	No	No	No					
097.128	···	···	No	No	No	No					
097.129	···	···	No	No	No	No					
097.130	···	···	W	W	No	No	VD	VD			
097.131	···	···	No	W	No	No		VD			
097.133	···	···	W	No	No	No	VD				1
097.134	···	···	No	No	No	No					
097.135	···	···	No	No	No	No					
097.136	···	59	No	No	No	No					
097.137	···	···	No	No	No	No					

Table 3.6 – *continued*

CGCG	Galaxy no.		Emission visibility				Emission Concentration				Notes
no.	C	D	A	B	C	D	A	B	C	D	
(1)	(2)	(3)	(4)	(5)	(6)	(7)	(8)	(9)	(10)	(11)	(12)
097.138	···	···	W	W	No	No		VD			
097.139	···	···	No	No	No	No					
097.140	···	···	No	No	No	No					
097.141	···	···	No	No	No	No					
097.142	···	···	No	W	No	No		VD			
097.143	···	···	No	No	No	No					
097.144	···	···	W	No	No	No					
097.147	···	···	No	No	No	No					
097.148	···	···	No	No	No	No					
097.149	···	···	No	No	No	No					
097.151	···	···	No	No	No	No					
097.152	···	···	No	No	No	No					
097.153	···	···	No	No	No	No					
097.154	···	69	No	No	No	No					
097.155	···	···	No	W	No	No		VD			
097.160	···	92	W	W	···	W	D	D	···	D	1
097.161	···	···	No	No	No	No					
097.162	···	···	No	W	No	No		VD			
097.168	···	89	W	W	···	No	VD	VD	···		
097.169	···	91	No	No	···	No			···		
097.172	···	···	W	No	···	No			···		
097.173	···	···	No	No	···	No			···		
097.174	···	···	No	No	···	No			···		
097.176	···	···	No	W	···	No		VD	···		
097.178	···	···	No	No	···	No			···		8
097.180	···	88	W	W	···	S	VD	D	···	VD	9
097.182	···	···	No	···	No	···		···		···	10
097.183	···	···	No	No	···	No			···		11
097.184*	···	···	···	···	No	···	···	···		···	
097.185	···	···	No	W	···	No		VD	···		12
126.073*	···	···	···	···	No	···	···	···		···	
126.074*	3	···	···	···	S	···	···	···	D	···	
126.075*	7	···	···	···	S	···	···	···		···	
126.077*	2	···	···	···	No	···	···	···		···	
126.081*	···	···	···	···	No	···	···	···		···	
126.083*	4	···	···	···	M	···	···	···		···	
126.091*	16	···	···	···	S	···	···	···	VD	···	
126.097	···	···	···	···	No	No	···	···			
126.100	23	4	···	···	No	No	···	···			
126.102	···	···	No	···	No	No		···			
126.103	24	6	W	W	M	M	VD	VD	VD	VD	
126.104	22	5	M	M	S	S	D	D	VD	VD	
126.106	···	···	No	No	···	···			···	···	
126.108	···	7	No	No	···	No			···		
126.110	20	13	S	S	S	S	VC	VC	VC	C	13
127.002	···	···	No	No	No	No					
127.006	···	···	No	W	No	···		VD		···	
127.007	···	···	No	No	No	···				···	

Table 3.6 – *continued*

CGCG	Galaxy no.		Emission visibility				Emission Concentration				Notes
no.	C	D	A	B	C	D	A	B	C	D	
(1)	(2)	(3)	(4)	(5)	(6)	(7)	(8)	(9)	(10)	(11)	(12)
127.009	···	···	No	No	No	No					
127.010	···	···	No	No	No	No					
127.011	21	···	No	No	W	No			VD		
127.012	···	···	No	W	No	···		VD		···	
127.013	···	···	No	No	No	No					
127.014	···	···	No	No	No	···				···	
127.015	···	···	No	No	No	No					
127.016	···	···	No	No	No	No					
127.017	···	···	No	No	No	No					
127.024	···	···	No	No	No	No					
127.032	···	···	No	No	No	No					
127.036	···	···	No	No	No	No					
127.040	···	···	No	No	No	No					
127.045	···	···	MW	MW	No	No	D	D			
127.046	49	25	M	M	S	No	D	D	C		
127.047	···	···	No	No	No	No					
127.048	···	···	No	No	No	No					
127.049	83	30	S	MS	S	S	C	VC			
127.050	···	···	No	No	No	No					
127.051	84	33	S	MS	S	S					14
127.052	85	···	MW	MW	W	No		C			
127.054	···	···	No	W	No	No					
127.055	82	64	M	M	S	S					
127.056	···	65	W	W	No	S	VD	VD		VD	
127.058	···	61	M	MW	···	M			···		
127.059	···	···	No	No	···	No			···		
127.062	···	···	No	No	···	No			···		
127.063	···	···	No	No	···	No			···		
127.066	···	···	No	No	···	No			···		
127.067	···	79	W	W	···	No	D	D	···		
127.068	···	75	W	W	···	W	VD	VD	···	VD	
127.069	···	···	No	W	···	No		VD	···		
127.070	···	···	No	No	···	No			···		
127.071	···	77	S	S	···	S	VC	VC	···		
127.072	···	···	No	No	···	No			···		
127.073	···	···	W	No	···	No			···		
127.074	···	78	M	M	···	S			···		
127.075	···	···	No	No	···	No			···		
127.076	···	···	No	No	···	No			···		
127.078	···	···	No	No	···	No			···		
127.079	···	···	No	No	···	No			···		
127.080	···	···	No	No	···	No			···		
127.082	···	80	W	W	···	M	VD	D	···	D	1
127.083	···	···	No	No	···	No			···		
127.085	···	···	W	W	···	No			···		
127.088	···	···	No	No	···	No			···		
127.089	···	···	No	No	···	No			···		
127.090	···	···	No	No	···	No			···		
127.092	···	···	No	No	···	No			···		
127.095	···	81	MW	MW	···	W			···		15

Table 3.6 – *continued*

CGCG	Galaxy no.		Emission visibility				Emission Concentration				Notes
no.	C	D	A	B	C	D	A	B	C	D	
(1)	(2)	(3)	(4)	(5)	(6)	(7)	(8)	(9)	(10)	(11)	(12)
127.096	...	...	No	No	...	No			...		
127.098	...	...	No	No	...	No			...		
127.100	...	...	No	No	...	No			...		

Explanation of columns.

Column 1. CGCG number from Zwicky & Herzog (1963). An asterix indicates that the object appears on one plate only.
Column 2. Galaxy identification number on plate C from the analysis of Moss, Whittle & Irwin (1988).
Column 3. Galaxy identification number on plate D from the analysis of Moss, Whittle & Irwin (1988).
Column 4. A visibility parameter (S strong, MS medium-strong, M medium, MW medium-weak, W weak) describing the visual appearance of the emission for galaxies on plate A. An ellipsis in this, and the next 7 columns indicates that the galaxy is not on the plate.
Column 5. A visibility parameter for galaxies on plate B.
Column 6. A visibility parameter for galaxies on plate C.
Column 7. A visibility parameter for galaxies on plate D.
Column 8. A concentration parameter (VD very diffuse, D diffuse, C concentrated, VC very concentrated) for galaxies on plate A. A blank in this, and the next 3 columns indicates that emission is not detected, or that the spectral appearance is unremarkable.
Column 9. A concentration parameter for galaxies on plate B.
Column 10. A concentration parameter for galaxies on plate C.
Column 11. A concentration parameter for galaxies on plate D.
Column 12. References to notes on individual objects, given below.

Notes on individual objects.

1. Galaxy spectrum is overlapped by a star on plates A,B,C,D.
2. The galaxy is near the edge of plate A.
3. A foreground galaxy. Several knots of emission are detected.
4. Four (or possibly five) distinct knots of emission are visible.
5. This galaxy is interacting with 097.093 (Moss & Whittle 1991).
6. This galaxy is interacting with 097.088 (Moss & Whittle 1991).
7. Also CGCG 127.042. Double system (Zwicky & Herzog, 1963).
8. Also CGCG 098.001.
9. Also CGCG 098.002.
10. Also CGCG 098.004.
11. Also CGCG 098.005.
12. Also CGCG 098.007.
13. The galaxy is near the edge of plate D. A second continuum source showing weak emission lies 7 arcsec west of the galaxy centre.
14. The galaxy showing emission is the SE component of a double galaxy system.
15. There is an emission knot at the centre and two emission knots which are 19 arcsec to the east and 17 arcsec to the west of the nucleus, respectively. These correspond to regions of high surface brightness at either end of the galactic bar visible on the PSS blue print.
16. Near the edge of plate B, spectrum is noisy.

Table 3.7: Emission-line galaxies in Abell 1367.

Galaxy Identification			R.A. (1950.0)	Dec. (1950.0)	m_p	Type	Emission		Plates	$V_\odot$ (km s^{-1})	Notes
CGCG	NGC/IC* UGC	MCG IRAS	h m s	° ′ ″			Vis.	Conc.		Refs.	
(1)	(2)	(3)	(4)	(5)	(6)	(7)	(8)	(9)	(10)	(11)	(12)
126.074*	701*	+04-27-051	11 28 23.5	+20 44 43	14.7	SBb*	S	D	C	6155	s
	06503	11284+2044								3	
126.075*	···	+03-29-061	11 28 26.6	+20 30 43	15.4	SBc*	S		C		
	···	11284+2030									
126.091*	707*	+04-27-064	11 31 07.8	+21 39 23	14.4	Sbc	S	VD	C	6575	
	06543	11311+2139								3	
126.103	···	···	11 32 46.7	+20 35 20	15.7	S0-a	MW	VD	A,B,C,D	10300	v
	···	···								13	
126.104	···	···	11 32 58.4	+20 46 57	15.6	S pec	MS	D	A,B,C,D	6679	
	···	···								3	
126.110	3758	+04-27-073	11 33 52.4	+21 52 25	14.8	Sab	S	VC	A,B,C,D	8897	b, c, w
	···	11338+2152								4	
097.027	···	+03-30-021	11 34 17.8	+20 16 24	14.6	S(B)a pec	W	VD	A,B	6630	d, s
	···	···								5	
097.026	···	+03-30-019	11 34 17.9	+20 14 51	13.9	S pec	S		A,B,C,D	6202	s
	06583	11342+2015								5	
097.033	···	+03-30-026	11 34 59.6	+20 26 23	15.6	S(B)a	W	VD	A,B	7736	d,x
	···	11347+2026								3	

Table 3.7 – *continued*

Galaxy Identification			R.A. (1950.0)	Dec. (1950.0)	m_p	Type	Emission		Plates	$V_\odot$ (km s^{-1})	Notes
CGCG	NGC/IC* UGC	MCG IRAS	h m s	° ′ ″			Vis.	Conc.		Refs.	
(1)	(2)	(3)	(4)	(5)	(6)	(7)	(8)	(9)	(10)	(11)	(12)
097.044	···	+03-30-031	11 37 11.5	+20 12 36	14.2	S pec	W	D	A,B,D	10964	a, s
	06625	11371+2012								7	
097.062	···	···	11 39 38.9	+20 15 12	15.5	Sa pec	M		A,B,C,D	7800	x
	···	···								8	
097.063	···	···	11 39 39.8	+20 19 32	15.7	S pec	W		A,B,D	6102	a, t
	···	···								5	
097.068	···	+03-30-051	11 39 48.7	+20 23 44	14.7	SBc	S		A,B,C,D	5960	
	···	11398+2023								3	
097.067	···	+03-30-053	11 39 53.7	+18 36 40	14.3	Sbc	MS	VC	A,B,C,D	918	e,x
	06670	11398+1836								2	
097.070	3827	+03-30-054	11 40 00.6	+19 07 25	13.6	Sbc	MS	D	A,B,C,D	3226	
	06673	11400+1907								9,10	
097.072	···	+03-30-055	11 40 09.4	+20 18 30	15.0	SBbc	W	VD	A,B,C,D	6334	
	···	···								8	
097.073	···	···	11 40 20.7	+20 14 37	15.6	Scd pec	M	D	A,B,D	7275	a,x
	···	···								5	
097.079	···	···	11 40 37.5	+20 16 54	15.7	S pec	S		A,B,C,D	7000	f, h, t, x
	···	···								5	

Table 3.7 – *continued*

Galaxy Identification			R.A. (1950.0)	Dec. (1950.0)	m_p	Type	Emission		Plates	$V_\odot$ (km s^{-1})	Notes
CGCG	NGC/IC* UGC	MCG IRAS	h m s	° ′ ″			Vis.	Conc.		Refs.	
(1)	(2)	(3)	(4)	(5)	(6)	(7)	(8)	(9)	(10)	(11)	(12)
097.087	···	+03-30-066	11 41 12.7	+20 14 52	14.3	Irr–Sd	S		A,B,C,D	6723	g, x
	06697	11412+2014								5	
097.092	···	···	11 41 22.5	+20 27 44	15.5	S0–a pec	S		A,B,C,D	6373	h, t
	···	···								5	
097.091	3840	+03-30-070	11 41 23.2	+20 21 14	14.7	Sbc	MS		A,B,C,D	7367	
	06702	11413+2021								3	
097.093	···	+03-30-071	11 41 26.3	+20 03 42	15.5	Sab	M		A,B,C,D	4924	i, x
	···	···								11	
097.114	···	+03-30-087	11 42 12.1	+20 03 02	15.4	S0–a pec	MS		A,B,C,D	8293	p, x
	···	···								5	
097.120	3860	+03-30-088	11 42 13.6	+20 04 21	14.5	SBab	M	D	A,B,D	5595	a, j, k
	06718	11422+2003								8	
097.122	3859	+03-30-091	11 42 16.8	+19 43 59	14.9	S pec	S		A,B,C,D	5466	
	06721	11423+1943								8	
097.125	···	+03-30-092	11 42 19.3	+20 03 15	15.6	Sa pec	M		A,B,C,D	8288	k
	···	11422+2003								5	
127.046	···	···	11 42 29.9	+21 41 24	15.6	S pec–Irr	M	D	A,B,C	7814	l
	···	11424+2141								3	

Table 3.7 – *continued*

Galaxy Identification			R.A. (1950.0)	Dec. (1950.0)	m_p	Type	Emission		Plates	$V_\odot$ (km s^{-1}) Refs.	Notes
CGCG	NGC/IC* UGC	MCG IRAS	h m s	° ′ ″			Vis.	Conc.			
(1)	(2)	(3)	(4)	(5)	(6)	(7)	(8)	(9)	(10)	(11)	(12)
127.045	...	+04-28-046	11 42 30.5	+20 42 57	14.5	Sb	MW	D	A,B	6878	d
	06725	...								7	
097.130	3864	+03-30-097	11 42 40.2	+19 40 13	15.5	Sa	W	VD	A,B	6697	d, m, t
	...	...								8	
097.138	...	...	11 43 09.3	+20 18 30	15.5	Scd	W	VD	A,B	5313	d, m
	...	...								8	
127.049	...	...	11 43 13.4	+20 54 24	15.5	SBb	S	C	A,B,C,D	7061	x
	...	...								3	
127.051	732*	+04-28-050	11 43 24.4	+20 43 01	15.1	SB0–a	S		A,B,C,D	7288	n, t
	...	...								5	
127.052	3884	+04-28-051	11 43 36.8	+20 40 08	14.0	Sa	MW		A,B,C	6842	l,w
	06746	...								8	
127.055	...	+04-28-054	11 44 11.2	+21 33 00	15.1	Sa	MS		A,B,C,D	6665	o
	...	...								12	
127.056	...	...	11 45 52.3	+21 26 05	15.7	Sb	M	VD	A,B,D	6834	a, x
	...	...								3	
127.058	...	...	11 46 13.4	+22 17 17	15.7	SBb	M		A,B,D		
	...	...									

Table 3.7 – *continued*

Galaxy Identification			R.A. (1950.0)	Dec. (1950.0)	m_p	Type	Emission		Plates	$V_\odot$ (km s^{-1})	Notes
CGCG	NGC/IC* UGC	MCG IRAS	h m s	° ′ ″			Vis.	Conc.		Refs.	
(1)	(2)	(3)	(4)	(5)	(6)	(7)	(8)	(9)	(10)	(11)	(12)
097.160	...	...	11 47 58.6	+18 08 10	15.6	S0–a	W	D	A,B,D		u
	...	...									
127.067	...	...	11 48 04.7	+21 11 07	15.5	S pec?	W	D	A,B		l
	...	...									
127.068	...	+04-28-063	11 48 17.7	+21 26 51	15.3	S pec	W	VD	A,B,D		s
	...	11483+2126									
127.071	...	+04-28-066	11 48 20.5	+21 25 26	15.4	pec	S	VC	A,B,D	6388	s
	...	...								5	
127.074	...	+04-28-070	11 48 39.8	+21 16 47	15.0	S0	M		A,B,D	3358	
	...	...								1	
097.168	...	...	11 49 13.9	+19 38 09	15.7	S	W	VD	A,B		l, x
	...	...									
127.082	...	+04-28-077	11 49 25.0	+21 23 13	14.7	Sbc	W	D	A,B,D	6654	p
	...	...								6	
127.085	...	...	11 49 55.9	+20 54 14	15.5	S(B)a	W		A,B		l, q
	...	...									
127.095	3947	+04-28-088	11 50 45.8	+21 01 49	14.2	SBb	W		A,B,D	6199	r
	06863	11507+2101								6	

Table 3.7 – *continued*

Galaxy Identification			R.A. (1950.0)	Dec. (1950.0)	m_p	Type	Emission		Plates	$V_\odot$ (km s^{-1})	Notes
CGCG	NGC/IC* UGC	MCG IRAS	h m s	° ′ ″			Vis.	Conc.		Refs.	
(1)	(2)	(3)	(4)	(5)	(6)	(7)	(8)	(9)	(10)	(11)	(12)
097.180	...	...	11 51 39.4	+20 18 19	15.6	Sab	M	VD	A,B,D	6187	x
098.002	...	...								3	

References: (1) Markarian *et al.* 1984. (2) Fisher & Tully 1981. (3) Bothun *et al.* 1985. (4) Petrosyan, Saakyan & Khachikyan 1979. (5) Gavazzi 1987. (6) Chincarini *et al.* 1983. (7) Huchra *et al.* 1983. (8) Giovanelli & Haynes 1985. (9) Dickens & Moss 1976. (10) Kirshner 1977. (11) Tifft 1978. (12) Denisyuk *et al.* 1976. (13) Moss & Whittle 1991.

Explanation of columns.

Column 1. CGCG number from Zwicky & Herzog 1963. An asterix indicates that the object is detected on one plate only. Line 2 is the alternate CGCG number.

Column 2. Line 1, NGC or IC number (with asterix); line 2, UGC number (Nilson 1973).

Column 3. Line 1, MCG number (Vorontsov-Velyaminov & Arkipova 1964); line 2, *IRAS* identification (Fullmer & Lonsdale 1989).

Columns 4. and 5. 1950.0 coordinates in HHMMSS.S+DDMMSS format.

Column 6. Photographic magnitude taken from CGCG.

Column 7. Morphological type. Galaxies were typed using plate G. Types with an asterix were determined from the PSS blue prints.

Column 8. A visibility parameter (S strong, MS medium-strong, M medium, MW medium-weak, W weak) describing the visual appearance of the emission, averaged from the appearance on the plates in column 10.

Column 9. A concentration parameter (VD very diffuse, D diffuse, C concentrated, VC very concentrated) averaged from the concentration on the plates in column 10. No entry indicates that the spectral appearance is unremarkable.

Column 10. Plates on which the galaxy is detected in emission.
Column 11. Heliocentric velocity (line 1) and references (line 2).
Column 12. References to notes on individual objects, described below.

Notes on individual objects.

a. The galaxy appears on plate C but no emission is visible.
b. The galaxy is near the edge of plate D.
c. A second continuum source showing weak emission lies 7 arcsec west of the galaxy centre.
d. The galaxy appears on plates C and D but no emission is visible.
e. A foreground galaxy. Several knots of emission are detected.
f. Double nebula (Zwicky & Herzog 1963). Spectrum is overlapped by a star on plates A,B,C,D.
g. Four (or possibly five) distinct knots of emission are visible.
h. Double nebula (Zwicky & Herzog 1963).
i. This galaxy is interacting with CGCG 097.088 (Moss & Whittle 1991).
j. Double system (Zwicky & Herzog 1963).
k. Galaxies 097.120 and 097.125 have the same *IRAS* identification as noted by Fullmer & Lonsdale (1989).
l. The galaxy appears on plate D but no emission is visible.
m. Diffuse (Zwicky & Herzog 1963).
n. The galaxy showing emission is the SE component of a double galaxy system.
o. Compact (Zwicky & Herzog 1963).
p. Spectrum is overlapped by a star on plates A,B,C,D.
q. Zwicky & Herzog (1963) incorrectly identify this object as IC 2958.
r. The central emission is concentrated. There are two emission knots which are 19 arcsec to the east and 17 arcsec to the west of the nucleus, respectively. These correspond to regions of high surface brightness at either end of the galactic bar visible on the PSS blue print.
s. Appears disturbed on plate G and/or the PSS blue print.
t. Appears to be interacting on plate G and/or the PSS blue print.
u. Spectrum is overlapped by a star on plates A, B and D.
v. Spectrum on plate B is too noisy to analyze.
w. Classified as Seyfert 1 by Véron-Cetty & Véron (1989).
x. Galaxy is edge-on.

CHAPTER IV

Redshift Measurements

4.1 Plate digitization

The objective prism plates were digitized using the Automatic Plate Measuring (APM) facility at Cambridge (Kibblewhite *et al.* 1984). A 10 μm (Gaussian FWHM) spot was stepped at 7.6 μm intervals to give a raster scan of 384 pixels in the dispersion direction and 256 pixels in the perpendicular direction. Between 30 and 120 pixels (depending on the width of the spectra) perpendicular to the dispersion direction were summed to produce a spectrum, and the sky background was subtracted. Four galaxies, CGCG nos. 097.067, 097.070, 097.087 and 097.122, exhibit emission that is "tilted" with respect to the dispersion direction due to the emission being in the plane of the galaxy, and the galaxy plane being inclined with respect to the dispersion direction. These galaxies were not included in the analysis which follows. Appendix A shows the 2-D pixel maps and spectra of each of the 42 galaxies exhibiting emission on the plates.

4.2 Redshifts

4.2.1 THE ONE-PLATE METHOD

The galaxy CGCG no. 126.075 has no previously measured redshift. In this case the "one-plate method" was employed to determine the redshift. The shape of the continuum of the prism spectra is determined by the filter-emulsion combination with the peak of the continuum coinciding with the peak sensitivity of the IIIaF emulsion (6717 Å), as described above in Section 3.2.1. Therefore, the offset of the Hα emission feature relative to the continuum peak may be used to estimate the galaxy redshifts. However, this method can only be used if a continuum is present and only if the centres of the Hα emission and continuum distributions are assumed to be spatially coincident in the dispersion direction, as noted by MWI.

Using the dispersion curve (for the 10° prism, since CGCG no. 126.075 was observed on plate C only), the redshift can be determined for a given offset between the Hα emission and the continuum peak. The 1σ uncertainty of redshifts determined in this way is $\sim$ 550 km s^{-1} (MWI). The velocity for CGCG no. 126.075 is 6600 km s^{-1}.

4.2.2 THE TWO-PLATE METHOD

For the galaxies in the overlap region of plates A and B, accurate redshifts can be obtained by measuring the separation between emission features on two plates taken with opposite dispersion directions. The separation of the Hα emission is directly related to the radial velocities of the galaxies.

The "two-plate method" used here was developed by Stock & Osborn

(1980) to measure radial velocities of stars and was first employed by MWI to determine galaxy redshifts. As explained by MWI, the two-plate technique has several advantages over the one-plate method: firstly, redshifts can be determined for faint emission-line galaxies with weak or no observed continuum, secondly, it is not necessary to assume that the centre of the Hα emission is spatially coincident with the galaxy continuum emission and, finally, the accuracy achievable is much greater ($\Delta v \sim 270$ km s^{-1}, *cf.* Section 4.2.2.b below) than that from the one-plate method ($\Delta v \sim 550$ km s^{-1}).

4.2.2.a plate-to-plate distortions

Before redshifts can be measured, correction for distortions in position introduced by the objective prism must be made. The distortions have a quadratic dependence on position. Once corrected, the separation between lines in the dispersion direction is monotonically related to the galaxy's radial velocity and may be calibrated with known velocities.

Stock & Osborn (1980) used absorption lines in a set of reference stars spread uniformly over the area of interest to determine and correct distortions. However, in this analysis the spectra have a limited bandpass centred near Hα; an area where few, if any, absorption features occur in stellar spectra. The general spectral shape is determined by the filter-emulsion combination with the peak of the continuum coinciding with the peak sensitivity of the IIIaF emulsion, at $\sim$ 6717 Å, (see Figure 3.2). To first order, the shape is independent of the colour of an object. Therefore, the continuum shape of reference stars distributed over the plates may be used to determine and correct the positional distortions. Accordingly, 58 reference stars, with magnitudes $\sim$ 12.5, in the field of the plates were selected from the Hubble Space Telescope

Guide Star Catalog (*cf.* Appendix C). The plates were scanned at the APM facility following the method of MWI, described below.

An input list of equatorial coordinates, for the objects of interest, was converted to X,Y positions on the APM plate table using an approximate conversion. The prism plate was aligned on the APM machine and X,Y positions were measured for typically 15 SAO stars. A least-squares solution was obtained for the linear relation between X,Y and standard coordinates (ξ, η; *i.e.*, equatorial coordinates projected on to the tangent plane, where the tangential point is the plate centre) for these stars. A standard scanning mode was used in which the input list of positions was employed to automatically drive the APM machine to each object position, where a pixel map (described above, Section 4.1; refer to Appendix A) of the object was produced and stored on magnetic tape for later processing.

The position of each reference star spectrum was determined by cross-correlation with an idealized, two-dimensional continuum shape using the FIGARO routine SCROSS. Two such positions were determined for each star, one for each plate (S_A and S_B). These positions were used to compute the plate-to-plate separations ($S_A - S_B$) for each reference star as a function of standard coordinates. Figure 4.2(a) depicts, schematically, these shifts. The separations include the quadratic distortions introduced by the objective prism, small linear systematic errors from the conversion of X,Y positions to standard coordinates and random errors from position measuring accuracy. These separations are plotted in Figure 4.1(a). The systematic errors are well modelled by a full quadratic fit of the form,

$$S = A\xi + B\eta + C + D\xi^2 + E\xi\eta + F\eta^2.$$

Table 4.1: Constants for the plate distortion model.

Constant	Value
A	$-1.59705058 \times 10^{-1}$
B	$-6.96754903 \times 10^{-2}$
C	$+2.34986432 \times 10^{-2}$
D	$-1.52076597 \times 10^{+1}$
E	$-1.52682483 \times 10^{-1}$
F	$-1.45001202 \times 10^{+1}$

Given the values of $S = S_A - S_B$ and (ξ, η) for each reference star, values for the six constants were determined using a standard least-squares method. Values for the general constants obtained in this manner are given in Table 4.1.

The modelled distortions for each position were then subtracted from the star's separations $(S_A - S_B)$ to check the procedure. The remaining residuals are shown in Figure 4.1(b) and are of the order a few pixels. They are the random errors involved in measuring the shifts.

4.2.2.b analysis of galaxy spectra

Galaxy spectra from each plate were then analyzed to determine the shift in position of the Hα emission between the plates (ΔS) and, hence, the redshift. The FIGARO routine ABLINE was used to fit a seventh order polynomial to the continuum; line limits were determined interactively and ABLINE provided the line centroid, allowing ΔS to be calculated. The procedure used

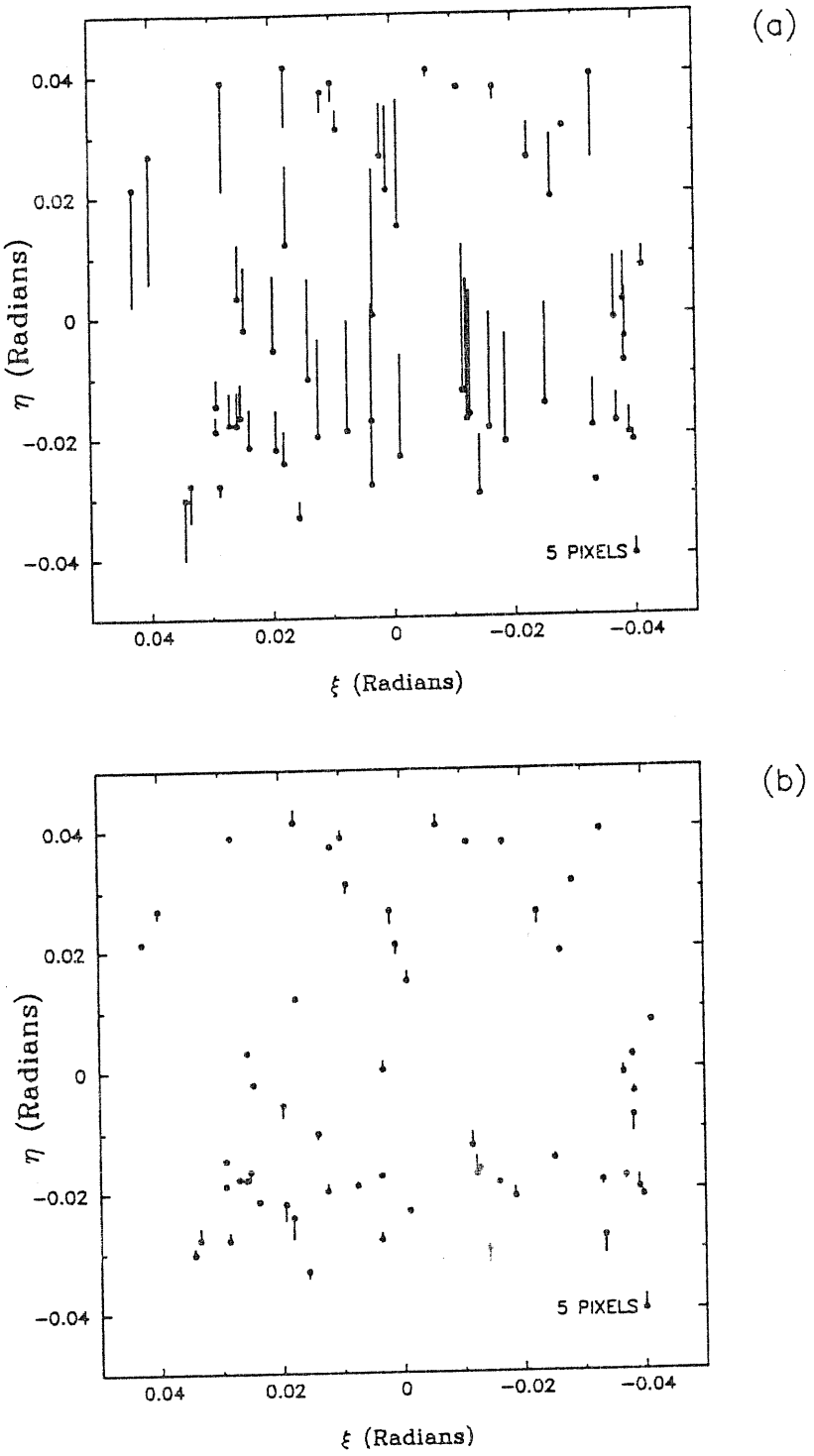

Figure 4.1: (a.) Map of the overlap region of plates A and B in standard coordinates, *i.e.*, equatorial coordinates projected onto the tangent plane, where the tangential point is the plate centre. Shown are the plate-to-plate separations in the positions of the objective prism plate spectra of reference stars. (b.) The same plot with the modelled quadratic distortions subtracted. A shift of five pixels is shown in the bottom right-hand corner of each plot.

is illustrated schematically in Figure 4.2(b). Quadratic positional distortions, modelled as discussed in Section 4.2.2.a, were then subtracted.

As a check to determine whether the continua affected the determination of the line centre, continua, fitted previously with ABLINE, were subtracted and the line centres remeasured. There were no apparent changes in the position of the line centres.

Because systematic errors have been removed we can be confident that the remaining errors in radial velocities are limited only by the information content (*i.e.*, signal-to-noise) on the plates. The position of line centres on plates A and B and the correction factor, S, for each object are given in Table 4.2. In this table, $\Delta S'$ is the corrected separation between the emission on both plates ($\Delta S'$ = line centre (A) – line centre (B) – S) and is a simple, monotonic function of radial velocity.

Of the 42 emission-line galaxies analyzed, 35 have previously measured redshifts which can be used to calibrate the two-plate method. Two galaxies, CGCG nos. 126.074 and 126.091, appear on one plate only and CGCG no. 126.103 has a usable spectrum on plate A only, and, hence, can not be used for this analysis, leaving us with 32 galaxies.

In Figure 4.3 the previously determined radial velocities are shown plotted against the shift in Hα, $\Delta S'$. The curve, a quadratic, is the best, least-squares fit. All 32 galaxies with previously measured redshifts in emission on plates A and B are plotted. The scatter about the curve corresponds to a (1σ) velocity uncertainty of $\sim$ 270 km s^{-1} for the sample as a whole, with no dependence on redshift, galaxy magnitude, the measure of emission concentration, flux or equivalent width. As stated by MWI, the accuracy obtainable for the galaxy redshifts is sufficient not only for estimating cluster membership

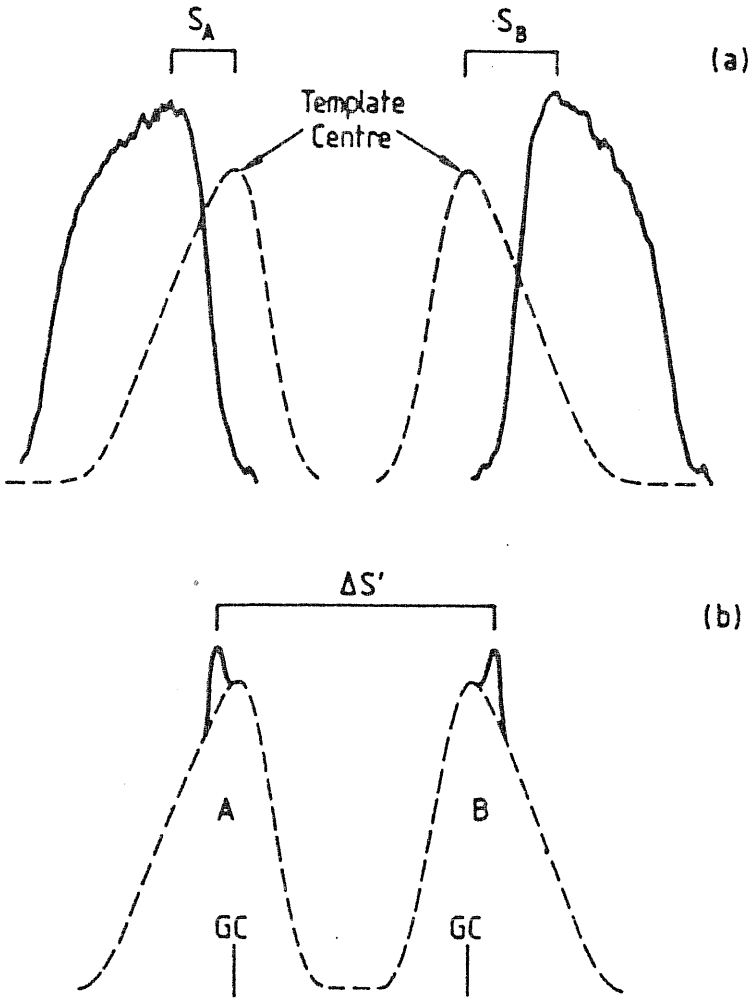

Figure 4.2: (a.) Schematic representation of the spectral shift due to distortions induced by the objective prism (exaggerated for clarity). Shown is a stellar spectrum on plate A (left) and plate B (right) and a template spectrum for each (dashed line). The position of the centre of the template is the same on both plates relative to the centroid of the target object. Shifts in the stellar spectrum away from the template centre on plates A and B (S_A and S_B, respectively) represent the distortion, $S = S_A - S_B$. S = 0 for distortion free plates. (b.) A highly exaggerated schematic representation of the shift, $\Delta S'$, between the line centre of the Hα emission of a galaxy on plate A and plate B. The centre of the galaxy spectrum (GC) is at the same position on plates A and B, after correcting for plate distortions.

Table 4.2: Plate-to-plate displacements for emission-line galaxies.

CGCG no.	Line centre Plate A (mm)	Line centre Plate B (mm)	Correction Factor (S) (mm)	$\Delta S'$ (mm)	Notes
(1)	(2)	(3)	(4)	(5)	(6)
126.104	1.4153	1.5397	0.0164	−0.1408	
126.110	1.3919	1.5527	−0.1378	−0.0230	
097.027	1.4036	1.4434	0.1427	−0.1825	
097.026	1.4353	1.4588	0.1441	−0.1676	
097.033	1.4086	1.3558	0.1701	−0.1173	
097.044	1.5934	1.2168	0.2790	0.0976	
097.062	1.5696	1.3285	0.3389	−0.0978	
097.063	1.5227	1.3534	0.3350	−0.1657	
097.068	1.4920	1.3330	0.3326	−0.1736	
097.072	1.4867	1.3177	0.3428	−0.1738	
097.073	1.6481	1.4241	0.3484	−0.1244	
097.079	1.5468	1.3184	0.3490	−0.1206	a
097.092	1.5168	1.3451	0.3406	−0.1698	
097.091	1.5756	1.3012	0.3485	−0.0741	
097.093	1.5122	1.3807	0.3620	−0.2305	
097.114	1.6189	1.3036	0.3614	−0.0461	b
097.120	1.5310	1.3590	0.3607	−0.1887	
097.125	1.6313	1.3282	0.3607	−0.0576	
127.046	1.5096	1.4761	0.1383	−0.1048	
127.045	1.5453	1.3872	0.3134	−0.1553	
097.130	1.6186	1.3981	0.3584	−0.1379	
097.138	1.5058	1.3788	0.3430	−0.2160	
127.049	1.5480	1.3883	0.2824	−0.1227	
127.051	1.5752	1.3685	0.3042	−0.0975	c
127.052	1.4879	1.3386	0.3066	−0.1573	
127.055	1.4794	1.4856	0.1491	−0.1553	
127.056	1.4695	1.4549	0.1303	−0.1157	
127.058	1.3849	1.4403	−0.1109	0.0555	c
097.160	1.3925	1.5492	0.0092	−0.1659	d
127.067	1.4271	1.4931	0.0880	−0.1540	
127.068	1.3983	1.5109	0.0259	−0.1385	
127.071	1.4159	1.5394	0.0285	−0.1520	
127.074	1.2813	1.6033	0.0402	−0.3622	
097.168	1.4909	1.4400	0.1387	−0.0878	
127.082	1.3837	1.5689	−0.0239	−0.1613	
127.085	1.4350	1.5282	0.0271	−0.1203	
127.095	1.3732	1.5893	−0.0476	−0.1685	
097.180	1.3460	1.5483	−0.0361	−0.1662	

Table 4.2 – *continued*

Explanation of columns.

Column 1. CGCG number from Zwicky & Herzog (1963).
Column 2. Position of the line centre of Hα emission on plate A, in mm.
Column 3. Position of the line centre of Hα emission on plate B, in mm.
Column 4. The modelled correction factor for plate distortions (S).
Column 5. The shift in Hα emission between plates A and B. $\Delta S'$ is the result of subtracting columns 2,3 and 4, in mm.
Column 6. Notes on individual objects, given below.

Notes on individual objects.

a. Overlapped by a stellar spectrum, see Appendix A.
b. Spectrum on plate A is partially overlapped by debris. A nearby galaxy distorts the continuum.
c. Noise spike due to dust (?) on plate A spectrum.
d. Nearby star distorts the continuum.

but also for determining the velocity dispersions of the emission-line galaxies within a cluster.

New redshift estimates for the six galaxies on plates A and B without previously measured radial velocities are shown in Table 4.3. They have a 1σ uncertainty of ~ 270 km s^{-1} and are determined from the curve in Figure 4.3.

4.2.3 DISPERSION CURVE FOR THE 2° + 4° PRISM COMBINATION

From the redshift analysis and Figure 4.3 the dispersion curve for the 2° + 4° prism can be obtained. In Figure 4.4 we plot one-half of the shift of emission between plates A and B ($1/2\Delta S'$) versus the wavelength of the Hα emission. In order to determine the dispersion we fit the data with a curve, differentiation of which gives the dispersion value. In this analysis, a straight line proved the best fit to the data, the reciprocal of the slope of which is the dispersion. For the 2° + 4° prism combination we find that the dispersion, $d\lambda/dX$, is 780 Å mm^{-1}, approximately twice the dispersion of the 10° prism.

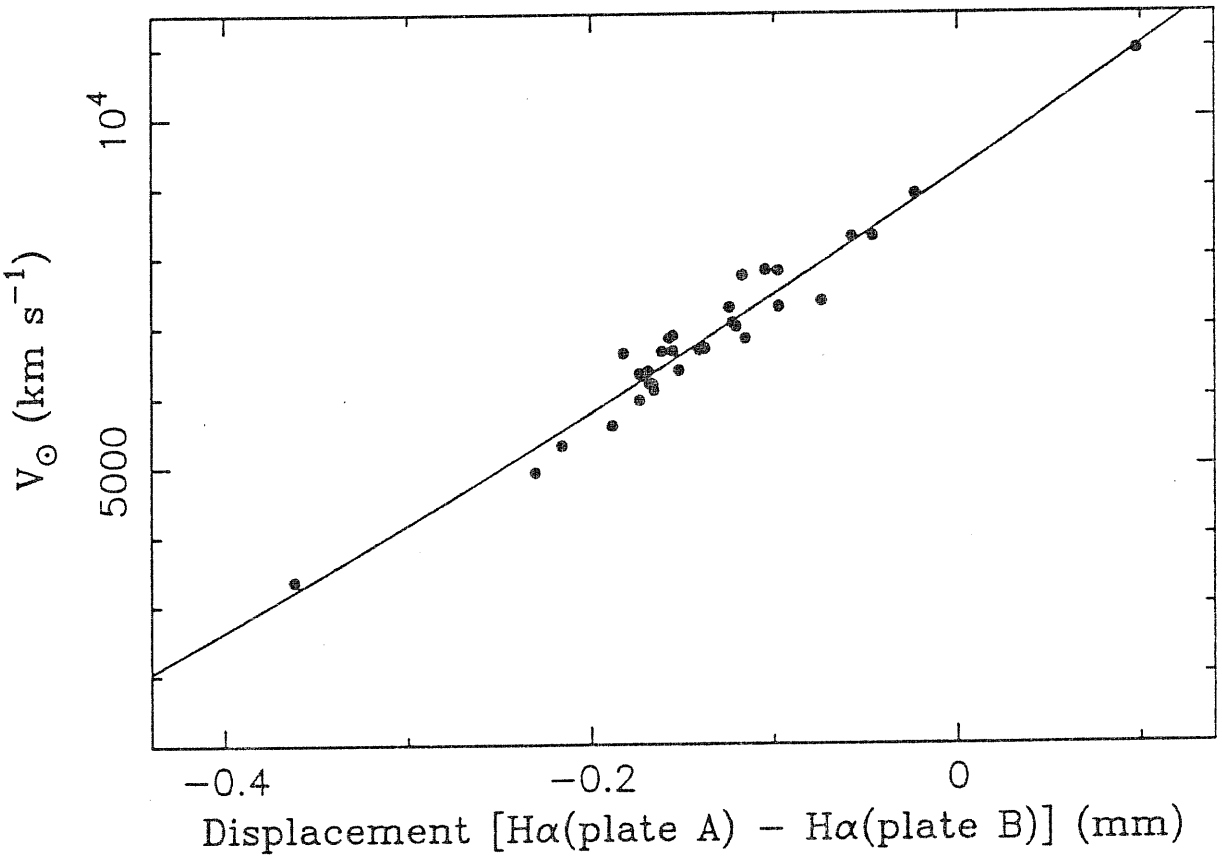

Figure 4.3: A plot of the plate-to-plate separations of Hα emission versus previously determined radial velocities for 32 galaxies in emission on plates A and B. The curve is the best, least squares fit to the data; a mild quadratic function. The scatter of points about the curve corresponds to a (1σ) velocity uncertainty of $\sim$ 270 km s^{-1} for the sample.

Table 4.3: Redshifts of emission-line galaxies (objective prism measurements).

CGCG no.	$V_\odot$ (km s^{-1})
126.075*	(6600)
127.058	10200
097.160	6300
127.067	6500
127.068	6800
097.168	7700
127.085	7100

The velocity in parentheses was obtained from a single plate and has a 1σ error of $\sim$ 550 km s^{-1}. All other velocity errors are $\sim$ 270 km s^{-1}.

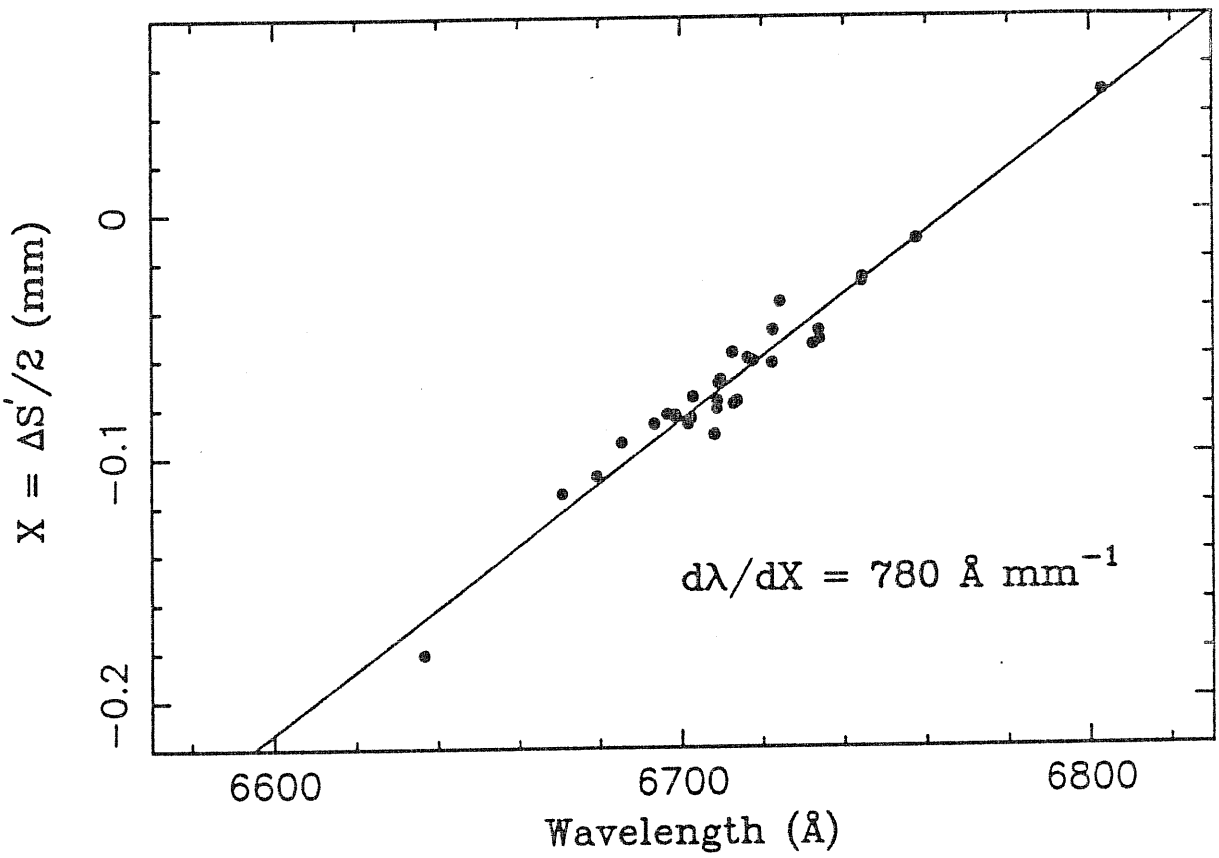

Figure 4.4: The dispersion curve for the 2° + 4° objective plate prism. Plotted are the wavelengths of the Hα emission versus X (one-half of $\Delta S'$, the shift of the Hα emission line between plates A and B; refer to Table 4.2). The best fit is a straight line, the reciprocal of the slope of which yields the dispersion, $d\lambda/dX = 780$ Å mm^{-1}.

CHAPTER V

Hα Fluxes and Equivalent Widths for Emission-line Galaxies

5.1 Flux measurements

In order to obtain flux measurements the emission-line galaxy spectra were smoothed, using a gaussian function with $\sigma = 1$ pixel, over eight pixels. For plates A and B, one pixel is equivalent to 7.6 μm or 5.9 Å. The continua were fit by a seventh order polynomial with the FIGARO routine, ABLINE. After the line limits were chosen interactively the continua were subtracted and the remaining Hα emission line was integrated to provide the total emitted flux.

Because the detector sensitivity varies over the wavelength region of interest, raw fluxes must be corrected to give the true values of the relative flux. The measured flux was divided by the normalized detector response (*cf.* Figure 3.2) at the observed wavelength of the Hα emission, to give a corrected flux value. For the main velocity region of interest, 5000 – 8000 km s^{-1}, the corrections are quite small; approximately 10 per cent or less. The correction is 20 per cent for velocities less than 2000 km s^{-1} and 40 per cent for velocities greater than 10 000 km s^{-1}. These corrected, relative fluxes were then converted to absolute flux units using measurements in common with Kennicutt *et al.* (1984) for 11 galaxies and Gavazzi (1990) for three galaxies.

Table 5.1 presents a comparison between values of the combined Hα + [NII] flux obtained with the objective prism methods and the values of Kennicutt *et al.* (1984) and Gavazzi (1990) obtained photoelectrically. Of the 14 values in common between the present study and those of Kennicutt *et al.* (1984) and Gavazzi (1990), four are uncertain values in the present study and have been marked with a colon. In order to compare the relative errors of individual flux measurements between the three samples (MWI, Kennicutt *et al.* (1984) + Gavazzi (1990) and the present study), the following error analysis was used.

A quantity (F_o) is measured independently three times with three methods, F_A, F_B and F_C, for an individual galaxy. Each measurement has unknown errors, ϵ, ϕ and ψ. Measurements are made on N_A, N_B and N_C galaxies in each sample:

$$
\begin{array}{lll}
F_{A,1} = F_{o,1} + \epsilon_1; & F_{B,1} = F_{o,1} + \phi_1; & F_{C,1} = F_{o,1} + \psi_1 \\
F_{A,2} = F_{o,2} + \epsilon_2; & F_{B,2} = F_{o,2} + \phi_2; & F_{C,2} = F_{o,2} + \psi_2 \\
F_{A,3} = F_{o,3} + \epsilon_3; & F_{B,3} = F_{o,3} + \phi_3; & F_{C,3} = F_{o,3} + \psi_3 \\
\cdot & \cdot & \cdot \\
\cdot & \cdot & \cdot \\
\cdot & \cdot & \cdot \\
F_{A,N_A} = F_{o,N_A} + \epsilon_{N_A}; & F_{B,N_B} = F_{o,N_B} + \phi_{N_B}; & F_{C,N_C} = F_{o,N_C} + \psi_{N_C}
\end{array}
$$

Comparing measurements A and B gives:

$$\sum_{i=1}^{N_{AB}} (F_{A,i} - F_{B,i})^2 = \sum_{i=1}^{N_{AB}} \{(F_{o,i} + \epsilon_i) - (F_{o,i} + \phi_i)\}^2$$

$$= \sum_{i=1}^{N_{AB}} (\epsilon_i^2 - 2\epsilon_i\phi_i + \phi_i^2).$$

Since ϵ_i and ϕ_i have equal probability of being positive or negative (*i.e.*, uncorrelated if they are really random), the cross terms cancel and,

$$\frac{1}{N_{AB}} \sum_{i=1}^{N_{AB}} (F_{A,i} - F_{B,i})^2 \approx \frac{1}{N_{AB}} (\sum_{i=1}^{N_{AB}} \epsilon_i^2 + \sum_{i=1}^{N_{AB}} \phi_i^2) = \langle \epsilon_i^2 \rangle + \langle \phi_i^2 \rangle.$$

Similarly, for comparison between measurements A and C:

$$\frac{1}{N_{AC}} \sum_{i=1}^{N_{AC}} (F_{A,i} - F_{C,i})^2 \approx \frac{1}{N_{AC}} (\sum_{i=1}^{N_{AC}} \epsilon_i^2 + \sum_{i=1}^{N_{AC}} \psi_i^2) = \langle \epsilon_i^2 \rangle + \langle \psi_i^2 \rangle,$$

and measurements B and C:

$$\frac{1}{N_{BC}} \sum_{i=1}^{N_{BC}} (F_{B,i} - F_{C,i})^2 \approx \frac{1}{N_{BC}} (\sum_{i=1}^{N_{BC}} \phi_i^2 + \sum_{i=1}^{N_{BC}} \psi_i^2) = \langle \phi_i^2 \rangle + \langle \psi_i^2 \rangle,$$

where N_{AB}, N_{AC} and N_{BC} are the number of galaxies in common between samples AB, AC and BC, respectively. The numbers do not have to be the same. The L.H.S. of the equations are measured quantities and hence, we have

Table 5.1: Comparison of flux and equivalent width measurements for emission-line galaxies in Abell 1367.

CGCG	Log f(Hα) (erg cm^{-2} s^{-1})				W_λ(Hα) (Å)			
no.	P	MWI	KBS	G	P	MWI	KBS	G
(1)	(2)	(3)	(4)	(5)	(6)	(7)	(8)	(9)
126.104	−12.67:	−12.72			93:	—		
126.110	−11.92	−12.00			66 ± 10	74 ± 5		
097.026	−12.08	−12.19	−12.26		76 ± 10	92 ± 4	88 ± 6	
097.044	−12.58	−12.57:			5 ± 10	—		
097.062	−13.22		−13.10		46 ± 10		45 ± 10	
097.068	−12.44	−12.83	−12.51		35 ± 10	(33)	44 ± 5	
097.072	−13.14:	−13.05:	−13.5:		7 ± 10	—	5 ± 3	
097.073	−13.04	−12.84	−12.84		80 ± 10	—	80 ± 12	
097.079	−12.27:	−12.54	−12.64		151 ± 10	—	145 ± 15	
097.092	−12.87	−13.06			29 ± 10	—		
097.091	−12.66	−12.92	−12.74		23 ± 10	20 ± 3	23 ± 3	
097.093	−12.73	−12.95			50 ± 10	59:		
097.114	−12.62	−12.82			59:	79:		
097.120	−13.17		−13.2:		3 ± 10		4 ± 2	
097.125	−12.75	−13.13			26 ± 10	29 ± 4		
127.046	−12.84	−13.05			50 ± 10	61 ± 11		
097.138	−13.28:		−13.09		34 ± 10		31 ± 4	
127.049	−12.58	−12.95			48 ± 10	59 ± 4		
127.051	−12.77:	−12.88		−12.83	33 ± 10	38 ± 3		26 ± 5
127.055	−12.60	−12.85			41 ± 10	43 ± 6		
127.068	−12.84			−13.14	20 ± 10			26 ± 7
127.071	−12.44	−12.72		−12.83	88 ± 10	72 ± 12		52 ± 5
127.074	−12.57	−12.75			37 ± 10	45 ± 4		
127.082	−13.09		−12.86		16 ± 10		22 ± 3	
127.095	−12.90		−12.63		10 ± 10		15 ± 3	
097.180	−13.27:	−13.03:			54:	—		
097.129			−12.58				10 ± 2	
127.054			−13.00				5 ± 3	
127.050			−12.80				16 ± 5	
127.100			−13.14				10 ± 3	
097.149				−13.38				13 ± 5

Explanation of columns.

Column 1: CGCG number from Zwicky & Herzog (1963).
Columns 2 & 3: Flux measurements from photographic surveys: this work (P) and MWI, respectively.
Columns 4 & 5: Flux measurements from wide aperture photoelectric surveys: Kennicutt *et al.* (1984) (KBS) and Gavazzi (1990) (G), respectively.
Columns 6 & 7: Integrated Hα equivalent widths from this work and MWI, respectively.
Columns 8 & 9: Integrated Hα equivalent widths from Kennicutt *et al.* (1984) and Gavazzi (1990), respectively.

three equations with which we can determine $\langle\epsilon^2\rangle, \langle\phi^2\rangle$ and $\langle\psi^2\rangle$, the variances of the errors for the three methods ($\langle\epsilon^2\rangle = \frac{1}{N}\sum_i \epsilon_i^2$).

Using an analysis of this sort for the log of the flux measurements in each of the studies, the present study, that of Kennicutt *et al.* (1984) and MWI, we obtain standard deviations of $\sigma_P = 0.18$, $\sigma_K = 0.17$ and $\sigma_M = 0.16$, respectively (in units of erg cm^{-2} s^{-1}). There are 14 galaxies in common between the present study and that of Kennicutt *et al.* (+ Gavazzi 1990), eight galaxies in common between Kennicutt *et al.* + Gavazzi and MWI and 20 galaxies in common between the present study and MWI. Because the errors are similar between the three analyses we can say that fluxes measured with the objective prism plate method have a similar accuracy to those measured with the photoelectric technique. Figure 5.1 shows a comparison of fluxes obtained with the photographic methods and photoelectric methods.

5.2 Equivalent width measurements

Equivalent widths for the emission-line galaxies were measured. The continua were fit with a cubic spline anchored at six positions in the spectra. After subtracting the continua, line boundaries were determined and the continua and lines integrated. Equivalent widths calculated in this way are in units of pixels and are then converted to angstroms (5.9 Å pixel^{-1}).

Comparisons with equivalent widths obtained via the photographic method of MWI and the photoelectric method of Kennicutt *et al.* (1984) and Gavazzi (1990) are given in Table 5.1. An error analysis, as described above in Section 5.1.1, was performed on the three independent samples of equivalent width measurements, the results of which are $\sigma_P = 6$ Å, $\sigma_K = 10$ Å and $\sigma_M =$

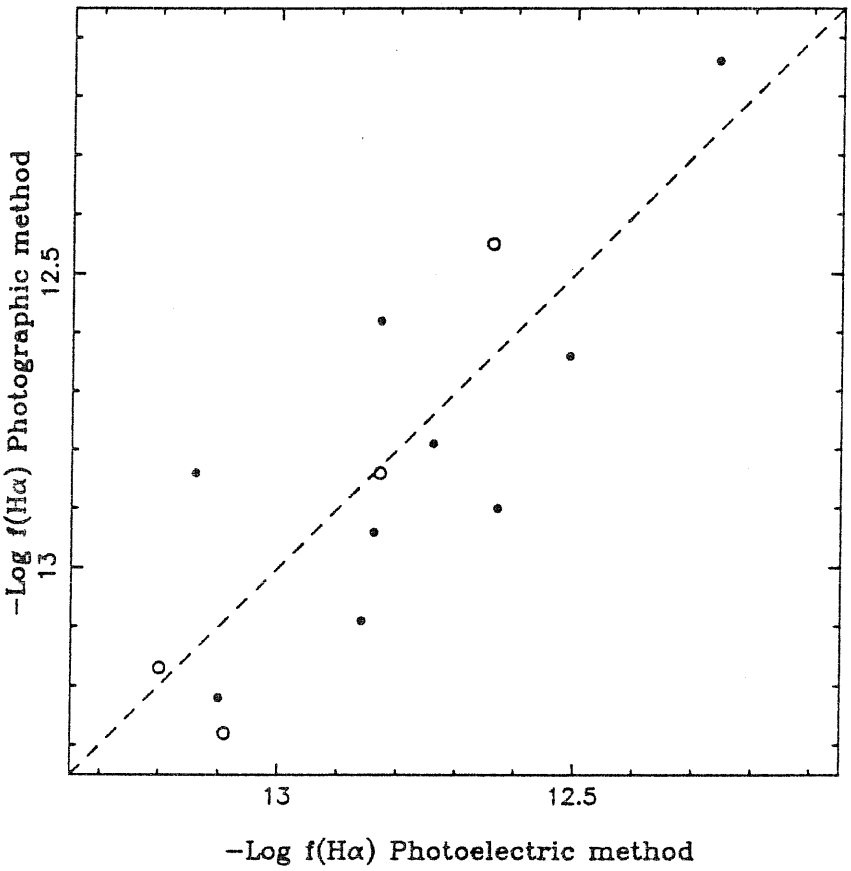

Figure 5.1: A comparison between values of global Hα + [NII] flux measured from objective prism spectra (mean values from this paper and MWI) and wide-aperture photoelectric photometry (Kennicutt *et al.* 1984 and Gavazzi 1990). The dashed line shows y = x and the open circles indicate uncertain values.

9 Å. Figure 5.2 shows a comparison between equivalent widths measured with the photographic methods and the photoelectric methods.

While the equivalent widths in this study agree favourably with those measured in other studies, it should be noted that equivalent widths are extremely difficult to measure with a prism of low dispersion. Continuum fitting was found to present a possible, large source of error, as seemingly small changes in the fit produced large differences in the equivalent widths. However, with this *caveat* in mind and with the knowledge of the general shape of continua (which vary little from galaxy to galaxy) it is possible to produce accurate fits and, hence, equivalent widths.

5.3 Flux and equivalent width values

Table 5.2 gives the values of flux and equivalent width for all emission-line galaxies in Abell 1367. The table gives the CGCG galaxy number in column 1. The log fluxes, in column 2, are weighted mean values. Column 3 gives the number of flux measurements used to compute the mean flux in column 2. The weighted mean values of equivalent width are given in column 4 and the number of measurements used to compute the mean are given in column 5. References to notes on individual objects are given in column 6.

Mean errors on equivalent widths are computed as follows. Well-determined errors on individual values in the studies of Kennicutt *et al.* (1984) and MWI are taken as published. Equivalent width uncertainties for the present study are not known, but are set to 10 Å, based on the error analysis performed above. The uncertainties on the weighted mean values are simply the inverse of the square root of the summed weights.

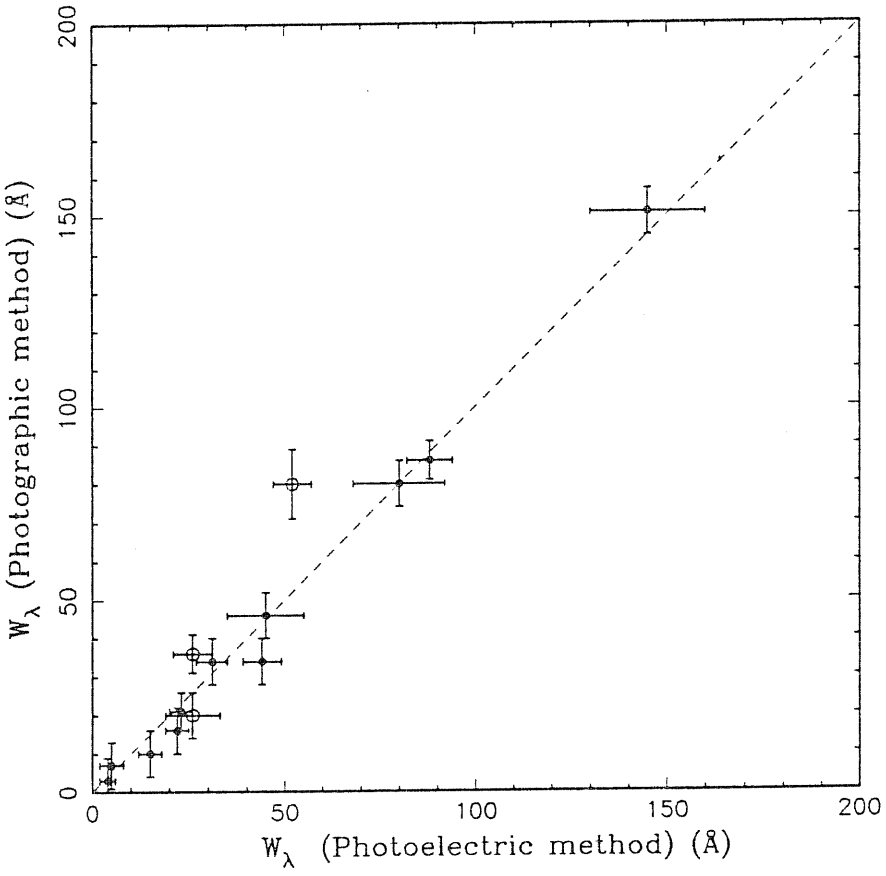

Figure 5.2: A comparison between values of global Hα + [NII] equivalent width measured from objective prism spectra (mean values of this study and MWI) and wide-aperture photoelectric photometry (Kennicutt *et al.* 1984 and Gavazzi 1990). The dashed line shows y = x. Filled circles are the data from Kennicutt *et al.* and open circles represent data from Gavazzi.

Table 5.2: Hα flux and equivalent width measurements for emission-line galaxies in Abell 1367.

CGCG no.	<Log f> (erg cm^{-2} s^{-1})	N	<W_λ> (Å)	N	Notes
(1)	(2)	(3)	(4)	(5)	(6)
126.074*	—	—	33 ± 10	1	
126.075*	—	—	50 ± 10	1	
126.091*	—	—	40 ± 10	1	
126.103	—	—	10 ± 10	1	
126.104	−12.70:	2	93:	1	e
126.110	−11.96	2	72 ± 4	2	
097.027	−13.41:	1	14 ± 10	1	a
097.026	−12.18	3	89 ± 3	3	
097.033	−12.91:	1	21:	1	d
097.044	−12.58:	2	5 ± 10	1	
097.062	−13.16	2	46 ± 7	2	
097.063	−13.67	1	15 ± 10	1	
097.068	−12.59	3	42 ± 5	2	
097.072	−13.23:	3	5 ± 3	2	b
097.073	−12.91	3	80 ± 8	2	
097.079	−12.55:	3	149 ± 8	2	c
097.092	−12.97	2	29 ± 10	1	
097.091	−12.77	3	22 ± 2	3	
097.093	−12.84	2	53 ± 10	2	
097.114	−12.72	2	69:	2	c
097.120	−13.18	2	4 ± 2	2	
097.125	−12.94	2	29 ± 4	2	
127.046	−12.95	2	55 ± 7	2	
127.045	−12.80	1	10 ± 10	1	
097.130	−13.31	1	7 ± 10	1	
097.138	−13.15:	2	31 ± 4	2	f
127.049	−12.77	2	57 ± 4	2	
127.051	−12.84:	3	35 ± 3	3	d
127.052	−13.42:	1	7 ± 10	1	a, b
127.055	−12.73	2	43 ± 5	2	
127.056	−12.86	1	21 ± 10	1	
127.058	−12.61:	1	48:	1	d
097.160	−13.10:	1	20:	1	c
127.067	−12.98	1	42 ± 10	1	
127.068	−12.99	2	24 ± 6	2	
127.071	−12.66	3	61 ± 4	3	
127.074	−12.66	2	44 ± 4	2	
097.168	−13.07	1	35 ± 10	1	
127.082	−12.98	2	22 ± 3	2	
127.085	−13.09	1	29 ± 10	2	
127.095	−12.77	2	15 ± 3	2	
097.180	−13.15:	2	54:	1	f

Table 5.2 – *continued*

Column 1: CGCG number from Zwicky & Herzog (1963).
Columns 2: Weighted mean of the Hα + [NII] flux measured from the objective prism spectra and photoelectric values.
Column 3: Number of measurements used to compute the mean flux.
Column 4: Weighted mean of Hα + [NII] equivalent width measured from the objective prism spectra and photoelectric values.
Column 5: Number of measurements used to compute the mean equivalent width.
Column 6: Notes on individual objects, listed below.

Notes:

All values of equivalent width and flux are the weighted mean of values in Table 5.1.

a.) Emission line on plate A is weak.
b.) Emission line on plate B is weak.
c.) Continua are contaminated by nearby stars on plates A and B.
d.) Spectra on plate A are contaminated by a noise spike.
e.) Spectra on plate B are contaminated by a noise spike.
f.) Spectra are noisy on plates A and B.

5.4 Galaxy detection limits

In the overlap region, Kennicutt *et al.* (1984) obtained Hα flux and equivalent width measurements for 18 galaxies. Of these, we detect 14 in the present study. Shown in Figure 5.3(a) and (b) are the distributions of equivalent width and flux, respectively, for detected (shaded boxes) and undetected (open boxes) galaxies. There is a sharp cutoff, in equivalent width, between detected and undetected galaxies at $W_\lambda = 20$ Å, as observed by MWI. For $W_\lambda \leq 20$ Å this study detects three out of seven galaxies, while for $W_\lambda > 20$ Å 11 out of 11 galaxies are detected. The flux cutoff appears to be less clear; for $f \leq 2 \times 10^{-13}$ erg cm^{-2} s^{-1} six out of nine galaxies are detected while for fluxes greater than this eight out of nine are detected. Again, this confirms the results of MWI.

Because both flux and equivalent widths are relevant to the detection of the emission, MWI suggest that the combined parameter of $f \times W_\lambda$ may be a good indicator of the ease of detection. For a cutoff of $f \times W_\lambda \leq 3 \times 10^{-12}$ erg cm^{-2} s^{-1} Å, the present study detects three out of six galaxies while for larger values, 11 out of 12 galaxies are detected. Thus, the most reliable limits appear to be the equivalent width ($W_\lambda = 20$ Å) and the combined flux and equivalent width parameter.

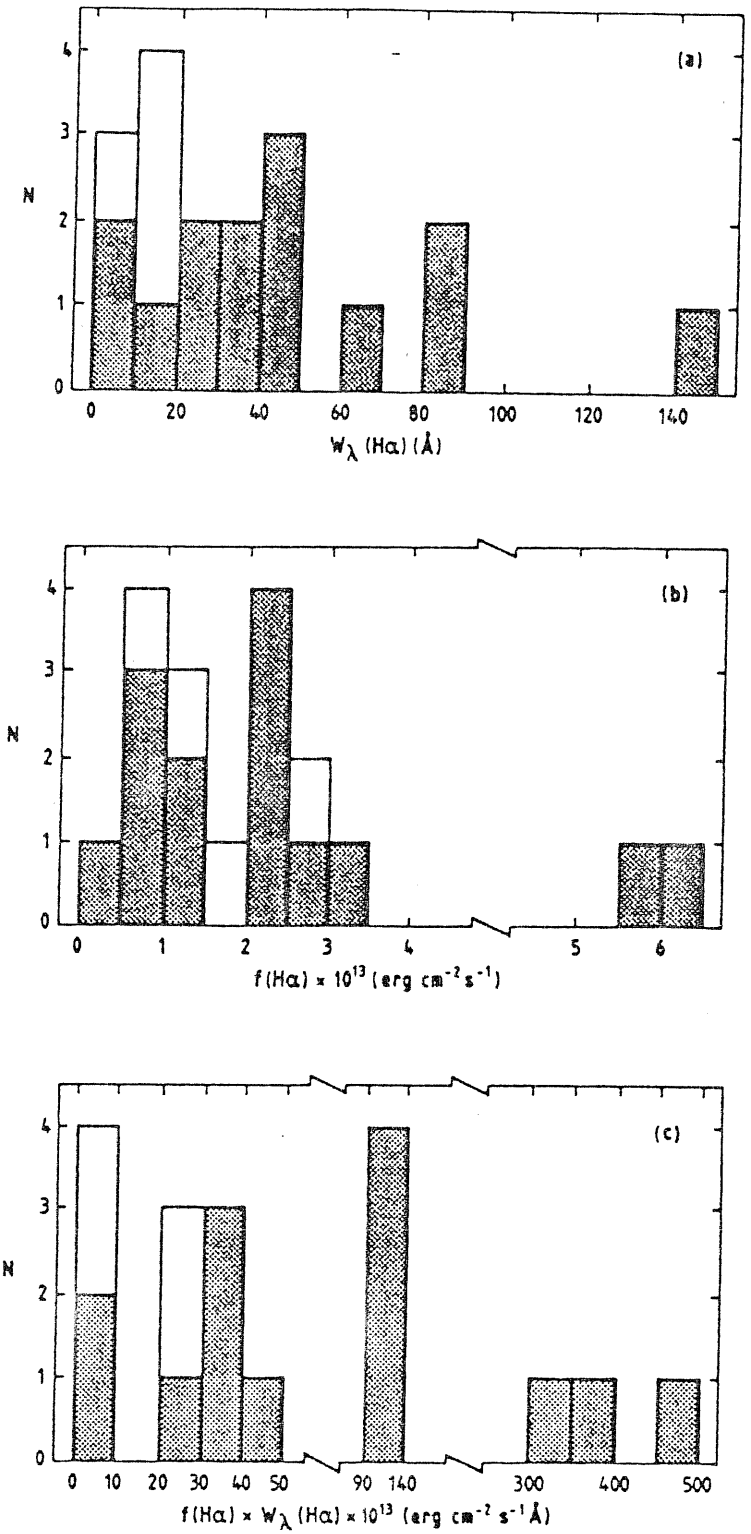

Figure 5.3: A sample of 18 galaxies in Abell 1367 detected in Hα emission by Kennicutt *et al.* (1984). The histograms show the distributions of galaxies detected (shaded) and not detected (open) using the objective prism technique. The distributions of detected and undetected galaxies with Hα equivalent width and flux are shown in (a) and (b), respectively. The distribution with a combined parameter, $f \times W_\lambda$, is shown in (c).

CHAPTER VI

A Survey for [OII] λ3727 Å Emission

A tracer of star formation is the [OII] λ3727 Å emission line, produced in star forming regions (Gallagher, Bushouse & Hunter 1989). Moss has proposed the method for detecting [OII] emission in galaxies, discussed below. The present objective prism survey is, as far as is known, the first of its kind to be performed.

Using the Burrell Schmidt telescope equipped with a UG5 filter, 4°.5 UV objective prism and using IIIaJ emulsion, two plates, E and F in Table 3.1 (above, Section 3.2.1) were obtained of Abell 1367. The experimental set-up is described thoroughly in Chapter III. As for the Hα analysis, the two plates allow for confirmation of questionable detections and are of a similar quality, although plate F is slightly better than E because of its longer exposure time. There are 201 CGCG galaxies in the overlap of the two plates.

The plates were scanned with a binocular microscope at $\times$ 12. Among the sample of 201 CGCG galaxies, nine (of which seven are cluster members) are detected in emission and are listed in Table 6.1. Emission was characterized by visibility using the same five-point scale as for the Hα survey (W, MW, M, MS, S) and by concentration (VD, D, normal, C, VC). We find that most galaxies exhibiting [OII] emission have medium-weak to medium-strong visibility.

The [OII] emission was rather difficult to detect and it is possible

Table 6.1: [OII] Emission-line Galaxies in Abell 1367.

Galaxy Identification			R.A. (1950.0)	Dec. (1950.0)	m_p	Type	Emission		Plates	$V_\odot$ (km s^{-1})	Notes
CGCG	NGC/IC* UGC	MCG IRAS	h m s	° ′ ″			Vis.	Conc.		Refs.	
(1)	(2)	(3)	(4)	(5)	(6)	(7)	(8)	(9)	(10)	(11)	(12)
126.104	...	...	11 32 58.4	+20 46 57	15.6	S pec	W	D	E,F	6679	
	...	...								3	
097.026	...	+03-30-019	11 34 17.9	+20 14 51	13.9	S pec	MS	C	E,F	6202	d
	06583	11342+2015								4	
097.067	...	+03-30-053	11 39 53.7	+18 36 40	14.3	Sbc	M	C	E,F	918	a, g
	06670	11398+1836								2	
097.073	...	...	11 40 20.7	+20 14 37	15.6	Scd pec	W	VD	E,F	7275	a, g
	...	...								4	
097.079	...	...	11 40 37.5	+20 16 54	15.7	S pec	M		E,F	7000	b, e, g
	...	...								4	
097.087	...	+03-30-066	11 41 12.7	+20 14 52	14.3	Irr–Sd	M		E,F	6723	c, g
	06697	11412+2014								4	
097.114	...	+03-30-087	11 42 12.1	+20 03 02	15.4	S0–a pec	W	VD	E,F	8293	g
	...	...								4	
127.052	3884	+04-28-051	11 43 36.8	+20 40 08	14.0	Sa	M		E,F	6842	f
	06746	...								5	
127.074	...	+04-28-070	11 48 39.8	+21 16 47	15.0	S0	MW		E,F	3358	
	...	...								1	

References: (1) Markarian *et al.* 1984. (2) Fisher & Tully 1981. (3) Bothun *et al.* 1985. (4) Gavazzi 1987. (5) Giovanelli & Haynes 1985.

Explanation of columns.

Column 1. CGCG number from Zwicky & Herzog 1963. An asterix indicates that the object is detected on one plate only. Line 2 is the alternate CGCG number.
Column 2. Line 1, NGC or IC number (with asterix); line 2, UGC number (Nilson 1973).
Column 3. Line 1, MCG number (Vorontsov-Velyaminov & Arkipova 1964); line 2, *IRAS* identification (Fullmer & Lonsdale 1989).
Columns 4. and 5. 1950.0 coordinates in HHMMSS.S+DDMMSS format.
Column 6. Photographic magnitude taken from CGCG.
Column 7. Morphological type. Galaxies were typed using plate G.
Column 8. A visibility parameter (S strong, MS medium-strong, M medium, MW medium-weak, W weak) describing the visual appearance of the emission, averaged from the appearance on the plates in column 10.
Column 9. A concentration parameter (VD very diffuse, D diffuse, C concentrated, VC very concentrated) averaged from the concentration on the plates in column 10. No entry indicates that the spectral appearance is unremarkable.
Column 10. Plates on which the galaxy is detected in emission.
Column 11. Heliocentric velocity (line 1) and references (line 2).
Column 12. References to notes on individual objects, described below.

Notes on individual objects.

a. A foreground galaxy. Several knots of emission are detected.
b. Double nebula (Zwicky & Herzog 1963).
c. Four distinct knots of emission are visible.
d. Appears disturbed on plate G and/or the PSS blue print.
e. Appears to be interacting on plate G and/or the PSS blue print.
f. Classified as Seyfert 1 by Véron-Cetty & Véron (1989).
g. Galaxy is edge-on.

that emission exists in more galaxies but their detection is beyond the limit of the present, visual inspection. There are several factors which contribute to the difficulty of detecting [OII] emission. Firstly, the [OII] emission is not as strong as Hα emission and, therefore, does not stand out from the background as well as the Hα emission. Secondly, unlike the spectral region of Hα, there are numerous emission and absorption lines near [OII]. These lines hinder the immediate identification of [OII]. Finally, strong [OII] emission simply may not be present in spiral galaxies.

All of the galaxies exhibiting [OII] emission are observed in Hα as well. These Hα emission-line galaxies are among the strongest emitters. The average Hα equivalent width for [OII] emission-line galaxies is 80 Å while for the rest of the Hα emission-line galaxies it is 30 Å. Figure 6.1 shows the number distribution of [OII] emission-line galaxies with Hα equivalent width. The stippled boxes indicate galaxies with [OII] emission.

Table 6.2 shows the emission statistics for [OII] and Hα emission-line galaxies. There is some suggestion that the [OII] emission, like the Hα emission, increases for later type galaxies, although the effect is not statistically significant due to the small number of galaxies detected. As can be seen in Table 6.3, 13 per cent of galaxies (of types Sa – Irr) within one Abell radius exhibit [OII] emission compared to only four per cent beyond this radius. Most (71 per cent, or five galaxies) of the [OII] emission-line galaxies have a given Hubble type but are also recognized as 'peculiar'. This can be compared with 65 per cent of Hα emission-line galaxies which are also recognized as peculiar (in addition to a given Hubble type) and only eight per cent of non-emission-line galaxies.

Since [OII] emission is associated with some of the strongest Hα emission-line galaxies, we have attempted to determine if there are other, unique proper-

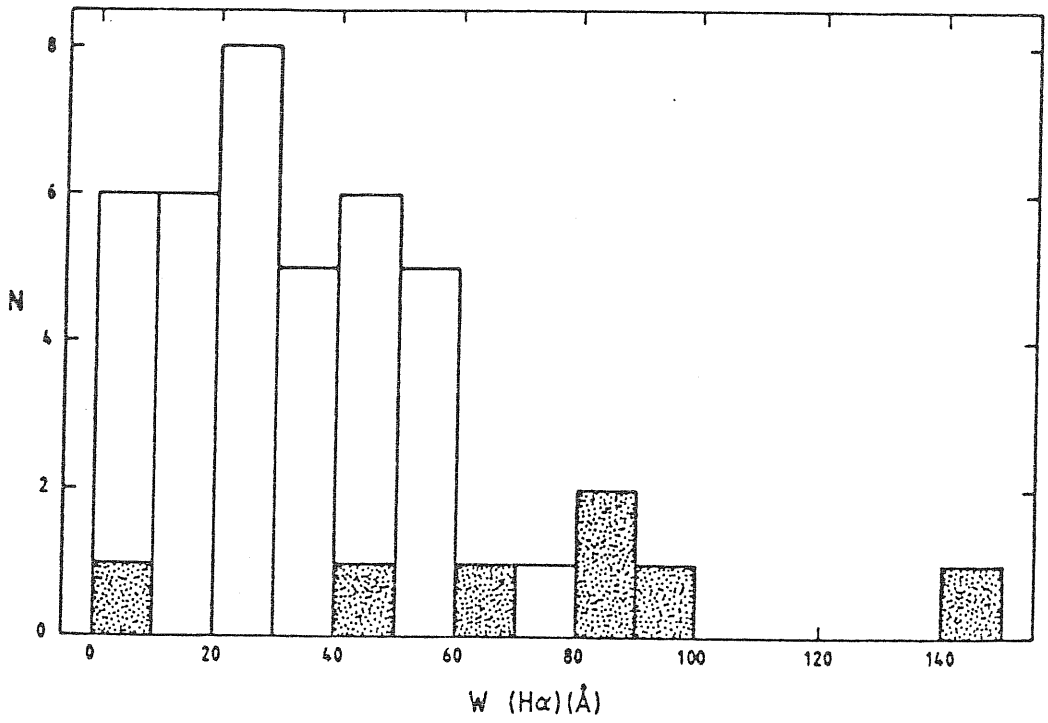

Figure 6.1: The number distribution of [OII] emission-line galaxies with Hα equivalent widths. The stippled boxes represent galaxies with [OII] emission.

Table 6.2: Comparison of [OII] and Hα Emission Statistics.

	$r_A \leq 1.0$					$r_A > 1.0$				
Type	Total	[OII]	Hα	% [OII]	% Hα	Total	[OII]	Hα	% [OII]	% Hα
(1)	(2)	(3)	(4)	(5)	(6)	(7)	(8)	(9)	(10)	(11)
S0, S0–a	32	1	3	3%	9%	19	0	1	—	5%
Sa – Sb	15	1	8	7%	53%	29	0	10	—	35%
Sbc – Irr	9	2	6	22%	67%	11	0	3	—	27%
S...	6	1	3	17%	50%	7	2	5	29%	71%

Explanation of Columns

Column 1: Morphological type.
Column 2: Total number of cluster galaxies within 1.0 Abell radius of the core.
Column 3: Number of galaxies within 1.0 Abell radius of the core exhibiting [OII] emission.
Column 4: Number of galaxies within 1.0 Abell radius of the core exhibiting Hα emission.
Columns 5 & 6. Percentage of galaxies within 1.0 Abell radius of the core exhibiting [OII] and Hα emission, respectively.
Columns 7 – 11, the same as columns 2 – 6 but for $r_A > 1.0$

Table 6.3: Location of [OII] emission-line galaxies in the cluster.

	$r_A \leq 1.0$	$r_A > 1.0$
Total Spirals (Sa-Irr)	30	47
[OII] emission galaxies	4 (13%)	2 (4%)
Hα emission galaxies ($W_\lambda > 60$ Å)	2 (7%)	4 (9%)

ties that these galaxies exhibit. The majority of Hα emission-line galaxies (83 per cent) with Hα equivalent widths greater than 60 Å exhibit [OII] emission (*cf.* Figure 6.1, above). In contrast, only seven per cent of Hα emission-line galaxies with Hα equivalent widths less than 60 Å have [OII] emission as well. However, there is no position dependence for galaxies with equivalent widths greater than 60 Å (*cf.* Table 6.3), though we must caution, once again, that the numbers are too small to make a definitive statement.

In conclusion, the [OII]-emission detection method is successful and we detect seven out of 172 cluster galaxies (or four per cent). However, [OII] emission *is* difficult to detect. The galaxies that exhibit [OII] emission tend to be among the strongest of Hα emitters as well. The average Hα equivalent width for these galaxies is 80 Å while it is only 30 Å for the rest of the Hα emission-line galaxies. Emission from [OII] may be position sensitive, since 13 per cent of galaxies within one Abell radius exhibit emission compared to four per cent beyond one Abell radius, and it *may* increase for later type galaxies. Most of the [OII] emission-line galaxies, in addition to a given Hubble type, are recognized as being peculiar. Much more work needs to be done, however, in order to say more about the results presented herein. For example, the lack of detection of [OII] emission may be due to the survey technique, but we do not have enough information to determine whether this is the case or not.

CHAPTER VII

Properties of Emission-line Galaxies in Abell 1367

7.1 The galaxy sample

Figure 7.1 shows the velocity histogram for all galaxies on one or more plates. As can be seen, the cluster extends from $\sim$ 5500 km s^{-1} to $\sim$ 7500 km s^{-1}, with many background galaxies and a small cluster of foreground galaxies at $\sim$ 3300 km s^{-1}. Galaxies with velocities beyond 3σ from the cluster mean velocity ($V_\odot > 8946$ km s^{-1} and $V_\odot < 3954$ km s^{-1}) have been removed leaving 177 galaxies in the sample as a whole and 40 emission-line galaxies (23 per cent). The galaxies without measured redshifts are assumed to be all cluster members, although one can expect that $\sim$ 11 per cent of them are either foreground or background objects. In this case, we could obtain a maximum of 25 per cent emission-line galaxies in Abell 1367. When restricted to include only galaxies in the overlap region (overlap of plates A and B), the sample consists of 153 galaxies of which 37 (or 24 per cent) show emission. This is the sample analyzed in what follows.

7.2 Frequency of emission as a function of galaxy magnitude

The sample of cluster galaxies was binned according to magnitude as in Table 7.1. This table gives the number of galaxies in each bin, the number

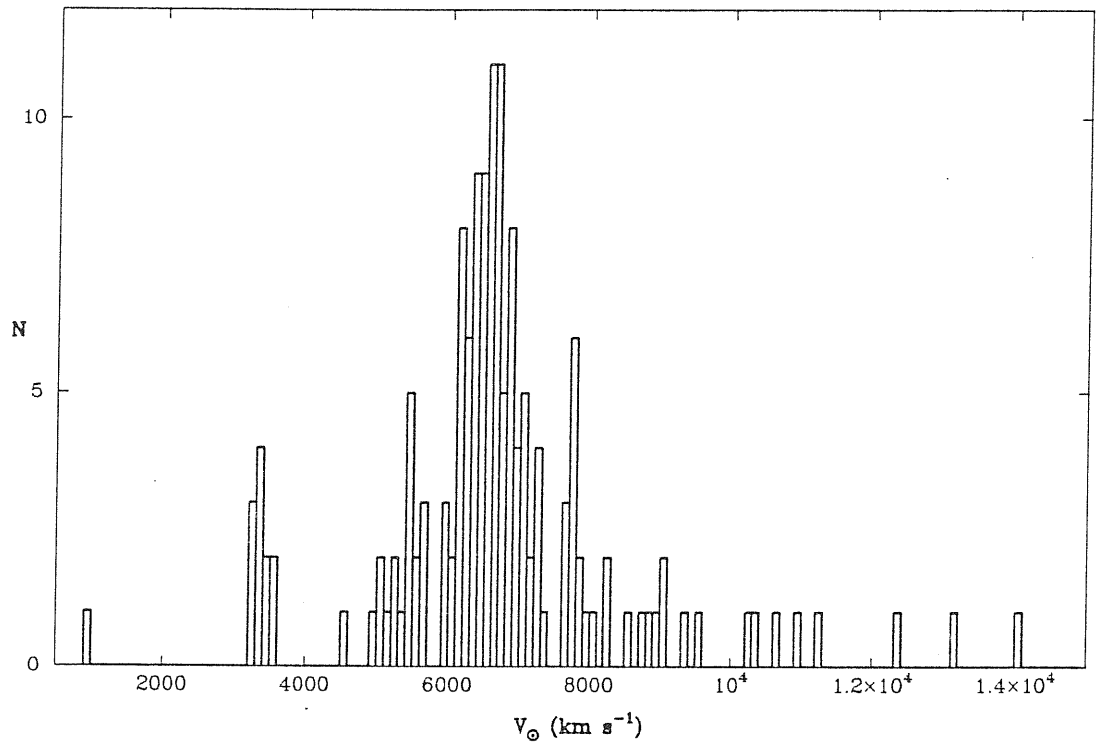

Figure 7.1: The velocity histogram for all galaxies on one or more plates. As can be seen, the cluster extends from $5600 \lesssim V_\odot \lesssim 7300$ km s^{-1}. There appears to be a small clustering of foreground galaxies at ~ 3300 km s^{-1}.

Table 7.1: Emission as a function of galaxy magnitude.

Magnitude Range	$13.3 \leq m_p \leq 14.2$	$14.3 \leq m_p \leq 14.7$	$14.8 \leq m_p \leq 15.2$	$15.3 \leq m_p \leq 15.7$
Total no. of galaxies	13	23	33	90
No. of emission-line galaxies	3	7	5	21
	—	—	—	—
% Observed in emission	23%	30%	15%	23%
% Expected in emission	23%	30%	20%	27%

Table 7.2: Emission as a function of galaxy magnitude for emission-line galaxies with $W_\lambda > 20$ Å.

Magnitude Range	$13.3 \leq m_p \leq 14.2$	$14.3 \leq m_p \leq 14.7$	$14.8 \leq m_p \leq 15.2$	$15.3 \leq m_p \leq 15.7$
Total no. of galaxies	11	21	31	90
No. of emission-line galaxies ($W_\lambda > 20$ Å)	1	5	3	21
% Observed in emission	9%	24%	13%	23%
% Expected in emission	18%	24%	14%	27%

of emission-line galaxies in each bin and their percentage. Also shown are the expected percentages of emission-line galaxies, computed as follows.

In each magnitude bin, the number of galaxies of each morphological type was counted. This number was multiplied by the percentage of galaxies in that morphological type exhibiting emission (refer to Table 7.3 on page 108). Summing the expected numbers over all morphological types gives the total number of galaxies expected to be in emission in each magnitude bin. The expected numbers compare favourably with the observed numbers ($\chi^2 = 0.95$, $p \sim 0.80$) and there is no evidence for a systematic effect in the detection frequency over the magnitude range. Because the values in Table 7.1 refer to cluster members only, the observed range in apparent magnitude can be taken to correspond to a range in absolute magnitude. Therefore, we see that there is no systematic effect with absolute magnitude either, in agreement with the findings of Kennicutt & Kent (1983).

Making use of our 20 Å equivalent width cutoff, Table 7.2 shows the emission as a function of magnitude, as in Table 7.1, but for emission-line galaxies with equivalent widths greater than 20 Å only. The observed numbers compare favourably with the expected numbers ($\chi^2 = 1.13$, $p \sim 0.75$).

7.3 Frequency of emission as a function of galaxy morphology

Table 7.3 shows the total number of galaxies, the number of emission-line galaxies and the fractions of galaxies in emission for each morphological type ('f' for individual galaxies; 'F' for combined types). Galaxies with a given Hubble type but also noted as peculiar galaxies are included in the relevant morphological type bins. No S0 galaxies are detected in emission and emission is seen to increase for S0 – a galaxies through later type spirals, although

the fraction of detected emission-line galaxies of combined types, Sa – Sab, Sb – Sbc and Sc – Irr, remains relatively constant. These combined types are discussed below, in Section 8.2. For obvious emission-line galaxies (*i.e.*, those with $W_\lambda > 20$ Å only), as in Table 7.4, this trend of emission frequency increasing for later type galaxies is more clearly seen. The results agree with the findings of Kennicutt and Kent (1983).

Table 7.5 shows the number of barred and unbarred galaxies in emission. The numbers in parentheses indicate the numbers of emission-line galaxies for which emission is characterized as very concentrated, concentrated or normal only. Edge-on galaxies have been removed from the sample. For all emission types, we find that there is no correlation between the presence of a bar and Hα emission ($\chi^2 = 0.47$, $p = 0.50$). Nor is there a correlation when the emission types are limited to very concentrated, concentrated and normal ($\chi^2 = 0.28$, $p = 0.59$). Although there are a slightly higher percentage of barred emission-line galaxies (26%) than unbarred emission-line galaxies (18%), this result is not significant due to the small sample size.

Finally, Table 7.6 compares the number of normal spirals in emission and those that have a given Hubble type but also appear peculiar. More emission-line galaxies are peculiar spirals (63%) than normal spirals (36%). A chi-squared test confirms this, although the result is only slightly significant ($\chi^2 = 3.3$, $p = 0.059$).

Table 7.3: Hα emission statistics for cluster galaxies in the overlap region.

Galaxy type:		E	E–S0	S0	S0–a	Sa	Sab	Sb	Sbc	Sc – Irr	S...	pec
Total number:		9	31	19	27	22	7	14	4	10	16	1
Number in emission:		0	0	0	4	8	4	5	3	4	8	1
	f	—	—	—	15%	36%	57%	36%	75%	40%	50%	100%
	F					41%		44%		40%		

Table 7.4: Hα emission statistics for cluster galaxies with $W_\lambda > 20$ Å in the overlap region.

Galaxy type:		E	E–S0	S0	S0–a	Sa	Sab	Sb	Sbc	Sc – Irr	S...	pec
Total number:		9	31	19	27	22	7	14	4	10	16	1
Number in emission:		0	0	0	3	5	3	4	3	4	7	1
	f	—	—	—	11%	23%	43%	29%	75%	40%	44%	100%
	F					28%		39%		40%		

Table 7.5: Emission in barred and unbarred galaxies.

	Barred	Unbarred
Galaxies with emission	7 (4)	19 (10)
Galaxies with no emission	20	88
Per cent in emission	26% (17%)	18% (10%)

Table 7.6: Emission and 'peculiar' spirals.

	'S' peculiar	normal
Galaxies with emission	12	20
Galaxies with no emission	7	36
Per cent in emission	63%	36%

CHAPTER VIII

Variation of Emission with Environment

8.1 Location within the cluster

In what follows, we define emission-line galaxies as those galaxies with Hα equivalent widths greater than 20 Å (our detection cutoff). Figure 8.1 shows a map of Abell 1367. Only the cluster galaxies in the overlap region are included. Filled circles represent the emission-line galaxies. There is a significant north-south asymmetry in the emission-line galaxies (*i.e.*, the arc of emission-line galaxies at approximately $-1.4\ r_A$). Shown in Figure 8.2(a) is the cumulative number distribution function for all cluster spiral galaxies, Sa and later (outside of the overlap region, as well). The solid line represents all non-emission-line spirals in the sample while the dashed line represents only the emission-line galaxies. There appear to be slightly more emission-line than non-emission-line galaxies in the inner $0.5\ r_A$, as was seen before, although the shapes of the distributions are essentially the same.

The cumulative number distribution of morphological types is shown in Figure 8.2(b). As can be seen, all types are present throughout cluster, with the inner 0.5 Abell radius dominated by elliptical and S0 galaxies, as expected. Rather unexpected, though, is the distribution of galaxies with given Hubble type but also noted as being "peculiar". These galaxies follow the distribution

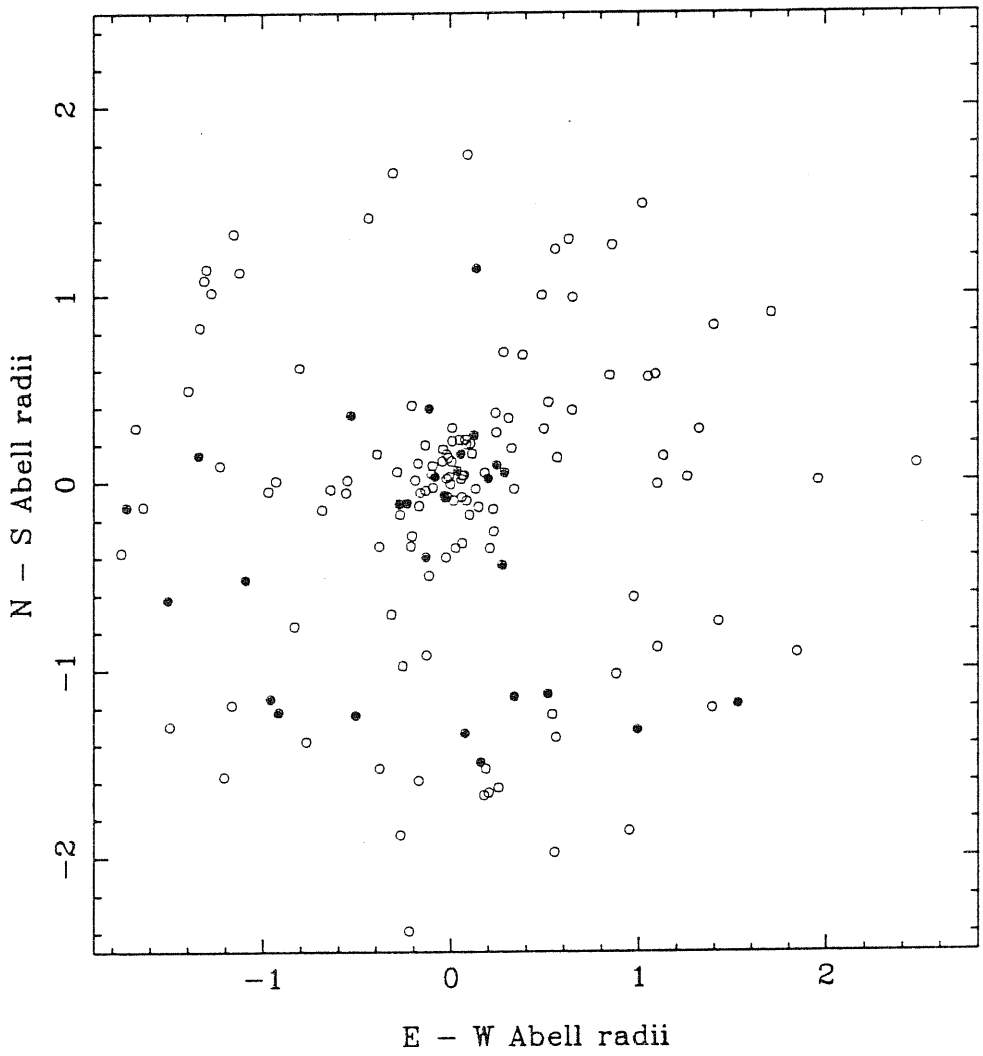

Figure 8.1: A map of Abell 1367; only cluster galaxies in the overlap region are depicted. Filled circles represent emission-line galaxies.

of the elliptical and S0 galaxies. Spiral galaxies, Sa – Irr, are present uniformly throughout the cluster.

It may be noted that the distributions of most galaxies except, perhaps Sbc – Irregular spirals, instead of leveling off at large Abell radii, as might be expected, start to rise again around 1.5 r_A. The rise in the distribution is clearly seen in Figure 8.2(a). We believe this unexpected increase in the number of galaxies at large Abell radii is due to substantial subclustering in the outer regions of Abell 1367. That is, within $\sim$ 1.5 r_A we are observing the cluster proper. The cumulative distribution increases and then levels off. Beyond 1.5 r_A, subclusters mimic the main cluster and we see the cumulative distribution rise and then level off, again, at about 2.6 r_A.

Although extremely interesting, this finding *may* mean that we can not compare galaxies throughout the range of Abell radii depicted in Figure 8.2 because they are not from the same "cluster". Because of this possible problem, we have determined the "local galaxy density" in the following manner. We count the number of galaxies within a circle of radius 0.2 r_A centred on all galaxies. The number obtained is defined as the local galaxy density (σ_{LGD}) and is not affected by the fact that galaxies at large Abell radii may not be part of Abell 1367, proper, but are members of subclusters instead. Local galaxy density ranges from 0 to 32 and, for $H_o = 50$ km s^{-1} Mpc^{-1}, this corresponds to projected galaxy densities of 0.9 to 29 galaxies Mpc^{-2}.

Figure 8.3 shows the distribution of galaxies with the local galaxy density. The solid line represents spiral galaxies, Sa – Irr, elliptical (E, E – S0) galaxies are the dashed line and the dotted line is S0 and S0 – a galaxies. As expected, most of the spirals are in the lower density regions while ellipticals and S0 galaxies are in the higher density regions, though a substantial number appear in the low density regions as well.

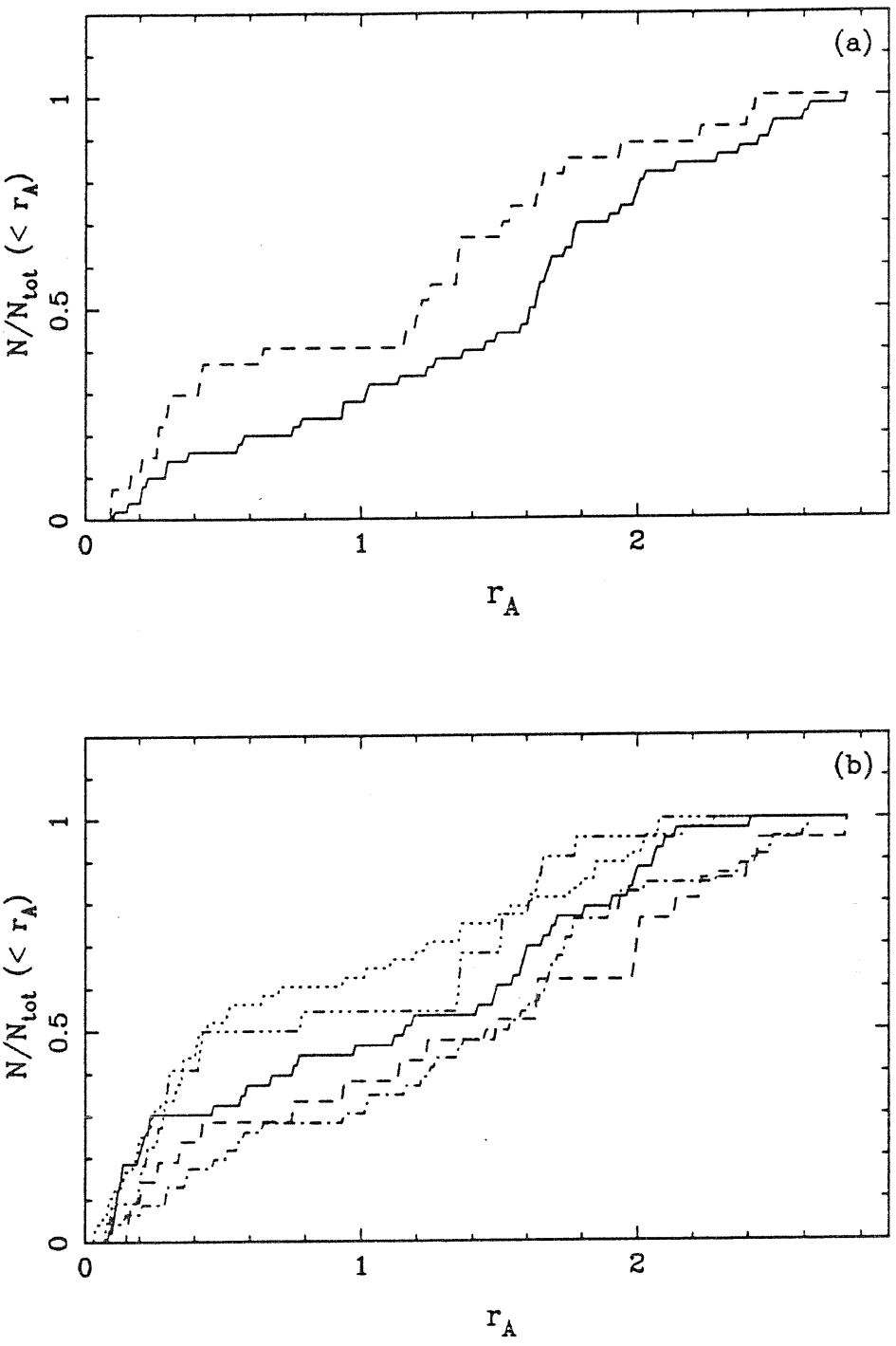

Figure 8.2: (a) The cumulative number distribution for cluster spiral galaxies. The solid line represents all non-emission-line spiral galaxies, Sa and later, while the dashed line represents only emission-line galaxies. (b) The cumulative number distribution for different morphological types. The solid line represents E and E – S0 galaxies, the dotted line, S0 and S0–a galaxies, the dot-dashed line is Sa – Sb galaxies, the dashed line is Sbc – Irregular galaxies and the dash-dot-dot-dot line represents all galaxies with a given Hubble type but also noted as "peculiar".

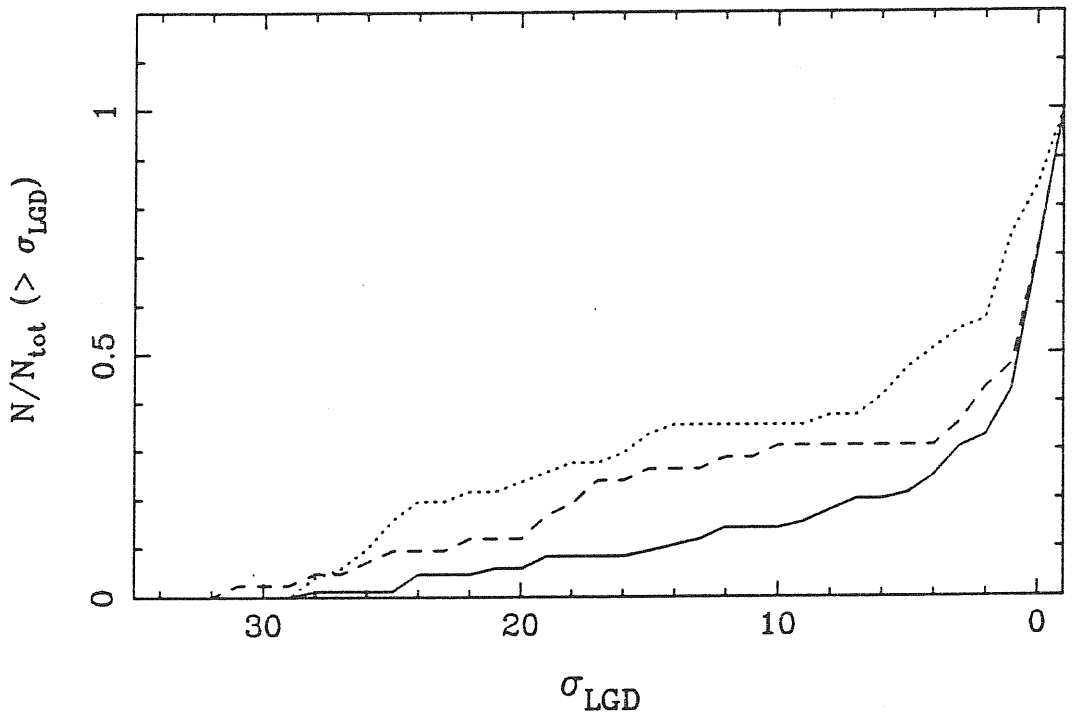

Figure 8.3: The distribution of cluster galaxies with the local galaxy density, σ_{LGD}. Shown are spiral galaxies (Sa – Irr) as the solid line, elliptical galaxies (E, E – S0) as the dashed line and S0, S0 – a galaxies with the dotted line.

Table 8.1: Emission and local galaxy density.

	Low Density (< 2)	High Density (≥ 2)
Emission-line galaxies	15	11
Non-emission-line galaxies	33	17
Per cent emission-line galaxies	31%	39%

We now test to see if there are a higher percentage of emission-line galaxies in the higher density regions. Figure 8.4 is a histogram of the number of Sa – Irr galaxies for given local galaxy densities. Emission-line galaxies are depicted as the stippled boxes. For spirals with no other galaxy within 0.2 r_A, emission-line galaxies make up 33 per cent of the sample (8 out of 24). The percentage is 29 per cent (7 out of 24) for a local galaxy density of one and increases to 39 per cent (11 out of 28) for local galaxy densities greater than one. If we define "high" density to signify $\sigma_{LGD} \geq 2$ and "low" density to signify $\sigma_{LGD} < 2$, Table 8.1 gives the results. (This local galaxy density is the approximate mean density of galaxies located at 0.5 r_A). Although there is a slight increase of emission-line galaxies for $\sigma_{LGD} \geq 2$, it is not significant ($\chi^2 = 0.21$, $p \sim 0.06$).

Figure 8.5(a) shows the histogram of spirals with local galaxy density. Emission-line galaxies with compact emission regions, defined as $d_e/D \leq 0.37$, are shown as the stippled boxes. Figure 8.5(b) shows the same histogram but for emission-line galaxies with diffuse ($d_e/D > 0.37$) emission regions. Comparisons between low and high density regions for emission-line galaxies with compact and diffuse emission regions are given in Tables 8.2 and 8.3, respec-

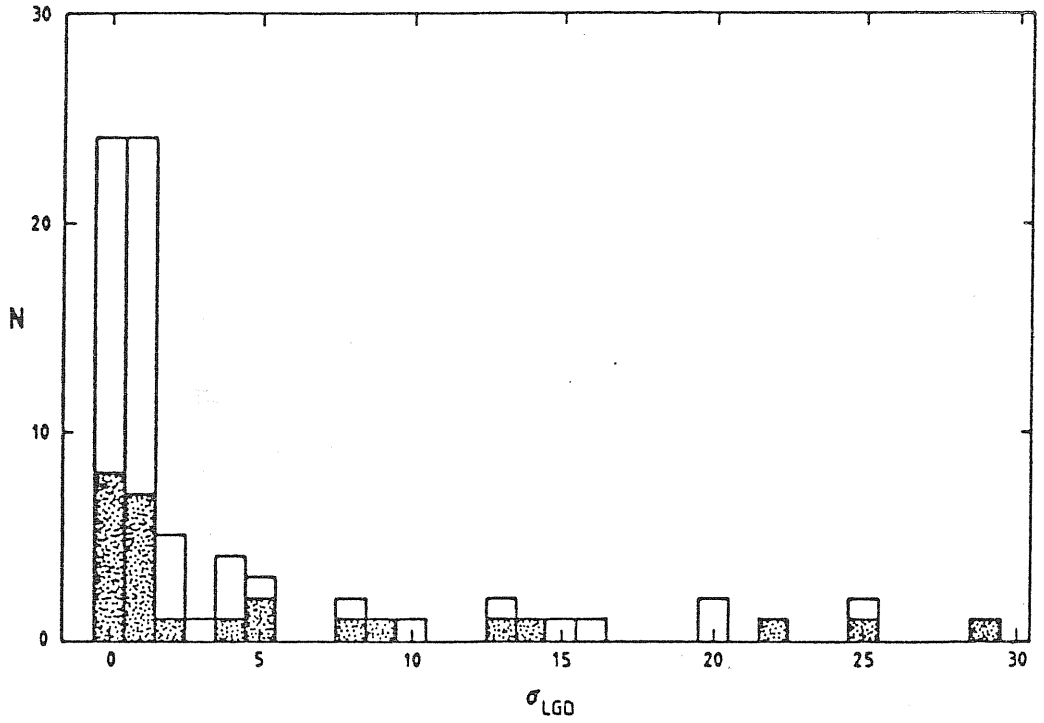

Figure 8.4: The number of cluster Sa – Irr galaxies with the local galaxy density, σ_{LGD}, defined in the text. The stippled boxes represent emission-line galaxies.

Table 8.2: Compact ($d_e/D \leq 0.37$) emission and local galaxy density.

	Low Density (< 2)	High Density (≥ 2)
Emission-line galaxies	3	5
Non-emission-line galaxies	45	23
Per cent emission-line galaxies	7%	18%

Table 8.3: Diffuse ($d_e/D > 0.37$) emission and local galaxy density.

	Low Density (< 2)	High Density (≥ 2)
Emission-line galaxies	12	6
Non-emission-line galaxies	36	22
Per cent emission-line galaxies	33%	21%

tively. We see that there are slightly more emission-line galaxies with compact emission in the higher density regions but this is not significant ($\chi^2 = 1.4$, $p \sim 0.25$) and that emission-line galaxies with diffuse emission are spread uniformly through all densities ($\chi^2 = 0.005$, $p \sim 0.96$).

Although it is difficult to tell for certain, the frequency of emission-line galaxies *may* increase with increasing local galaxy density. However, this is not significant since the numbers are small. In addition, there may be a slight tendency for emission-line galaxies with compact emission to be predominately in the higher (≥ 2) density regions (but, again, this is not significant).

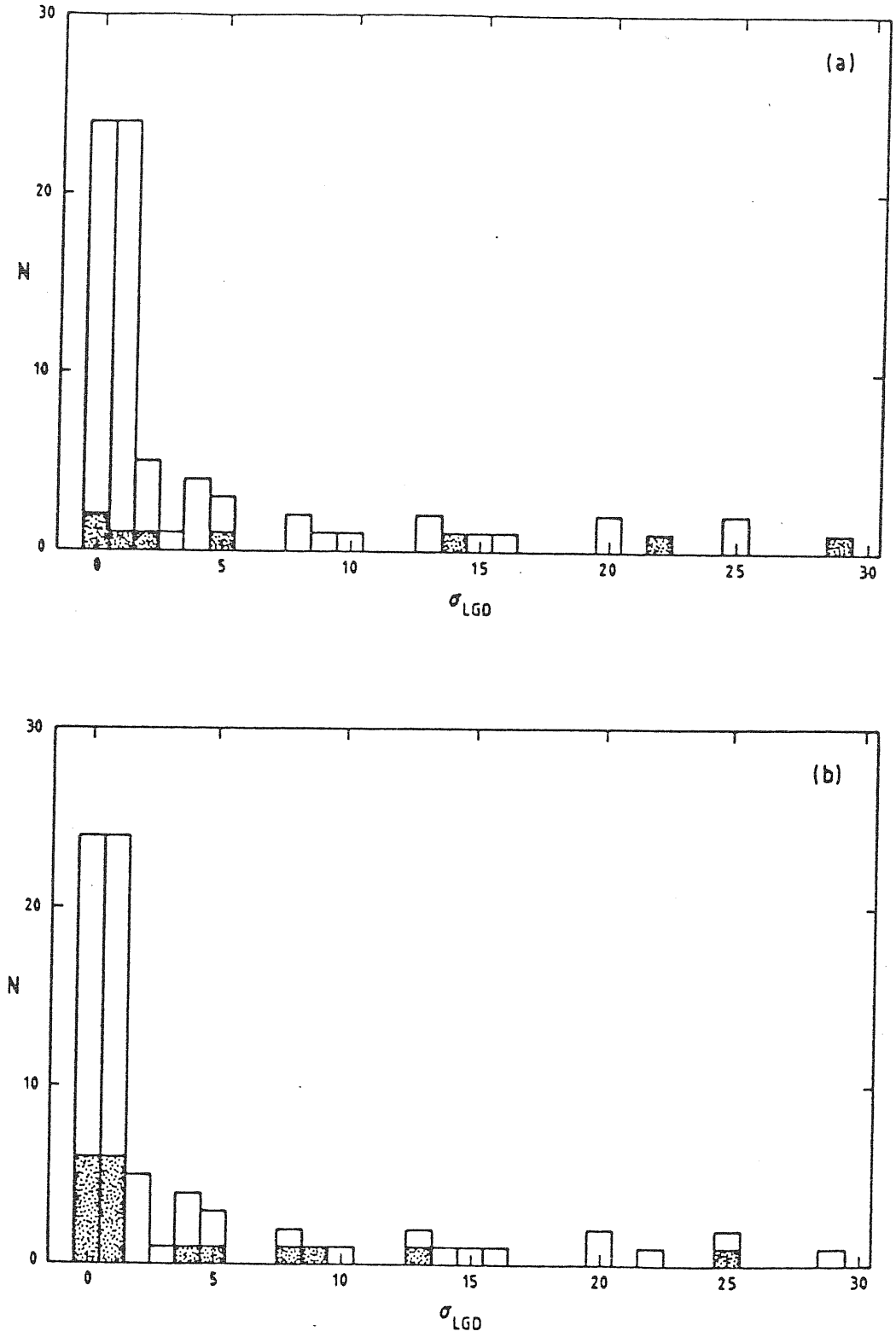

Figure 8.5: The number of cluster Sa – Irr galaxies with the local galaxy density, σ_{LGD}. (a) The stippled boxes represent emission-line galaxies with compact, $d_e/D \leq 0.37$, emission regions. (b) The same histogram but for emission-line galaxies with diffuse, $d_e/D > 0.37$ emission regions.

8.2 Comparison of Hα equivalent widths for field and cluster galaxies

We now wish to compare the Hα emission in cluster galaxies with that in field galaxies. To this end, we have selected 134 field galaxies from the study of Kennicutt & Kent (1983). Figure 8.6 is a comparison of the distribution of cluster and field galaxy Hα equivalent widths. Three galaxy morphological types are compared, Sa – Sab, Sb – Sbc and Sc – Irr. These three groups exhibit similar percentages of emission-line galaxies (*cf.* Section 7.3, above). Cluster galaxies are represented with filled symbols: filled circles are normal galaxies and filled triangles are galaxies of a given Hubble type also noted as being peculiar. For the field sample, crosses indicate normal galaxies and open triangles, the peculiar galaxies. Arrows signify upper limits for non-detected cluster galaxies. The horizontal, dashed line is the 20 Å equivalent width detection cutoff determined in Section 5.4. We choose this detection cutoff because above it we detect 100 per cent of galaxies in emission while below it we only detect some ill-defined fraction. Galaxies classified as 'S...', 'S pec' or simply 'pec' have not been included.

As can be seen in Figure 8.6, cluster Sa – Sab galaxies are significantly different than the field galaxies, in that cluster galaxies show **more**, strong emission ($\chi^2 = 8.9$, $p = 3.5 \times 10^{-3}$). Cluster and field Sb – Sbc galaxies are not substantially different ($\chi^2 = 0.6$, $p = 0.44$). Late-type spirals and irregulars are different than field galaxies of the same type, exhibiting **less** emission than expected ($\chi^2 = 14.2$, $p < 5 \times 10^{-4}$). We note that of the six Sa – Sab peculiar cluster galaxies, four are within one Abell radius of the cluster centre.

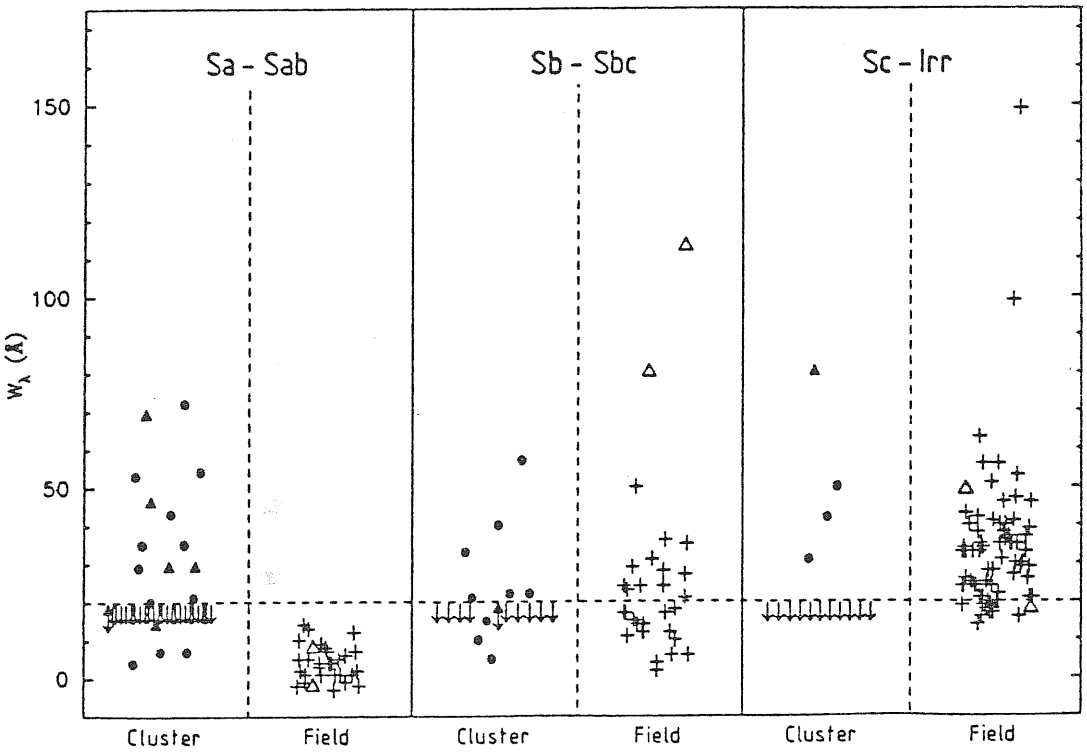

Figure 8.6: A comparison of Hα equivalent width distributions for cluster and field galaxies (from Kennicutt & Kent 1983). The horizontal, dashed line indicates the 20 Å equivalent width cutoff. Normal cluster galaxies are indicated with filled circles and cluster galaxies of a given Hubble type also noted as being peculiar with filled triangles. Arrows indicate upper limits for non-detected galaxies. Field galaxies are marked with crosses (normal) and open triangles (peculiar).

Several points should be addressed concerning these observations. The Kennicutt & Kent (1983) sample is magnitude limited and it is possible that the field galaxies are intrinsically fainter than the cluster galaxies. While there appears to be no dependence of Hα equivalent width on magnitude or luminosity (Kennicutt & Kent 1983), one could expect that brighter field galaxies may exhibit stronger emission.

In order to test whether there is, indeed, a difference between the absolute magnitudes of the cluster and field samples, we have taken absolute blue magnitudes for the field galaxy sample from the *Revised Shapley-Ames Catalog of Bright Galaxies* (RSA: Sandage & Tammann 1981) and computed absolute photographic magnitudes for the cluster galaxies. For both calculations of absolute magnitude, $H_o = 50$ km s^{-1} Mpc^{-1} has been assumed. Although the blue and photographic magnitudes are not the same, the difference between the two systems should be slight and is, in any case, dominated by uncertainties in the distance modulus for the cluster galaxies.

Figure 8.7 shows the number distribution of absolute magnitudes for the Sa – Sab galaxies in the two samples. The cluster galaxies are in the lower panel and with a dashed line. Stippled boxes signify cluster emission-line galaxies. The mean absolute magnitude and standard deviation for the field galaxies is -21.09 ± 0.73, while for cluster galaxies the mean absolute magnitude is -20.54 ± 0.61. There is no significant difference between the two samples.

We obtain similar results when the absolute magnitudes for field and cluster Sc – Irr galaxies are compared, as in Figure 8.8. The mean absolute

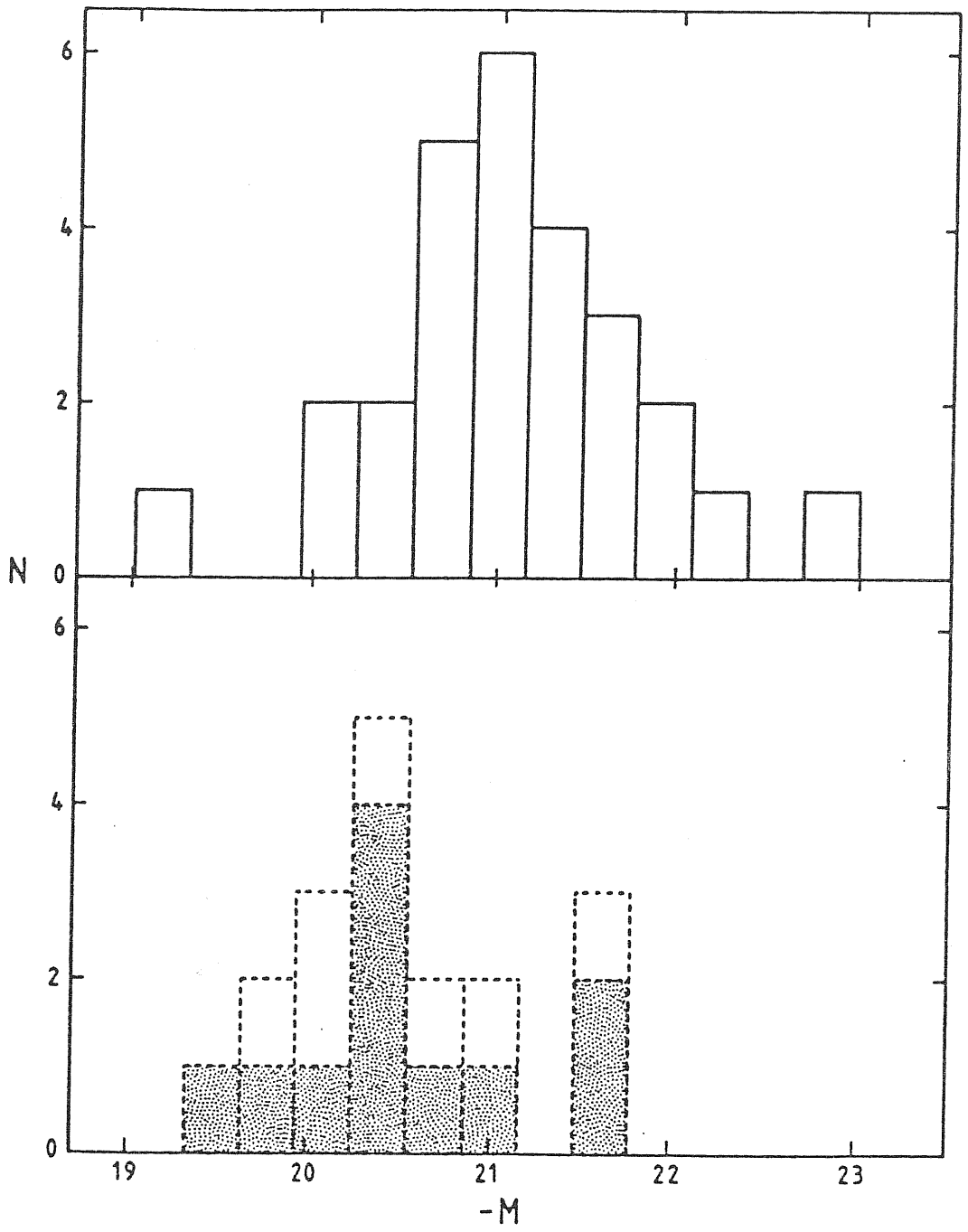

Figure 8.7: A comparison of the absolute blue magnitudes for the sample of Sa – Sab field galaxies (from Kennicutt & Kent 1983) taken from the RSA and the absolute photographic magnitudes of the cluster Sa – Sab galaxies. The number distribution of the absolute magnitudes for field galaxies is shown in the upper panel and that for cluster galaxies is shown in the lower panel, with the dashed line. Stippled boxes signify cluster emission-line galaxies.

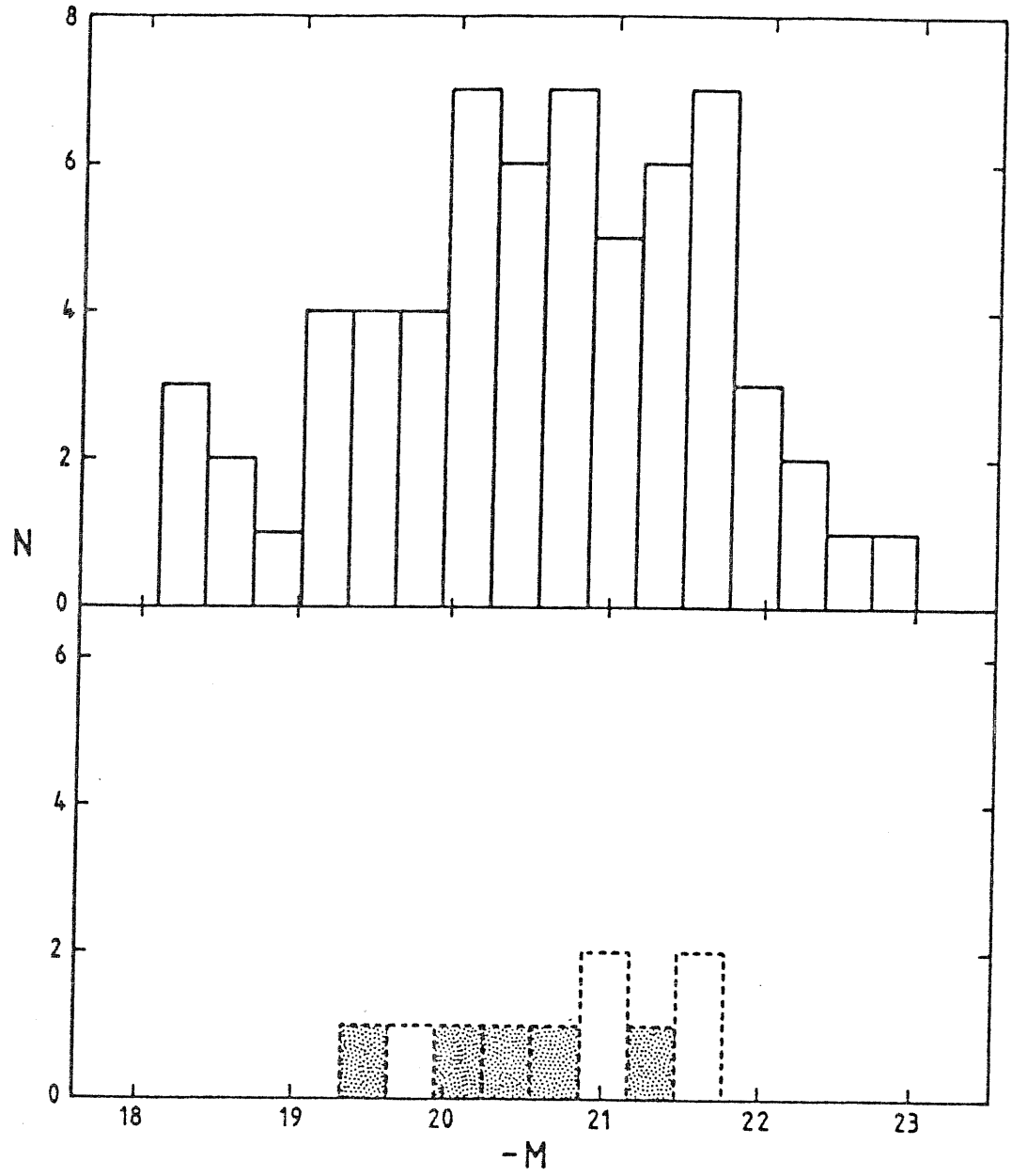

Figure 8.8: A comparison of the absolute blue magnitudes for the sample of Sc – Irr field galaxies (from Kennicutt & Kent 1983) taken from the RSA and the absolute photographic magnitudes of the cluster Sc – Irr galaxies. The number distribution of the absolute magnitudes for field galaxies is shown in the upper panel and that for cluster galaxies is shown in the lower panel, with the dashed line. Stippled boxes signify cluster emission-line galaxies.

magnitude for the field galaxies is -20.52 ± 1.09 and for the cluster galaxies, -20.69 ± 0.71. Therefore, the assumption that we can compare the two samples fairly, in regard to absolute magnitude at least, is valid.

8.2.2 MORPHOLOGICAL TYPE CLASSIFICATIONS

Another factor which might possibly lead to the results discussed above in Section 8.2 is the misclassification of morphological types. In order to determine if galaxies have been misclassified in the present study, types are compared to galaxy types from the study of Moss & Whittle (1991).

Table 8.4 shows the morphological classifications from the present study in the rows and those from Moss & Whittle in the columns. The numbers indicate the number of galaxies given each type by both studies. Exact agreement would cause all galaxies to lie on the diagonal line from upper left to lower right. The agreement between the classifications from the two independent studies is good and hence we do not expect that serious misclassification has caused the results discussed above.

8.2.3 TRANSFORMATION OF MORPHOLOGICAL TYPE

Cluster Sa – Sab spirals may really be Sb – Sbc galaxies that have been modified by the cluster environment to look like Sa – Sab galaxies. In fact, the *cluster* Sa – Sab galaxies, when compared to the *field* Sb – Sbc galaxies are **not** significantly different than the field galaxies. This hypothesis is discussed below on page 135.

Table 8.4: Comparison of morphological type classifications.

P \ MW	E	E – S0	S0	S0 – a	Sa	Sab	Sb	Sbc	Sc	Scd	Sd	Irr
E	4	3	1									
E – S0		11	5									
S0			22	1								
S0 – a			12	8	1							
Sa			6	2	10							
Sab					2	2		1				
Sb			2		2	2	10	1				
Sbc					1	1	2	1	2	1		
Sc										3		
Scd											1	
Sd												
Irr								1				

8.3 Discussion

For the sample of emission-line galaxies in the cluster, early-type galaxies Sa – Sab exhibit *more* emission and late-type galaxies, Sc – Irr, exhibit *less* emission when compared to a similar sample of field galaxies. This finding is in agreement with Moss (1988). In addition, these results appear to be real and not an effect of magnitude differences between the two samples or misclassification of galaxy morphological types.

Less emission in late-type galaxies compared to the field galaxies of the same type can be explained by the fact that these galaxies have been stripped of their interstellar gas. Stripping could be expected to affect a late-type galaxy more than a galaxy of earlier type since the gas is less tightly bound. However, the explanation for enhancement of emission in early-type spirals is more problematic. To reiterate, we observe a pronounced enhancement of Hα emission for early-type, Sa – Sab, galaxies when compared to field Sa – Sab galaxies. The enhancement might be explained by ram pressure effects (*i.e.*, interactions between the intracluster gas and the galaxies; *cf.* Chapter I, Section 1.4.1). Another, attractive hypothesis is that interactions between galaxy and cluster or galaxy and galaxy may explain our observations. Such interactions are discussed in the sections that follow.

8.3.1 GALAXY–CLUSTER INTERACTIONS: TIDAL EFFECTS

Byrd & Valtonen (1990) find that cloud – cloud collisions within a galaxy, due to tidal interaction between galaxies and the cluster field, are much more effective at inducing clouds to collapse and, therefore triggering star formation, than are ram pressure effects of the intracluster medium. This

is because the intracluster medium is thin compared to the internal density of molecular clouds. The greatest effects of interactions with the intracluster medium would be the removal of gas from the outer disk and halo of a spiral galaxy, while tidal perturbations would create both disk and nuclear activity.

The tidal field of a cluster should have effects on gas-rich spirals. Such spirals venturing to within several core radii of the centre of the cluster ($\sim$ 800 kpc) should be triggered into activity (nuclear inflow and disk star formation).

8.3.2 GALAXY–GALAXY INTERACTIONS

Many workers (*e.g.* Toomre & Toomre 1972; Eneev, Kovlov & Sunyaev 1973) have shown that when galaxies experience grazing encounters (more common than the direct Spitzer–Baade encounters, *cf.* Chapter I, Section 1.4.1) and when the encounter velocity is of the same order as the maximum rotational velocity (*i.e.*, 200 – 300 km s^{-1}) then loops and streamers of gas and stars are liberated and significant tidal distortions occur.

Galaxies with nearby companions possess significantly higher *nuclear* emission line luminosities and equivalent width and their nuclei exhibit significantly higher levels of ionization, on average, according to a study by Kennicutt & Keel (1984). Tidal disruptions of the disk during a close encounter may drive the gas into the nuclear regions and either fuel nuclear activity directly or lead to a burst of star formation within the inner nuclear disk (Byrd *et al.* 1986; Noguchi 1988; Byrd & Valtonen 1990).

In a sample of 13 isolated spirals and 13 interacting pairs, CO (2.6μm line) and *IRAS* observations by Young *et al.* (1986) showed that while the interacting and field galaxies have similar H_2 mass and molecular gas content, L_{IR}/L_B ratios are greatly enhanced in the interacting population. If infrared

luminosity is a measure of star formation rates and if CO luminosity is a measure of the mass of molecular hydrogen, then the ratio, L_{IR}/M_{H_2}, reflects the globally averaged star formation efficiency (SFE). The mean SFE is 12 $L_\odot/M_\odot$ in isolated galaxies but 78 $L_\odot/M_\odot$ in the interacting systems of the study. The authors suggest that galaxy interactions may cause new star formation mechanisms to operate such that more stars form per unit mass of molecular gas, or, physical processes of star formation may be the same but interactions enhance the efficiency. Because cloud–cloud collisions increase due to interactions, SFE is expected to increase if cloud–cloud collisions are responsible for massive star formation.

Bushouse (1986) finds that the vast majority of his sample of violently interacting spirals show emission that can be classified as arising from H II-like regions (as opposed to a Seyfert or LINER classification). The emission, therefore, represents normal star formation activity. He cautions that while galaxy–galaxy interactions can lead to enhanced levels of star formation activity, this is not true in all cases.

In a later study of global star formation rates from the Hα luminosity, Bushouse (1987) reports that Hα emission (and, hence, the current star formation rate) is heavily concentrated near the nuclear regions of most of the interacting galaxies. Interaction induced star formation usually does not follow the same pattern as pre-interaction star formation activity, but preferentially occurs in and around the nuclear regions of a galaxy. Modest disk enhancements of the star formation rate may also occur. In this sample of interacting galaxies, global star formation rates derived from Hα emission are, on average, a factor of 2.5 times higher than for isolated galaxies and star formation rates derived from infrared luminosity are 6 times higher. Emission from Hα in interacting galaxies is confirmed by Moss (1988) and by Laurikainen & Moles

(1989) who find the global star formation rate for interacting spirals higher than for field galaxies, with the activity concentrated toward the central parts of the galaxies.

Kennicutt *et al.* (1987) used Hα and far-infrared observations of interacting spiral and irregular galaxies to assess the influence of the interactions. Emissions from Hα and far-infrared are enhanced in interacting systems but the degree of the enhancement varies enormously. Variations indicate that the induced star formation is sensitive to the kinematic properties of the interaction and the ambient properties of the galaxy disks.

In most of the interacting galaxies the nuclear contribution to the integrated flux is small (13 per cent on average) and hence integrated emission is dominated by disk star formation. However, the nucleus appears to be more sensitive to interactions than the disk. Kennicutt *et al.* find no correlations between disk and nuclear emission. *Therefore, observations of the nuclear regions* **alone** *do not tell us anything about the global star formation rates.*

The difficulty with galaxy–galaxy interactions is that the relatively high velocity dispersion in clusters does not allow such interactions to be significant. Moss (1988) has shown, however, that disturbed galaxies and those of a given Hubble type but also noted as being peculiar in the two clusters he studied can be separated into pairs and small groups with low relative velocity dispersions, although the velocity dispersion of the whole sample is high. Clumping and subclustering may be necessary for galaxy–galaxy tidal interactions to occur.

White (1976), with an N-body simulation of cluster formation, found that extensive and inhomogeneous subclustering during early stages of the model would provide a natural explanation for the lumpy distribution of galaxies in systems like the Virgo cluster. Similarly, Roos & Norman (1979), with

their N-body simulation, found that multiple mergers can be found in subclumps that form before the collapse of the cluster and afterwards in the central regions of the cluster. That is, subclustering does occur and appears to be a common consequence of the formation process of a cluster.

8.3.3 DISTURBED GALAXIES

Clues to whether ram pressure or interaction effects are operating may be provided by the appearance of a galaxy. Ram pressure affects the gas of a galaxy only and does not necessarily lead to a change in appearance. On the other hand, tidal encounters will affect the stars and cause a galaxy to appear disturbed in some way (the classic examples being the galaxies studied by, for example, Toomre & Toomre 1972).

With this in mind, we compare the Hα emission with the appearance of galaxies for types Sa and later. Moss & Whittle (1991) classify the appearance of galaxies in their sample from undisturbed through varying degrees of disturbance. These classifications are used here, for our sample of spirals, but we only consider the galaxies to be either disturbed or not. Not included in the analysis are galaxies classified only as 'peculiar' since it is difficult to tell if they are disturbed or not.

To test whether undisturbed galaxies have predominantly large, diffuse emission regions and disturbed galaxies have small, compact emission regions we first compare the number of emission- and non-emission-line galaxies that are disturbed and undisturbed, in Table 8.5. There is no difference between undisturbed and disturbed galaxies.

Table 8.5: Disturbance and emission in galaxies.

	Disturbed	Undisturbed
Emission-line galaxies	6	9
Non-emission-line galaxies	6	9
Per cent emission-line galaxies	50%	50%

Table 8.6: Disturbance and emission in galaxies with VC, C or normal emission.

	Disturbed	Undisturbed
Emission-line galaxies (VC,C or —)	4	5
Non-emission-line galaxies	6	9
Per cent emission-line galaxies	40%	36%

Now consider two categories of emission-line galaxies, those with compact or diffuse emission regions. We define compact emission regions as exhibiting VC, C or normal emission and diffuse regions as exhibiting VD or D emission. Table 8.6 gives the number of non-emission- and emission-line galaxies, with emission categorized as VC, C or normal, that are disturbed and undisturbed. The numbers of emission-line galaxies with VD and D emission are given in Table 8.7. Again, our results are the same. There is no difference between disturbed and undisturbed galaxies (for emission-line galaxies with VC, C or normal emission, a Fisher test gives $p = 0.32$, while for emission-line galaxies with VD or D emission $p = 0.37$).

We can also define compact and diffuse emission based on the size of the emission region. Accordingly, Table 8.8 gives the number of non-emission-

Table 8.7: Disturbance and emission in galaxies with VD or D emission.

	Disturbed	Undisturbed
Emission-line galaxies (VD or D)	2	4
Non-emission-line galaxies	6	9
Per cent emission-line galaxies	25%	31%

Table 8.8: Disturbance and emission in galaxies with $d_e/D \leq 0.37$.

	Disturbed	Undisturbed
Emission-line galaxies ($d_e/D \leq 0.37$)	2	3
Non-emission-line galaxies	6	9
Per cent emission-line galaxies	25%	25%

and compact emission-line galaxies, those with $d_e/D \leq 0.37$, that are disturbed and undisturbed. Table 8.9 shows the numbers for diffuse ($d_e/D > 0.37$) emission-line galaxies. There are no significant differences between disturbed and undisturbed galaxies; for compact emission the Fisher test gives $p = 0.40$, and for diffuse emission $p = 0.32$.

A further test was performed by comparing d_e/D with the measure of emission concentration for two groups, galaxies with concentrated emission (VC, C and normal) and diffuse emission (VD and D), shown in Table 8.10. A Fisher test indicates no significance between the two groups and d_e/D ($p = 0.15$).

These results do not show an expected correlation of emission and

Table 8.9: Disturbance and emission in galaxies with $d_e/D > 0.37$.

	Disturbed	Undisturbed
Emission-line galaxies ($d_e/D > 0.37$)	4	6
Non-emission-line galaxies	6	9
Per cent emission-line galaxies	40%	40%

Table 8.10: Concentration and emission-region size.

	$d_e/D \leq 0.37$	$d_e/D > 0.37$
VC, C normal	5	4
VD, D	1	5

emission size with disturbance. Such correlations have been seen by other workers (*e.g.* Moss 1988). The numbers in the present analysis are, however, too small to make any significant statement regarding disturbance and emission.

Finally, Figure 8.9 shows a comparison between field galaxies (from Kennicutt & Kent 1983) and cluster galaxies categorized as disturbed. Figure 8.10 shows the same comparison but for undisturbed cluster galaxies. Although the numbers are small for disturbed galaxies, early-type galaxies in the cluster exhibit more emission than field Sa – Sab galaxies while the other galaxy types in the cluster are not significantly different than their counterparts in the field (χ^2 and significance levels for Sa – Sab, Sb – Sbc and Sc – Irr are, 34, 0.3 and 0.03; $< 5 \times 10^{-4}$, 0.59 and 0.85, respectively). The undisturbed sample is similar to the sample as a whole (*cf.* Figure 8.6) in that

early-type cluster galaxies exhibit more emission ($\chi^2 = 9.2$, $p = 3 \times 10^{-3}$) and late-type cluster galaxies exhibit less emission than galaxies of similar types in the field ($\chi^2 = 6.3$, $p = 1.2 \times 10^{-2}$).

These results and those in Section 8.2 are consistent with Elmegreen *et al.* (1990) who find that barred, binary systems are predominantly of early type (77 per cent) compared with unbarred galaxies in all environments (44 per cent). Based on N-body simulations, these authors conclude that galaxy interactions, because of their torques, lead to bar formation and a significant mass inflow from the disk. They suggest that for a prolonged encounter, the mass inflow can *change an unbarred spiral galaxy of intermediate type, Sbc - Scd, into a barred galaxy of early type, SBa - SBb*, by making the galaxy density larger in the inner regions and by removing a significant amount of the gas mass, and hence star formation, from the outer disk. Thus, **interactions may be transmuting Sb galaxies into Sa galaxies in the cluster** *and* **enhancing star formation in the process** (since merely changing an Sb galaxy into an Sa galaxy, which would normally have *less* star formation, would not match our observations).

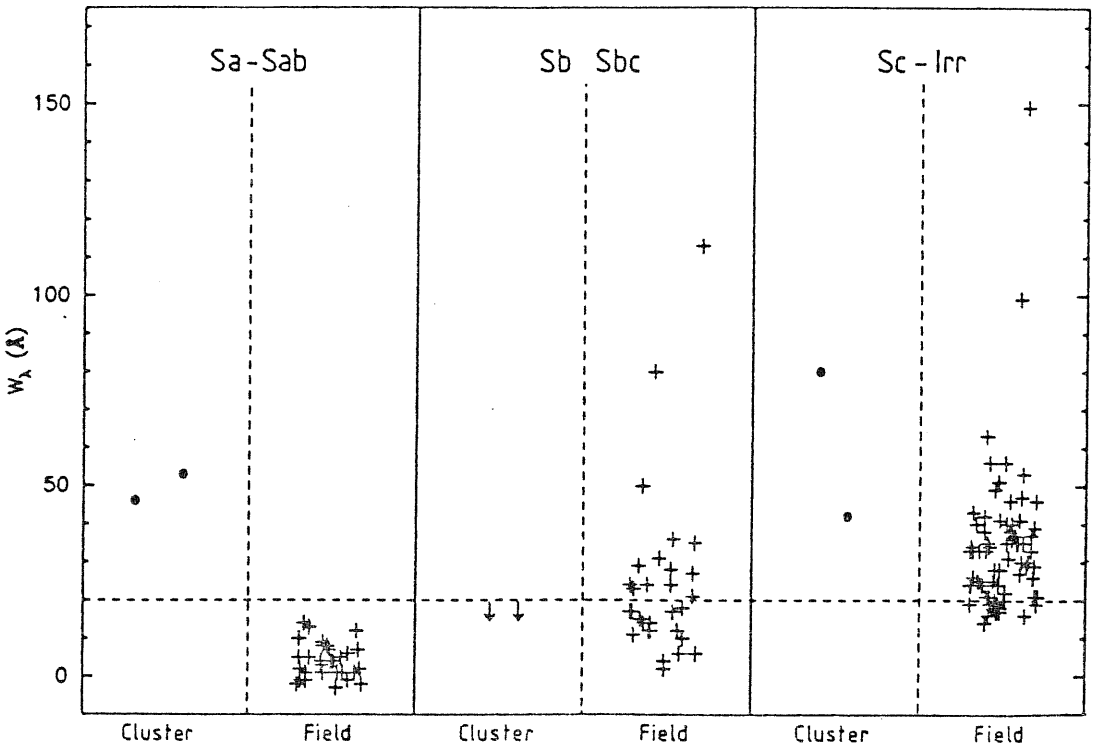

Figure 8.9: A comparison of Hα equivalent width distributions for field galaxies (from Kennicutt & Kent 1983) and disturbed cluster galaxies. The horizontal, dashed line indicates the 20 Å equivalent width cutoff. Arrows indicate upper limits for non-detected galaxies. Cluster galaxies are marked with filled circles and field galaxies are marked with crosses. Galaxies classified as 'S...', 'S pec' or 'pec' have not been included.

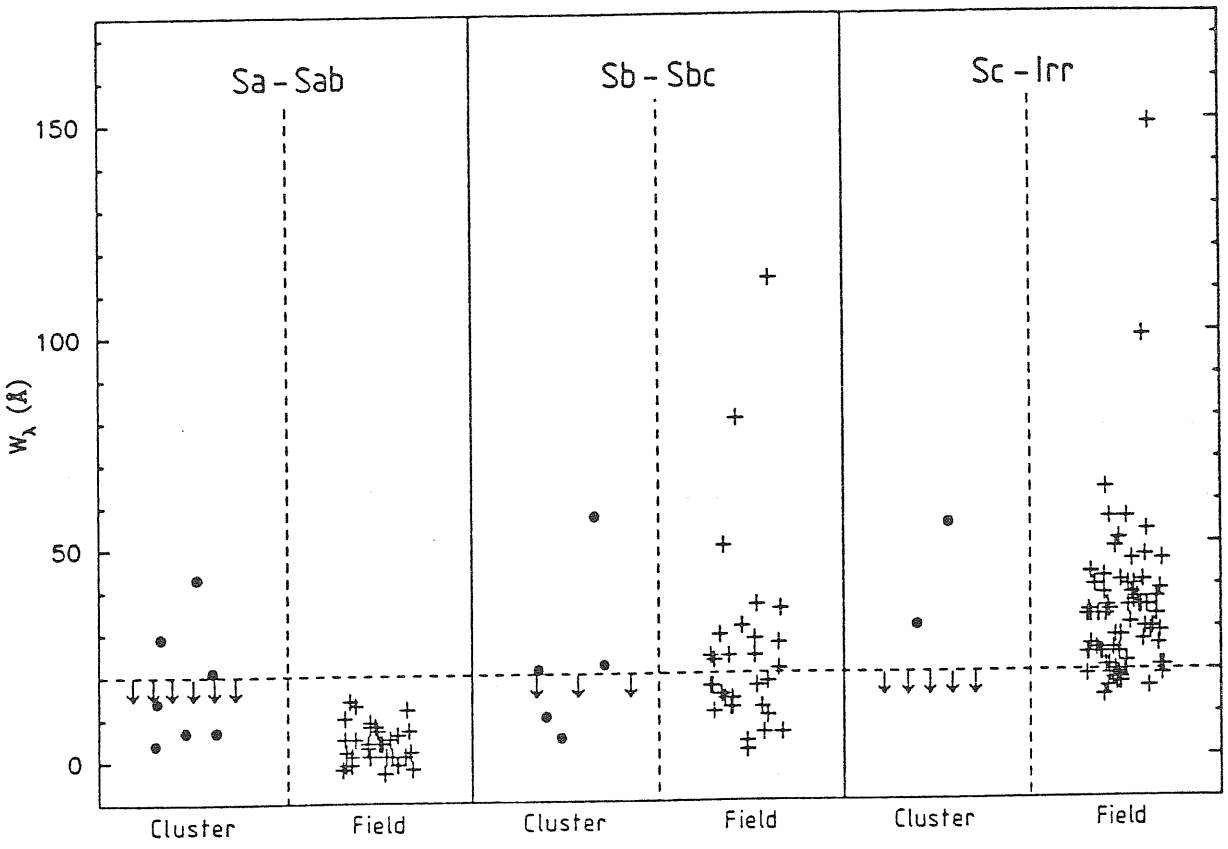

Figure 8.10: A comparison of Hα equivalent width distributions for field and undisturbed cluster galaxies. See Figure 8.9 for a description of the symbols.

CHAPTER IX

Conclusions

As postulated by MWI, the objective prism/filter combination provides a useful means for surveying entire clusters of galaxies for emission in individual galaxies. MWI employed the Burrell Schmidt telescope on Kitt Peak equipped with a 10° objective prism and a circular RG 630 filter. The present analysis uses the same telescope equipped with a 2° + 4° and a square RG 645 filter. The latter system, with the lower dispersion prism, performs just as well as the former, or at least no worse. Seeing is, perhaps, the single most important factor in determining the quality of observations. The method can be employed for galaxies with velocity $\leq$ 12 000 km s^{-1}.

The emission survey also enables one to determine redshifts accurately (σ = 270 km s^{-1}, in the present study). Redshifts were determined for seven galaxies without previously measured redshifts. In addition, the 2° + 4° prism is found to have a dispersion of 780 Å mm^{-1} at the rest wavelength of Hα.

The irregular cluster Abell 1367 was surveyed for Hα emission in a total of 201 galaxies of which 177 are cluster members. Forty cluster members (or 23 per cent) exhibit Hα emission.

An objective prism survey for [OII] λ3727 Å emission was made for the first time. Seven galaxies (or four per cent) show emission. These galaxies are also the strongest Hα emitters, with an average Hα equivalent width of 80 Å compared to an average of 30 Å for the rest of the Hα emission-line

galaxies. Thirteen per cent of galaxies within one Abell radius exhibit [OII] emission compared to only four per cent beyond one Abell radius and most [OII] emission-line galaxies are classified as peculiar in addition to a given Hubble type (77 per cent compared to 65 per cent of the Hα emission-line galaxies and eight per cent of the non-emission-line galaxies). The numbers are too small in the present sample to make any definitive statements and more work needs to be done in order to determine the efficiency of the technique for detecting [OII] emission-line galaxies.

Fluxes and equivalent widths were measured for the sample of emission-line galaxies and these were found to be of comparable accuracy with the equivalent width and flux measurements obtained by other photographic methods (MWI) and photoelectrically (Kennicutt *et al.* 1984 and Gavazzi 1990). For the present analysis, the error on the log of the flux measurements is $\sigma_P = 0.18$, while for the for the Kennicutt *et al.* and Gavazzi samples and the MWI samples the errors are $\sigma_K = 0.17$ and $\sigma_M = 0.16$ (in units of erg cm^{-2} s^{-1}). Errors on equivalent widths for the present sample, the Kennicutt *et al.* and Gavazzi sample and the MWI sample are, $\sigma_P = 6$ Å, $\sigma_K = 10$ Å and $\sigma_M = 9$ Å, respectively. However, with a prism of relatively low dispersion, it was found to be rather difficult to fit continua precisely and, hence, to determine the equivalent widths easily. Detection limits for emission-line galaxies were found to be $W_\lambda = 20$ Å, $f = 2 \times 10^{-13}$ erg cm^{-2} s^{-1} and 3×10^{-12} erg cm^{-2} s^{-1} Å for the combined parameter, $f \times W_\lambda$, in agreement with the findings of MWI.

Emission-line galaxies were analyzed thoroughly to determine other properties of the Hα emission. The fraction of spirals in emission increases with decreasing Abell radii, although there is no correlation between position and Hα equivalent width. There is no correlation between emission and galaxy

magnitude. Although emission frequency may increase for later type galaxies, it is relatively constant (at about 40 per cent) for the three groups, Sa – Sab, Sb – Sbc and Sc – Irr.

In the present analysis we have observed several unexpected results. The first is that instead of leveling off at approximately 1.5 r_A as expected, the cumulative distribution of galaxies begins to increase, again, at this radius and then levels off at around 2.6 r_A. We believe that this is caused by subclusters in the periphery of Abell 1367. The other surprising observation is that galaxies with a given Hubble type but which appear peculiar as well follow the distribution of the elliptical and S0 galaxies, although the majority of them are peculiar spirals. Galaxies of other types behave as expected, with ellipticals and S0 predominating in the central regions and spiral galaxies spread relatively uniformly throughout the cluster.

The fact that we might be observing galaxies in subclusters instead of galaxies in the field, at large Abell radii, means that we may not be able to compare galaxies in the inner Abell radius with galaxies in the outer Abell radii. We have, therefore, defined a quantity, the "local galaxy density", which provides us with information regarding emission-line galaxies that is independent of any effects introduced by subclusters. The local galaxy density is the number of galaxies within 0.2 r_A radius of a given galaxy. For all spirals, Sa and later, there is an increase in the frequency of emission with increasing local galaxy density, although this increase is slight. There is a small tendency for emission-line galaxies with compact emission to be in high ($\geq$ 2) density regions while emission-line galaxies with diffuse emission are spread throughout the range of densities.

Using the equivalent width threshold of 20 Å, we compare cluster spiral galaxies with a sample of field spiral galaxies. In particular, early-type

Sa – Sab cluster galaxies exhibit more, strong emission and late-type Sc – Irr cluster galaxies exhibit less emission than similarly typed galaxies in the field. These observations appear to be real and are not due to differences in absolute magnitude between the two samples or misidentification of cluster galaxy morphological types. We take this to imply that the cluster environment has affected both types of cluster galaxies; by removing gas from the late-type galaxies and perhaps by causing morphological changes in the early-type galaxies.

The enhanced emission found in early-type spirals may be caused by tidal interactions rather than ram pressure effects. While ram pressure effects disrupt mainly gas, tidal interactions will disrupt stars and change the appearance of a galaxy. Hence, disturbed appearance in galaxies could be taken as a sign of tidal interactions. This study does not show convincing correlations between Hα emission and disturbed appearance or between the ratio of emission-region size and galaxy size and disturbance. Such correlations are seen in other studies. However, the numbers are small in the present study.

One attractive, alternative hypothesis has been proposed by Elmegreen *et al.* (1990) who suggest that interactions change unbarred spirals of intermediate types into barred spirals of early types. If interactions also enhance star formation in these early type galaxies, this hypothesis may account for our observations of more cluster Sa – Sab galaxies in emission when compared to similar galaxies in the field.

The present survey has a high detection threshold and our sample of emission-line galaxies is dominated by cluster spirals with strong star formation (*i.e.*, the minority). Earlier surveys using slit spectroscopy and large telescopes (Gisler 1978; Dressler, Thompson & Schectman 1985) have lower detections limits. Their samples are dominated by the majority of cluster spirals which

may have lower disk star formation rates. Therefore, it is not surprising that these surveys find fewer emission-line galaxies in the cluster than in the field, while our survey and other, similar ones (Kennicutt, Bothun & Schommer 1984; Moss 1988) find more spirals with very high star formation rates in the cluster than in the field.

Once again, to reiterate, the most important finding of this work is that early-type cluster spiral galaxies, Sa – Sab, exhibit **more** emission than field spirals of the same type. Conversely, late-type cluster spirals, Sc – Irr, exhibit **less** emission than late-type field spirals. The decreased emission in late-type spirals can be explained by the fact that they have less gas. However, it is more difficult to explain the enhanced emission in the early-type cluster spirals. While ram pressure effects may be causing enhancement of emission, we see no variations of emission with cluster position and there are strong emitters in the periphery of Abell 1367. These observations are not expected if ram pressure effects are operating.

Interactions may be the causes of enhanced emission, as well, but we have no evidence in the present analysis to suggest this. Disturbance, which may be the result of interactions, was not found to correlate with emission or emission size in our galaxies. However, our sample sizes are too small to make any definitive statement concerning disturbance and enhanced emission.

APPENDICES

APPENDIX A

2-D pixel Maps and Spectra

The following pages show the 2-D pixel maps (lower panel of each galaxy) and spectra (upper panel) of the 42 emission-line galaxies on plates A (left) and B (right), produced by scanning the plates with the Automatic Plate Measuring machine. Each pixel map is 384 pixels, in the dispersion direction, by 256 pixels. The spectra are summed perpendicularly to the dispersion direction over 30 – 120 pixels depending upon the width of the galaxy. The ordinate is arbitrary flux density units and the abscissa is in pixels. Emission lines, in those cases where there is ambiguity, are marked with arrows.

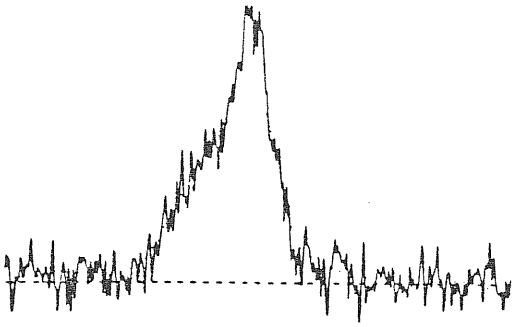

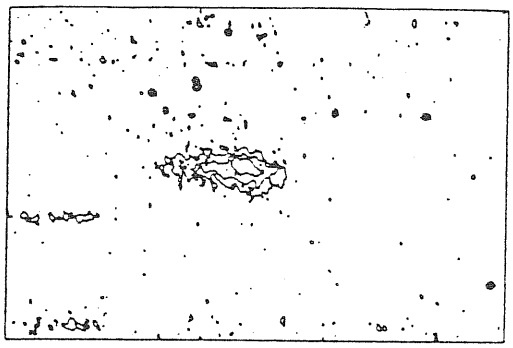

126.104: PLATE A

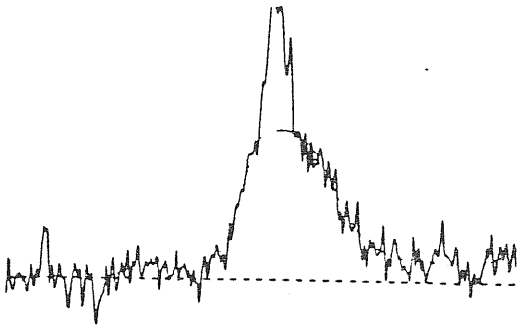

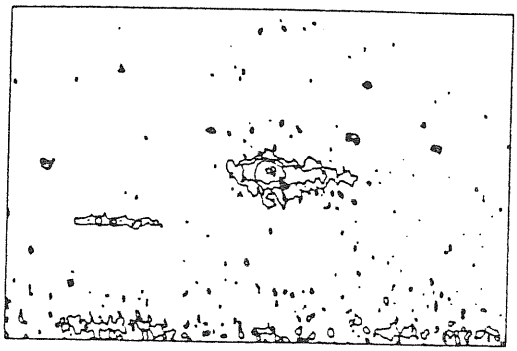

126.104: PLATE B

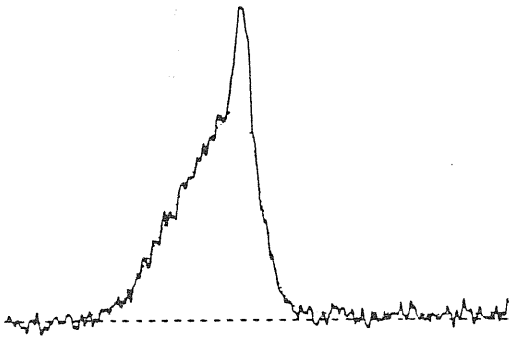

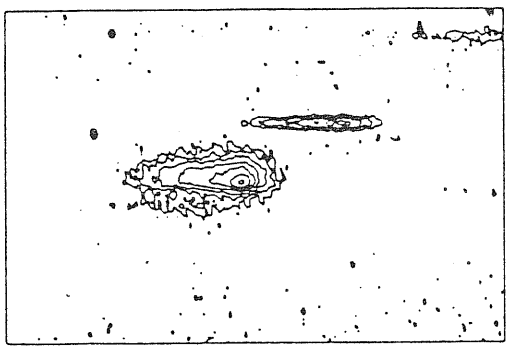

126.110: PLATE A

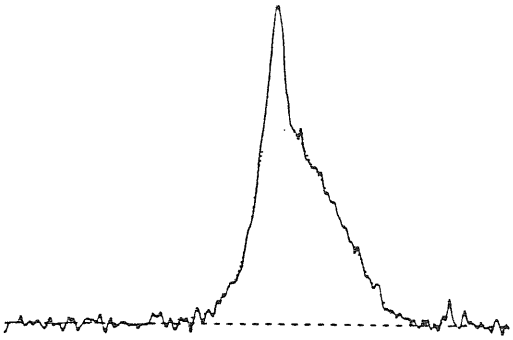

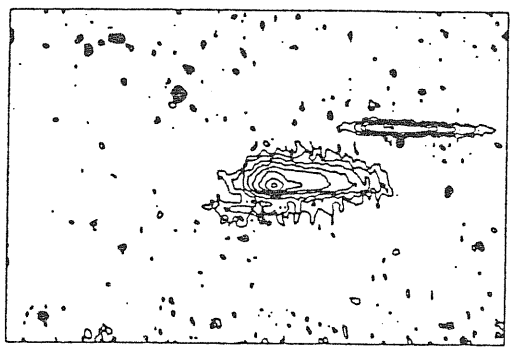

126.110: PLATE B

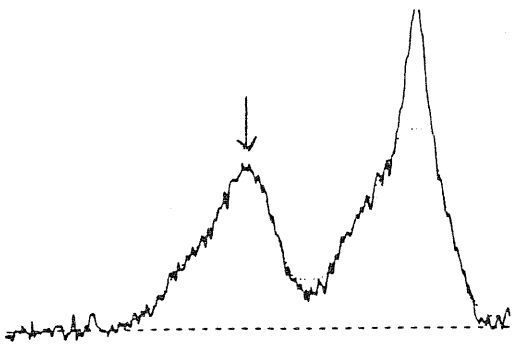

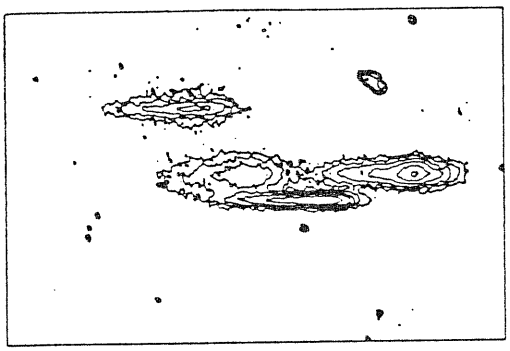

097.027: PLATE A

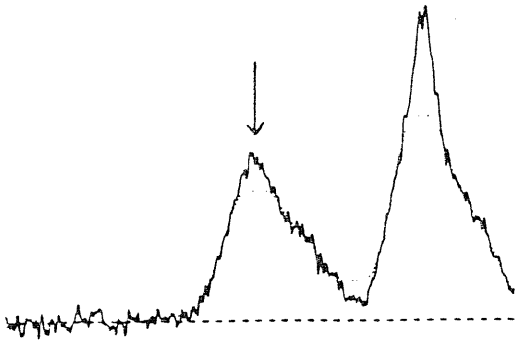

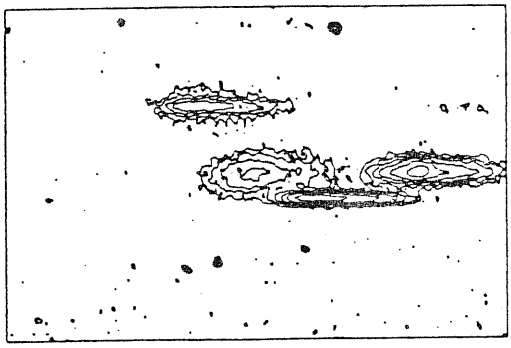

097.027: PLATE B

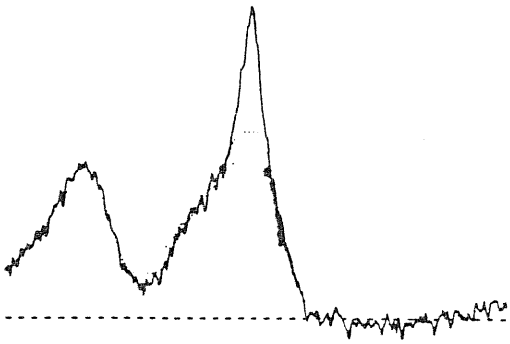

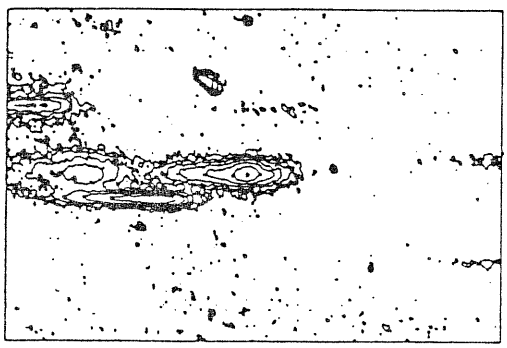

097.026: PLATE A

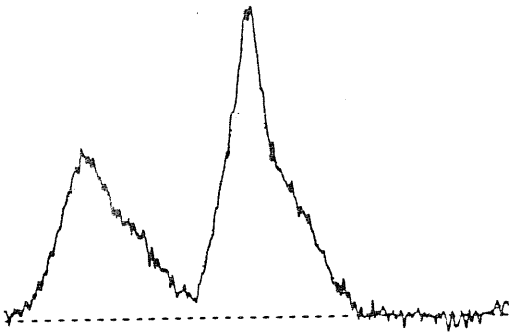

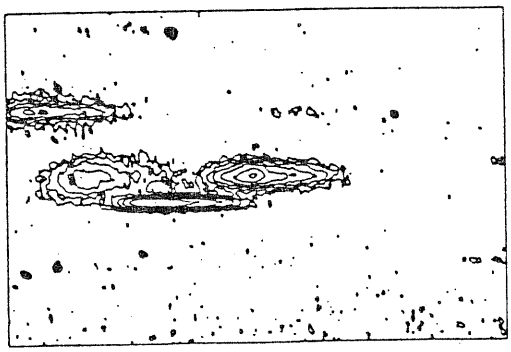

097.026: PLATE B

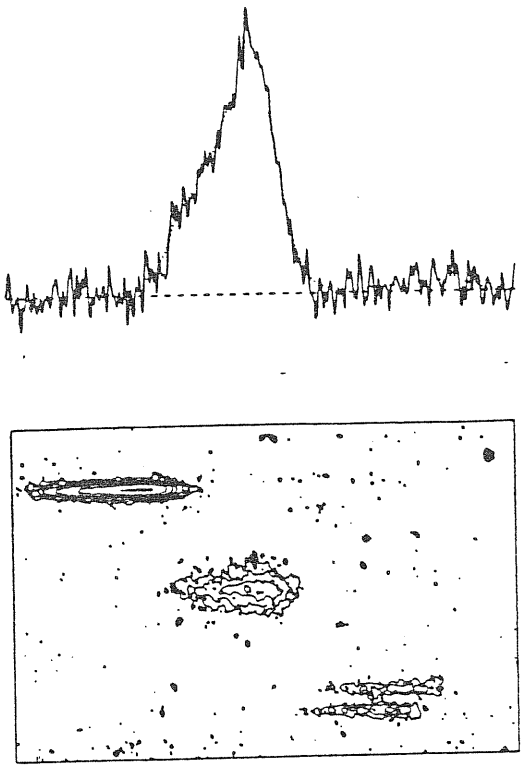

097.033: PLATE A

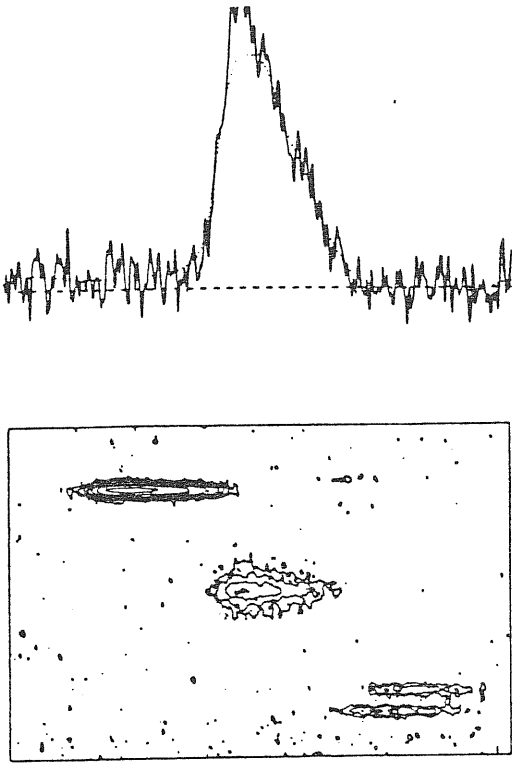

097.033: PLATE B

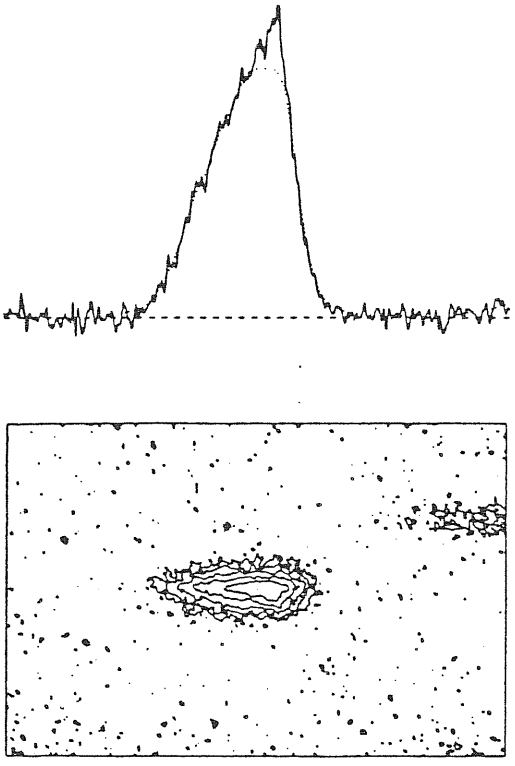

097.044: PLATE A

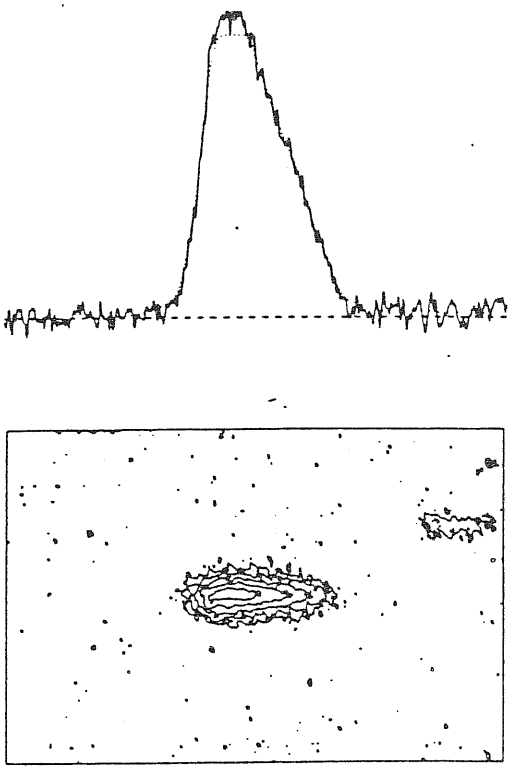

097.044: PLATE B

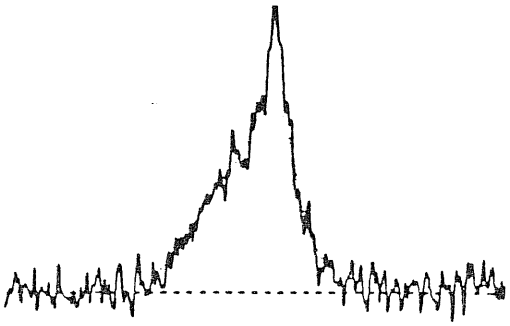

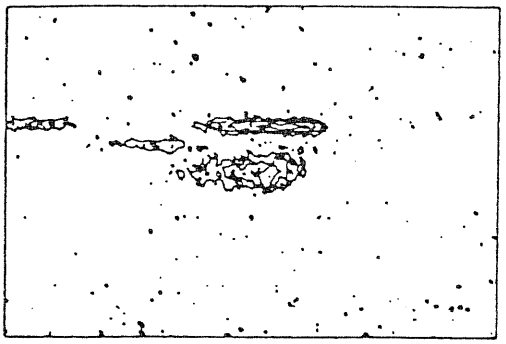

097.062: PLATE A

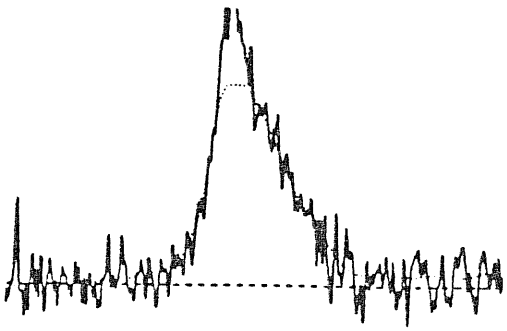

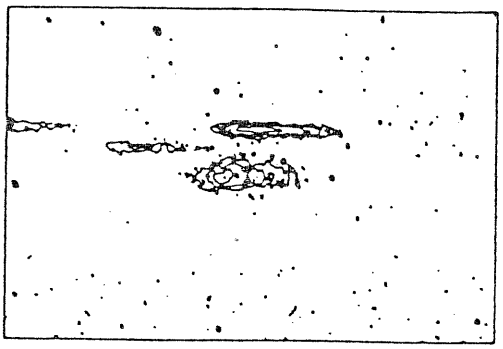

097.062: PLATE B

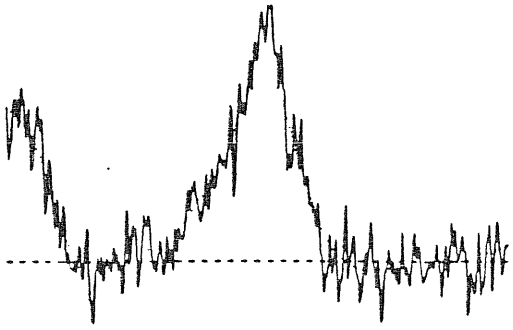

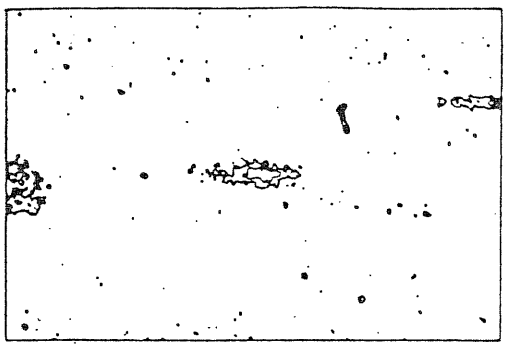

097.063: PLATE A

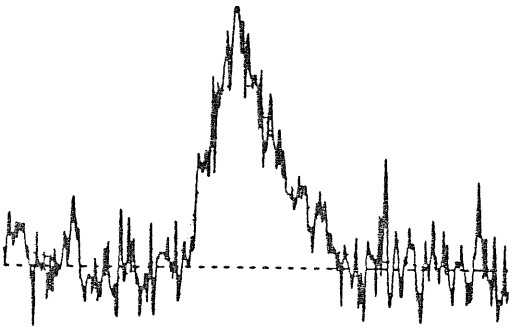

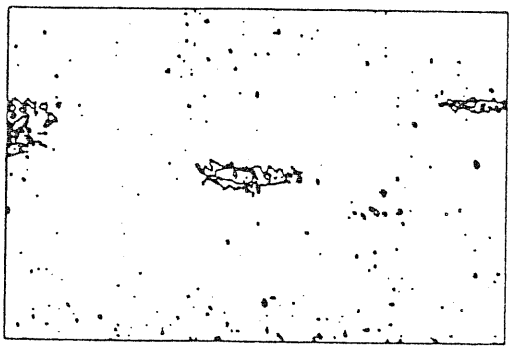

097.063: PLATE B

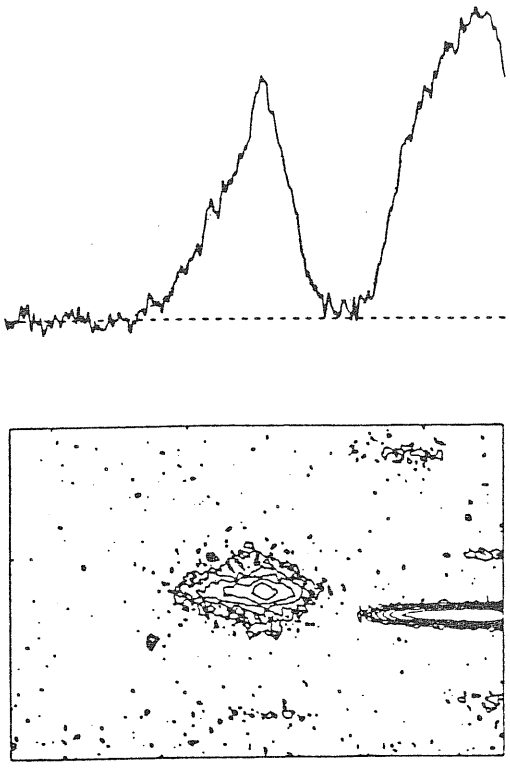

097.068: PLATE A

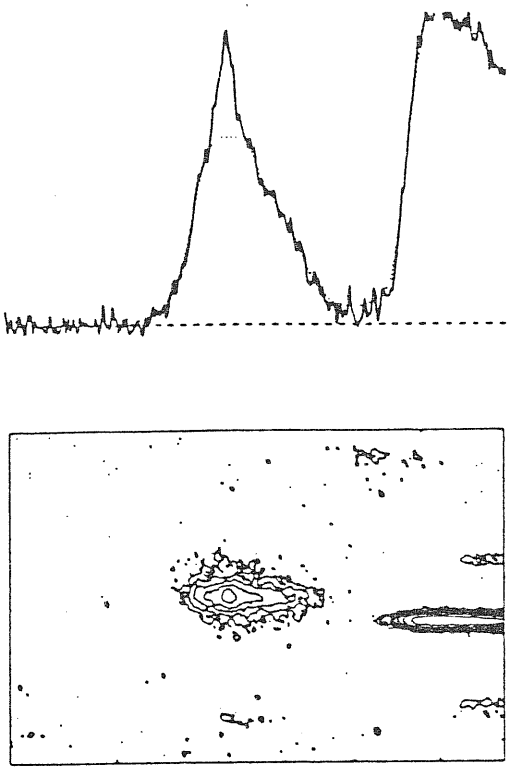

097.068: PLATE B

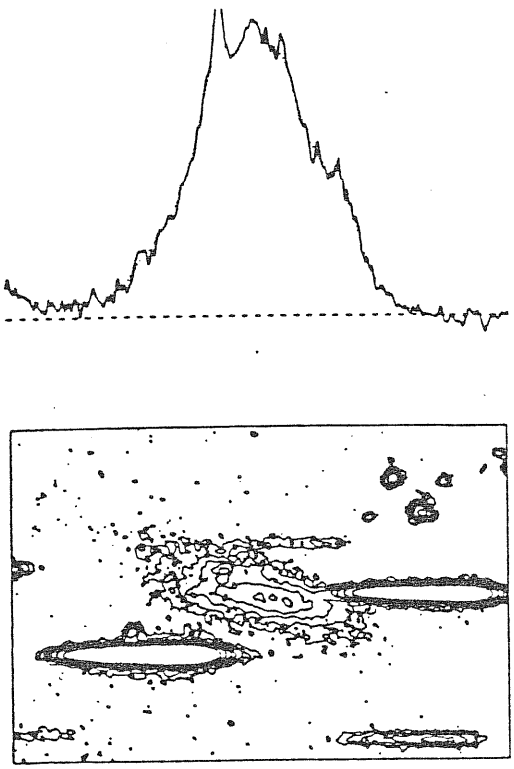

097.067: PLATE A

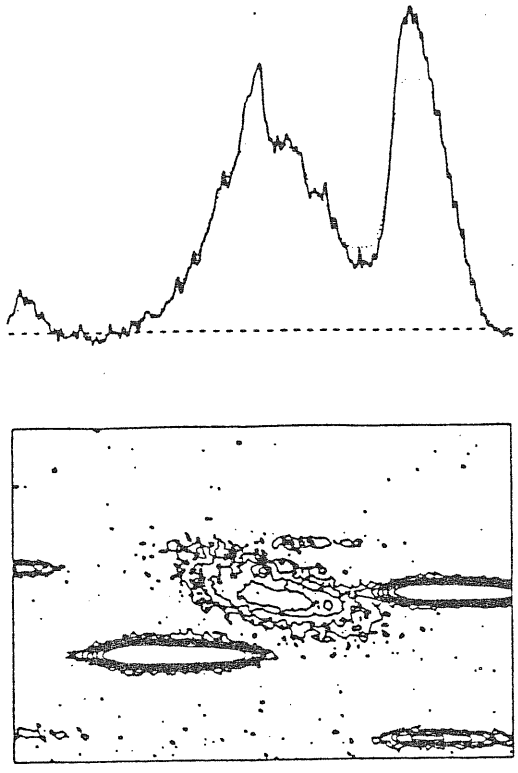

097.067: PLATE B

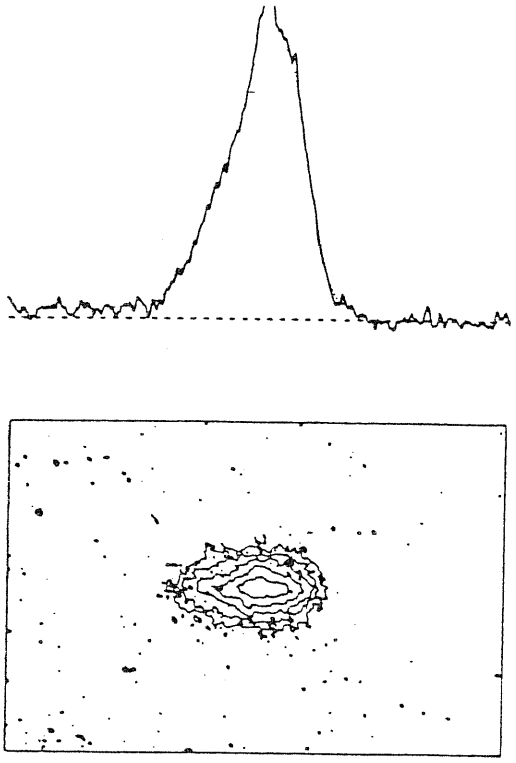

097.070: PLATE A

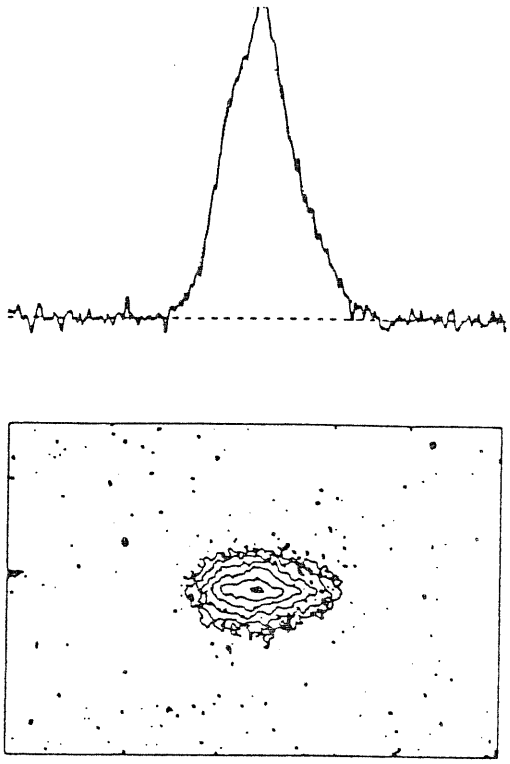

097.070: PLATE B

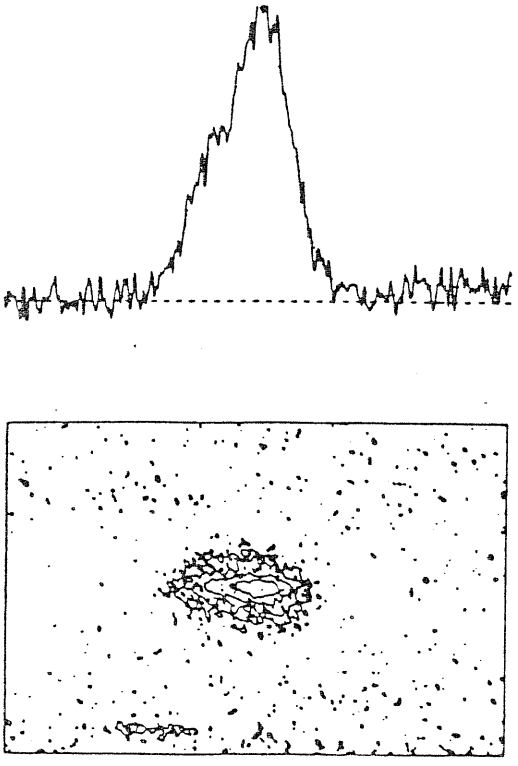

097.072: PLATE A

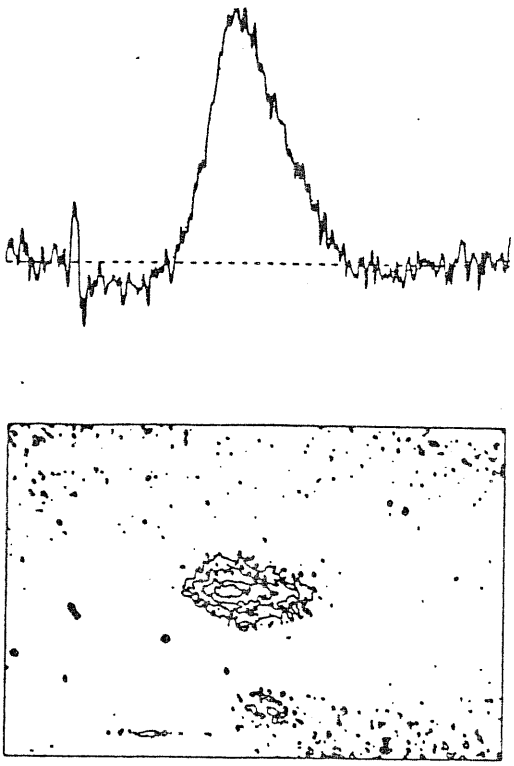

097.072: PLATE B

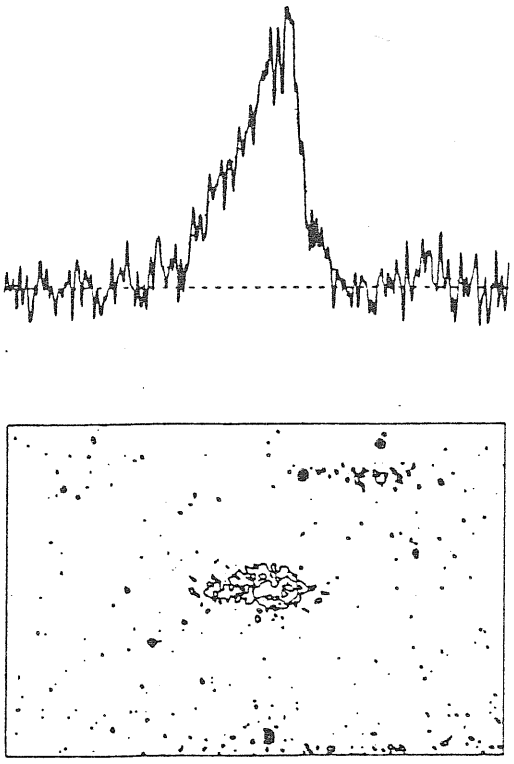

097.073: PLATE A

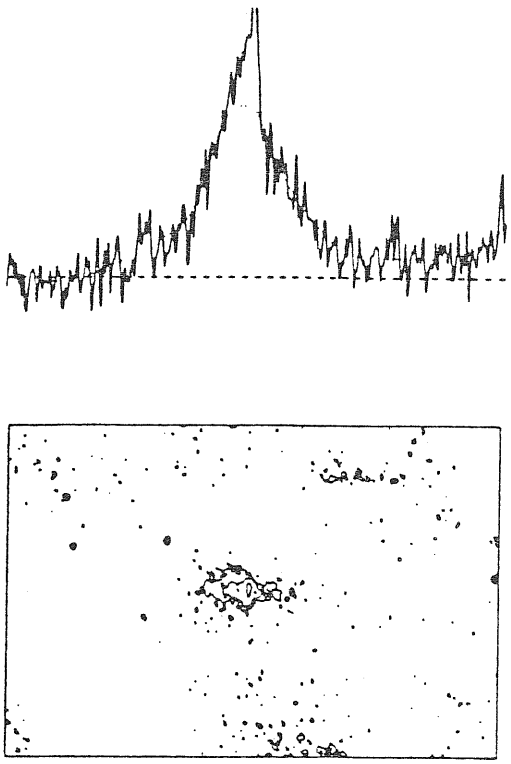

097.073: PLATE B

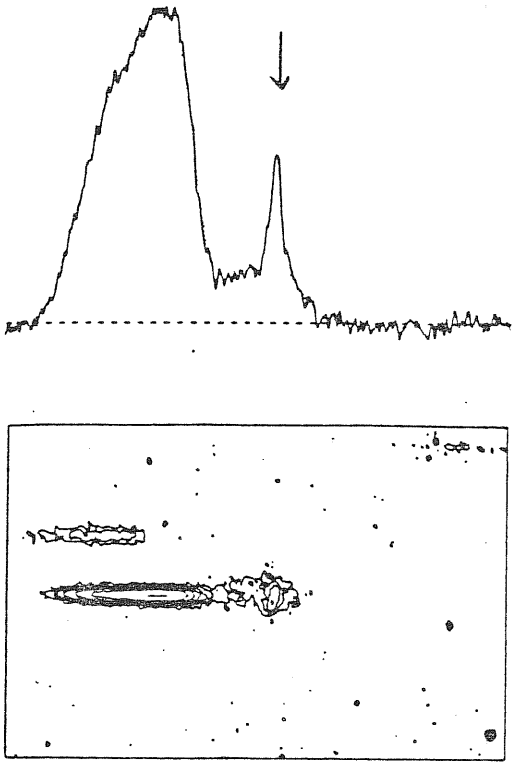

097.079: PLATE A

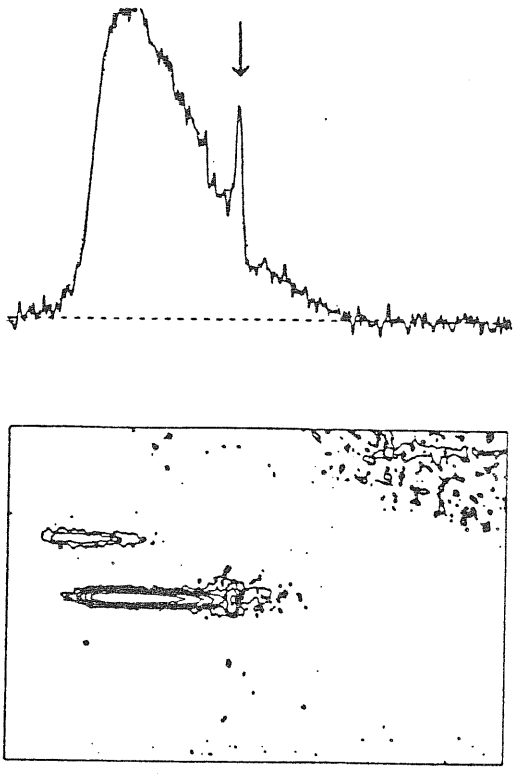

097.079: PLATE B

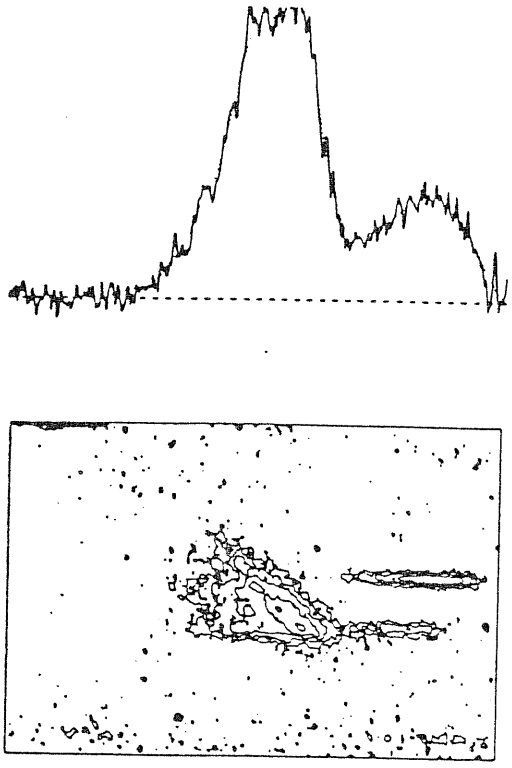

097.087: PLATE A

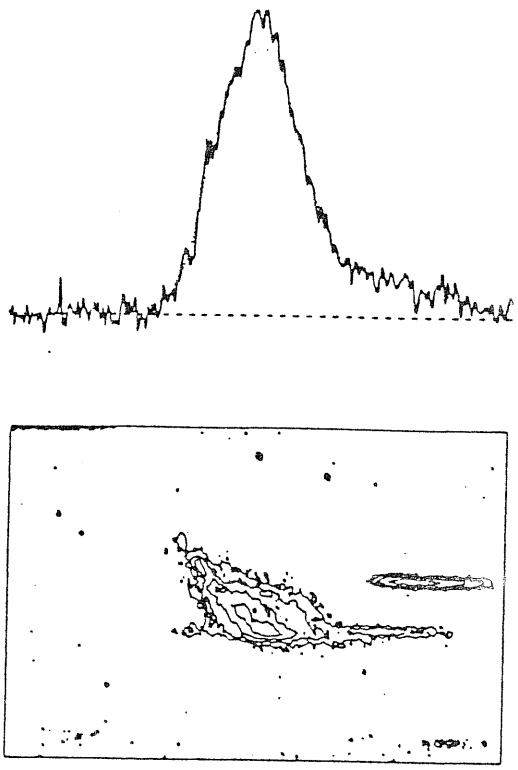

097.087: PLATE B

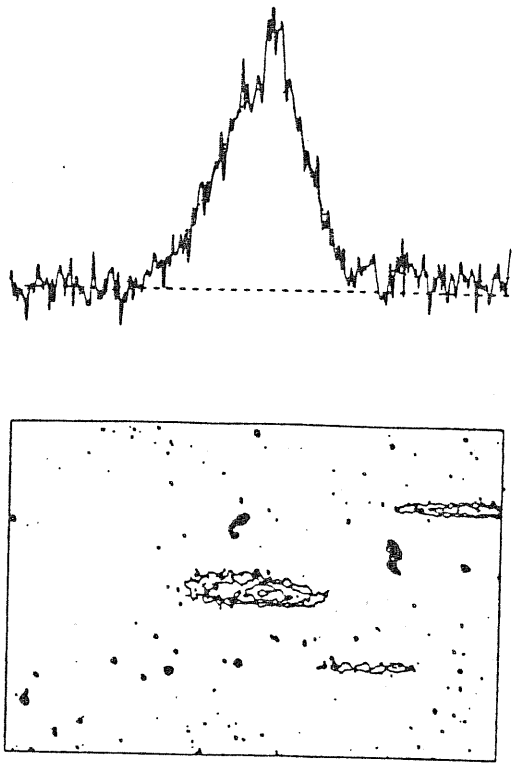

097.092: PLATE A

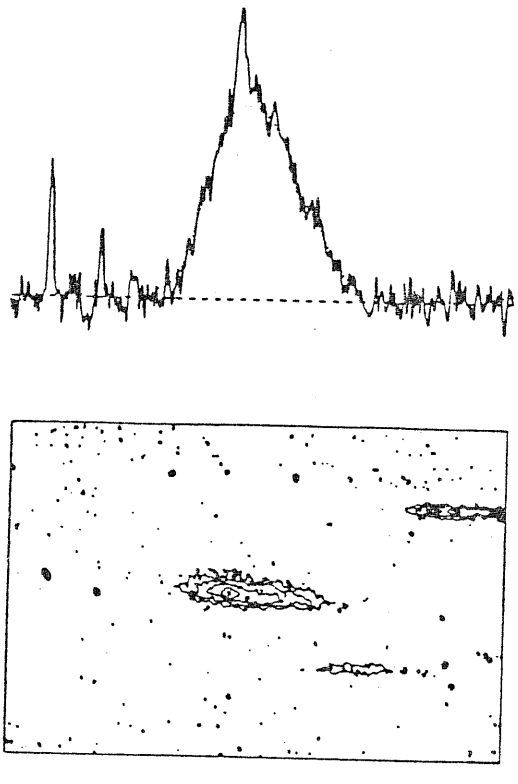

097.092: PLATE B

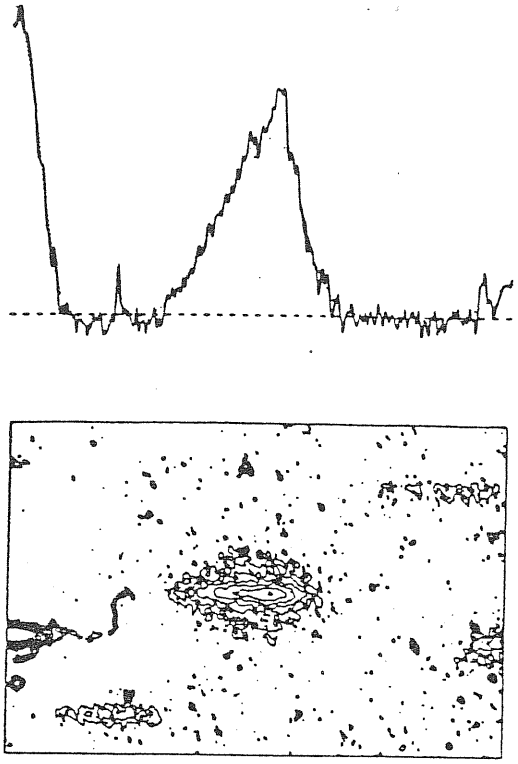

097.091: PLATE A

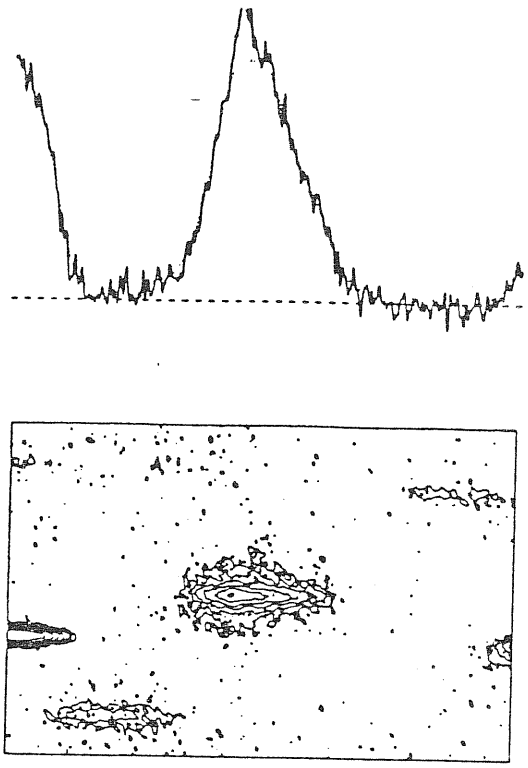

097.091: PLATE B

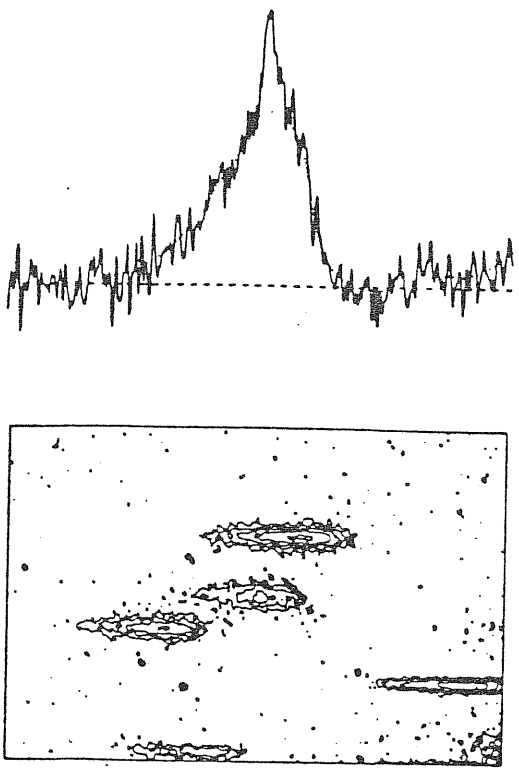

097.093: PLATE A

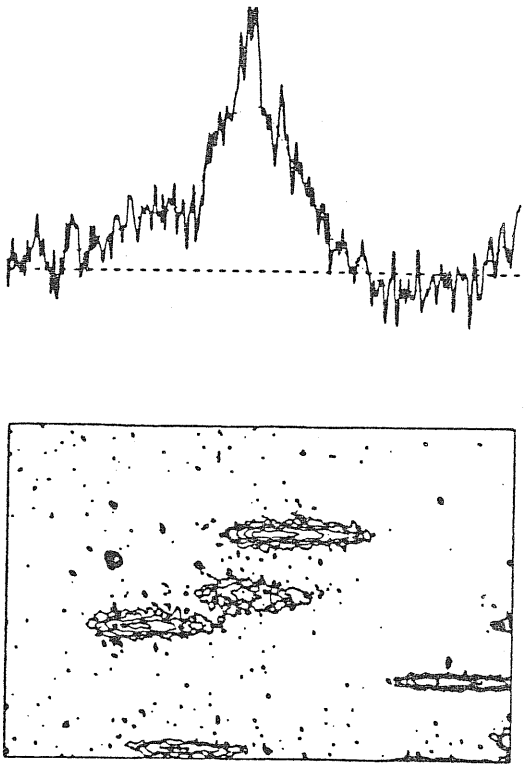

097.093: PLATE B

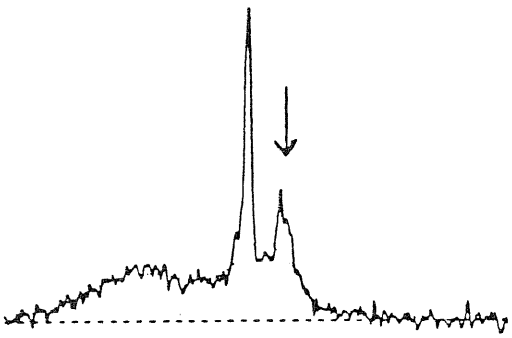

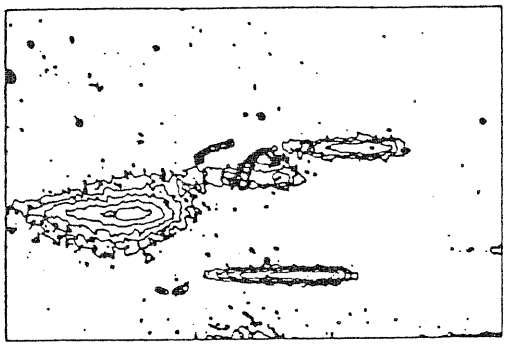

097.114: PLATE A

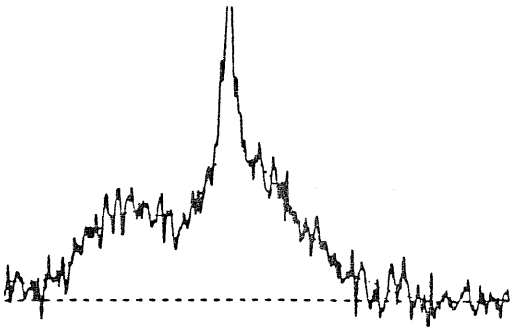

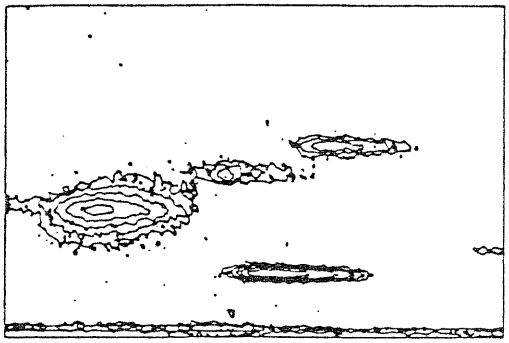

097.114: PLATE B

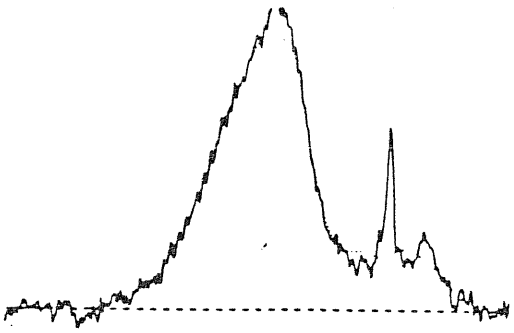

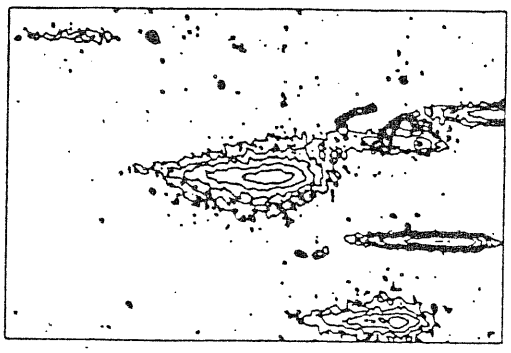

097.120: PLATE A

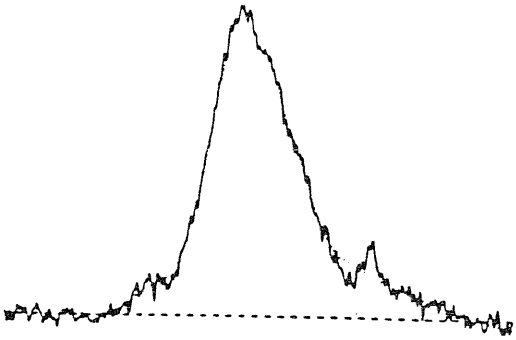

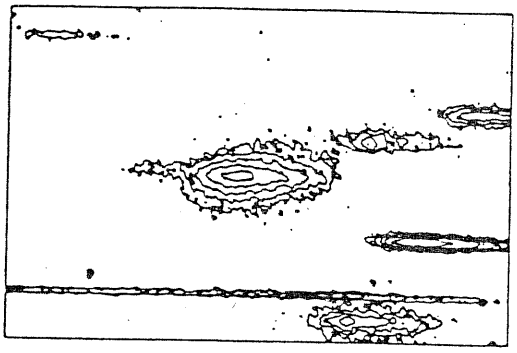

097.120: PLATE B

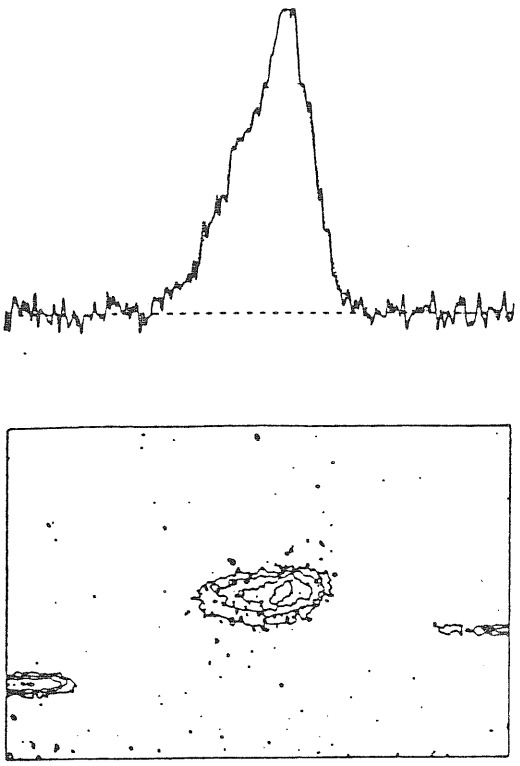

097.122: PLATE A

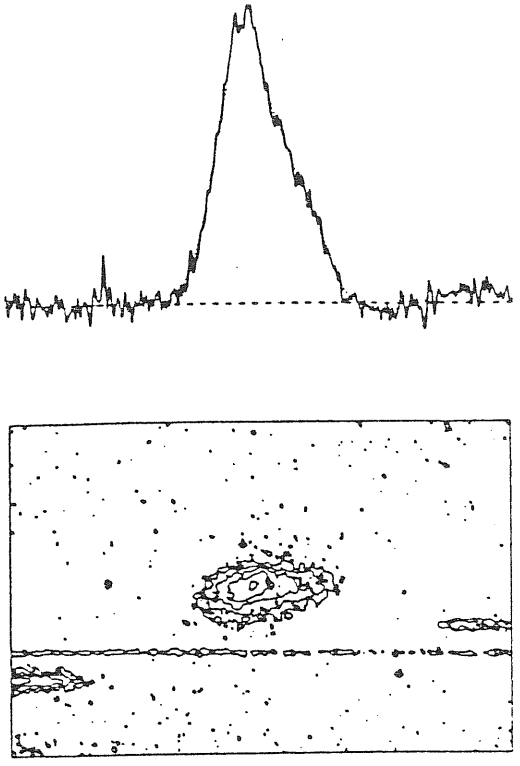

097.122: PLATE B

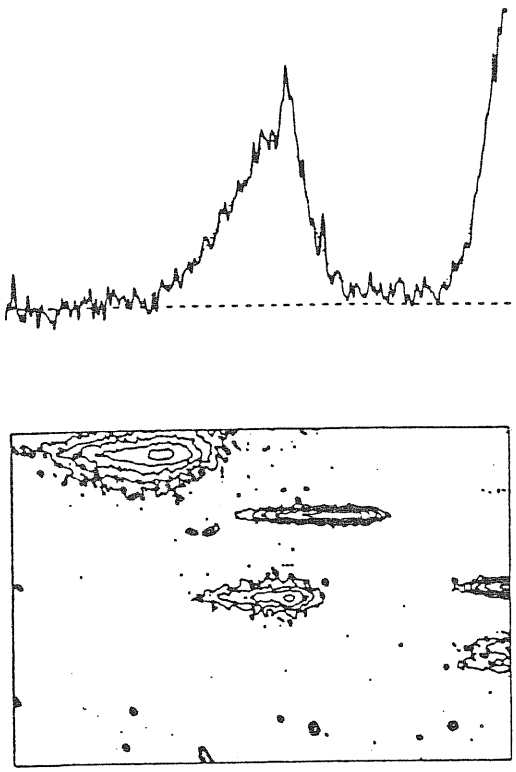

097.125: PLATE A

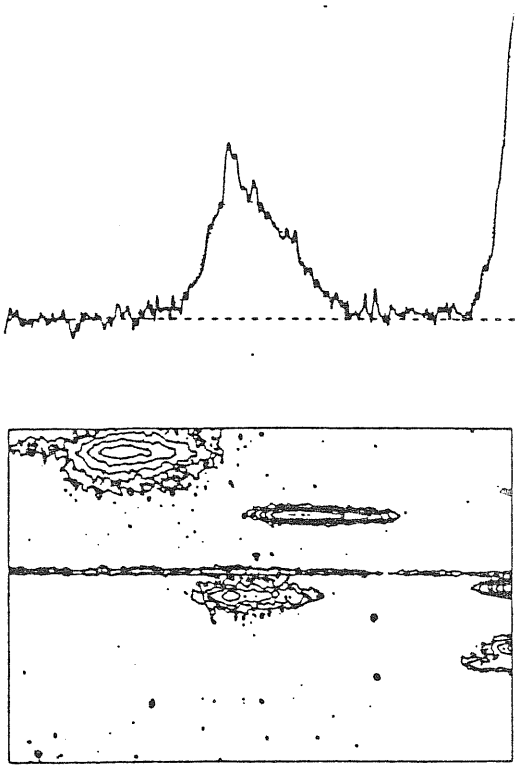

097.125: PLATE B

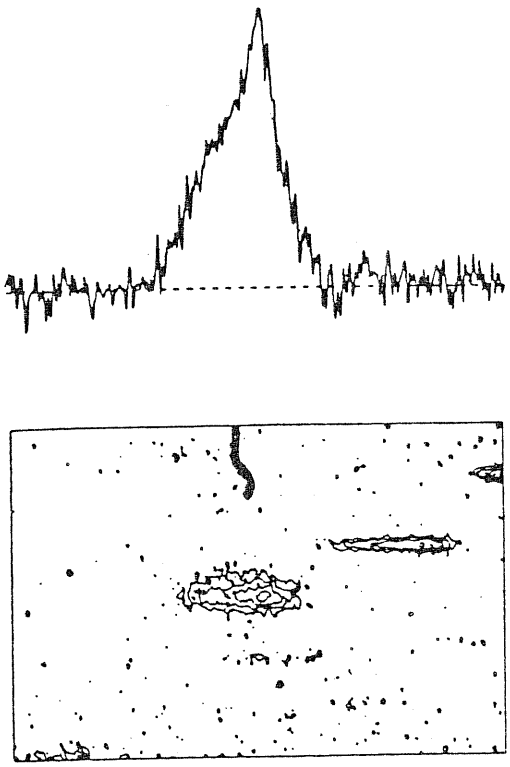

127.046: PLATE A

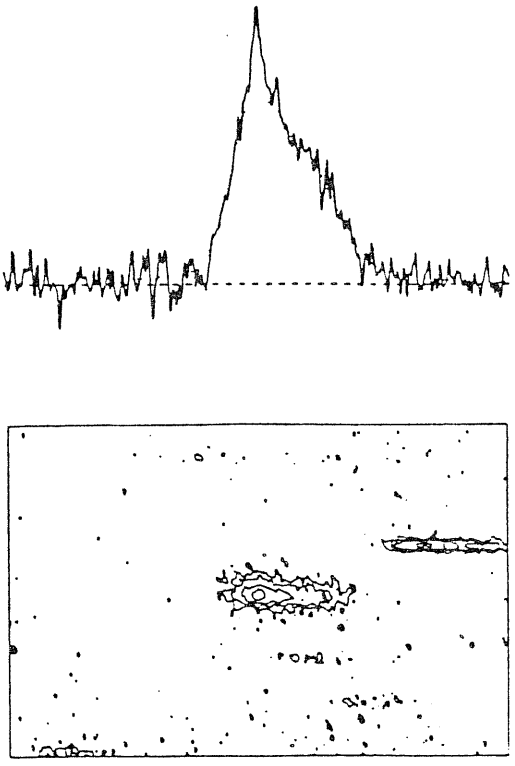

127.046: PLATE B

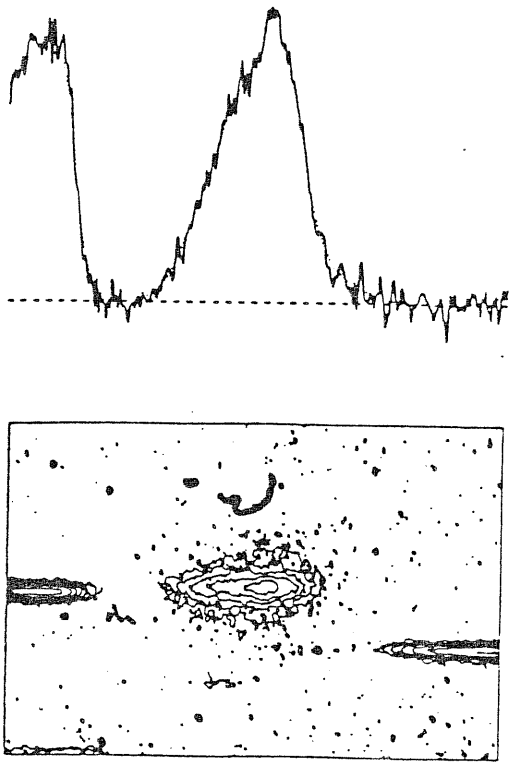

127.045: PLATE A

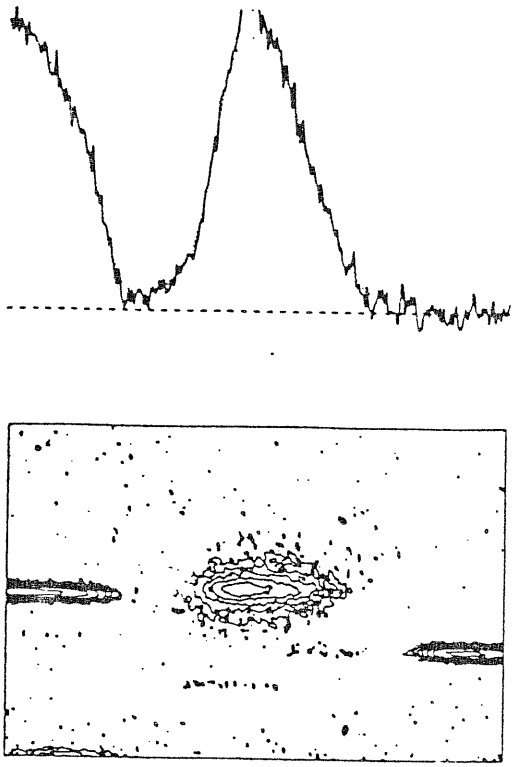

127.045: PLATE B

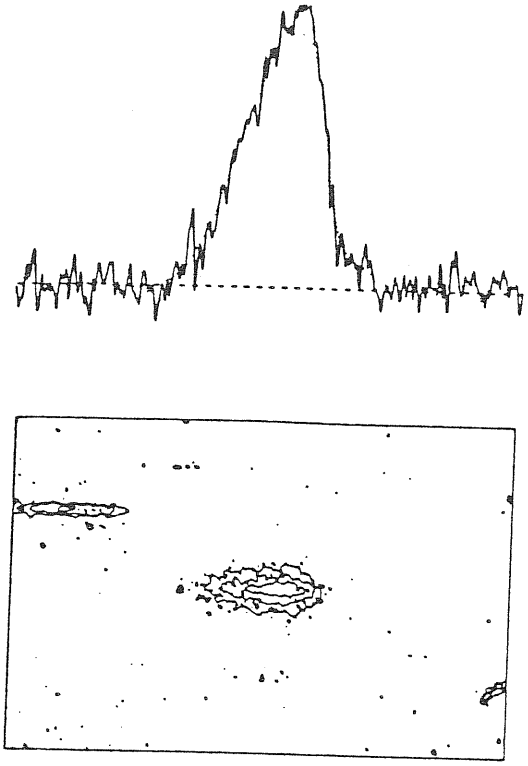

097.130: PLATE A

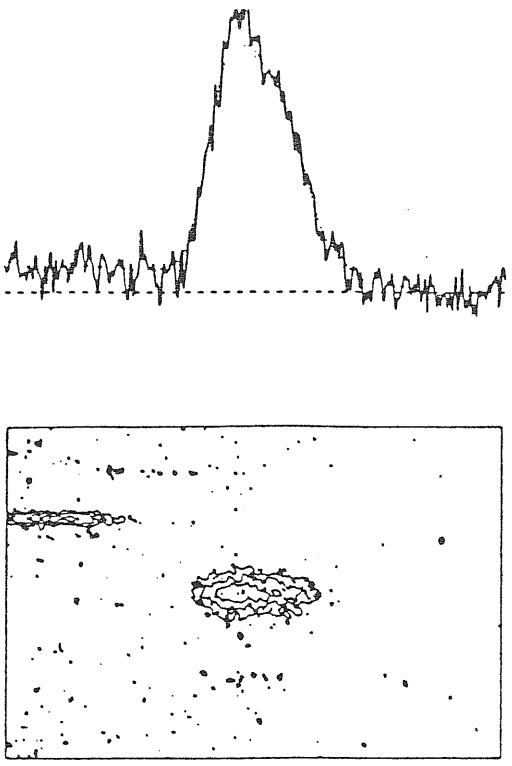

097.130: PLATE B

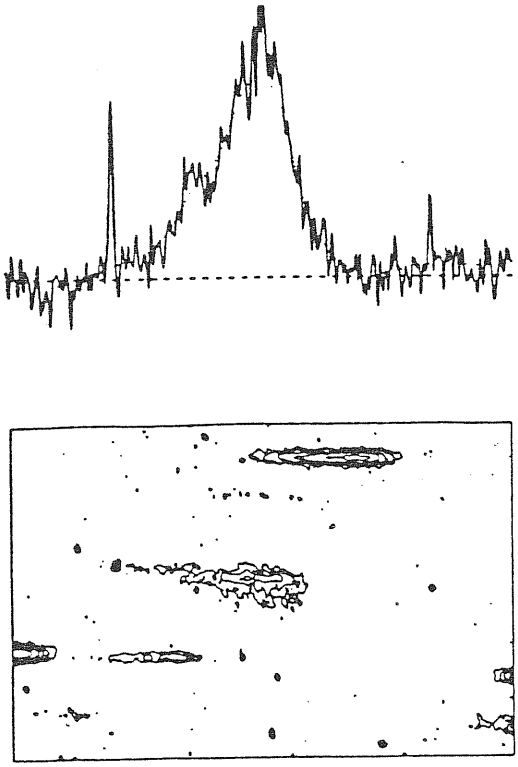

097.138: PLATE A

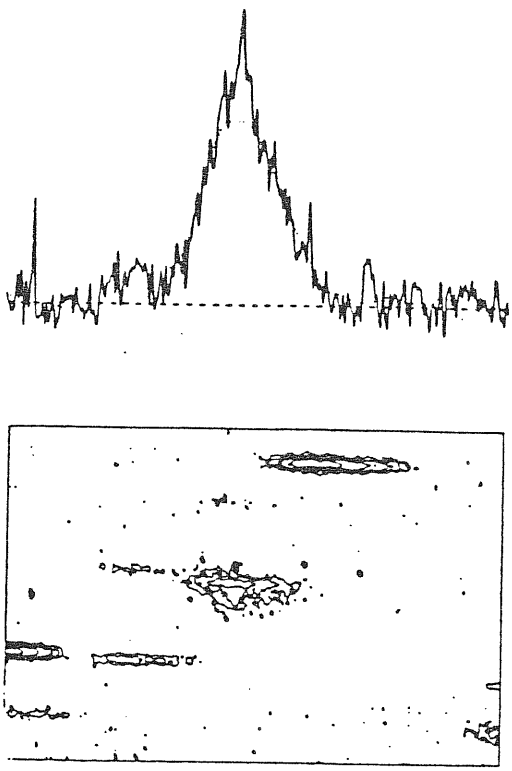

097.138: PLATE B

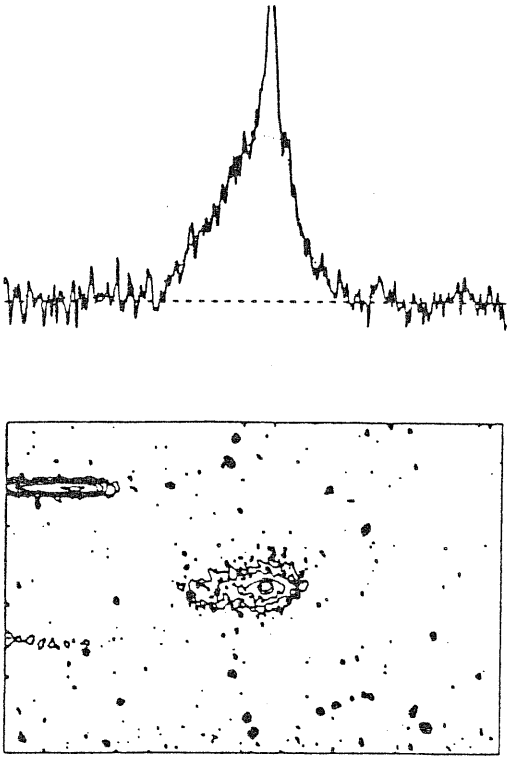

127.049: PLATE A

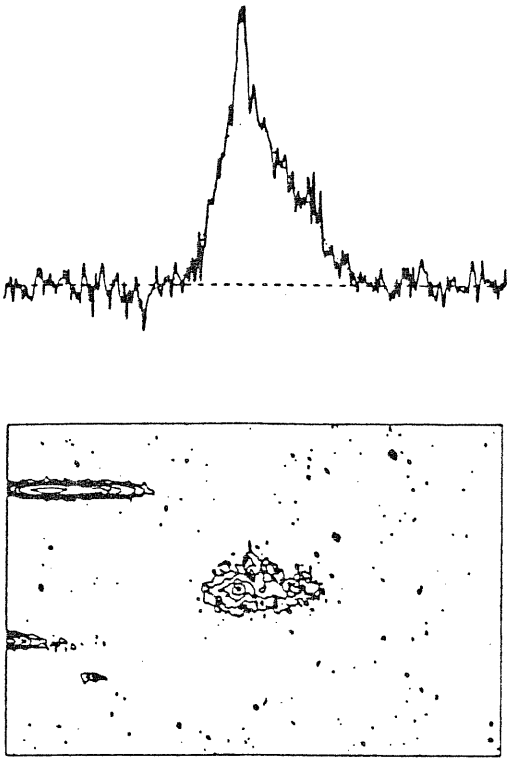

127.049: PLATE B

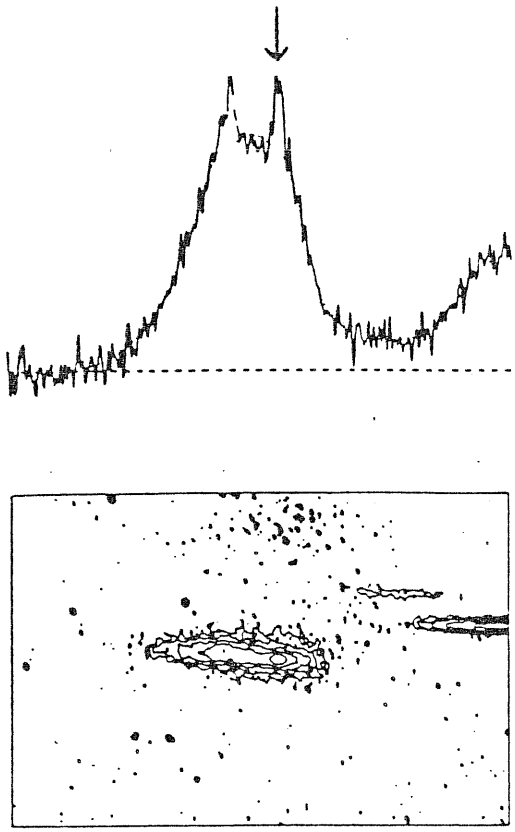

127.051: PLATE A

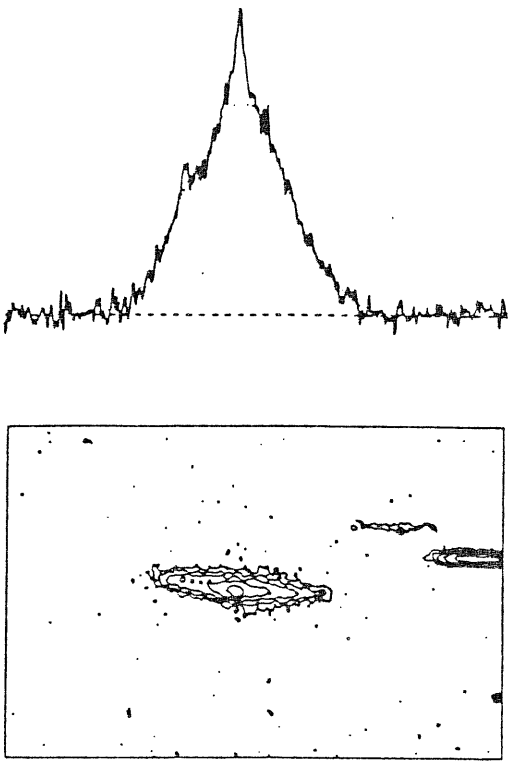

127.051: PLATE B

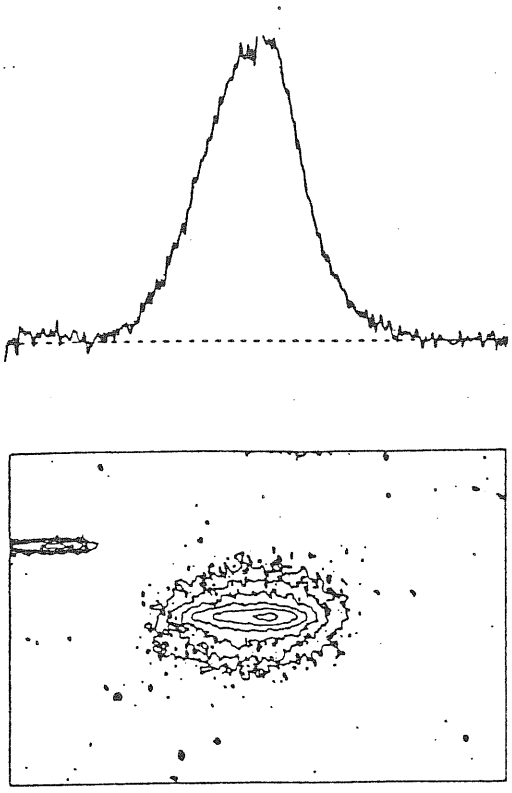

127.052: PLATE A

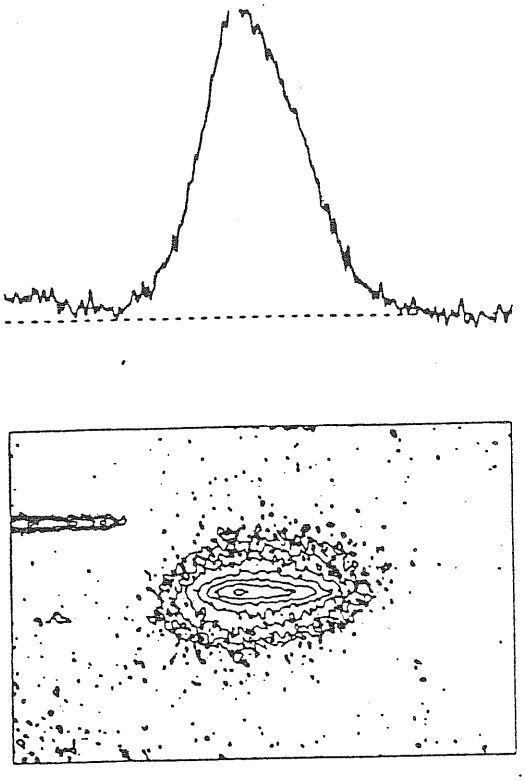

127.052: PLATE B

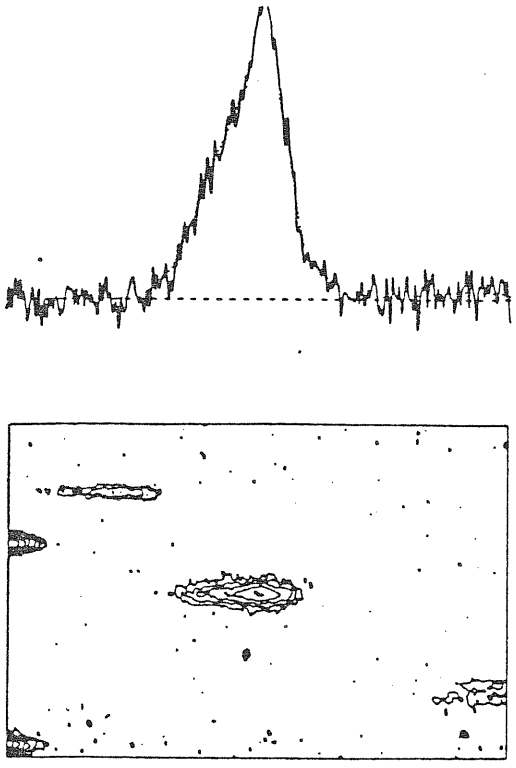

127.055: PLATE A

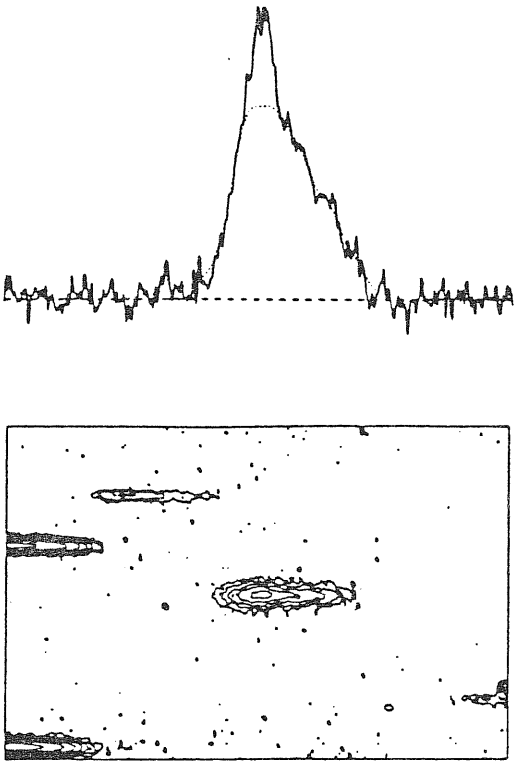

127.055: PLATE B

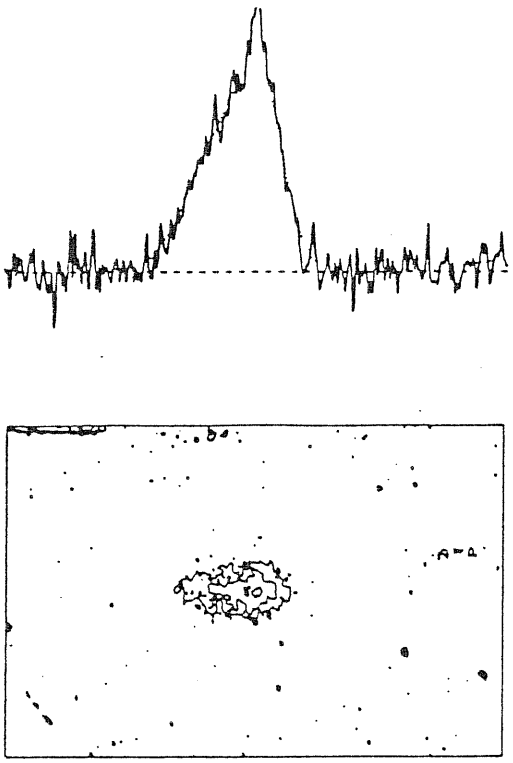

127.056: PLATE A

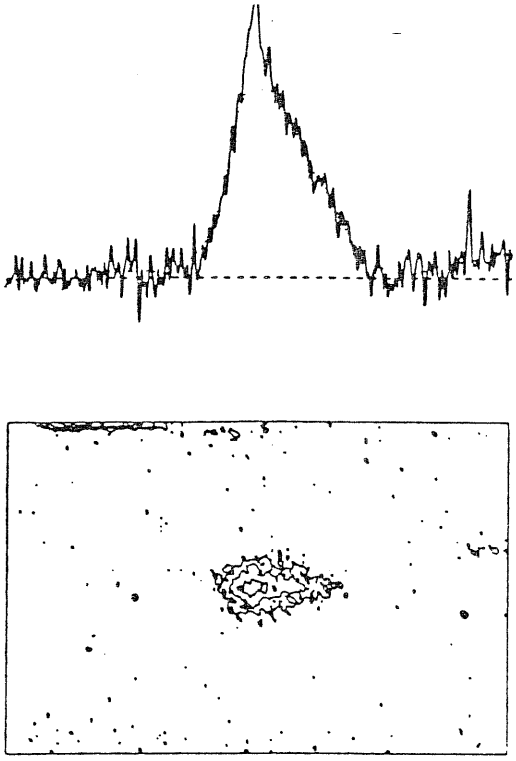

127.056: PLATE B

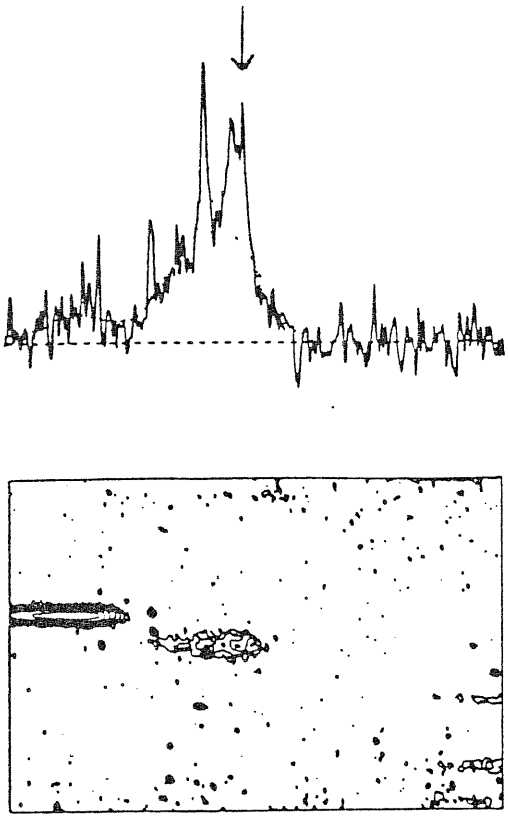

127.058: PLATE A

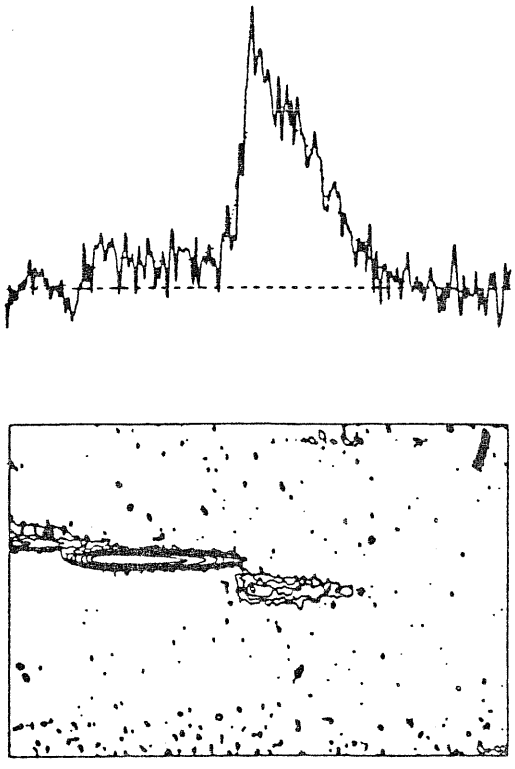

127.058: PLATE B

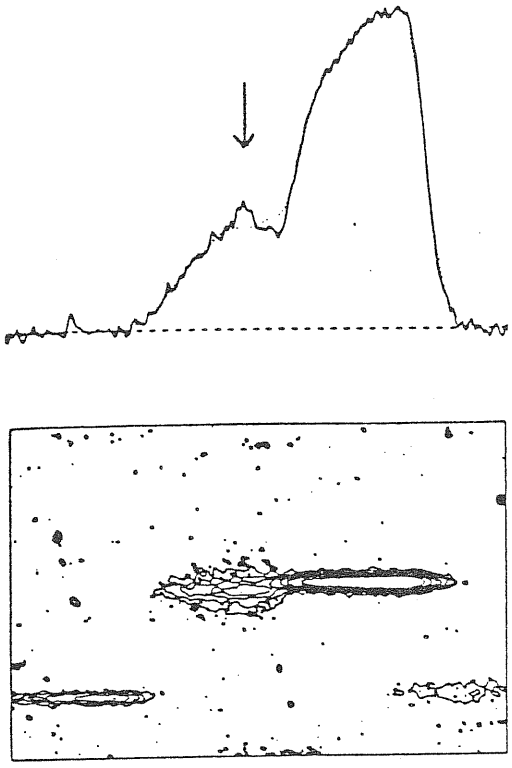

097.160: PLATE A

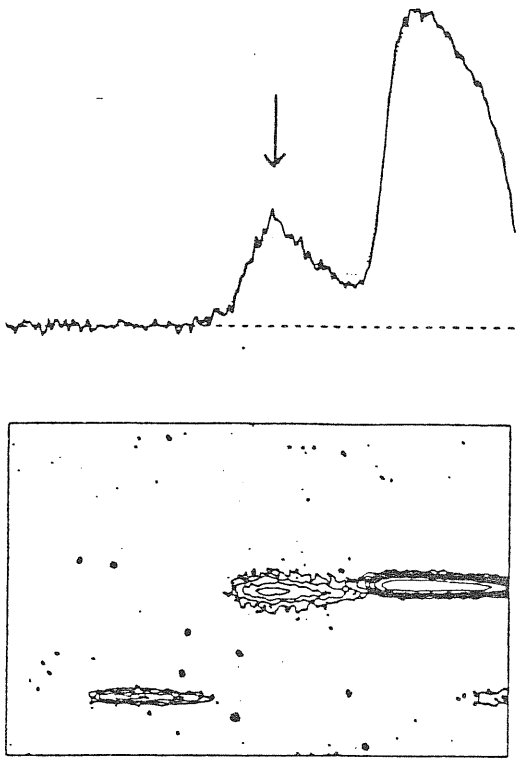

097.160: PLATE B

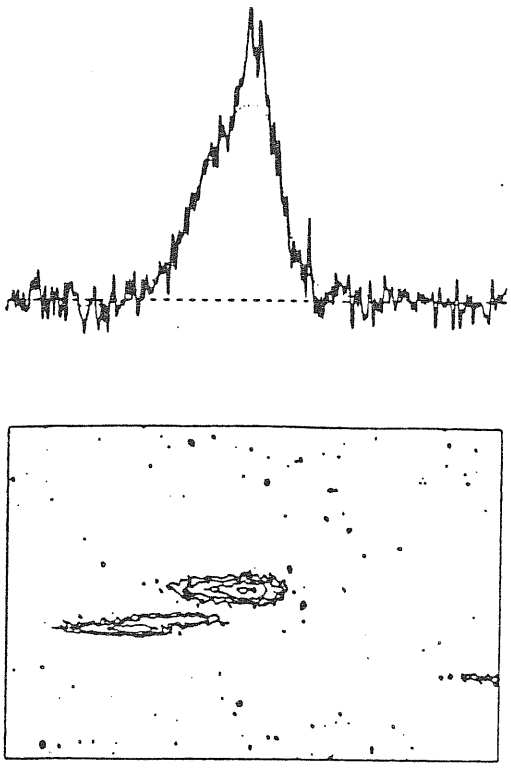

127.067: PLATE A

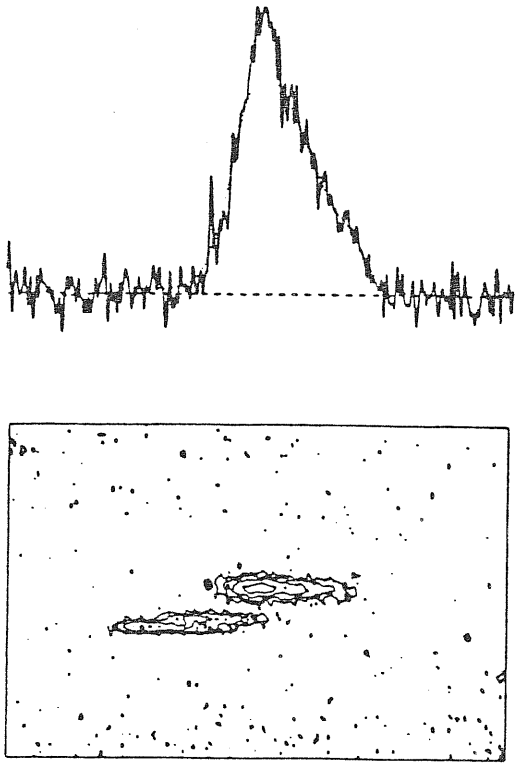

127.067: PLATE B

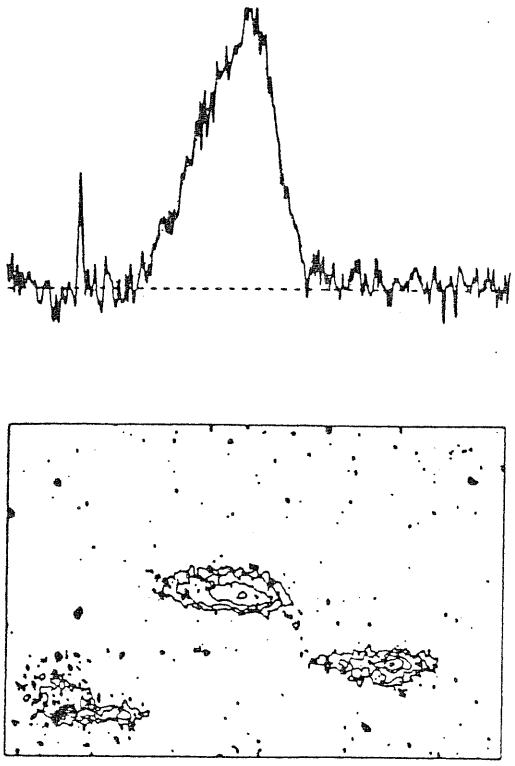

127.068: PLATE A

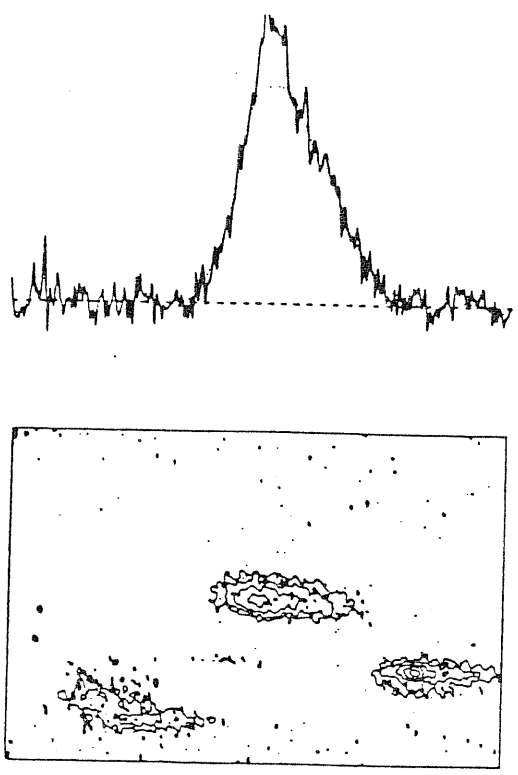

127.068: PLATE B

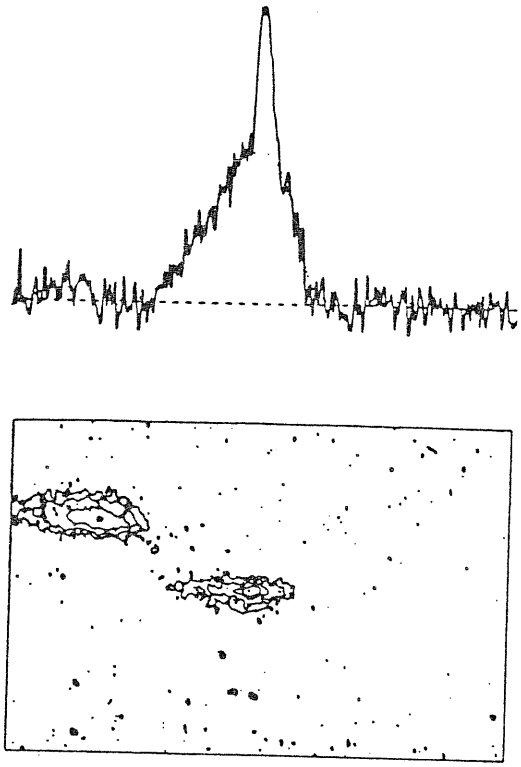

127.071: PLATE A

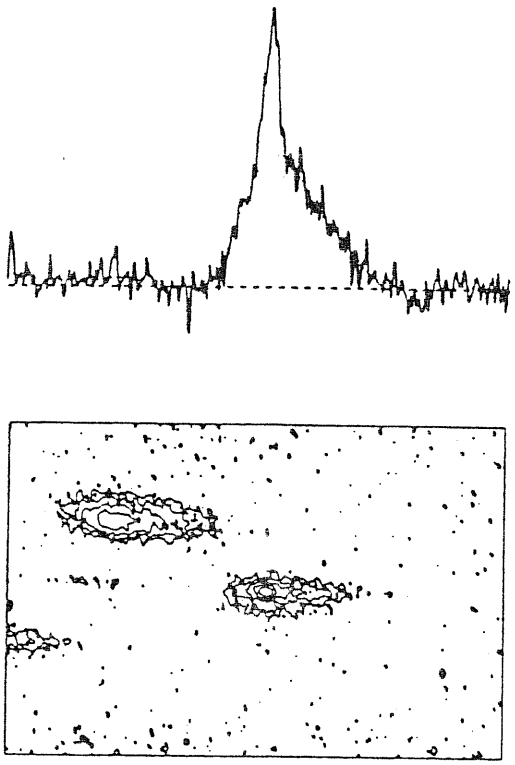

127.071: PLATE B

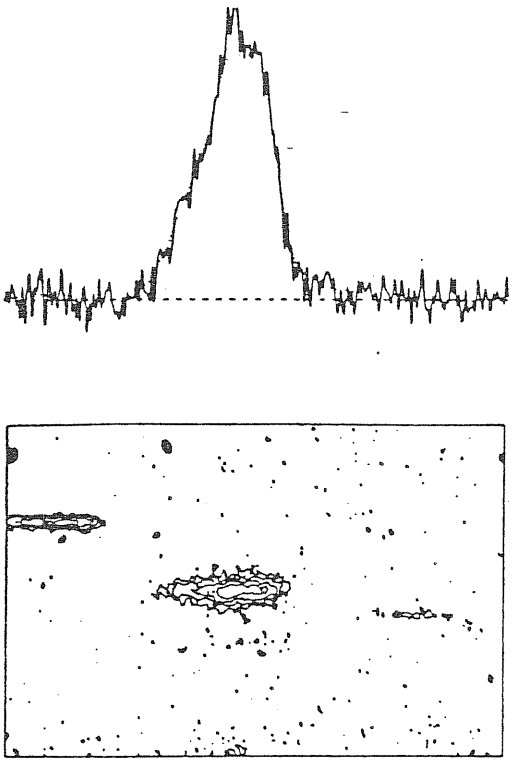

127.074: PLATE A

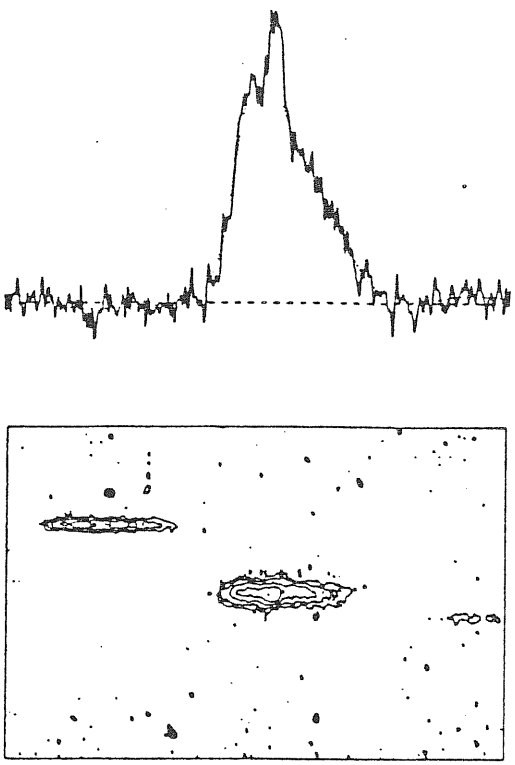

127.074: PLATE B

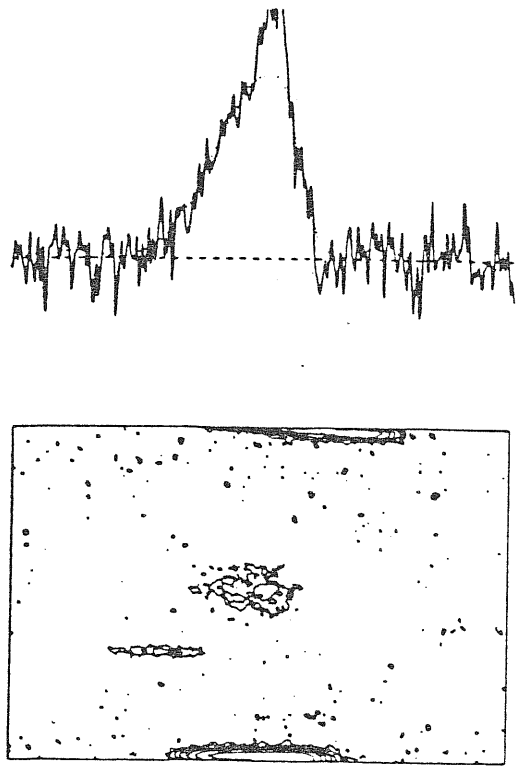

097.168: PLATE A

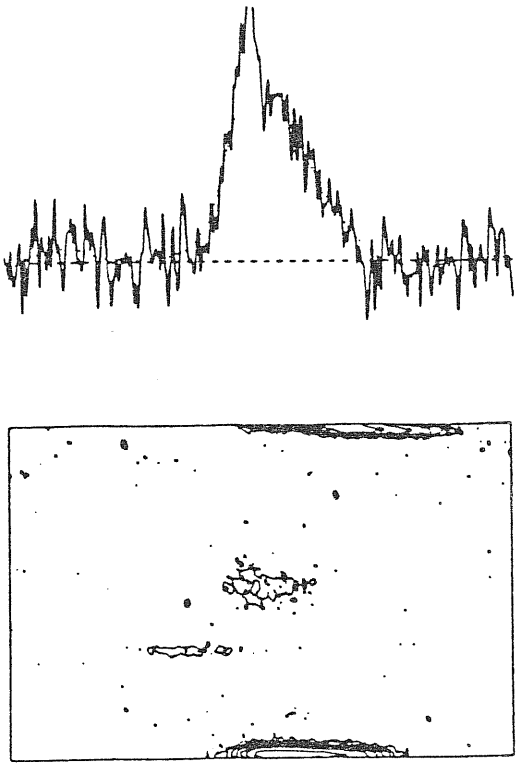

097.168: PLATE B

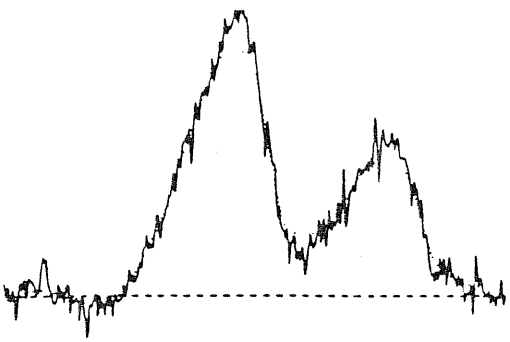

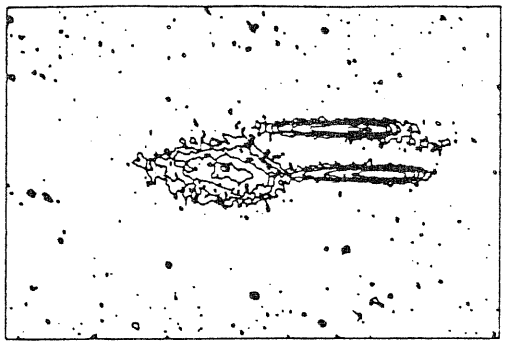

127.082: PLATE A

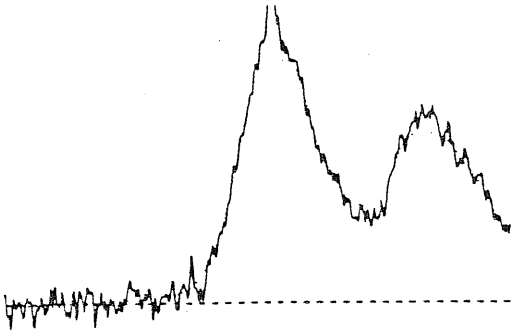

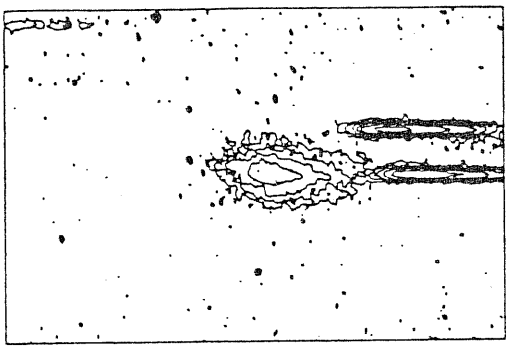

127.082: PLATE B

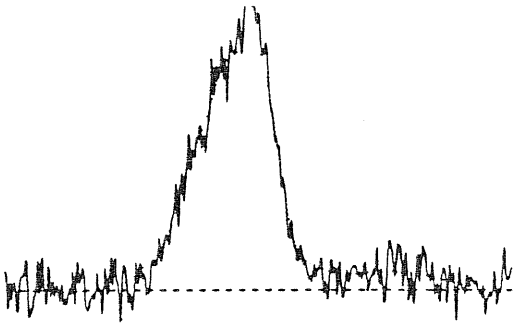

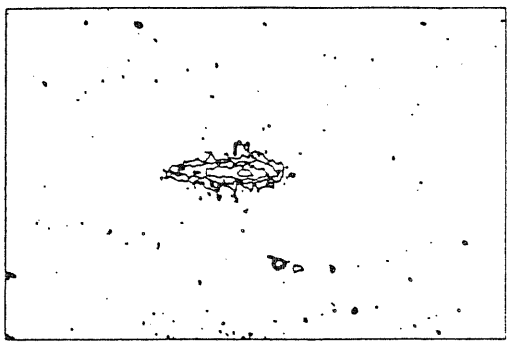

127.085: PLATE A

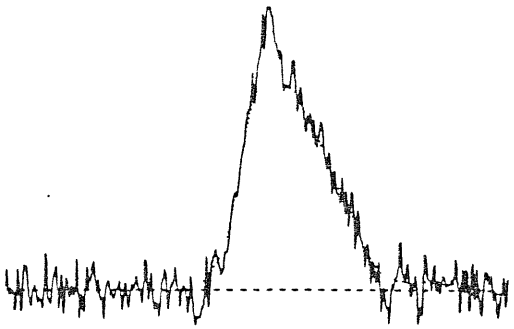

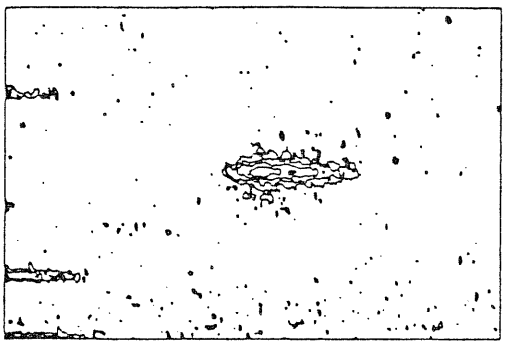

127.085: PLATE B

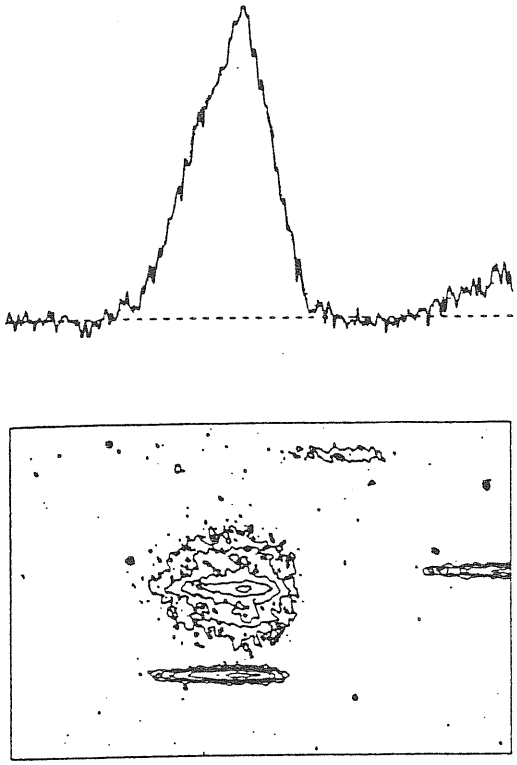

127.095: PLATE A

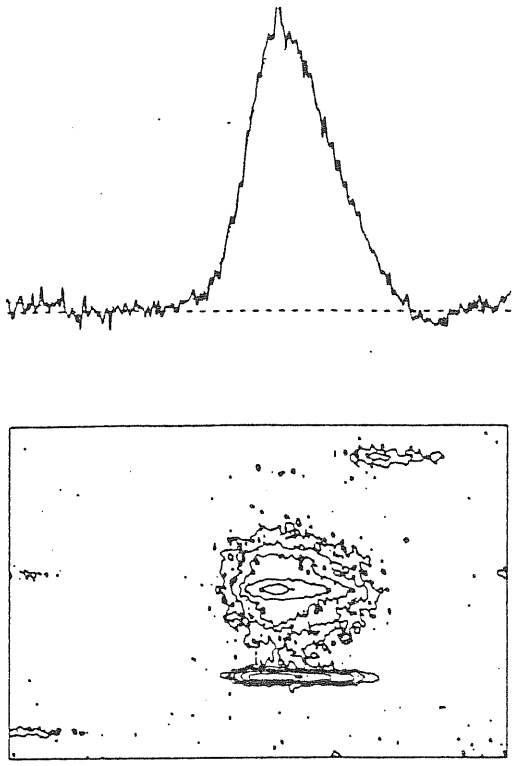

127.095: PLATE B

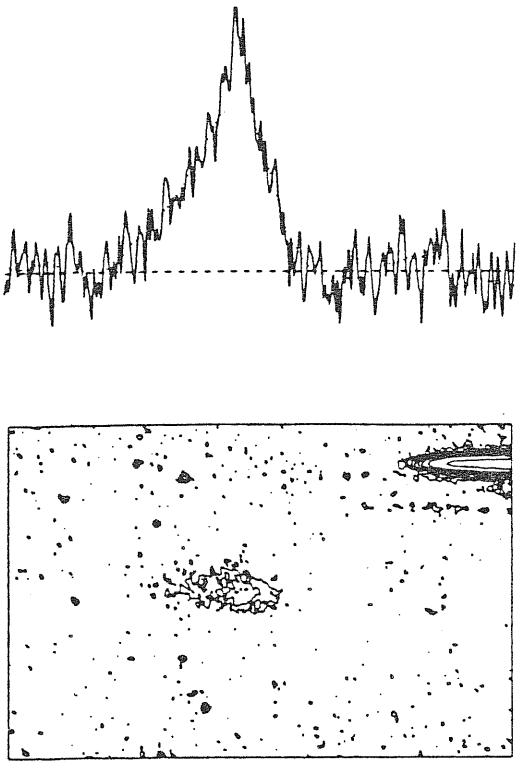

097.180: PLATE A

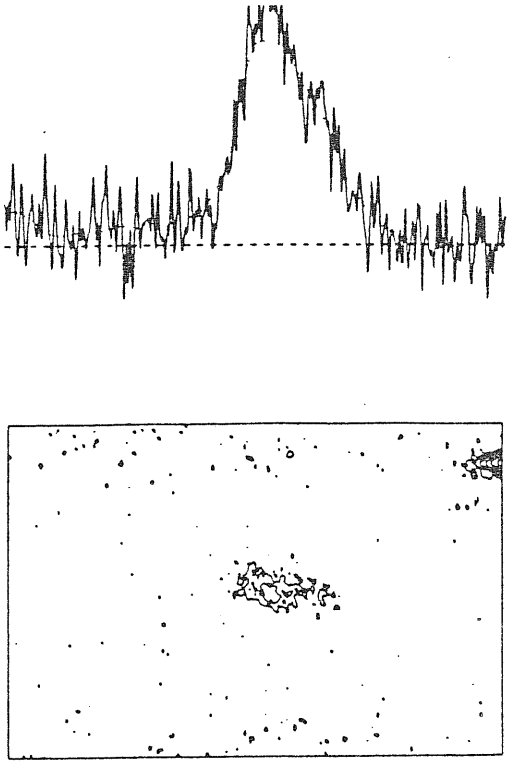

097.180: PLATE B

APPENDIX B

Spectra and Code on Magnetic Tape

The following are descriptions of data files and code used in the analysis. Information is stored on magnetic tape, labelled "Chris," a directory of which is at the end of this appendix.

B.1 Spectra

IMAGES_PLATEA.DAT
IMAGES_PLATEB.DAT
PLATEA.DAT
PLATEB.DAT

These are raw data files containing galaxy and stellar spectra, their use is described below.

GALAXYA1-44.DAT
GALAXYA1-44.DST

The raw galaxy spectra from plates A and B are located in the files with the ".DAT" extension while the ".DST" extension signifies FIGARO format files. The numbers, from 1 to 44, signify the galaxy number given in Table B.1.

126_074.DAT
126_075.DAT
126_091.DAT
126_100.DAT
126_103.DAT
097_022CCC.DAT

These are spectra of galaxies on one plate. The ".DST" extension is for FIGARO format files.

Files beginning with "C" are galaxy continua output from ABLINE, while the "S" indicates smoothed spectra. "SUB" are smoothed, continua

subtracted spectra. File ONEA.DAT is a false continuum set to a level of one. Finally, files TEMPLATE_A/B.DAT are the templates used to determine the shifts in the stellar spectra and STARA/B.DAT and STARA/B.DST are typical stellar spectra.

N.B.: For all files, plates A or B are indicated with an "A" or "B".

B.2 Code

Using the raw 2-D information provided by the APM (stored on tape: "APM", 23-03-90) as input, FITSR.FOR creates the files PLATEA/B.DAT. Running TOM.FOR, with PLATEA/B.DAT as inputs extracts the spectra and creates the files IMAGES_PLATEA/B.DAT.

The FORTRAN files CONV.FOR and DS_MODEL.FOR compute the shifts between spectra on different plates and the modelled corrections, respectively. The file READ.FOR is a subsection of CONV.FOR and is used to read-in raw spectra, while EW.FOR computes the equivalent widths. Finally, TRI.FOR creates the templates used to determine shifts in the stellar spectra and KENDALL.FOR computes Kendall-Rank correlations.

Table B.1: Galaxy numbers for archival data.

CGCG no.	Archival Number
126.104	1
126.110	2
097.027	3
097.026	4
097.033	5
097.044	6
097.052	7
097.062	8
097.063	9
097.068	10
097.067	11
097.070	12
097.072	13
097.073	14
097.079	15
097.087	16
097.092	17
097.091	18
097.093	19
097.114	20
097.120	21
097.122	22
097.125	23
127.046	24
127.045	25
097.130	26
097.138	27
127.049	28
127.051	29
127.052	30
127.055	31
127.056	32
127.058	33
097.160	34
127.067	35
127.068	36
127.071	37
127.074	38
097.168	39
097.169	40
127.082	41
127.085	42
127.095	43
097.180	44

```
Listing of save set(s)

Save set:             GAL.BCK
Written by:           JEP1
UIC:                  [000024,000031]
Date:                  7-DEC-1990 14:05:56.35
Operating system:     VAX/VMS version V5.3
BACKUP version:       V5.3
CPU ID register:      0A000005
Node name:            _CAMV0::
Written on:           _CAMV0$MSA0:
Block size:           8192
Group size:           10
Buffer count:         32

[JEP1.RAW]IMAGES_PLATEA.DAT;1      308  11-APR-1990 13:08
[JEP1.RAW]IMAGES_PLATEB.DAT;1      308  11-APR-1990 13:05
[JEP1.RAW]PLATEA.DAT;1             46848   6-APR-1990 12:41
[JEP1.RAW]PLATEB.DAT;1             47232   6-APR-1990 12:55
[JEP1.RAW]STARS_PLATEA.DAT;1       405   9-APR-1990 17:17
[JEP1.RAW]STARS_PLATEB.DAT;1       405  11-APR-1990 13:23
[JEP1.RAW]STAR_LIST.DAT;1          10  20-APR-1990 17:02
[JEP1.DAT]126_074.DAT;1            8  25-AUG-1990 17:08
[JEP1.DAT]126_074.DST;1            8  29-JUN-1990 11:08
[JEP1.DAT]126_075.DAT;1            8  25-AUG-1990 17:18
[JEP1.DAT]126_075.DST;1            16  30-MAY-1990 11:18
[JEP1.DAT]126_091.DAT;1            8  25-AUG-1990 17:18
[JEP1.DAT]126_091.DST;1            8  29-JUN-1990 11:29
[JEP1.DAT]126_100.DAT;1            8  29-MAY-1990 15:17
[JEP1.DAT]126_100.DST;1            16  30-MAY-1990 11:19
[JEP1.DAT]126_103.DAT;1            8  25-AUG-1990 17:19
[JEP1.DAT]126_103.DST;1            8  29-JUN-1990 11:35
[JEP1.DAT]97_022CCC.DAT;1          8  29-MAY-1990 15:37
[JEP1.DAT]97_022CCC.DST;1          16  31-MAY-1990 10:54
[JEP1.DAT]CA1.DST;1                8  20-JUN-1990 17:46
[JEP1.DAT]CA10.DST;1               8  20-JUN-1990 13:51
[JEP1.DAT]CA13.DST;1               8  20-JUN-1990 13:57
[JEP1.DAT]CA14.DST;1               8  20-JUN-1990 14:02
[JEP1.DAT]CA15.DST;1               8  20-JUN-1990 14:07
[JEP1.DAT]CA17.DST;1               8  20-JUN-1990 14:12
[JEP1.DAT]CA18.DST;1               8  20-JUN-1990 14:17
[JEP1.DAT]CA19.DST;1               8  20-JUN-1990 14:21
[JEP1.DAT]CA2.DST;1                8  20-JUN-1990 17:47
[JEP1.DAT]CA20.DST;1               8  20-JUN-1990 14:26
[JEP1.DAT]CA21.DST;1               8  20-JUN-1990 14:33
[JEP1.DAT]CA23.DST;1               8  20-JUN-1990 14:37
[JEP1.DAT]CA24.DST;1               8  20-JUN-1990 14:41
[JEP1.DAT]CA25.DST;1               8  20-JUN-1990 14:46
[JEP1.DAT]CA27.DST;1               8  20-JUN-1990 15:14
[JEP1.DAT]CA28.DST;1               8  20-JUN-1990 15:18
[JEP1.DAT]CA29.DST;1               8  20-JUN-1990 15:23
[JEP1.DAT]CA3.DST;1                8  20-JUN-1990 17:48
[JEP1.DAT]CA30.DST;1               8  20-JUN-1990 15:30
[JEP1.DAT]CA31.DST;1               8  20-JUN-1990 15:39
[JEP1.DAT]CA32.DST;1               8  20-JUN-1990 15:43
[JEP1.DAT]CA33.DST;1               8  20-JUN-1990 16:52
[JEP1.DAT]CA34.DST;1               8  20-JUN-1990 16:57
[JEP1.DAT]CA35.DST;1               8  20-JUN-1990 17:03
[JEP1.DAT]CA36.DST;1               8  20-JUN-1990 17:12
[JEP1.DAT]CA37.DST;1               8  20-JUN-1990 17:15
```

```
[JEP1.DAT]CA38.DST;1                 8  20-JUN-1990 17:19
[JEP1.DAT]CA39.DST;1                 8  20-JUN-1990 17:25
[JEP1.DAT]CA4.DST;1                  8  20-JUN-1990 13:17
[JEP1.DAT]CA40.DST;1                 8  22-JUN-1990 15:29
[JEP1.DAT]CA41.DST;1                 8  20-JUN-1990 17:29
[JEP1.DAT]CA42.DST;1                 8  20-JUN-1990 17:33
[JEP1.DAT]CA43.DST;1                 8  20-JUN-1990 17:37
[JEP1.DAT]CA44.DST;1                 8  20-JUN-1990 17:41
[JEP1.DAT]CA5.DST;1                  8  20-JUN-1990 13:22
[JEP1.DAT]CA6.DST;1                  8  20-JUN-1990 13:25
[JEP1.DAT]CA7.DST;1                  8  20-JUN-1990 13:32
[JEP1.DAT]CA8.DST;1                  8  20-JUN-1990 13:37
[JEP1.DAT]CA9.DST;1                  8  20-JUN-1990 13:44
[JEP1.DAT]CB1.DST;1                  8  20-JUN-1990 17:50
[JEP1.DAT]CB10.DST;1                 8  20-JUN-1990 13:53
[JEP1.DAT]CB13.DST;1                 8  20-JUN-1990 13:59
[JEP1.DAT]CB14.DST;1                 8  20-JUN-1990 14:04
[JEP1.DAT]CB15.DST;1                 8  20-JUN-1990 14:09
[JEP1.DAT]CB17.DST;1                 8  20-JUN-1990 14:14
[JEP1.DAT]CB18.DST;1                 8  20-JUN-1990 14:19
[JEP1.DAT]CB19.DST;1                 8  20-JUN-1990 14:24
[JEP1.DAT]CB2.DST;1                  8  20-JUN-1990 17:51
[JEP1.DAT]CB20.DST;1                 8  20-JUN-1990 14:29
[JEP1.DAT]CB21.DST;1                 8  20-JUN-1990 14:35
[JEP1.DAT]CB23.DST;1                 8  20-JUN-1990 14:39
[JEP1.DAT]CB24.DST;1                 8  20-JUN-1990 14:44
[JEP1.DAT]CB25.DST;1                 8  20-JUN-1990 14:51
[JEP1.DAT]CB27.DST;1                 8  20-JUN-1990 15:16
[JEP1.DAT]CB28.DST;1                 8  20-JUN-1990 15:20
[JEP1.DAT]CB29.DST;1                 8  20-JUN-1990 15:25
[JEP1.DAT]CB3.DST;1                  8  20-JUN-1990 13:15
[JEP1.DAT]CB30.DST;1                 8  20-JUN-1990 15:37
[JEP1.DAT]CB31.DST;1                 8  20-JUN-1990 15:41
[JEP1.DAT]CB32.DST;1                 8  20-JUN-1990 15:45
[JEP1.DAT]CB33.DST;1                 8  20-JUN-1990 16:55
[JEP1.DAT]CB34.DST;1                 8  20-JUN-1990 17:01
[JEP1.DAT]CB35.DST;1                 8  21-JUN-1990 11:29
[JEP1.DAT]CB36.DST;1                 8  20-JUN-1990 17:13
[JEP1.DAT]CB37.DST;1                 8  21-JUN-1990 11:43
[JEP1.DAT]CB38.DST;1                 8  20-JUN-1990 17:22
[JEP1.DAT]CB39.DST;1                 8  20-JUN-1990 17:26
[JEP1.DAT]CB4.DST;1                  8  20-JUN-1990 13:19
[JEP1.DAT]CB40.DST;1                 8  22-JUN-1990 15:31
[JEP1.DAT]CB41.DST;1                 8  20-JUN-1990 17:31
[JEP1.DAT]CB42.DST;1                 8  20-JUN-1990 17:35
[JEP1.DAT]CB43.DST;1                 8  20-JUN-1990 17:39
[JEP1.DAT]CB44.DST;1                 8  20-JUN-1990 17:43
[JEP1.DAT]CB5.DST;1                  8  20-JUN-1990 13:24
[JEP1.DAT]CB6.DST;1                  8  20-JUN-1990 13:30
[JEP1.DAT]CB7.DST;1                  8  20-JUN-1990 13:33
[JEP1.DAT]CB8.DST;1                  8  20-JUN-1990 13:42
[JEP1.DAT]CB9.DST;1                  8  21-JUN-1990 12:07
[JEP1.DAT]GALAXYA1.DAT;1            31   3-MAY-1990 15:37
[JEP1.DAT]GALAXYA10.DAT;1           31  24-AUG-1990 09:35
[JEP1.DAT]GALAXYA13.DAT;1           31   3-MAY-1990 15:38
[JEP1.DAT]GALAXYA14.DAT;1           31   3-MAY-1990 15:38
[JEP1.DAT]GALAXYA15.DAT;1           31   3-MAY-1990 17:43
[JEP1.DAT]GALAXYA17.DAT;1           31   3-MAY-1990 15:38
[JEP1.DAT]GALAXYA18.DAT;1           31  24-AUG-1990 09:36
[JEP1.DAT]GALAXYA19.DAT;1           31   3-MAY-1990 15:38
```

```
[JEP1.DAT]GALAXYA2.DAT;1                31   3-MAY-1990 15:37
[JEP1.DAT]GALAXYA20.DAT;1               31   3-MAY-1990 17:54
[JEP1.DAT]GALAXYA21.DAT;1               31   3-MAY-1990 15:38
[JEP1.DAT]GALAXYA23.DAT;1               31   3-MAY-1990 15:38
[JEP1.DAT]GALAXYA24.DAT;1               31   3-MAY-1990 15:38
[JEP1.DAT]GALAXYA25.DAT;1               31   3-MAY-1990 15:38
[JEP1.DAT]GALAXYA26.DAT;1               31   3-MAY-1990 15:38
[JEP1.DAT]GALAXYA27.DAT;1               31   3-MAY-1990 15:38
[JEP1.DAT]GALAXYA28.DAT;1               31   3-MAY-1990 15:38
[JEP1.DAT]GALAXYA29.DAT;1               31   3-MAY-1990 18:26
[JEP1.DAT]GALAXYA3.DAT;1                31   3-MAY-1990 15:37
[JEP1.DAT]GALAXYA30.DAT;1               31   3-MAY-1990 15:38
[JEP1.DAT]GALAXYA31.DAT;1               31   3-MAY-1990 15:38
[JEP1.DAT]GALAXYA32.DAT;1               31   3-MAY-1990 15:38
[JEP1.DAT]GALAXYA33.DAT;1               31   3-MAY-1990 18:02
[JEP1.DAT]GALAXYA34.DAT;1               31   3-MAY-1990 18:05
[JEP1.DAT]GALAXYA35.DAT;1               31   3-MAY-1990 15:39
[JEP1.DAT]GALAXYA36.DAT;1               31   3-MAY-1990 15:39
[JEP1.DAT]GALAXYA37.DAT;1               31   3-MAY-1990 15:39
[JEP1.DAT]GALAXYA38.DAT;1               31   3-MAY-1990 15:39
[JEP1.DAT]GALAXYA39.DAT;1               31   3-MAY-1990 15:39
[JEP1.DAT]GALAXYA4.DAT;1                31   3-MAY-1990 15:37
[JEP1.DAT]GALAXYA41.DAT;1               31   3-MAY-1990 18:17
[JEP1.DAT]GALAXYA42.DAT;1               31   3-MAY-1990 15:39
[JEP1.DAT]GALAXYA43.DAT;1               31   3-MAY-1990 15:39
[JEP1.DAT]GALAXYA44.DAT;1               16   3-MAY-1990 15:39
[JEP1.DAT]GALAXYA5.DAT;1                31   3-MAY-1990 15:37
[JEP1.DAT]GALAXYA6.DAT;1                31   3-MAY-1990 15:37
[JEP1.DAT]GALAXYA8.DAT;1                31   3-MAY-1990 15:38
[JEP1.DAT]GALAXYA9.DAT;1                31   3-MAY-1990 18:37
[JEP1.DAT]GALAXYB1.DAT;1                31   3-MAY-1990 15:37
[JEP1.DAT]GALAXYB10.DAT;1               31  24-AUG-1990 09:35
[JEP1.DAT]GALAXYB13.DAT;1               31   3-MAY-1990 15:38
[JEP1.DAT]GALAXYB14.DAT;1               31   3-MAY-1990 15:38
[JEP1.DAT]GALAXYB15.DAT;1               31   3-MAY-1990 17:48
[JEP1.DAT]GALAXYB17.DAT;1               31   3-MAY-1990 15:38
[JEP1.DAT]GALAXYB18.DAT;1               31  24-AUG-1990 09:36
[JEP1.DAT]GALAXYB19.DAT;1               31   3-MAY-1990 15:38
[JEP1.DAT]GALAXYB2.DAT;1                31   3-MAY-1990 15:37
[JEP1.DAT]GALAXYB20.DAT;1               31   3-MAY-1990 15:38
[JEP1.DAT]GALAXYB21.DAT;1               31   3-MAY-1990 18:21
[JEP1.DAT]GALAXYB23.DAT;1               31   3-MAY-1990 15:38
[JEP1.DAT]GALAXYB24.DAT;1               31   3-MAY-1990 15:38
[JEP1.DAT]GALAXYB25.DAT;1               31   3-MAY-1990 15:38
[JEP1.DAT]GALAXYB26.DAT;1               31   3-MAY-1990 15:38
[JEP1.DAT]GALAXYB27.DAT;1               31   3-MAY-1990 15:38
[JEP1.DAT]GALAXYB28.DAT;1               31   3-MAY-1990 15:38
[JEP1.DAT]GALAXYB29.DAT;1               31   3-MAY-1990 15:38
[JEP1.DAT]GALAXYB3.DAT;1                31   3-MAY-1990 15:37
[JEP1.DAT]GALAXYB30.DAT;1               31   3-MAY-1990 15:38
[JEP1.DAT]GALAXYB31.DAT;1               31   3-MAY-1990 15:38
[JEP1.DAT]GALAXYB32.DAT;1               31   3-MAY-1990 15:38
[JEP1.DAT]GALAXYB33.DAT;1               31   3-MAY-1990 15:39
[JEP1.DAT]GALAXYB34.DAT;1               31   3-MAY-1990 18:08
[JEP1.DAT]GALAXYB35.DAT;1               31   3-MAY-1990 15:39
[JEP1.DAT]GALAXYB36.DAT;1               31   3-MAY-1990 15:39
[JEP1.DAT]GALAXYB37.DAT;1               31   3-MAY-1990 15:39
[JEP1.DAT]GALAXYB38.DAT;1               31   3-MAY-1990 15:39
[JEP1.DAT]GALAXYB39.DAT;1               31   3-MAY-1990 15:39
[JEP1.DAT]GALAXYB4.DAT;1                31  24-AUG-1990 09:36
```

```
[JEP1.DAT]GALAXYB41.DAT;1      31   3-MAY-1990 18:16
[JEP1.DAT]GALAXYB42.DAT;1      31   3-MAY-1990 15:39
[JEP1.DAT]GALAXYB43.DAT;1      31   3-MAY-1990 15:39
[JEP1.DAT]GALAXYB44.DAT;1      16   3-MAY-1990 15:39
[JEP1.DAT]GALAXYB5.DAT;1       31   3-MAY-1990 15:37
[JEP1.DAT]GALAXYB6.DAT;1       31   3-MAY-1990 15:48
[JEP1.DAT]GALAXYB8.DAT;1       31   3-MAY-1990 15:38
[JEP1.DAT]GALAXYB9.DAT;1       31   3-MAY-1990 18:42
[JEP1.DAT]ONEA.DST;1            8  21-JUN-1990 13:50
[JEP1.DAT]ONEB.DST;1            8  21-JUN-1990 13:53
[JEP1.DAT]SA1.DST;1             8  19-JUN-1990 15:23
[JEP1.DAT]SA10.DST;1            8  19-JUN-1990 15:29
[JEP1.DAT]SA11.DST;1            8  19-JUN-1990 15:29
[JEP1.DAT]SA12.DST;1            8  19-JUN-1990 15:30
[JEP1.DAT]SA13.DST;1            8  19-JUN-1990 15:30
[JEP1.DAT]SA14.DST;1            8  19-JUN-1990 15:30
[JEP1.DAT]SA15.DST;1            8  19-JUN-1990 15:30
[JEP1.DAT]SA17.DST;1            8  19-JUN-1990 16:30
[JEP1.DAT]SA18.DST;1            8  19-JUN-1990 15:53
[JEP1.DAT]SA19.DST;1            8  19-JUN-1990 16:30
[JEP1.DAT]SA2.DST;1             8  19-JUN-1990 15:24
[JEP1.DAT]SA20.DST;1            8  19-JUN-1990 16:30
[JEP1.DAT]SA21.DST;1            8  19-JUN-1990 16:31
[JEP1.DAT]SA22.DST;1            8  19-JUN-1990 16:31
[JEP1.DAT]SA23.DST;1            8  19-JUN-1990 16:31
[JEP1.DAT]SA24.DST;1            8  19-JUN-1990 16:31
[JEP1.DAT]SA25.DST;1            8  19-JUN-1990 16:32
[JEP1.DAT]SA26.DST;1            8  19-JUN-1990 16:32
[JEP1.DAT]SA27.DST;1            8  19-JUN-1990 16:32
[JEP1.DAT]SA28.DST;1            8  19-JUN-1990 16:32
[JEP1.DAT]SA29.DST;1            8  19-JUN-1990 16:33
[JEP1.DAT]SA3.DST;1             8  19-JUN-1990 15:24
[JEP1.DAT]SA30.DST;1            8  19-JUN-1990 16:33
[JEP1.DAT]SA31.DST;1            8  19-JUN-1990 16:33
[JEP1.DAT]SA32.DST;1            8  19-JUN-1990 16:33
[JEP1.DAT]SA33.DST;1            8  19-JUN-1990 16:33
[JEP1.DAT]SA34.DST;1            8  19-JUN-1990 16:34
[JEP1.DAT]SA35.DST;1            8  19-JUN-1990 16:34
[JEP1.DAT]SA36.DST;1            8  19-JUN-1990 16:34
[JEP1.DAT]SA37.DST;1            8  19-JUN-1990 16:34
[JEP1.DAT]SA38.DST;1            8  19-JUN-1990 16:34
[JEP1.DAT]SA39.DST;1            8  19-JUN-1990 16:35
[JEP1.DAT]SA4.DST;1             8  19-JUN-1990 15:25
[JEP1.DAT]SA40.DST;1            8  19-JUN-1990 16:35
[JEP1.DAT]SA41.DST;1            8  19-JUN-1990 16:35
[JEP1.DAT]SA42.DST;1            8  19-JUN-1990 16:35
[JEP1.DAT]SA43.DST;1            8  19-JUN-1990 16:35
[JEP1.DAT]SA44.DST;1            8  19-JUN-1990 16:36
[JEP1.DAT]SA5.DST;1             8  19-JUN-1990 15:25
[JEP1.DAT]SA6.DST;1             8  19-JUN-1990 15:26
[JEP1.DAT]SA7.DST;1             8  19-JUN-1990 15:27
[JEP1.DAT]SA8.DST;1             8  19-JUN-1990 15:28
[JEP1.DAT]SA9.DST;1             8  19-JUN-1990 15:28
[JEP1.DAT]SB1.DST;1             8  19-JUN-1990 16:37
[JEP1.DAT]SB10.DST;1            8  19-JUN-1990 16:39
[JEP1.DAT]SB11.DST;1            8  19-JUN-1990 16:39
[JEP1.DAT]SB12.DST;1            8  19-JUN-1990 16:40
[JEP1.DAT]SB13.DST;1            8  19-JUN-1990 16:40
[JEP1.DAT]SB14.DST;1            8  19-JUN-1990 16:40
[JEP1.DAT]SB15.DST;1            8  19-JUN-1990 16:40
```

```
[JEP1.DAT]SB17.DST;1          8  19-JUN-1990 16:41
[JEP1.DAT]SB18.DST;1          8  19-JUN-1990 16:41
[JEP1.DAT]SB19.DST;1          8  19-JUN-1990 16:41
[JEP1.DAT]SB2.DST;1           8  19-JUN-1990 16:38
[JEP1.DAT]SB20.DST;1          8  19-JUN-1990 16:41
[JEP1.DAT]SB21.DST;1          8  19-JUN-1990 16:42
[JEP1.DAT]SB22.DST;1          8  19-JUN-1990 16:42
[JEP1.DAT]SB23.DST;1          8  19-JUN-1990 16:42
[JEP1.DAT]SB24.DST;1          8  19-JUN-1990 16:42
[JEP1.DAT]SB25.DST;1          8  19-JUN-1990 16:42
[JEP1.DAT]SB26.DST;1          8  19-JUN-1990 16:43
[JEP1.DAT]SB27.DST;1          8  19-JUN-1990 16:43
[JEP1.DAT]SB28.DST;1          8  19-JUN-1990 16:43
[JEP1.DAT]SB29.DST;1          8  19-JUN-1990 16:43
[JEP1.DAT]SB3.DST;1           8  19-JUN-1990 16:38
[JEP1.DAT]SB30.DST;1          8  20-JUN-1990 15:33
[JEP1.DAT]SB31.DST;1          8  19-JUN-1990 16:43
[JEP1.DAT]SB32.DST;1          8  19-JUN-1990 16:44
[JEP1.DAT]SB33.DST;1          8  19-JUN-1990 16:44
[JEP1.DAT]SB34.DST;1          8  19-JUN-1990 16:44
[JEP1.DAT]SB35.DST;1          8  19-JUN-1990 16:44
[JEP1.DAT]SB36.DST;1          8  19-JUN-1990 16:44
[JEP1.DAT]SB37.DST;1          8  19-JUN-1990 16:45
[JEP1.DAT]SB38.DST;1          8  19-JUN-1990 16:45
[JEP1.DAT]SB39.DST;1          8  19-JUN-1990 16:45
[JEP1.DAT]SB4.DST;1           8  19-JUN-1990 16:38
[JEP1.DAT]SB40.DST;1          8  19-JUN-1990 16:45
[JEP1.DAT]SB41.DST;1          8  19-JUN-1990 16:45
[JEP1.DAT]SB42.DST;1          8  19-JUN-1990 16:45
[JEP1.DAT]SB43.DST;1          8  19-JUN-1990 16:46
[JEP1.DAT]SB44.DST;1          8  19-JUN-1990 16:46
[JEP1.DAT]SB5.DST;1           8  19-JUN-1990 16:38
[JEP1.DAT]SB6.DST;1           8  20-JUN-1990 13:28
[JEP1.DAT]SB7.DST;1           8  19-JUN-1990 16:39
[JEP1.DAT]SB8.DST;1           8  19-JUN-1990 16:39
[JEP1.DAT]SB9.DST;1           8  20-JUN-1990 13:46
[JEP1.DAT]STARA.DAT;1         8  29-MAY-1990 15:26
[JEP1.DAT]STARA.DST;1        16  29-MAY-1990 16:41
[JEP1.DAT]STARB.DAT;1         8  29-MAY-1990 15:47
[JEP1.DAT]STARB.DST;1        16  29-MAY-1990 16:42
[JEP1.DAT]SUBA1.DST;1         8  21-JUN-1990 12:30
[JEP1.DAT]SUBA10.DST;1        8  21-JUN-1990 12:33
[JEP1.DAT]SUBA13.DST;1        8  21-JUN-1990 12:34
[JEP1.DAT]SUBA14.DST;1        8  21-JUN-1990 12:35
[JEP1.DAT]SUBA15.DST;1        8  21-JUN-1990 12:35
[JEP1.DAT]SUBA17.DST;1        8  21-JUN-1990 12:36
[JEP1.DAT]SUBA18.DST;1        8  21-JUN-1990 12:36
[JEP1.DAT]SUBA19.DST;1        8  21-JUN-1990 12:37
[JEP1.DAT]SUBA2.DST;1         8  21-JUN-1990 12:30
[JEP1.DAT]SUBA20.DST;1        8  21-JUN-1990 12:37
[JEP1.DAT]SUBA21.DST;1        8  21-JUN-1990 12:37
[JEP1.DAT]SUBA23.DST;1        8  21-JUN-1990 12:38
[JEP1.DAT]SUBA24.DST;1        8  21-JUN-1990 12:38
[JEP1.DAT]SUBA25.DST;1        8  21-JUN-1990 12:39
[JEP1.DAT]SUBA26.DST;1        8  21-JUN-1990 12:39
[JEP1.DAT]SUBA27.DST;1        8  21-JUN-1990 12:39
[JEP1.DAT]SUBA28.DST;1        8  21-JUN-1990 12:40
[JEP1.DAT]SUBA29.DST;1        8  21-JUN-1990 12:40
[JEP1.DAT]SUBA3.DST;1         8  21-JUN-1990 12:31
[JEP1.DAT]SUBA30.DST;1        8  21-JUN-1990 12:41
```

```
[JEP1.DAT]SUBA31.DST;1                8  21-JUN-1990 12:41
[JEP1.DAT]SUBA32.DST;1                8  21-JUN-1990 12:42
[JEP1.DAT]SUBA33.DST;1                8  21-JUN-1990 12:42
[JEP1.DAT]SUBA34.DST;1                8  21-JUN-1990 12:43
[JEP1.DAT]SUBA35.DST;1                8  21-JUN-1990 12:43
[JEP1.DAT]SUBA36.DST;1                8  21-JUN-1990 12:43
[JEP1.DAT]SUBA37.DST;1                8  21-JUN-1990 12:44
[JEP1.DAT]SUBA38.DST;1                8  21-JUN-1990 12:44
[JEP1.DAT]SUBA39.DST;1                8  21-JUN-1990 12:45
[JEP1.DAT]SUBA4.DST;1                 8  21-JUN-1990 12:31
[JEP1.DAT]SUBA41.DST;1                8  21-JUN-1990 12:45
[JEP1.DAT]SUBA42.DST;1                8  21-JUN-1990 12:46
[JEP1.DAT]SUBA43.DST;1                8  21-JUN-1990 12:46
[JEP1.DAT]SUBA44.DST;1                8  21-JUN-1990 12:47
[JEP1.DAT]SUBA5.DST;1                 8  21-JUN-1990 12:31
[JEP1.DAT]SUBA6.DST;1                 8  21-JUN-1990 12:32
[JEP1.DAT]SUBA7.DST;1                 8  21-JUN-1990 12:32
[JEP1.DAT]SUBA8.DST;1                 8  21-JUN-1990 12:32
[JEP1.DAT]SUBA9.DST;1                 8  21-JUN-1990 12:33
[JEP1.DAT]SUBB1.DST;1                 8  21-JUN-1990 12:47
[JEP1.DAT]SUBB10.DST;1                8  21-JUN-1990 12:51
[JEP1.DAT]SUBB13.DST;1                8  21-JUN-1990 12:51
[JEP1.DAT]SUBB14.DST;1                8  21-JUN-1990 12:51
[JEP1.DAT]SUBB15.DST;1                8  21-JUN-1990 12:52
[JEP1.DAT]SUBB17.DST;1                8  21-JUN-1990 12:52
[JEP1.DAT]SUBB18.DST;1                8  21-JUN-1990 12:53
[JEP1.DAT]SUBB19.DST;1                8  21-JUN-1990 12:53
[JEP1.DAT]SUBB2.DST;1                 8  21-JUN-1990 12:48
[JEP1.DAT]SUBB20.DST;1                8  21-JUN-1990 12:54
[JEP1.DAT]SUBB21.DST;1                8  21-JUN-1990 12:54
[JEP1.DAT]SUBB23.DST;1                8  21-JUN-1990 12:54
[JEP1.DAT]SUBB24.DST;1                8  21-JUN-1990 12:55
[JEP1.DAT]SUBB25.DST;1                8  21-JUN-1990 12:55
[JEP1.DAT]SUBB26.DST;1                8  21-JUN-1990 12:56
[JEP1.DAT]SUBB27.DST;1                8  21-JUN-1990 12:56
[JEP1.DAT]SUBB28.DST;1                8  21-JUN-1990 12:57
[JEP1.DAT]SUBB29.DST;1                8  21-JUN-1990 12:57
[JEP1.DAT]SUBB3.DST;1                 8  21-JUN-1990 12:48
[JEP1.DAT]SUBB30.DST;1                8  21-JUN-1990 12:58
[JEP1.DAT]SUBB31.DST;1                8  21-JUN-1990 12:58
[JEP1.DAT]SUBB32.DST;1                8  21-JUN-1990 12:58
[JEP1.DAT]SUBB33.DST;1                8  21-JUN-1990 12:59
[JEP1.DAT]SUBB34.DST;1                8  21-JUN-1990 12:59
[JEP1.DAT]SUBB35.DST;1                8  21-JUN-1990 13:00
[JEP1.DAT]SUBB36.DST;1                8  21-JUN-1990 13:00
[JEP1.DAT]SUBB37.DST;1                8  21-JUN-1990 13:01
[JEP1.DAT]SUBB38.DST;1                8  21-JUN-1990 13:01
[JEP1.DAT]SUBB39.DST;1                8  21-JUN-1990 13:01
[JEP1.DAT]SUBB4.DST;1                 8  21-JUN-1990 12:48
[JEP1.DAT]SUBB41.DST;1                8  21-JUN-1990 13:02
[JEP1.DAT]SUBB42.DST;1                8  21-JUN-1990 13:02
[JEP1.DAT]SUBB43.DST;1                8  21-JUN-1990 13:03
[JEP1.DAT]SUBB44.DST;1                8  21-JUN-1990 13:03
[JEP1.DAT]SUBB5.DST;1                 8  21-JUN-1990 12:49
[JEP1.DAT]SUBB6.DST;1                 8  21-JUN-1990 12:49
[JEP1.DAT]SUBB7.DST;1                 8  21-JUN-1990 12:49
[JEP1.DAT]SUBB8.DST;1                 8  21-JUN-1990 12:50
[JEP1.DAT]SUBB9.DST;1                 8  21-JUN-1990 12:50
[JEP1.DAT]TEMPLATE_A.DAT;1           17   7-MAY-1990 11:05
[JEP1.DAT]TEMPLATE_A.DST;1           15  24-APR-1990 18:07
```

```
[JEP1.DAT]TEMPLATE_B.DAT;1          17  24-APR-1990 18:06
[JEP1.DAT]TEMPLATE_B.DST;1          15  24-APR-1990 18:07
[JEP1.CODE]CONV.FOR;1               15   2-MAY-1990 12:32
[JEP1.CODE]DS_MODEL.FOR;1           16   7-MAY-1990 14:36
[JEP1.CODE]EW.FOR;1                 3  25-AUG-1990 17:13
[JEP1.CODE]FITSR.FOR;1              13  12-JAN-1990 12:02
[JEP1.CODE]KENDALL.FOR;1            4  27-AUG-1990 14:12
[JEP1.CODE]READ.FOR;1               5   3-MAY-1990 11:04
[JEP1.CODE]TOM.FOR;1                17   3-APR-1990 15:04
[JEP1.CODE]TRI.FOR;1                4  24-APR-1990 18:13

Total of 355 files, 100103 blocks
```

APPENDIX C

Stars Used to Determine Plate-to-plate Separations

Table C.1 lists the stars used to determine the plate-to-plate distortion correction (*cf.* Section 4.2.2.a). They were randomly chosen from the Hubble Guide Star Catalog (Lasker, Jenkner & Russell 1989). The information below is saved in the file STAR_LIST.DAT on the magnetic tape discussed in Appendix B.

Table C.1: Stars used for the plate-to-plate distortion correction.

R.A. (1950.0)	Dec.	m_p
h m s	° ′ ″	
11 32 51.9	20 25 50.8	12.12
11 33 20.6	18 46 55.3	12.73
11 33 29.6	18 51 25.4	12.24
11 33 36.8	19 45 41.9	12.53
11 33 38.6	20 06 35.5	12.22
11 33 39.5	19 32 18.6	12.80
11 34 01.0	18 58 13.0	12.75
11 34 01.6	19 56 40.4	12.13
11 34 47.1	22 15 58.0	12.55
11 34 53.0	18 24 32.3	12.43
11 34 57.2	18 55 55.6	12.74
11 35 58.6	21 46 49.5	12.52
11 36 30.8	21 06 39.4	12.12
11 36 51.6	19 09 17.5	12.76
11 37 25.9	21 29 31.1	12.90
11 38 28.0	18 48 00.9	12.29
11 38 46.8	22 09 48.6	12.90
11 39 06.1	18 56 12.2	12.89
11 39 22.9	21 59 32.8	12.78
11 39 31.9	18 18 34.3	12.99
11 39 51.6	19 04 01.2	12.93
11 39 59.3	19 01 13.0	12.41
11 40 09.3	19 17 20.0	12.34
11 40 13.9	22 10 01.7	12.57
11 41 30.0	22 19 56.0	12.53
11 42 42.6	18 40 25.8	12.59
11 42 45.1	20 51 16.7	12.31
11 43 11.9	21 12 10.9	12.71
11 43 26.2	21 31 20.3	12.88
11 43 45.7	20 00 54.0	12.95
11 43 50.2	19 00 47.8	12.90
11 43 50.3	18 24 11.6	12.11
11 44 47.5	18 55 06.8	12.42
11 45 09.6	22 42 28.6	12.79
11 45 24.1	22 13 19.5	12.55
11 45 50.0	22 08 06.8	12.80
11 45 57.9	18 52 01.8	12.28
11 46 21.5	19 24 46.8	12.85

Table C.1 – *continued*

R.A. (1950.0)	Dec. (1950.0)	m_p
h m s	° ′ ″	
11 46 43.7	18 05 59.5	12.47
11 47 15.9	20 41 13.3	12.26
11 47 19.8	22 22 09.1	12.41
11 47 21.0	18 36 52.7	12.94
11 47 39.5	18 44 34.8	12.93
11 47 46.0	19 41 04.9	12.87
11 48 43.3	18 46 05.5	12.97
11 48 57.4	19 52 37.0	12.46
11 49 04.4	19 03 01.2	12.86
11 49 12.4	20 10 34.5	12.46
11 49 13.0	18 58 28.1	12.56
11 49 31.0	18 58 40.7	12.54
11 49 53.3	18 23 55.7	12.59
11 49 53.7	22 13 21.2	12.38
11 50 02.6	19 09 27.7	12.62
11 50 03.0	18 55 05.1	12.97
11 51 02.7	18 24 00.9	12.86
11 51 15.5	18 15 42.8	12.96
11 52 49.9	21 31 23.6	12.90
11 53 29.1	21 12 22.0	12.68

References

Abell, G.O., 1958. *Astrophys. J. Suppl. Ser.*, **3**, 211.

Abell, G.O., 1975. In: *Galaxies and the Universe*, eds. A. Sandage, M. Sandage & J. Kristian, 601.

Arp, H., 1966. *Atlas of Peculiar Galaxies*, California Institute of Technology, Pasadena, California.

Bahcall N.A., 1977. *Astrophys. J. Lett.*, **218**, L93.

Barbon, R., Cappellaro, E. & Turatto, M., 1989. *Astron. & Astrophys. Suppl. Ser.*, **81**, 421.

Barnes, J.E., 1988. *Astrophys. J.*, **331**, 699.

Bautz, L. P. & Morgan, W. W., 1970. *Astrophys. J. Lett.*, **162**, L149.

Bechtold, J., Forman, W., Giacconi, R., Jones, C., Schwarz, J., Tucker, W. & Van Speybroeck, L., 1983. *Astrophys. J.*, **265**, 26.

Bicay, M.D. & Giovanelli, R., 1987. *Astrophys. J.*, **321**, 645.

Bothun, G.D., 1982. *Astrophys. J.*, **50**, 39.

Bothun, G.D., Schommer, R.A. & Sullivan, W.T., 1982. *Astron. J.*, **87**, 725.

Bothun, G.D., Aaronson, M., Schommer, B., Mould, J., Huchra, J. & Sullivan, W.T., 1985. *Astrophys. J. Suppl.*, **57**, 423.

Burns, J.O., Hanisch, R.J., White, R.A., Nelson, E.R., Morrisette, K.A. & Moody, J.W., 1987. *Astron. J.*, **94**, 587.

Bushouse, H.A., 1986. *Astron. J.*, **91**, 255.

Bushouse, H.A., 1987. *Astrophys. J.*, **320**, 49.

Butcher, H. & Oemler, A., 1978. *Astrophys. J.*, **219**, 18.

Byrd, G., Valtonen, M., Sundelius, B & Valtaoja, L., 1986. *Astron. Astrophys.*, **166**, 75.

Byrd, G. & Valtonen, M., 1990. *Astrophys. J.*, **350**, 89.

Chamaraux, P., Balkowski, C. & Gerard, E., 1980. *Astron. & Astrophys.*, **83**, 38.

Chincarini, G., Giovanelli, R. & Haynes, M.P., 1983. *Astrophys. J.*, **269**, 13.

Christensen, C.G., 1975. *Astron. J.*, **80**, 282.

Cohen, J.G., 1976. *Astrophys. J.*, **203**, 587.

Cowie, L.L. & Songaila, A., 1977. *Nature*, **266**, 501.

Davies, R.D. & Lewis, B.M., 1973. *Mon. Not. R. astr. Soc.*, **165**, 231.

de Jong, T., Clegg, P.E., Soiter, B.T., Rowan-Robinson, M., Habing, H.J., Houck, J.R., Aumann, H.H. & Raimond, E., 1984. *Astrophys. J. Lett.*, **278**, L67.

Denisyuk, E.K., Lipovetskii, V.A. & Afansiev, V.L., 1976. *Astrofiz*, **12**, 665.

Dickens, R.J. & Moss, C., 1976. *Mon. Not. R. astr. Soc.*, **174**, 47.

Dressler, A., 1980. *Astrophys. J.*, **236**, 351.

Dressler, A., 1984. *Ann. Rev. Astron. Astrophys.*, **22**, 185.

Dressler, A. & Gunn, J.E., 1982. *Astrophys. J.*, **263**, 533.

Dressler, A., Gunn, J.E. & Schneider, D.D., 1985. *Astrophys. J.*, **294**, 70.

Dressler, A. Thompson, I.B. & Shectman, S.A., 1985. *Astrophys. J.*, **288**, 481.

Elmegreen, B.G. & Lada, C.J., 1977. *Astrophys. J.*, **214**, 725.

Elmegreen, D.M., Elmegreen, B.G. & Bellin, A.D., 1990. *Astrophys. J.*, **364**, 415.

Eneev, T.M., Kovlov, N.N. & Sunyaev, R.A., 1973. *Astron. & Astrophys.*, **22**, 41.

Fisher, J.R. & Tully, R.B., 1981. *Astrophys. J. Suppl.*, **47**, 139.

Fitt, A.J., Alexander, P. & Cox, M.J., 1988. *Mon. Not. R. astr. Soc.*, **233**, 907.

Fullmer, L. & Lonsdale, C., 1989. *Cataloged Galaxies and Quasars Observed in the IRAS Survey.* Pasedena, California.

Gallagher, J.S., Bushouse, H. & Hunter, D.A., 1989. *Astron. J.*, **97**, 700.

Gavazzi, G., 1987. *Astrophys. J.*, **320**, 96.

Gavazzi, G., 1990. Private Communication.

Gavazzi, G. & Jaffe, W., 1985. *Astrophys. J. Lett.*, **294**, L89.

Gavazzi, G. & Jaffe, W., 1986. *Astrophys. J.*, **310**, 53.

Gavazzi, G., Tarenghi, M., Jaffe, W., Butcher, H. & Boksenberg, A., 1984. *Astron. Astrophys.*, **137**, 235.

Giovanardi, C., Helou, G., Krumm, N. & Salpeter, E.E., 1983. *Astrophys. J.*, **267**, 35.

Giovanelli, R. & Haynes, M.P., 1983. *Astron. J.*, **88**, 881.

Giovanelli, R. & Haynes, M.P., 1985. *Astrophys. J.*, **292**, 404.

Gisler, G.R., 1978. *Mon. Not. R. astr. Soc.*, **183**, 633.

Gott, J.R., 1977. *Ann. Rev. Astron. Astrophys.*, **15**, 235.

Gott, J.R. & Thuan, T.X., 1976. *Astrophys. J.*, **204**, 649.

Gregory, S.A. & Thompson, L.A., 1978. *Astrophys. J.*, **222**, 784.

Gudehus, D.H., 1976. *Astrophys. J.*, **208**, 267.

Gunn, J.E. & Gott, J.R., 1972. *Astrophys. J.*, **176**, 1.

Hanisch, R.J., 1980. *Astron. J.*, **85**, 1565.

Haynes, M.P. & Giovanelli, R., 1986. *Astrophys. J.*, **306**, 466.

Huchra, J.P., 1988. In: *Starbursts and Galactic Evolution*, eds. T.X. Thuan, T. Montmerle & J. Tran Thanh Van, 199.

Huchra, J., Davis, M., Latham, D. & Tonry, D., 1983. *Astrophys. J. Suppl.*, **52**, 89.

Jaffe, W. & Gavazzi, G., 1986. *Astron. J.*, **91**, 204.

Jaffe, W., Gavazzi, G & Valentijn, E., 1986. *Astron. J.*, **91**, 199.

Johnstone, R.M. & Fabian, A.C., 1989. *Mon. Not. R. astr. Soc.*, **237**, 27p.

Jones, C., Mandel, E., Schwarz, J., Forman, W., Murray, S.S. & Harnden, F.R., 1979. *Astrophys. J. Lett.*, **234**, L21.

Keel, W.C., 1983. *Astrophys. J.*, **268**, 632.

Kenney, J.D.P. & Young, J.S., 1989. *Astrophys. J.*, **344**, 171.

Kennicutt, R.C., 1983a. *Astron. J.*, **88**, 483.

Kennicutt, R.C., 1983b. *Astrophys. J.*, **272**, 54.

Kennicutt, R.C., Bothun, G.D. & Schommer, R.A., 1984. *Astron. J.*, **89**, 1279.

Kennicutt, R.C. & Keel, W.C., 1984. *Astrophys. J. Lett.*, **279**, L5.

Kennicutt, R.C., Keel, W.C., van der Hulst, J.M., Hummel, E. & Roettiger, K.A., 1987. *Astron. J.*, **93**, 1011.

Kennicutt, R.C. & Kent, S.M., 1983. *Astron. J.*, **88**, 1094.

Kibblewhite, E.J., Bridgeland, M.T., Bunclark, P. and Irwin, M.J., 1984. In: *Astronomical Microdensitometry Conference,* ed. D.A. Klinglesmith, 277.

Kirshner, R., 1977. *Astrophys. J.*, **212**, 319.

Lamb, S.A., Bushouse, H.A., Werner, M.W. & Smith, B.F., 1988. In: *Comets to Cosmology*, ed. A. Lawrence, 257.

Larson, R.B. & Tinsley, B.M., 1978. *Astrophys. J.*, **219**, 46.

Lasker, B.M., Jenkner, H. & Russell, J.C., 1989. *The Hubble Guide Star Catalog*, Space Telescope Science Institute, Baltimore, Maryland.

Laurikainen, E. & Moles, M., 1989. *Astrophys. J.*, **345**, 176.

Majewski, S. R., 1989. In: *The Epoch of Galaxy Formation*, ed. C.S. Frenk, R.S. Ellis, T. Shanks, A.F. Heavens & J.A. Peacock, 85.

Markarian, B.E., Lipovetskii, V.A. & Stepanyan, Dzh. A., 1984. *Astrofiz*, **20**, 419.

McCarthy, M.F. & Treanor, P.J., 1970. *Observatory*, **90**, 108.

Morgan, W.W., 1962. *Astrophys. J.*, **135**, 1.

Moss, C., 1988. In: *Starbursts and Galaxy Evolution*, eds. T.X. Thuan & Th. Montmerle, 341.

Moss, C. & Dickens, R.J., 1977. *Mon. Not. R. astr. Soc.*, **178**, 701.

Moss, C. & Whittle, M., 1991. In preparation.

Moss, C., Whittle, M. & Irwin, M.J., 1988. *Mon. Not. R. astr. Soc.*, **232**, 381. (MWI).

Mueller, M.W. & Arnett, W.D., 1976. *Astrophys. J.*, **210**, 670.

Mushotzky, R.F., 1984. *Phys. Scripta*, **T7**, 157.

Nilson, P., 1973. *Uppsala General Catalogue of Galaxies, Uppsala astr. Obs. Ann.*, **6**.

Noguchi, M., 1988. *Astron. Astrophys.*, **201**, 37.

Norman, C. & Silk, J., 1979. *Astrophys. J. Lett.*, **233**, L1.

Oemler, A., 1974. *Astrophys. J.*, **194**, 1.

Osterbrock, D.E., 1960. *Astrophys. J.*, **132**, 325.

Osterbrock, D.E., 1989. *Astrophysics of Gaseous Nebulae and Active Galactic Nuclei*, University Science Books.

Paturel, G., Fouqué, P., Bottinelli, L. & Gouguenheim, L., 1989. *Aston. Astrophys. Suppl. Ser.*, **80**, 299.

Peebles, P.J.E., 1989. In: *The Epoch of Galaxy Formation*, ed. C.S. Frenk, R.S. Ellis, T. Shanks, A.F. Heavens & J.A. Peacock, 1.

Petrosyan, A.R., Saakyan, K.A. & Khachikyan, E.E., 1979. *Astrofiz*, **15**, 373.

Roos, N. & Norman, C.A., 1979. *Astron. & Astrophys.*, **76**, 75.

Sandage, A., 1961. *The Hubble Atlas of Galaxies*, Carnegie Institution of Washington, Washington, D.C.

Sandage, A. & Tammann, G.A., 1981. *A Revised Shapley-Ames Catalog of Bright Galaxies*, Publ. No. 635 (Carnegie Institution of Washington, Washington, D.C.) (RSA).

Sarazin, C.L., 1979. *Astrophys. Lett.*, **20**, 93.

Sarazin, C.L., 1988. *X-ray Emission From Clusters of Galaxies,* Cambridge University Press, Cambridge.

Schneider, S.E., Helou, G., Salpeter, E.E. & Terzian, T., 1986. *Astron. J.*, **92**, 742.

Schweizer, F., 1983. In: *Internal Kinematics and Dynamics of Galaxies*, ed. E. Athanassoula, 319.

Schweizer, F., 1987. In: *Nearly Normal Galaxies: From Planck Time to the Present*, ed. S.M. Faber, 18.

Shu, F.H., Milione, V., Gebel, W., Yuan, C., Goldsmith, D.W. & Roberts, W.W., 1972. *Astrophys. J.*, **173**, 557.

Sodre, L., Capelato, H.V., Steiner J.E. & Mazure, A., 1989. *Astron. J.* **97**, 1279.

Spitzer, L. & Baade, W., 1951. *Astrophys. J.*, **113**, 413.

Stauffer, J.R., 1983. *Astrophys. J.*, **264**, 14.

Stock, J. & Osborn, W., 1980. *Astron. J.*, **85**, 1366.

Struble, M. F. & Rood, H. J., 1987. *Astrophys. J. Suppl. Ser.*, **63**, 543.

Tammann, G.A. & Binggeli, B., 1987. In: *High Redshift and Primeval Galaxies*, eds. J. Bergeron, D. Kunth, B. Rocca-Volmerange, J. Tran Thanh Van, 149.

Tifft, W.G., 1978. *Astrophys. J.*, **222**, 54.

Toomre, A., 1977. In: *The Evolution of Galaxies and Stellar Populations,* eds.. B. M. Tinsley & K. B. Larson, 401.

Toomre, A. & Toomre, J., 1972. *Astrophys. J.*, **178**, 623.

Tremaine, S., 1990. In: *Dynamics and Interactions in Galaxies*, ed. R. Wielen, 394.

Trinchieri, G., Fabbiano, G., Bandiera, R., 1989. *Astrophys. J.*, **342**, 759.

van den Bergh, S., 1990. In: *Dynamics and Interactions in Galaxies*, ed. R. Wielen, 492.

Véron-Cetty, M.-P. & Véron, P., 1989. *ESO Scientific Report*, #7, March 1989.

Vorontsov-Velyaminov, B.A. & Arkipova, V.P., 1964. *Morphological Catalogue of Galaxies*, Part II, Moscow State University.

Weiler, K.W. & Sramek, R.A., 1988. *Ann. Rev. Astron. Astrophys.*, **26**, 295.

White, S.D.M., 1976. *Mon. Not. R. astr. Soc.*, **177**, 717.

Young, J.S., Kenney, J.D., Tacconi, L., Claussen, M.J., Huang, Y.-L., Tacconi,-Garman, L., Xie, S. & Schloerb, F.P., 1986. *Astrophys. J. Lett.*, **311**, L17.

Young, J.S., Scoville, N.Z. & Brady, E., 1985. *Astrophys. J.*, **288**, 487.

Zwicky, F. & Herzog, E., 1963. *Catalogue of Galaxies and Clusters of Galaxies*, vol. II.